Orientational glasses

U.T. Höchli, K. Knorr, Alois Loidl

Angaben zur Veröffentlichung / Publication details:

Höchli, U.T., K. Knorr, and Alois Loidl. 1990. "Orientational glasses." *Advances in Physics* 39 (5): 405–615. https://doi.org/10.1080/00018739000101521.

Orientational glasses

By U. T. Höchli

IBM Research Division, Zürich Research Laboratory, 8803 Rüschlikon, Switzerland

K. Knorr and A. Loidl

Universität Mainz, Institut für Physik, 6500 Mainz, F.R. Germany

Abstract

This review summarizes experimental evidence for the freezing of reorienting moments in solids. The moments may be of dipolar or quadrupolar nature, or both; they belong to one of the constituents of a mixed-crystal solid. Extensive results are reported for the following systems: KCl doped with hydroxyl, potassium tantalate doped with Li, Na and Nb, alkali halide cyanides and alkali–alkali cyanides, rubidium ammonium dihydrogen phosphate, solid *ortho–para* hydrogen and argon–nitrogen mixtures. These have clearly glass-like properties. In other systems, results are limited to one or two methods hinting at glass formation; some of those are also reported. Clustering phenomena and the slow-down of reorientations at the freezing temperature are observed in susceptibility measurements and by local probing on nuclear spins. The modulation of the structure by cluster formation is revealed by diffraction experiments. These phenomena are confronted with model predictions and numerical simulations.

Contents

1. Introduction

We apply the term 'orientational glass' to a solid consisting of a regular lattice some of whose sites are occupied by constituents containing a dipole or quadrupole moment. These moments have orientational degrees of freedom; they interact with one another and, below some freezing temperature T_f, their motion slows and they freeze into a configuration devoid of long-range order. A typical example is KCl doped with OH molecules that replace Cl at random sites. At 10 K the dipoles associated with the OH molecules reorient rapidly, whereas at 0·1 K their orientations are static on experimental time scales, yet there is no macroscopic (spontaneous) polarization. Early investigations of this orientational-glass prototype (of the subspecies 'dipole glass') were performed by Känzig *et al.* (1964). Brout (1965) considered its short-range order and pointed out the analogy with what was to become the spin-glass prototype, Cu doped with Mn, where Mn has a spin of $\frac{5}{2}$ and therefore contains magnetic degrees of freedom.

The use of the word 'glass' suggests a similarity with what we call 'canonical glasses' (the prototype of which is fused silica, SiO_2), in order to distinguish them from orientational and spin glasses. There are indeed orientational degrees of freedom in SiO_2, in addition to rapid freezing of the moments and a low-temperature configuration devoid of order. Owing to the lack of an underlying lattice, however, it is impossible to associate moments at site i with interactions between moments at sites i and j, which is a pre-requisite for modelling a glass in terms of a Hamiltonian.

Spin-glass models are based almost entirely on the existence of a Hamiltonian containing interactions between spins and their coupling to a magnetic field. The interactions chosen to model spin glasses are, in general, totally unspecific for spins. They are usually probabilistic distributions of interaction strengths with a variance $\mathrm{Var}J_{ij}$ much larger than their average $\bar{J}_{ij}$ and with both quantities independent of $i - j$. The picture of spin glasses given on the basis of such crude models is quite reasonable, and the crude models are sufficiently general to be applied to dipole and quadrupole glasses as well (at least in principle).

It will become evident in the following that orientational glasses are not simply analogous to spin glasses but they also have more variety. The closest spin-glass analogues are perhaps glasses like KCl:OH, $KTaO_3$:Li and KBr:CN near the threshold concentration for glass formation. In these glasses, some minimum threshold concentration of impurities is required to form a glass state, and, upon increasing the concentration, the freezing temperature T_f rises. Obviously, an increase in the concentration of impurities leads to enhancement of the interaction between them. The form of the interaction, however, may also change. As in spin glasses, the average interaction may increase more quickly than its variance such that above a

second threshold the orientational degrees of freedom become ordered. Schematic (x, T) phase diagrams of A : B mixed crystals exhibiting an orientational-glass state are shown in figures 1.1 and 1.2. A characteristic phase diagram of solid solutions of an orientationally ordered component B ($T \leqslant T_c$) with a constituent A without multipolar moments is given in figure 1.1 (KCl : OH, KBr : KCN, o–p-H_2, Ar : N_2, Kr : CH_4, $KTaO_3$: Li). Figure 1.2 shows mixtures of two orientationally ordered

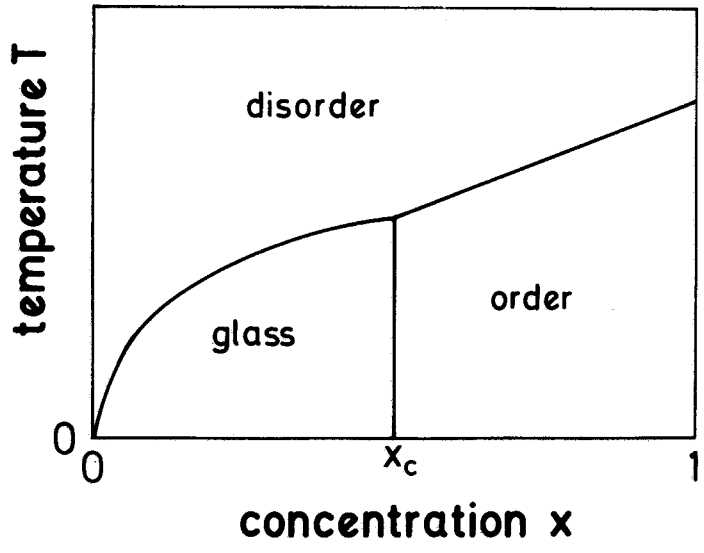

Figure 1.1. Schematic (x, T) phase diagram of $A_{1-x}B_x$ mixed crystal. B denotes a molecular compound (e.g. KCN, N_2, o-H_2), while A denotes a compound with no orientational degrees of freedom (e.g. KBr, Ar, p-H_2).

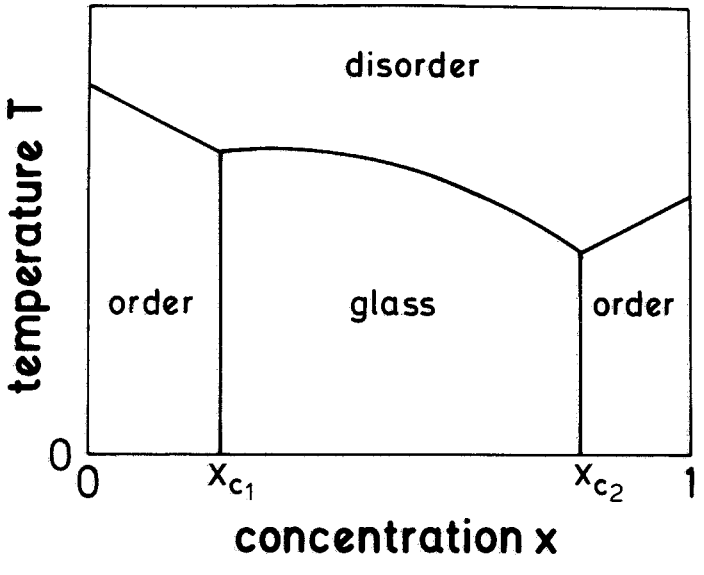

Figure 1.2. Schematic (x, T) phase diagram of $A_{1-x}B_x$ mixed crystals. Both pure compounds are elastically or electrically ordered. The high-temperature phase is para-elastic (plastic) or para-electric.

compounds A and B that exhibit a disordered low-temperature state at intermediate concentrations (the glass state occurs as a result of competing interactions or random fields). Examples are mixtures of ferroelectric and antiferroelectric compounds such as rubidium ammonium dihydrogen phosphate (RADP) and mixtures of elastically ordered NaCN and KCN. A situation that does not occur with spin glasses is the rapid growth of quadrupolar interaction with concentration such that cross-over from dipolar to quadrupolar behaviour takes place at the second threshold. In all these phase diagrams it is assumed that there is no diffusion (i.e. the composition x is a quenched variable). By 'motion', we always mean the reorientation of moments in the following.

Most of the evidence for the mechanism of glass formation has been obtained from investigations near the freezing temperature. In this respect, experimental research on orientational glasses is largely influenced by methods applied to the study of structural phase transitions. Various responses are measured as functions of T, on a vertical line in our phase diagrams. Like the structural phase transition, the glass transition divides the temperature regime into one (with $T > T_f$) in which responses are fluctuation-driven, and another (with $T < T_f$), in which they are interaction-driven. If we designate by p_i the local polarization then we may define the susceptibility as

$$\chi = \partial \sum_i p_i / \partial E$$

where E is the electric field. An analogous definition holds for local strain and stress. We expect χ to rise and its dispersion region to extend to increasingly lower frequencies upon lowering T. This suggests that we define a freezing temperature T_f below which the system is static. This definition, however, is impractical for experimental purposes: even at the lowest accessible frequencies ω, in the millihertz range, T_f still depends on ω, and it will become evident that reasonable extrapolation of $T_f(\omega)$ to $\omega = 0$ yields values for $T_f(0)$ that have no physical relevance. We therefore resort to defining an operational T_f as the temperature at which an orientational glass is frozen on the time scale set by ordinary low-frequency measurements—typically 1 Hz. The value of T_f reflects the fact that the fluctuation-driven and interaction-driven regimes are not separated at a critical temperature T_c but that competition is manifest over a broader temperature range. Investigations of static behaviour are performed with space-resolving experiments: structural and light-scattering methods are expected to reveal that the moments p_i are correlated to some finite distance ξ in space, where ξ is a measure of order for the low-temperature state. Investigations of orientational glasses have also profited from methods applied to canonical glasses. In particular, a plot of the leading relaxation time (or inverse dispersion frequency) *versus* reciprocal temperature yields parameters for the hindering barrier and the freezing temperature. The energy landscape accounting for these findings gives rise to tunnel states that are indicated by the unusual low-temperature ($T \ll T_f$) behaviour of most responses.

We are aware of compatibility problems that arise when responses of a glass are measured with methods devised for other research areas, and we note in particular that the frequency windows are radically different for magnetic, electric-dipole and elastic-quadrupole susceptibilities. The same applies for the spatial-resolution window or diffraction, light-transmission and scattering methods. We have thus made

a special effort to present experimental results disentangled from their interpretation by their authors. This is intended to help the reader as it has also helped us form an independent opinion as to the relevance of the data. The use of widespread methods for experimental investigation has prompted us to summarize the principal methods for later reference (section 2). The main body of this paper is contained in the sections on experimental results for KCl : OH (section 3), $KTaO_3$: (Li, Na and Nb) (section 4), KBr : CN and NaCN : KCN (section 5), RADP (section 6) and molecular solids such as *ortho–para*-H_2 (section 7), Ar : N_2 (section 8), Kr : CH_4 and others (section 9).

Selected data are evaluated in terms of a model specifically designed and probably valid only for a particular system. The evaluation of such data and the essential features of the model are treated in the appropriate chapter.

Some of the findings are quite general, and independent of the particular system under study. We have attempted to summarize such evidence in section 10, where reference is made to the experimental situation in canonical glasses and spin glasses. Section 11 summarizes the result of theories intended to account for unifying features in orientational glasses and references to the literature of canonical glasses. We have taken the liberty of developing our own philosophy on glass research in section 12, we hope without unduly imposing the lowest common denominator of our consolidated view on the reader.

From our point of view, it is essential that the low-temperature glass state is established by a cooperative freezing-in of the orientational degrees of freedom. Molecular crystals for which the reorienting moments simply slow down in a thermally activated process in the crystal field of the neighbouring atoms are explicitly excluded. Well known examples of this case are carbon monoxide (CO) and nitrous oxide (N_2O). These molecular compounds carry small dipolar moments but exhibit no head-to-tail order at low temperatures. In these crystals, the dipolar disorder is frozen in well above the hypothetical ordering temperatures because of the high activation energies required for relaxational processes compared with the ordering energy. For example, the hindering barriers in N_2O are of order 7000 K while the 'ordering temperature' has been evaluated to be of order 11 K. The freezing process in these materials is characterized by an Arrhenius equation for the rate processes and an almost monodispersive relaxation in the experimentally accessible time window. We neglect interaction and find that the reorienting moments continuously freeze into a 'static' low-temperature disordered state. As the temperature is reduced, longer and longer times must be allowed in order to detect reorientation processes (Böhmer and Loidl 1990a).

Frozen-in orientational disorder also occurs in undiluted molecular crystals. In thermodynamic equilibrium, these substances exhibit a plastic phase and a stable ordered low-temperature state. Upon rapid cooling, the rotor phase can be frozen-in and the long-range orientational order becomes suppressed. Cyclohexanol is an excellent example of this (Suga 1986). Another system in which the plastic phase can be supercooled is cyanoadamantane (Descamps and Caucheteux 1987). Both systems exhibit a thermal anomaly at the glass transition, analogous to the findings in canonical glasses. The cooling rate and the steric hindrance of the molecules with respect to reorientations are the important parameters to reach the glassy state in undiluted molecular crystals, which are usually termed glassy crystals. We do not treat glassy crystals, but rather refer to reviews by Suga and Seki (1974) and Suga (1986).

2. Experimental methods for the study of vitrification

This section contains a brief account of the experimental methods used to investigate orientational glasses. At the same time, it serves to introduce common relations. It contains no new physics and can be skipped by an experienced experimentalist.

The formation of an orientational glass bears some resemblance to the transition to a structural phase. In both processes, some constituents containing orientational degrees of freedom take a fixed position when the temperature is lowered. A structural phase has periodic symmetry, whereas a glass does not. The orientational degrees of freedom are thus correlated in a structural phase and uncorrelated in a glass on a macroscopic scale. The dynamics leading to periodic or aperiodic structures differ accordingly: formation of a periodic structure requires freezing of a particular motion of infinite wavelength or a single k vector, whereas aperiodic structures, such as glasses, are formed by freezing of motion in parts of the solid with continuously distributed wavelength. The distribution of resonance frequencies or relaxation rates is thus discrete in periodic systems, since only $3N - 3$ modes are allowed (N is the number of particles per unit cell), and continuous in glasses. Of these distributions, only one usually plays an active role in the ordered transition process.

Experimental methods for the study of glasses are similar to those used for the study of phase transitions. They are mainly aimed at resolving the dynamics of the freezing process and at resolving spatial inhomogeneity. To resolve the dynamics, susceptibilities (dielectric and elastic) need to be known over large ranges of frequencies. Spatial resolution is achieved by light scattering, second-harmonic light generation and diffraction by X-rays and neutrons. These methods are supplemented by nuclear magnetic resonance techniques, which provide information on local properties.

Here these methods are reviewed briefly to provide quick reference to data presented later and to facilitate access to pertinent literature on experimentation. No original data will be presented in this section.

2.1. *Dielectric susceptibilities*

The standard way (Jonscher 1983) of expressing the dielectric response is in terms of a frequency-dependent susceptibility, which relates the spectral component of the macroscopic polarization $P(\omega)$ to the a.c. field $E(\omega)$ in amplitude and phase. The value for $\varepsilon = 1 + \varepsilon_0^{-1} \partial P(\omega)/\partial E(\omega)$ is readily measured on commercial bridges on the basis of comparison of the simple characteristics with built-in standards, $\varepsilon_0 = 8{\cdot}85\,\mathrm{pF\,m^{-1}}$. The lower frequency limit is determined by impedance matching of the sample to the bridge, and is about 0·01 Hz; the upper limit is set by problems related to the calibration of transmission lines between input head and sample, often in a cryogenic environment. It is of the order of 10 GHz.

At frequencies below about 10 Hz, it is more convenient to measure the discharge current density $i(t)$ of a sample after subjecting it to a field for times that are large compared with the discharge. Susceptibilities and discharge currents are related by the Fourier transform

$$\varepsilon^* - \varepsilon_\infty = \varepsilon_0^{-1} E^{-1} (2\pi)^{-1} \int \mathrm{e}^{\mathrm{i}\omega t}\, i(t)\, \mathrm{d}t, \tag{2.1}$$

where ε_∞ is the value of ε at frequencies above the dispersive regime and E is the applied field, which must be kept low to ensure linearity between P and E.

The decay current is sometimes considered a result of independent (parallel) relaxation mechanisms, each with its own relaxation times. If $g(\tau)$ is the distribution

of relaxation times then the current density

$$i(t) = \int e^{-t/\tau} g(\tau)\,d\tau = \mathscr{L}[g(\tau)], \tag{2.2a}$$

and inversion gives

$$g(\tau) = \frac{1}{2\pi i}\int_{\gamma-i\infty}^{\gamma+i\infty} i(t)\, e^{\gamma t}\,dt = \mathscr{L}^{-1}[i(t)], \tag{2.2b}$$

where $\mathscr{L}$ is the Laplace transform and $\mathscr{L}^{-1}$ its inverse. Equations (2.1) and (2.2) imply a direct mathematical relationship between $\varepsilon(\omega)$ and $g(\tau)$. This was given by Wagner (1913) on the basis of the Debye model (Jonscher 1983) and is

$$\varepsilon^*(\omega) - \varepsilon_\infty = \int \frac{g(\tau)\,d\tau}{1 + i\omega\tau}. \tag{2.3}$$

The inverse transform involving the imaginary part $\varepsilon_2(\omega)$ was derived from the inverse Laplace transform by Fuoss and Kirkwood (1941):

$$g\left(\ln\frac{\tau}{\tau_0}\right) = \pi^{-1}\left[\varepsilon_2(\ln\omega\tau_0 + \tfrac{1}{2}i\pi) + \varepsilon_2(\ln\omega\tau_0 - \tfrac{1}{2}i\pi)\right]. \tag{2.4}$$

The fact that the arguments $\ln\omega\tau_0 \pm \frac{1}{2}i\pi$ of ε_2 are complex requires that ε_2 be at least piecewise-analytical, in order to allow analytical continuation of $\varepsilon(\omega)$ to imaginary ω. A similar expression is obtained from $\varepsilon_1(\omega)$ by applying the Kramers–Kronig relation between ε_1 and ε_2.

We summarize these connections in matrix form in table 2.1 and note that knowledge of either $i(t)$, $g(\tau)$, $\varepsilon_1(\omega)$ or $\varepsilon_2(\omega)$ is sufficient to describe the entire dielectric response except for ε_∞. As an example, exponential decay of the polarization implies

$$i(t) = E\Delta\varepsilon\,\alpha e^{-\alpha t},$$

from which it follows that

$$g(\tau) = \delta(1/\alpha - \tau),$$

$$\varepsilon_1 = \Delta\varepsilon/(1 + \omega^2\tau^2) + \varepsilon_\infty$$

$$\varepsilon_2 = \Delta\varepsilon\,\omega\tau/(1 + \omega^2\tau^2).$$

$\Delta\varepsilon$ is the size of the relaxation step. The transformations are given below in table 2.1. The Kramers–Kronig relation between ε_1 and ε_2 is given in Lines and Glass (1977, p. 138).

The choice of the variable in terms of which dielectric results are presented is thus a matter of personal preference and is often influenced by the experimental method. We recall generalizations of the Debye functions to a form $[1 + i(\omega\tau)^\alpha]^\beta$, where α and β are adjustable parameters (Jonscher 1983), the Gaussian distribution of logarithmic relaxation times (Wagner 1913, Höchli 1982, Birge *et al.* 1984) and the Kohlrausch (1854)–Williams–Watts (1970) function

$$P(t) \sim \exp[-(t/\tau)^\beta]$$

Table 2.1. Transformation matrix for dielectric responses.

	$\varepsilon(\omega)$ Transform, equation	$i(t)$ Transform, equation	$g(\tau)$ Transform, equation
$\varepsilon(\omega)$	1	Fourier, (2.1)	Wagner–Debye, (2.3)
$i(t)$	(Fourier)$^{-1}$, (2.1)	1	Laplace, (2.2)
$g(\tau)$	(Laplace)$^{-1}$, (2.2)	Fuoss–Kirkwood, (2.4)	1

for the decay of the polarization with

$$i(t) = \frac{\partial P(t)}{\partial t}.$$

The characteristic times τ in these expressions are often measured at different temperatures. Some results are fitted to an Arrhenius law

$$\tau = \tau_0 \exp\left(\frac{E_b}{k_B T}\right), \tag{2.5}$$

with E_b being identified as an activation energy for dipolar relaxation and τ_0^{-1} as the attempted frequency. A generalization inspired by research on canonical glasses is

$$\tau = \tau_0' \exp[E_b'/k_B(T - T_{VF})],$$

where T_{VF} is an empirical Vogel–Fulcher temperature.

2.2. *Static polarization*

If the polarization can be switched at fixed temperature, it is called 'spontaneous', and the standard Sawyer–Tower circuit can readily be used for its determination (Lines and Glass 1977). For glasses, this is usually not the case; therefore their polarization has to be generated by field-cooling the sample and then measuring the current integral upon reheating, much as discussed in section 2.1. The polarization generated in this way is called remanent. Usually, the field is successively increased until the maximum (saturation) polarization is obtained. In view of the nonlinear relationship between P and E at saturation, the transformation properties of section 2.1 do not hold for remanent polarization.

2.3. *Acoustic properties*

The acoustic analogue of the polarization, the strain $\mathbf{S}$, can in principle be measured upon application of a stress field $\mathbf{T}$. This method is not customary; instead, use is made of the propagation characteristics of strain waves: given the (tensor) susceptibility of a solid

$$\mathbf{s} = \frac{\partial \mathbf{S}}{\partial \mathbf{T}}, \tag{2.6}$$

the sound velocities v_i in different directions are related to $\mathbf{s}$ by $\det(\mathbf{s}^{-1} - \rho\mathbf{vv}) = 0$. For symmetry directions of propagation, this may reduce to

$$v_i = (\rho s_i)^{-1/2}, \tag{2.7}$$

where ρ is the mass density and $i = 1, 2, 3$ denote longitudinal and $i = 4, 5, 6$ transverse modes. At kilohertz frequencies the wavelength of the sound $\lambda = v/\nu$ is typical of sample dimensions. This lends itself to a determination of v by resonance methods (Mason 1950). At higher frequencies, propagation methods are used (Truell *et al.* 1969). They require mounting a sound generator (transducer) on an optically polished surface, a method that works from 10^7 to 10^{10} Hz. Since transducers themselves are resonant elements, the determination of an acoustic dispersion curve $s(\omega)$ requires cutting samples and/or transducers for each frequency. We are not aware of any systematic effort to determine $s(\omega)$ to such an extent as in dielectrics. Much of the

experimental data can be expressed in terms of the elastic constant

$$\mathbf{c} = \frac{\partial \mathbf{T}}{\partial \mathbf{S}}.$$

Obviously, $\mathbf{c} = \mathbf{s}^{-1}$.

2.4. *Birefringence*

Light propagating through a homogeneous solid has a speed c/n, where the refractive index n depends on crystal symmetry as well as on the propagation direction and polarization. For propagation along z, the difference of speeds with polarizations x and y is (Lines and Glass 1977)

$$\frac{\Delta c}{c} = g(P_x^2 - P_y^2), \tag{2.8}$$

where g is an electro-optical coefficient. This speed difference, also called retardation, is revealed by linear birefringence techniques. In this geometry, it probes the component of the quadrupole moment $P_x^2 - P_y^2$. If this is a constant over a large area of the crystal then conventional birefringence patterns are observed, as in $BaTiO_3$, which allow P_x to be determined.

If the speed of light propagation, and thus the refractive index, varies over distances comparable to λ then irregular birefringence patterns may be observed. Prater *et al.* (1981a–c) were among the first to point out the pitfalls of the birefringence method for zero-field-cooled orientational glasses. For one-dimensional inhomogeneities, like a stack of layers each with a difference of n, solutions for propagation and birefringence can be found in Liddell (1981).

2.5. *Heat capacity*

The heat capacity and, in particular, anomalies at phase and glass transition temperatures are usually recorded by the quasi-adiabatic Nernst method, where a known amount of Joule heat is introduced into the sample and the subsequent temperature changes are measured. In standard experiments, the temperature versus time profiles are analysed by computerized control and data-acquisition systems. Measurements using commercial differential-scanning calorimeters are less time-consuming but yield a considerably reduced precision of the c_P data.

Transient pulse techniques, with pulse widths of 1 μs, have been developed by Loponen *et al.* (1980, 1982) and Meißner and Spitzmann (1981) to measure the time dependence of the heat capacity in glasses. These measurements allow the observation of internal temperature relaxations within a time window of $0{\cdot}1\,\text{ms} < t < 0{\cdot}1\,\text{s}$. An experimental set-up for the measurements of long-time (100 s) thermal relaxations in amorphous solids has been described by Zimmermann and Weber (1981). Both techniques have usually been applied below 3 K. At higher temperatures, in the regime of the excess heat capacity, adiabatic calorimetry has been used.

2.6. *Inelastic light scattering*

Light may be scattered by a phonon, to which energy and momentum are transferred. Depending on the nature of the phonon, either 'acoustic' or 'optic', the phenomenon bears the name of its discoverer, either Brillouin or Raman. The customary energy transfer for Brillouin scattering is $\omega \approx 10^{11}\,\text{s}^{-1}$, and the shift of the

light frequency is determined with the help of a dispersive element, usually a Fabry–Perot étalon. Raman scattering implies shifts of some 10^{12}–$10^{13}\,s^{-1}$ and detection by grating diffractometers.

A record of scattered-light intensity against frequency shift provides information about the properties of the phonon, its energy as a function of the wave-vector and its dissipation. In crystalline material, the symmetry of the phonon eigenvector is determined from the dependence of the scattering efficiency of the polarization of the incident and scattered light beams (Long 1976). In orientational glasses, such selection rules can be broken or may depend on previous field treatments of the sample. Glass formation implies a local reduction of symmetry. The consequences may be as follows. (1) A phonon that is unable to scatter light in the high-symmetry phase can do so in those portions of the crystal where this symmetry is broken. This is called the defect-induced Raman effect and depends on the correlation of the 'defective' structure in space. (2) The phonon itself is scattered at the boundaries where local symmetry changes (Stephen and Cwilich 1987, Tamura and Wolf 1987, Merlin 1988a,b). (3) The phonon is split or shifted in frequency at the temperature where the local symmetry begins to be broken. This should happen when the phonon eigenvector has the same symmetry as the local distortion (see section 4.6). Light scattering has also been observed in canonical glasses, where no symmetry relation persists and where the scattering intensity after suitable normalization has been interpreted in terms of the density of phonon states (Alben *et al.* 1975).

When translational periodicity of the solid is broken, acoustic and optical phonons are no longer distinct, but the frequency separation between nearly optical and nearly acoustic branches may be preserved. For these cases, we adopt the customary methods and nomenclature.

2.7. *Second-harmonic-generation and light-mixing techniques*

We assume that a dynamic lattice polarization $P(\omega_3)$ can be achieved by applying fields $E_1(\omega_1)$ and $E_2(\omega_2)$ simultaneously. Then we can define a susceptibility χ by

$$P_3(\omega_3) = \chi E_1(\omega_1)E_2(\omega_2), \tag{2.9}$$

where χ has odd parity. In a homogeneous crystal, a measurement of the mixed-beam intensity at ω_3 allows χ to be determined (Vogt 1974). In an orientational glass, χ is proportional to the local polarization. If this is correlated over a long distance $\xi >> \lambda$, the intensities of the mixed beams cumulate. If, however, $\xi \lesssim \lambda$, interference reduces the mixing efficiency and no mixed beam is observed in the limit $\xi \to 0$. The special case $\omega_3 = 2\omega_1 = 2\omega_2$, called second-harmonic generation, allows a quantitative analysis of the beam intensity in terms of polar correlation (Banfi *et al.* 1988, 1989).

2.8. *X-ray and neutron scattering*

In X-ray scattering experiments, the intensity scattered from the sample is analysed in terms of momentum transfer of the initial photon to the sample. A rigid, perfect lattice scatters X-rays into Bragg points that are infinitely sharp in q-space. In practice, the Bragg spots observed have finite width. This may stem from variations of the lattice parameters as in cold-worked metals and defective crystal materials, but in particular from frozen-in glass-like disorder in mixed crystals. Either kind of disorder leads to diffuse scattering, whose intensity is spread around the exact Bragg spot. The most familiar form of diffuse intensity is caused by the thermal agitation of

the crystal. Here the diffuse intensity at $Q = \tau_{hkl} + q$ peaks with respect to frequency at $\omega = \omega(q)$, where $\omega(q)$ is the frequency of a phonon with wave-vector q. The intensity is proportional to the dynamic structure factor $S(Q, \omega)$. In X-ray experiments, the diffuse intensity measured at a given Q samples the contributions of all modes with the wave-vector q. The X-ray intensity is proportional to $\int_{-\infty}^{+\infty} S(Q, \omega) \mathrm{d}\omega$. At low q, where the acoustic phonons are most important, the X-ray intensity is proportional to q^{-2}. With neutrons, both the static and dynamic structure factors can be resolved.

Collective orientational excitations in an orientationally ordered state can be treated as optical phonons. In the disordered state, where the orientations of moments differ from cell to cell, jumps of moments between equivalent crystallographic directions give rise to additional diffuse scattering. The Q and ω distribution of this diffuse intensity reflects the correlations of the orientations in space and time. At high temperatures, the frequency distribution follows a quasi-elastic Lorentzian profile centred at $\omega = 0$, and the Lorentzian half-width is given by the diffusion rate.

Modulated patterns of displacements, tilts or orientations lead to satellite peaks at the positions $q = \tau_{hkl} \pm q_0$, where q_0 is the propagation vector of the modulation. A measurement of energy transfer in the neutron experiment can determine whether the modulation is static or dynamic. The width of the satellite peaks is related to the coherence length of the modulated pattern.

Energy- and momentum-transfer data can in principle resolve time and spatial correlation of orientational defects. In practice, lattice defects contribute to momentum transfer as well and render the identification of all the sources of diffuse scattering difficult. Detailed accounts of the potential of X-ray and neutron scattering are found in Guinier (1956) and Bacon (1962) respectively.

2.9. *Evidence from local probes; magnetic resonances*

Some constituents of the lattice, or the impurities, may carry a magnetic moment. This may be used to probe the local surroundings of the atom carrying the moment. For nuclear spins $I \geqslant 1$, magnetic resonances are split if the environment has less than cubic symmetry. The splitting ν_Q is proportional to the distortion squared and thus probes the local quadrupole moment at the site of the nucleus, for a review, see Rigamonti (1984). Fluctuations in time of this quadrupole moment give rise to nuclear magnetic relaxation (NMR) of a spin with a time constant T_1 related to the quadrupole fluctuation rate τ_c by

$$T_1^{-1} = \nu_Q^2 \tau_c / (1 + \omega_L^2 \tau_c^2),$$

where ω_L is the resonance (Larmor) frequency of the nuclear spin in a magnetic field. In the case of isolated impurities, there is a linear relation between ε_2 and T_1^{-1}. In the case of interacting impurities, this relation is broken: magnetic interactions establish a spin equilibrium, i.e. homogeneity, in a time given by $T_2 \ll T_1$, such that the magnetization still decays exponentially with time T_1. Dipolar interactions do not establish homogeneity, and accordingly the decay becomes non-exponential. From an Arrhenius plot of T_1^{-1} against $1/T$, the barrier may be determined that the quadrupole has to cross in order to change its orientation. In cubic crystals with [100] oriented moments these are 90° changes of orientation and involve a change of the dipole moment as well. Dipolar changes by 180° (i.e. inversions) are ineffective for quadrupolar reorientation and are not revealed by NMR or ultrasound.

NMR can thus resolve the static local environment of a nuclear spin, like distortions, and its distribution in case of sample inhomogeneity. In addition, it can determine how rapidly such local distortions react to perturbations. The method is thus sensitive to essential parameters describing glass formation. However, NMR cannot tell whether the slowing down of a motion and the distribution of lattice distortions are due to collective effects and thus associated with glass formation. Circumstantial evidence such as the composition dependence of NMR parameters can help establish this connection.

Magnetic moments may be introduced by doping with elements of the transition groups. The techniques for detecting their resonances are related to those of NMR (Abragam and Bleaney 1970). In view of the local distortions created by these additional impurities, their spectra and their role are difficult to interpret.

3. Alkali halides doped with hydroxyl and Li ions

The pioneering work by Känzig *et al.* (1964) contains much of the experimental information necessary for an understanding of the formation of glass by impurity dipoles in alkali halides. They investigated a series of samples doped with different OH concentrations and found that the temperature of maximum susceptibility scaled with concentration, reaching about 5 K at 500 p.p.m., and they provided evidence for non-Debye dispersion. These findings have obvious similarities with those in what was to become the spin-glass prototype: CuMn (Binder and Young 1986). Brout's (1965) suggestion that KCl : OH was glass-like and the detailed report by Knop and Känzig (1974) (in German) on KBr : OH were apparently forgotten and are only rarely cited in the abundant spin-glass literature. Thus we review some of these results here, despite their age, in the hope that interpretation in terms of models not available at the time may give new insights into this phenomenon. At the same time, we draw attention to the need for supporting evidence by structural methods not yet exploited. In part, such reinterpretations have been attempted and new data added, which we also report. For properties regarding the single-particle response of dipoles in alkali halide, we refer the reader to the review by Narayanamurti and Pohl (1970).

3.1. *Dielectric susceptibility*

Hydroxyl ions give rise to frequency and temperature-dependent dielectric susceptibilities. The temperature maxima of the susceptibility found by Känzig *et al.* (1964) were first assigned to the onset of a ferroelectric phase, but then Brout (1965) suggested that dipolar alignment below T_f was 'randomly antiferromagnetic' (Klein and Brout 1963). Li ions substitute for K at random sites, take an off-centre position and accordingly carry a dipole moment. They give rise to similar effects to those due to OH ions (Fiory 1970). Early data on their susceptibility at high temperatures were presented in the context of effective-field theories (Böttcher and Bordewijk 1978), and the temperatures of the susceptibility maxima were interpreted in terms of dipole-pair interactions, but without quantitative agreement (Potter and Anderson 1981) with the classical Clausius–Mosotti expressions.

A study of dielectric relaxation of hydroxyl ions in several alkali halides yielded perhaps the most detailed information on random fields and dynamics in this system (Knop and Känzig 1972, 1974). They plotted their dispersion curves as $\varepsilon(T)$, with ω as a parameter. $\varepsilon_s(T)$ was maximum at a concentration-dependent temperature $T_f(x)$. Knop and Känzig identified this temperature as the ferroelectric Curie–Weiss

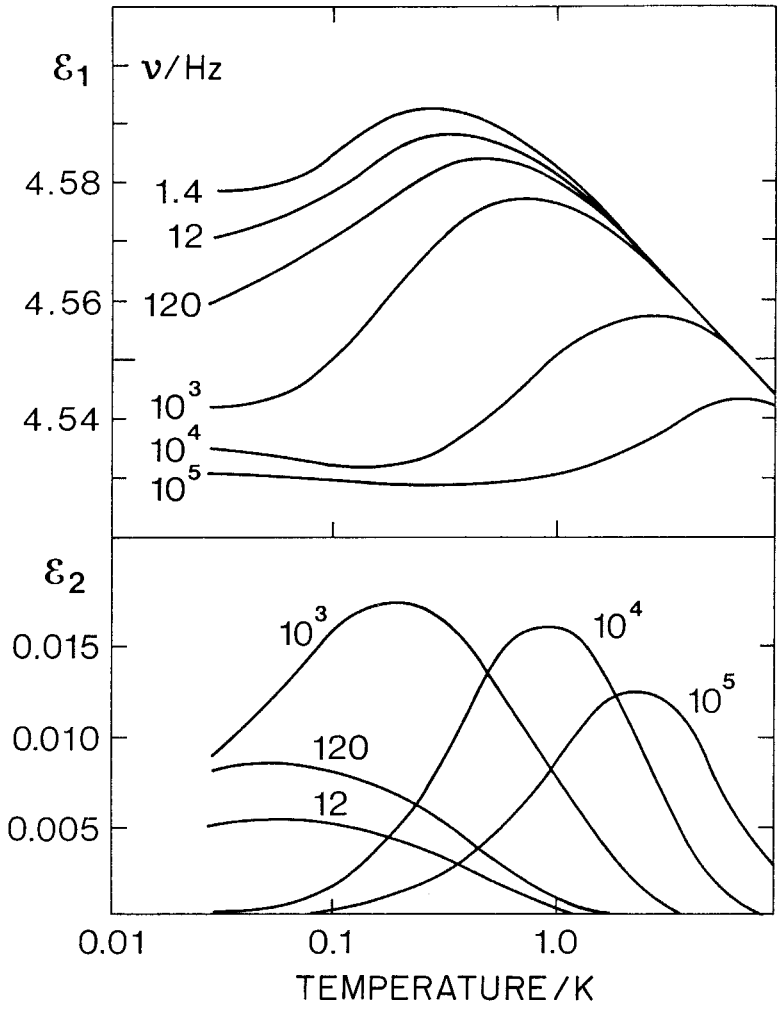

Figure 3.1. Real and imaginary parts of the complex differential dielectric constant $\varepsilon = \varepsilon_1 - i\varepsilon_2$ along [001] for KBr : OH^- ($N_d = 4{\cdot}5 \times 10^{17}\,cm^{-3}$) at different frequencies. From Knop and Känzig (1974).

temperature, implying that the polar phase of KCl : OH was ordered. They fitted their data (figure 3.1) to

$$\varepsilon^* - \varepsilon_\infty = \int \frac{g(\tau)\,d\tau/\tau}{1 + i\omega\tau}, \tag{3.1}$$

by choosing $g(\tau) = [\ln(\tau_1/\tau_2)]^{-1}$ for $\tau_1 < \tau < \tau_2$ and zero otherwise (Fröhlich 1958). An alternative is a Gaussian

$$g(\tau) = [\Delta(\ln\tau)]^{-1} \exp\{-[\ln(\tau/\tau_0)]^2/[\Delta(\ln\tau)]^2\} \tag{3.2}$$

(Wagner 1913). Either fit is satisfactory, in contrast with the fit to simple Debye behaviour $g(\tau) = \delta(\tau - \tau_0)$. The data thus provide evidence for a broadening of the relaxation time distribution growing from about one decade (at 2 K) to three decades (at 0·3 K). From this, Knop and Känzig (1974) concluded that the potentials

responsible for the relaxation process had random character. From the field-dependent static susceptibility, they were able to deduce expressions for the random field distribution at the dipole sites in terms of the Holtzmark (1919) distribution

$$H(E) = \pi E_0 \int_0^\infty \cos(xE_1/E_0)\exp(-x^{3/2})\,dx \tag{3.3}$$

of random site charges, and alternatively, for a Gaussian whose shape is not too different. The values for the random field are spread around $0{\cdot}5\,\mathrm{MV\,m^{-1}}$ for KCl:OH, KCl:OD, NaCl:OH and NaCl:OD, (D = deuterium) and around $2\,\mathrm{MV\,m^{-1}}$ for KBr:OH and RbCl:OH. Knop and Känzig attributed these fields to the conjectured presence of Ca^{2+} and Sr^{2+} impurities (50 parts per billion). However, in view of the presence of many more dipolar impurities, it is natural to assume that the random fields are a consequence of random bonds between OH ions, a point that was made by Fischer and Klein (1976, 1979) and to which we shall return later in this paper.

Estimates for dipolar fields have been given by Potter and Anderson (1981) on the basis of relaxation peaks, which they attributed to coherent flips of dipole pairs. They attempted to relate these fields to classical dipolar interaction in a polarizable lattice, thus accounting for the Lorentz correction. Interestingly, they found an apparent reduction of $\varepsilon_{\text{lattice}}$ by a factor of 2·4 for closest pairs. Intrigued by the progress made in spin glasses since then, Moy *et al.* (1983) reanalysed their data and performed annealing tests to determine the origin of the random fields. From the fact that they saw 'only rounded maxima' of $\varepsilon(T)$ and no cusp, they suggested that KCl:OH is not analogous to a spin glass. In view of the similarity of the Knop–Känzig results for KCl:OH with those of Hüser *et al.* (1983, 1986) for Cu:Mn, however, this interpretation is not supported.

The dielectric susceptibility at very low temperatures and high frequencies can probe low-lying energy levels by direct resonance processes. This method provided evidence for a distinct energy of 7 mK ($\sim 10^{-25}$ J) in $RbCl:OH^-$, which could relate to a single-ion tunnel level, thus leaving open the question of glass formation (Hess and De Conde 1981).

Saint-Paul and Gilchrist (1986) have measured the time variation of the susceptibility after switching the polarization with a field in KCl:OH. This provided evidence for a wide distribution of relaxation times. They also measured nonlinear susceptibilities in the frequency range from 30 Hz to 20 kHz. From the fact that their nonlinear susceptibilities did not diverge, they excluded spin-glass behaviour and adopted a model 'superparaelectric' cluster, whose size they determined to be ten dipoles. We note, however, that OH^- dipoles flip so slowly near the transition temperature that a.c. susceptibility measurements do not test static behaviour. Accordingly, no divergence of $\partial\varepsilon/\partial(E^2)$ as in spin glasses is expected (Omary *et al.* 1983), but rather dynamical critical behaviour as found by Lévy and Ogielski (1986) in Ag:Mn.

3.2. *Remanent polarization*

We are aware of only one attempt to determine the remanent polarization in alkali halides: Fiory (1971) investigated samples of KCl:Li in which Li substitutes for K at an off-centre position and thus carries a local polar moment. Hysteresis loops taken at a frequency of 16·7 mHz (1 cycle $\mathrm{min^{-1}}$) (figure 3.2) show that only a small fraction of dipoles stays aligned when the field is taken to zero. The poling efficiency is enhanced by cooling the crystal with an applied field, but in no instance do the dipoles stay aligned. Fiory was able to detect a nearly logarithmic decay of P_s with time down

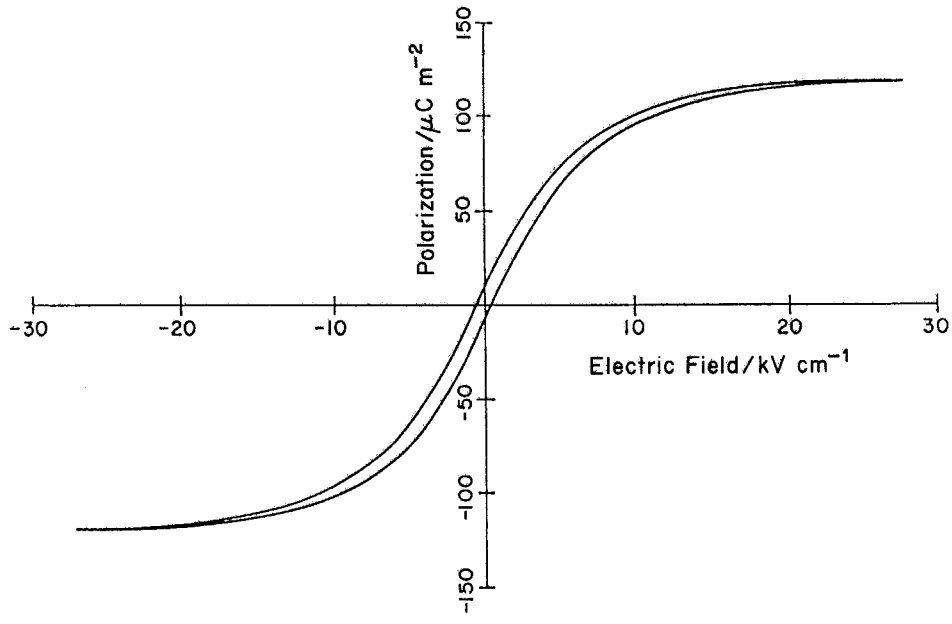

Figure 3.2. Low-temperature hysteresis loop of KCl:Li ($N = 7 \times 10^{18}\,\mathrm{cm}^{-3}$) taken at 16·7 mHz (1 cycle min^{-1}) at 0·06 K. From Fiory (1971).

to 0·17 K. These findings differ from those of classical ferroelectrics, in which at $T << T_c$ alignment of dipoles is nearly perfect and stable. Fiory clearly distinguished between these effects, and called them 'remanent' (rather than 'spontaneous') polarization, a designation we have adopted, and which even then had its magnetic analogue, Au:Fe (Souletie and Tournier 1969).

3.3. *Sound propagation*

OH impurities have not only an electric dipole moment but also an elastic quadrupole moment. By using the term 'elastic quadrupole' rather than 'elastic dipole' (as did Känzig *et al.* (1964)), we emphasize the symmetry property of elastic moments. They have inversion symmetry and thus interact not with electric fields but with the strain of propagating sound and gives rise to sound dispersion. On the basis of Brillouin-scattering data (figure 3.3), Berret *et al.* (1983) concluded that quadrupolar motion rapidly slows near T_f. On the other hand, the distribution of relaxation was not nearly as wide as that found in spin glasses (Hüser *et al.* 1986) (figure 3.4) or canonical glasses (Hunklinger and von Schickfus 1981). This view of limited analogy between KCl:OH and glasses was confirmed by Saint-Paul *et al.* (1984) on the basis of ultrasound experiments.

We point out that the crucial states in KCl:OH are of dipolar nature, that broad distributions near T_f have been reported and that high-frequency dielectric in addition to acoustic measurements should be performed and analysed in order to determine the dipole-glass character of KCl:OH.

3.4. *Heat capacity*

Peressini *et al.* (1969) and Fiory (1971) were the first to measure heat-capacity data. On the basis of his plot of $\log C$ *versus* $\log T$, Fiory concluded that the data at low T were compatible with $C \sim T^{3/2}$ as predicted by Gopal (1966, p. 90). An

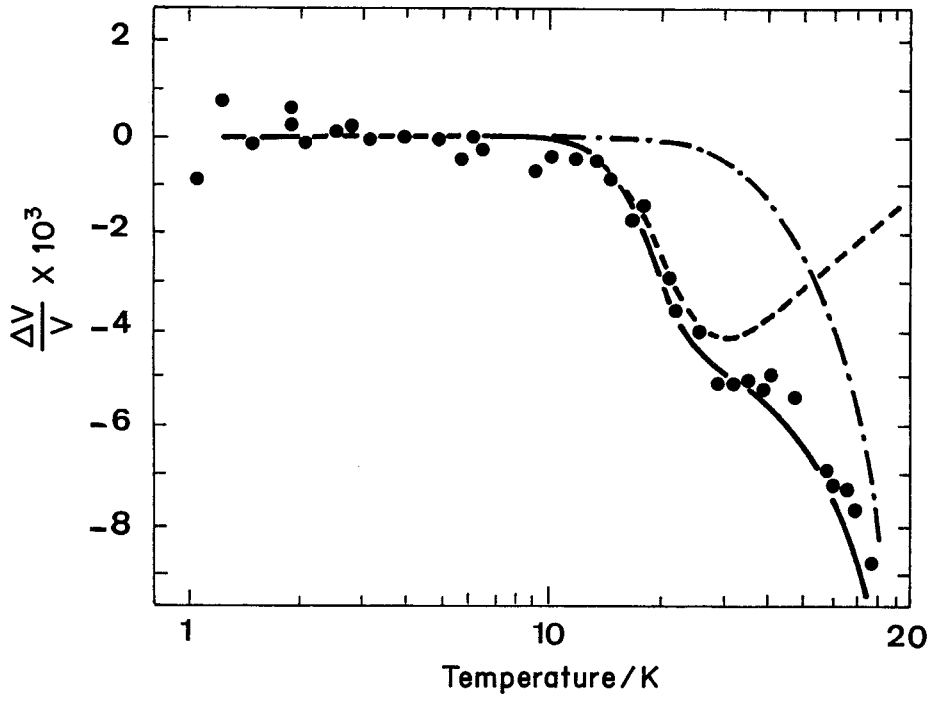

Figure 3.3. Comparison of experimental values and calculation for the velocity change in KCl : OH doped with 1000 p.p.m.: (·—·), contribution of anharmonic phonon–phonon interactions taken from pure KCl; (– – –), thermally activated relaxation process; (——), sum of both contributions. From Berret *et al.* (1983).

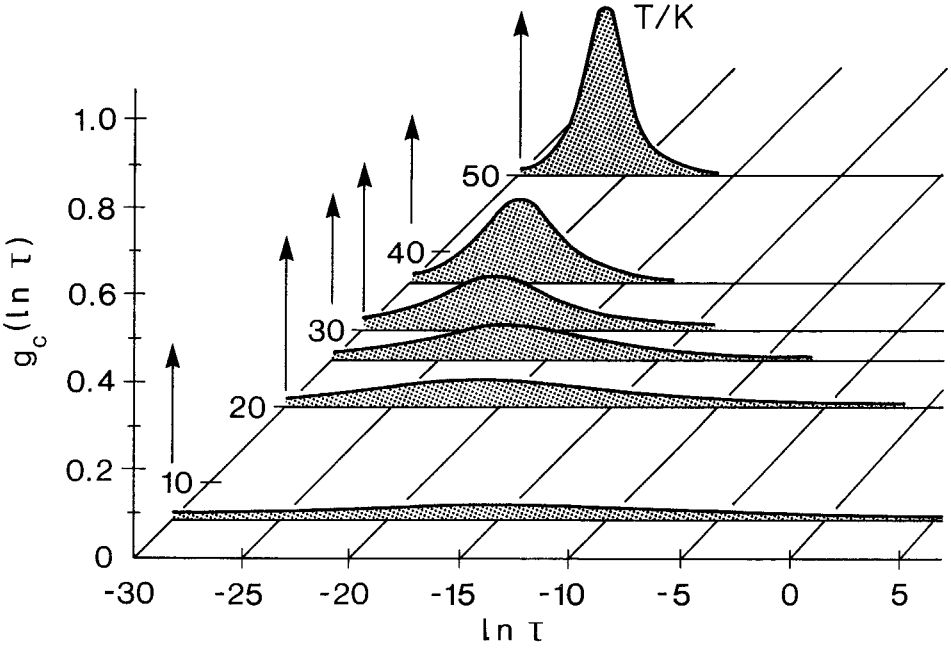

Figure 3.4. Distribution function g_c ($\ln \tau$) of cluster relaxation times for CuMn : 5 at.% at several temperatures. From Hüser *et al.* (1986).

inspection of his figure 12, however, suggests that lower exponents would fit the data even better. Lasjaunias and Löhneysen (1981) extended Fiory's measurements on KCl : OH at 1% doping to even lower temperatures and found compatibility with Fiory's data and a best fit to $C \sim T^{1\cdot1}$. This points to the presence of a wide distribution of activation energies typical of glasses (Hunklinger and von Schickfus 1981). At lower OH concentrations, however, the exponents are different.

3.5. *Structure-resolving experiments and local probes*

Aldermann and Cotts (1970) have investigated the off-centre ^{7}Li site using NMR, but present no evidence for collective effects.

3.6. *Summary of experimental evidence*

We are not aware of any investigations using particle and light scattering, or of local probes, namely ^{7}Li nuclei, being used to determine single-particle responses only. Most of the relevant information on glass formation is based on an analysis of susceptibility data, and some support is provided by sound-propagation and heat-capacity data. On the basis of these results, we conclude that dipolar impurities in alkali halides slow down their disordered motion progressively as $T \to 0$. At low T, there is evidence of a wide distribution of two-level systems. Disorder of motion and two-level systems are signs of a breakdown of long-range order. We thus believe that the low-T state of KCl : OH is glass-like despite the deplorable lack of evidence from spatial resolution.

3.7. *Theoretical models*

Early attempts to model KCl : OH are restricted to estimates of dipolar interaction in polarizable alkali halide lattices (Najaranamurti and Pohl 1970). Attempts to treat the motion of dipoles in an effective field have also been reported. The true field acting on a dipole, however, is given by the position and orientation of the other dipoles, and is therefore time-dependent. A pioneering attempt to model KCl : OH was undertaken by Fischer and Klein (1976), prior to the development of spin-glass theories. They started with the dipolar interaction between OH ions screened by a factor ε. Then they introduced the second moment of polarization and field distribution, and solved the model self-consistently. This moment was found to vanish above T_c, which was given as a function of concentration, and both the linear and nonlinear susceptibilities were found to be anomalous at T_c. When Fischer and Klein (1976) compared these results with data on KCl : OH (Knop and Känzig 1974), they realized that the anomalies were not as sharp as predicted by their model. In the light of general theories (see section 11, and Binder and Young (1986)) not available then, we can now express the interaction in terms of approximate first and second moments of nearest-neighbour dipolar interactions:

$$\bar{J} = 0, \qquad \mathrm{Var}(J) = \left(\frac{8}{5}\right)^{1/2} \frac{p^2}{\varepsilon_l \varepsilon_0 d^3 x}, \tag{3.4}$$

where $p = 1\cdot3 \times 10^{-29}\,\mathrm{C\,m}$, $\varepsilon_l = 4$ (Moy *et al.* 1983). With the use of

$$T_f = \mathrm{Var}(J)/k_B, \tag{3.5}$$

this allows $T_f = 5 \times 10^4 x$ and

$$\varepsilon_s \sim (Np^2/3k_B T\varepsilon_0)x \tag{3.6}$$

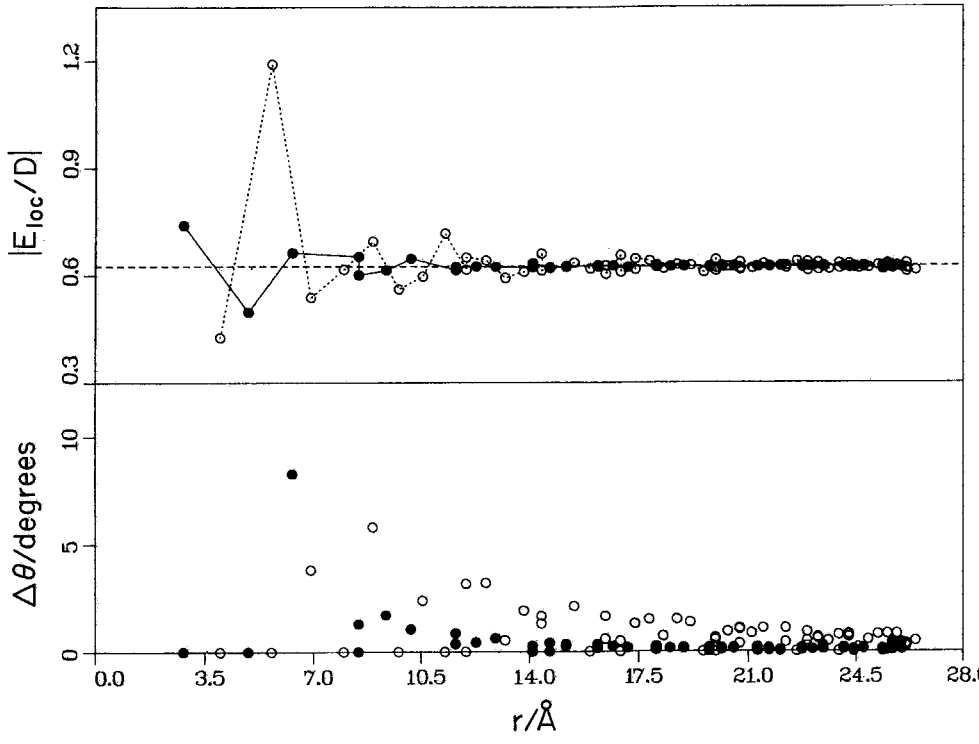

Figure 3.5. Calculated magnitudes of the local fields (top) and the angular deviations from the radial directions (bottom) at ions near an Na* vacancy in the NaCl crystal: ○, Na^+ ion; ●, Cl^- ion. The vacancy is located at $r = 0$. The horizontal dashed line represents $|E_{loc}/D| = (\varepsilon + 2)/3\varepsilon$ derived from the Clausius–Mossotti relation for large r. From Wang (1980).

to be estimated for $T > T_f$ and

$$\varepsilon_s = (Np^2/3k_B T_f \varepsilon_0)x = \frac{1}{3}\left(\frac{8}{5}\right)^{1/2} \varepsilon_l \varepsilon_0 \tag{3.7}$$

below T_f, independently of x and T. Of these predictions referred to as Parisi (1979) susceptibility, the first two are in reasonable agreement with experimental results, although a reduction of Var(J) by a factor of three would improve the agreement. Owing to lack of truly static values for ε, the third prediction is not experimentally tested. To calculate Var(J) quantitatively, more than just nearest neighbours should be considered, and the influence of the lattice on the effective interaction should be taken into account. Wang's (1980) computer simulation of effective interaction between dipoles in NaCl may be of great help for such an evaluation of $\bar{J}$ and Var(J) (figure 3.5).

3.8. *Conclusions*

Dipolar impurities in KCl give rise to collective effects, in particular to a polar phase that is stable below a concentration-dependent freezing temperature T_f. Evidence for disorder is gained from the peculiar dielectric response, from heat-capacity data and in part from sound-propagation data. On the other hand, there is evidence

for the formation of pairs and other small clusters. More than in other mixed crystals, this raises the question as to whether the dipolar impurities in KCl are really random-site impurities. Controlled growth conditions and a study of ionic migration could promote KCl:OH to the status of a dipolar-glass prototype.

4. Potassium tantalate mixed crystals

Pure potassium tantalate, $KTaO_3$, has a cubic perovskite structure that is known to have little stability against polar distortions; its isomorph $KNbO_3$ is ferroelectric up to 700 K. $KTaO_3$ does not become ferroelectric, but has a dielectric susceptibility that rises to 4500 at 4 K (Lines and Glass 1977). When doped with moderate amounts of Li, Na or Nb, polar distortions emerge, the character of which depends on the particular composition.

Several authors have performed measurements on $KTaO_3$ crystals doped with impurities. These crystals have been of various origins, so a comparison of results requires some knowledge of the crystal characteristics. Early investigations (Yacoby and Linz 1973) used crystals grown with the top-seed method from a solution with excess K_2CO_3 and Li_2CO_3. Spontaneous nucleation (Boatner *et al.* 1977b) of molten $KTaO_3$ led to crystallization as well, but its impurity content is difficult to control. Controlled nucleation (Rytz and Scheel 1982) in K_2CO_3 flux and characterization of impurity content (van der Klink and Rytz 1982) laid the basis for many of the subsequent investigations, including a study of migration of hydrogen (Engstrom *et al.* 1980) and its isotopes in $KTaO_3$.

In this section we review the characteristics of $KTaO_3$ mixed crystals and try to relate them to the properties of the constituents.

4.1. *Li doping*

Li substitutes for K and thus has twelve nearest oxygen neighbours. The oxygen cage fits well with the K^+ ion, which has a radius of 1·3 Å but is too large to host Li^+

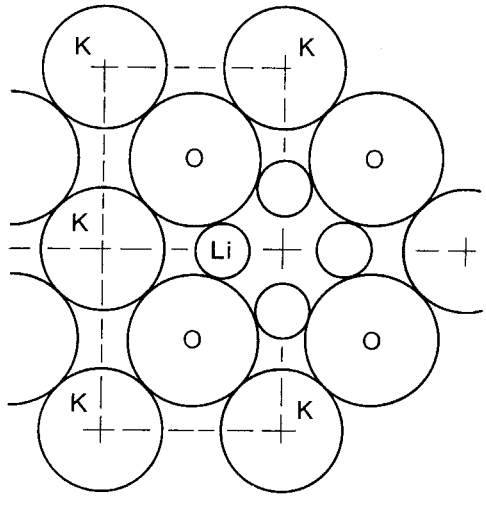

Figure 4.1. Cut through [100] plane of perovskite $KTaO_3$. Note displacement of small-size Li. Drawing of ionic radii and structure to scale; K–K distance 4 Å. Of the four equivalent off-centre positions shown (plus two out of plane, not shown), only one is occupied by Li. From Höchli and Maglione (1989).

($r = 0{\cdot}69$ Å) properly. Accordingly, Li takes an off-centre position (Yacoby and Just 1974) in the [100] direction with respect to the centrosymmetric K^+ site (figure 4.1). It thus carries a dipole moment, which interacts with the lattice and with neighbouring Li dipoles. These dipoles give rise to peculiar effects, which have been studied by the methods outlined in section 2.

Of the three impurities in $KTaO_3$ treated in this chapter, Li has the largest ionic misfit $(r_{Li} - r_K)/r_K = -0{\cdot}55$, and thus the largest dipole moment. It is the only impurity that gives rise to observable single-particle relaxation effects well separated from collective relaxational behaviour. This system is particularly suited to dielectric studies. Data from scattering experiments with light, neutrons and X-rays are also abundant. Their interpretation, however, is more difficult because of the small contribution of the Li scattering efficiency to the total response. We proceed by reviewing the available data.

4.1.1. *Dielectric spectroscopy*

A typical dielectric spectrum ε^* against $\log\omega$ is shown in figure 4.2 for $K_{1-x}Li_xTaO_3$, $x = 0{\cdot}015$, $T = 45$ K. We note two peaks for ε_2 against $\log\omega$, both nearly symmetric in $\log\omega\tau_\alpha$ but not of the same width (Höchli and Maglione 1989). The index α denotes either lattice (ℓ) or impurity (i). The most probable relaxation rates for the respective

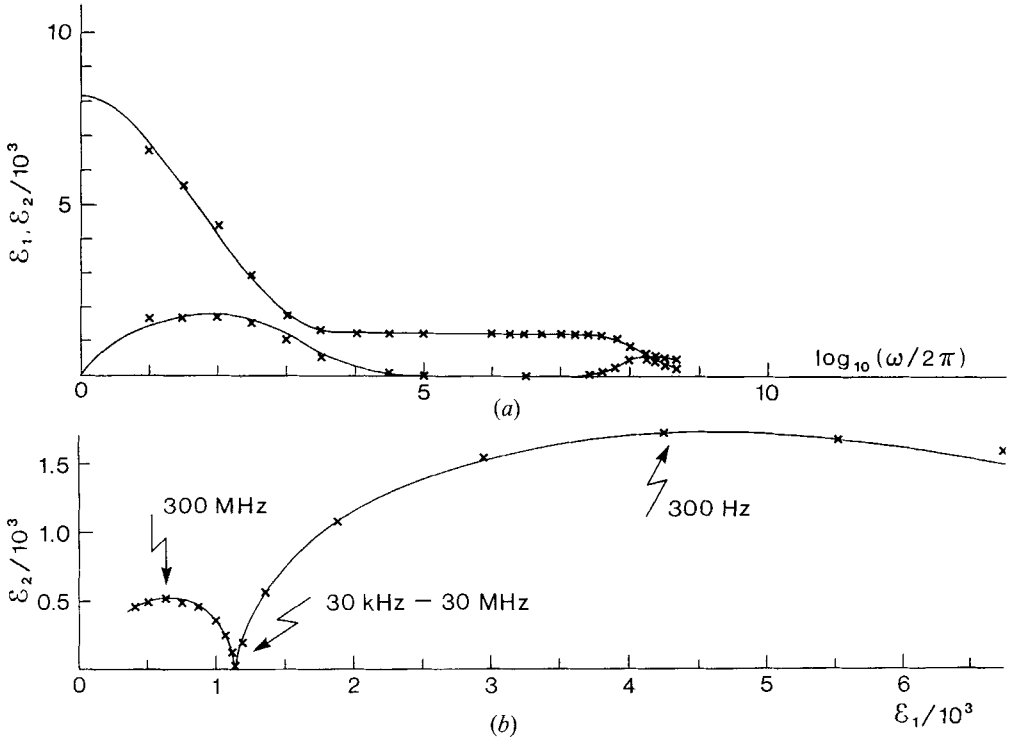

Figure 4.2. (*a*) Real and imaginary parts of susceptibility *versus* $\log(\omega/2\pi)$ and a fit to equations (4.1) and (4.2) of text. The sample is $K_{0{\cdot}985}Li_{0{\cdot}015}TaO_3$, $T = 45$ K. (*b*) Real *versus* imaginary part of susceptibility (Cole–Cole plot) for the same data. Note that the high-frequency mode is described by a semicircle centred at the abscissa corresponding to the Debye expression. The low-frequency mode is described by a flat curve with $\varepsilon_{2\max}/\Delta\varepsilon < \frac{1}{2}$. The flattening is a measure of the width of the distribution of relaxation times. From Höchli and Maglione (1989).

branches are $\tau_\ell^{-1} = 6 \times 10^8\,s^{-1}$ and $\tau_i^{-1} = 6 \times 10^3\,s^{-1}$. Associated with these two peaks are two steps of $\varepsilon_1(\log\omega)$. The measurement of ε^* at 10 temperatures, 10 concentrations and 100 frequencies produces 10^4 data points for the $K_{1-x}Li_xTaO_3$ system alone. The data are thus expressed in terms of analytic functions and their parameters are given as functions of external variables, such as T, x and E. Inspection of early data (Höchli *et al.* 1979) indicated that the size of the impurity peak at ε_2 increases in proportion to x up to about $x = 0{\cdot}012$. The size of the lattice peak, however, depends only slightly on x; in particular, it is non-zero for $x = 0$ (i.e. for pure $KTaO_3$) (Maglione *et al.* 1987). This has allowed association of the low-frequency relaxation mode with impurity relaxation and of the high-frequency relaxation mode with lattice relaxation. A quantitative analysis of the size, time and width parameters ε_α, τ_α and $\Delta_\alpha(\ln\tau)$, where $\alpha = i$ or ℓ, requires that the data be fitted to an equation of the form

$$\varepsilon_2(\omega) = \sum_\alpha \varepsilon_\alpha \int d\tau \frac{g(\tau)\omega\tau}{1 + \omega^2\tau^2}, \tag{4.1}$$

where ε_α are the amplitudes of the dielectric step. If ε_2 is a symmetric function of $\log\omega\tau_\alpha$, as is (approximately) the case for each of the well separated peaks in figure 4.2, then the distributions $g(\tau)$ are symmetric in $\log(\tau/\tau_\alpha)$ and may be chosen as Gaussians

$$g(\tau') = \pi^{-1}\Delta_\alpha(\ln\tau)\exp\left[-\frac{(\ln\tau' - \ln\tau)^2}{\Delta_\alpha^2(\ln\tau)}\right] \tag{4.2}$$

centred at the most probable relaxation times τ_α and with widths $\Delta_\alpha(\ln\tau)$. In addition to ε_∞, which is negligibly small in these compounds, there are three parameters to be determined per branch. One of them, $\Delta_\alpha(\ln\tau)$, may vanish, thereby reducing equation (4.2) to the Debye expression equation (2.3). For $x = 0{\cdot}015$, $\Delta_\ell(\ln\tau)$ must be close to zero, whereas $\Delta_i(\ln\tau)$ is several units, judging from the width of $\varepsilon(\omega)$ in terms of decades (figure 4.2).

Equation (4.2) is based on a physical model: a single particle jumps between two wells in a most probable rate of τ, which has a standard deviation since the barrier between two wells is also distributed. Evaluation of the data in figure 4.2 with (4.2) yields sets of fitting parameters: $\Delta\varepsilon_\ell = 1140 \pm 100$, $(\tau_\ell)^{-1} = 6 \times 10^8\,s^{-1}$, $\Delta(\ln\tau_\ell) = 0{\cdot}0 \pm 0{\cdot}2$; and $\Delta\varepsilon_i = 7 \times 10^3$, $(\tau_i)^{-1} = 6 \times 10^3\,s^{-1}$, $\Delta(\ln\tau_i) = 3 \pm 0{\cdot}3$.

The values of the parameters depend only insignificantly on the choice of the distribution, whether Gaussian, Lorentzian or even rectangular. These and the following data were parametrized with the help of (4.2) and a Gaussian distribution $g(\tau)$. A full curve in figure 4.2 fits the data satisfactorily. In addition, evaluation of ε_1 data gives $\varepsilon_\infty = 100 \pm 100$. Some readers may be more familiar with plots of ε_2 *versus* ε_1, which are also shown in figure 4.2. The fit of the data (to the left) to a perfect semicircle centred at the abscissa indicates that (4.1) is obeyed for these high-frequency data, while the curve drawn through the data, approximately a semicircle centred *below* the abscissa, indicates that this is not true for the low-frequency data. Plots of ε_2 against ε_1 are sufficient for quick reference, but are a poor analytical tool since all explicit information on frequency is lacking.

In the following, we give all experimental evidence in terms of step size, centre of dispersion peak and width of relaxation distribution on a logarithmic time scale, $\Delta\varepsilon$, $\bar{\tau}$ and $\Delta(\ln\tau)$.

Relaxation peaks were given by Höchli and Maglione (1989) in different samples at different temperatures. For the lowest concentration, $x = 0{\cdot}006$, the inverses of

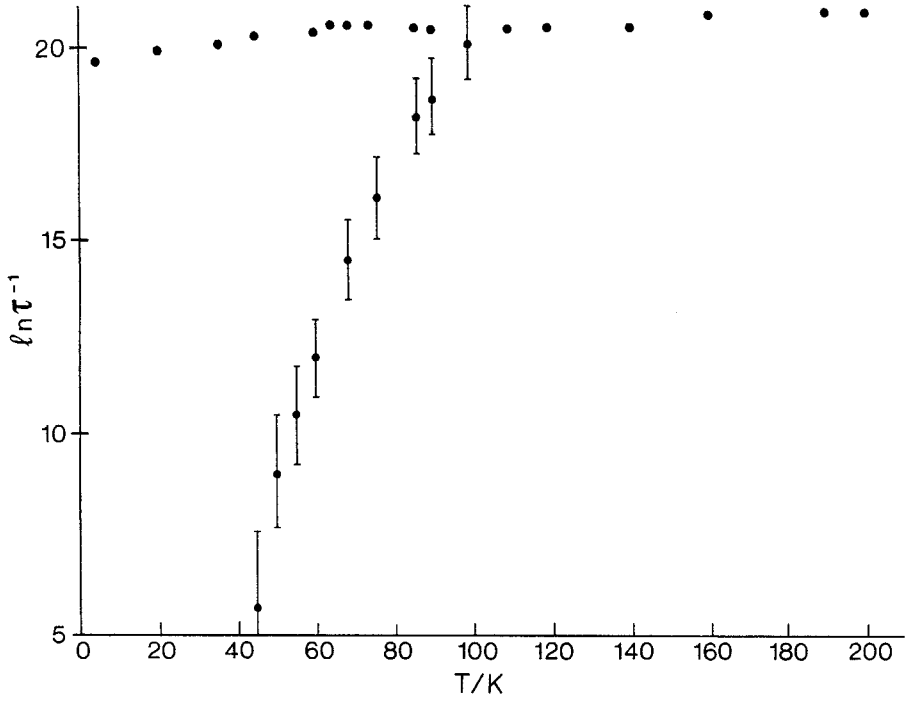

Figure 4.3. Lattice relaxation rates (represented by dots, near 20 on natural logarithmic scale) and impurity relaxation rates (dots and bars), strongly temperature-dependent. The error bars indicate the Gaussian width of the distributions, not the experimental error. Sample is $K_{0\cdot985}Li_{0\cdot015}TaO_3$. From Höchli and Maglione (1989).

$\varepsilon_\ell(x)$ and $\varepsilon_i(x)$ were found to be approximately linear functions of T, which in dielectric jargon indicates fits to Curie–Weiss laws $\varepsilon_\alpha^{-1} = C_\alpha^{-1}(T - T_\alpha^C)$. The Curie points T_α^C are given as $T_i^C = 22 \pm 8\,K$ and $T_\ell^C = -17 \pm 5\,K$; the Curie constants are $C_i = (2\cdot0 \pm 0\cdot3) \times 10^4\,K$, $C_\ell = (7\cdot2 \pm 0\cdot7) \times 10^4\,K$. Relaxation rates are displayed in figure 4.3 for $x = 0\cdot015$ as a function of temperature. We observe a strongly temperature-dependent and broadened impurity branch together with a monodispersive relaxation mode. These modes are mostly well separated, and where they superimpose (near 100 K) each branch retains its character: there appears to be little cross-relaxation. The dispersion step of ε_i becomes maximum at $T_f = 43\,K$ (i.e. even more positive than for $x = 0\cdot006$), and the lattice susceptibility extrapolates to a divergence at $T_\ell^C = -34\,K$ (i.e. even more negative than for $x = 0\cdot006$); furthermore, $C_i = 2\cdot5 \times 10^4\,K$ and $C_\ell = 7 \times 10^4\,K$.

Similar findings have been obtained for $K_{0\cdot974}Li_{0\cdot026}TaO_3$ (Höchli 1982). For this sample, it was shown that a Gaussian distribution of activation energies fitted the data somewhat better than the other distributions (figure 4.4), that its width increased as $T \to T_f^+$, and that the relaxation rate showed a nonlinear $\log\tau$ against T^{-1} dependence (figure 4.5). From the original data, which were fitted to $AT^{-1} + BT^{-2}$, one can readily derive an equivalent fit of the form $\ln(\tau/\tau_0) = E_b/(T - T_{VF})$. This form, named after Vogel (1921) and Fulcher (1925), seems to indicate that τ diverges and the system becomes static at T_{VF}. We find $T_{VF} = 6\,K$, which is significantly different from 0 but even more significantly lower than $T_f = 50\,K$, as defined by the maximum of the dielectric susceptibility at the lowest available frequency or, equivalently, by the

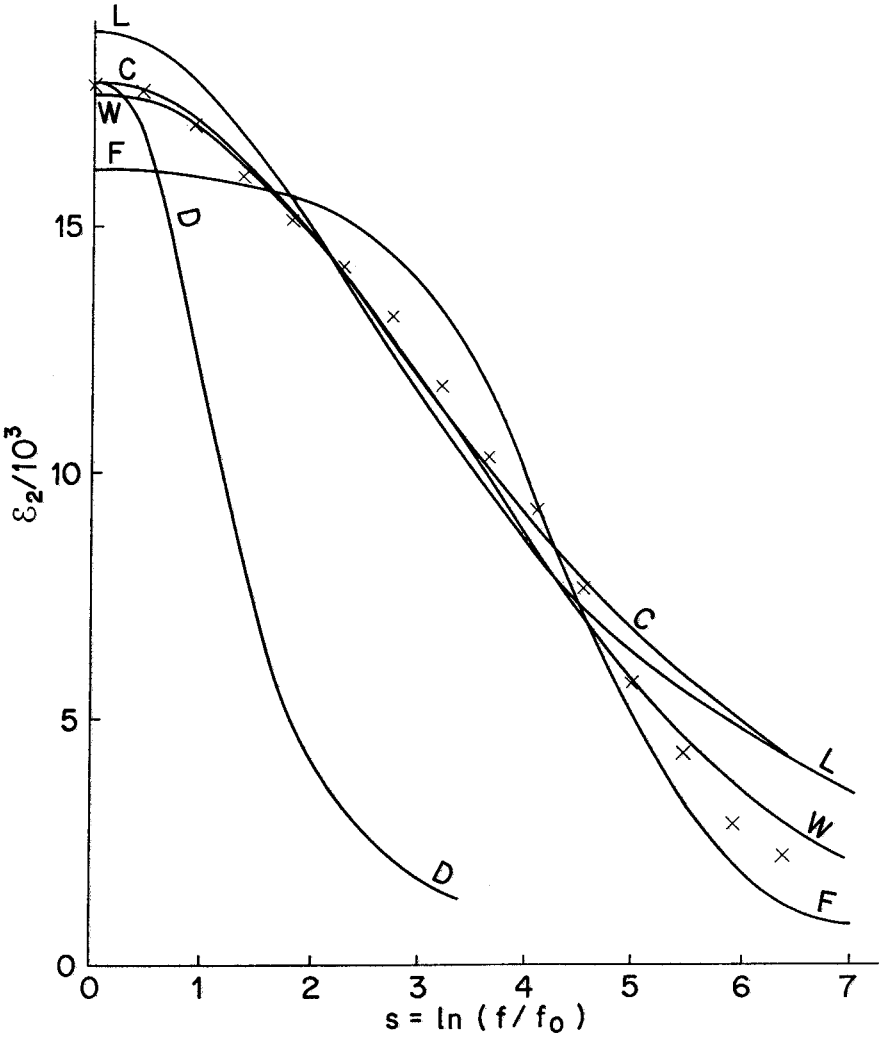

Figure 4.4. Imaginary part of the dielectric susceptibility as a function of frequency at $T = 57{\cdot}2$ K. Theoretical curves are from the convolution of the Debye relaxation formula $\omega_\tau/(1 + \omega^2\tau^2)$ with the following relaxation distributions: C, Cole; L, Lorentz; W, Wagner, F, Fröhlich and D, Debye. Li concentration is 0·026. From Höchli (1982).

limit of stability for non-zero polarization at zero field. Thus T_{VF} cannot be attained, it is a mere fitting parameter without physical significance (see section 10).

The zero-field characteristics may also be given in an ε_1 against T representation with ω as parameter (figure 4.6). Each ε against T curve shows a cusp whose size grows continuously as ω decreases. This plot stresses the analogy with spin glasses (Binder and Young 1986). With increasing concentration, the impurity branch becomes stronger and shifts to higher temperatures, showing the collective nature of the freezing process. We argue for the case of $KTaO_3$: Li—and shall show for the case of $KTaO_3$: Na (section 4.2)—that the sharp drop of $\varepsilon(T)$ below T_f is an artefact arising from the inability to approach the limit $\omega \to 0$. The lattice branch has temperature-independent size and zero width; its Curie–Weiss temperature, which is slightly negative for $x = 0$, drops even further with increasing x. Addition of Li

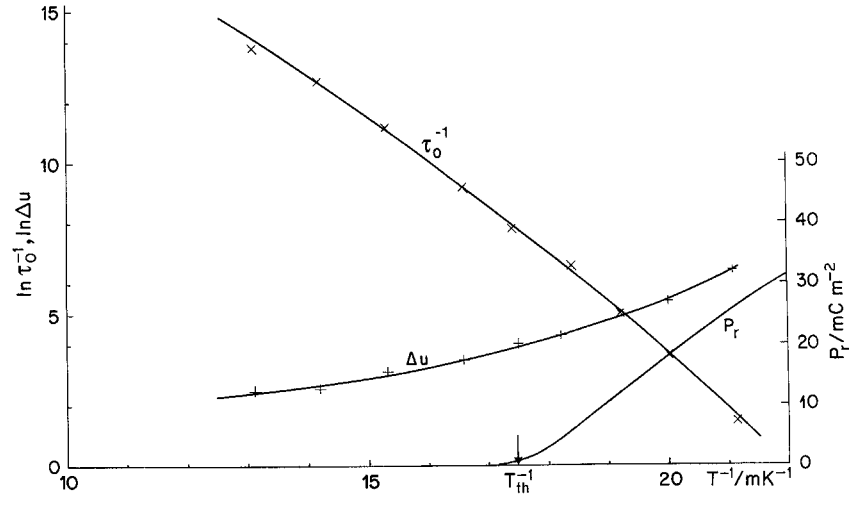

Figure 4.5. Most probable relaxation rate τ_0^{-1} and width of distribution Δu, $u = \ln \tau$, as functions of T^{-1}. Parameters for best-fit curves are given in the text. Also shown is the remanent polarization P_r from pyroelectric effect below the thawing temperature T_{th} taken on the same sample. Li concentration is 0·026. From Höchli (1982).

impurities stabilizes the $KTaO_3$ against ferroelectric distortions rather than inducing ferroelectricity, as was formerly widely believed (Yacoby and Just 1974).

The fact that the freezing temperature of the impurity mode grows with x indicates that the impurities interact increasingly as x grows. The susceptibility of the impurity is of course renormalized by the temperature-dependent lattice polarizability; therefore the type of interaction leading to freezing cannot be determined on the basis of ε_i^{-1} against T plots. This information needs to be derived from the dynamical nature of the freezing process.

At this point, it is useful to note that for conditions of nearly independent Li relaxation, i.e. low x and high T, the values found for the impurity relaxation step exceed those for the classic Debye expression $\varepsilon = N_i p_i^2 / 3 k_B T \varepsilon_0$ (N_i is the number density of Li and p_i an estimate for its local moment, which is about 1 eÅ) by two orders of magnitude. Accordingly, p_i is one order of magnitude larger than the bare local Li polarization. This point is pursued further in connection with data on static polarization.

Dielectric susceptibilities were also measured in a bias d.c. field, first at a fixed frequency of 10 Hz by Yacoby *et al.* (1983), then in the entire dispersion region of the impurity mode by Höchli *et al.* (1984). Yacoby's finding that ε_1 at 10 Hz is enhanced by a small field and decreases in a large field was confirmed for special sets of parameters, but Yacoby's identification of ε_1 (10 Hz) with ε_{static} was not. Instead, it was found that a field reduces, sharpens and accelerates the dispersion step continuously (Höchli *et al.* 1984). Contrary to early belief, $KTaO_3$: Li does not undergo a simple first-order transition to a ferroelectric phase.

At concentrations exceeding 4%, dielectric relaxation changes its character. A summary of the findings as plotted in Cole–Cole representation by van der Klink *et al.* (1983) is shown in figure 4.7: there are two impurity-related dispersion regimes; the one at low temperatures is characterized by a strong broadening at T_f and decreases in size as x increases; that at high temperature is not as broad and increases

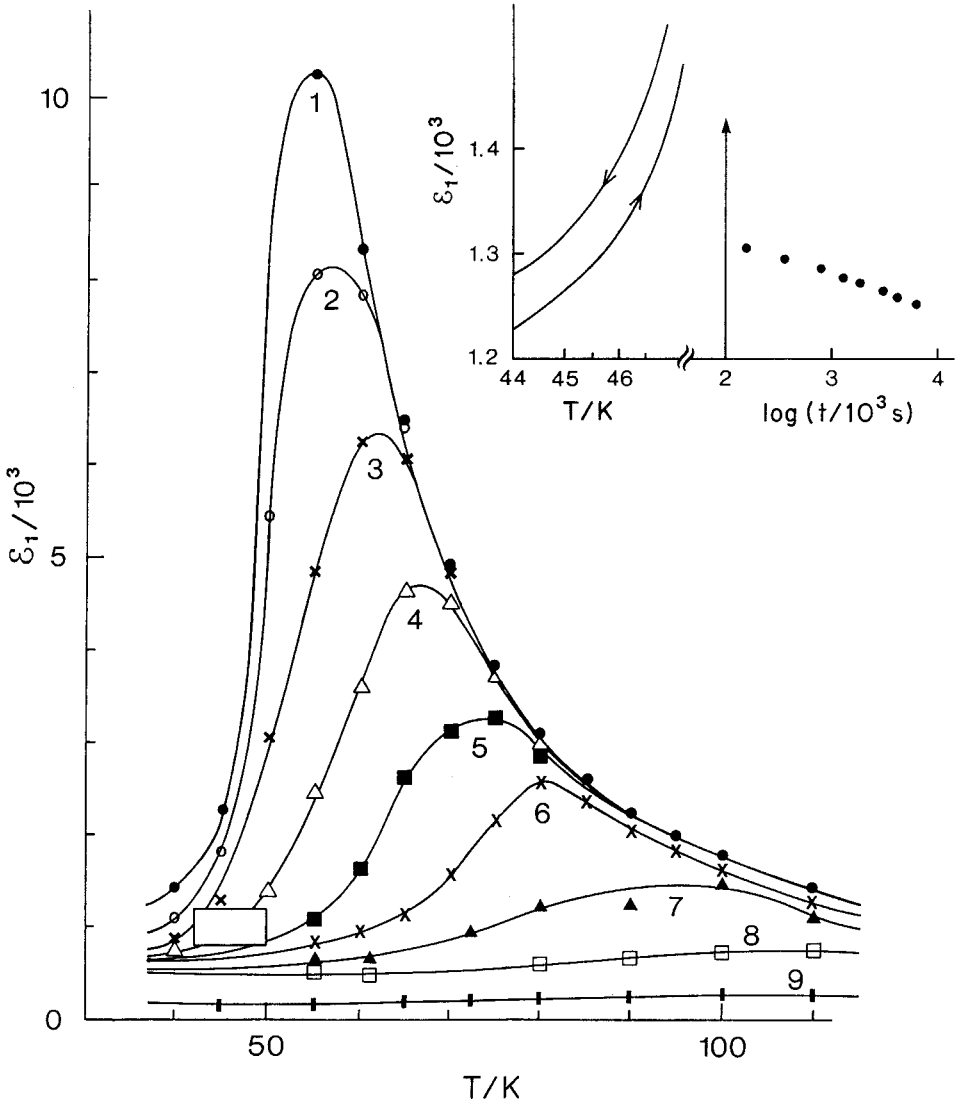

Figure 4.6. Real part of dielectric susceptibility as a function of temperature with $\log_{10}$ (frequency) as parameter. Sample is $K_{0.974}Li_{0.026}TaO_3$, from the same growth as that used by Kleemann *et al.* (1987). The boxed area is the region where Kleeman *et al.* observed hysteresis effects. The inset shows the hysteresis effect within the small boxed area and the time effect on ε_1 at $T = 45{\cdot}3$ K. From Höchli and Maglione (1989).

in size more than linearly with concentration. These findings may be summarized in terms of a phase diagram (figure 4.8). The solid line denotes the concentration-dependent temperature for which ε_1 (10 Hz) is maximum. Double-dispersion peaks have also been found by Smolenski *et al.* (1986) for $x = 0{\cdot}1$. They attempt—but not convincingly—to fit their data by semicircles, implying monodispersion (figure 4.9). We feel that, when properly evaluated (in terms of the Fuoss–Kirkwood transform), their data will supply evidence for enormously broad, possibly double-peaked, distributions of $g(\tau)$. In view of the disorder manifest at high concentration and of the

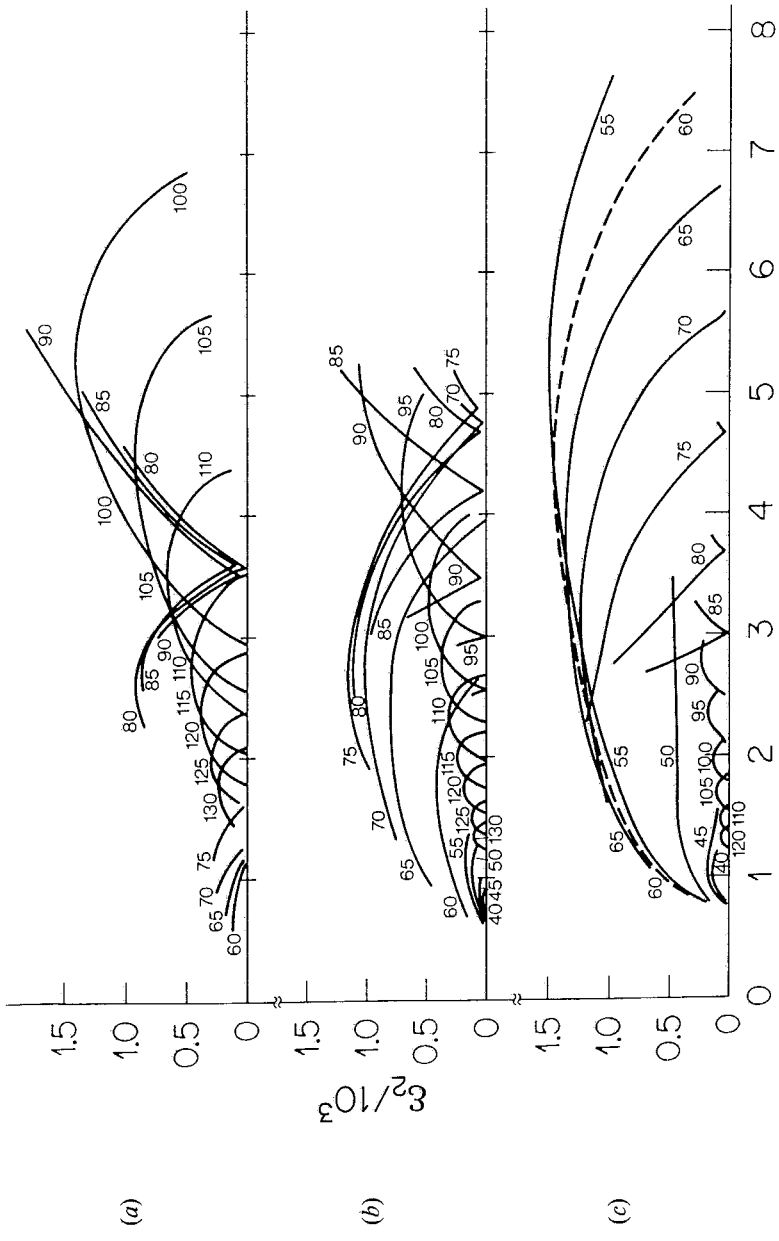

Figure 4.7. Cole–Cole plot of the dielectric susceptibility in $K_{1-x}Li_xTaO_3$ against temperature. From van der Klink *et al.* (1983). (*a*) $x = 0{\cdot}063$; (*b*) 0·049; (*c*) 0·036.

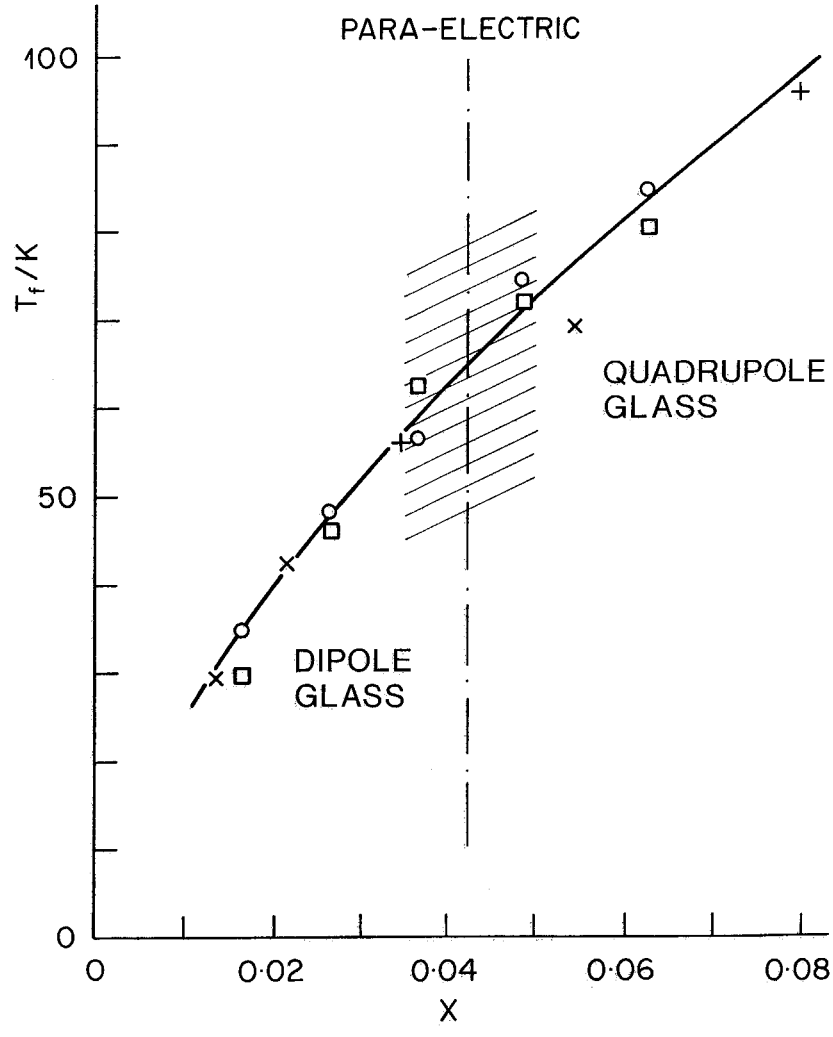

Figure 4.8. Configuration diagram of $K_{1-x}Li_xTaO_3$. Data for T_f from van der Klink *et al.* (1983). The solid line dividing high-temperature and low-temperature configurations is the theoretical best fit (Fischer and Klein 1976). The division between high- and low-concentration configurations is made according to the Vugmeister and Glinchuk (1979) criterion. The hatched area denotes the region of coexistence of dipolar and quadrupolar relaxations. From Höchli and Baeriswyl (1984).

dominant role of quadrupolar interaction in this concentration range (see also section 4.1.10), we have tentatively assigned this phase to a quadrupolar glass.

There is also evidence for asymmetric dielectric response (in terms of ε_2 against $\log \omega\tau_i$) for samples with $x = 0{\cdot}034$, particularly at $T \sim T_f$. A set of depolarization data (related to $\varepsilon(\omega)$ by the Fourier transform) is shown in figure 4.10. These curves were obtained (Höchli *et al.* 1990) after subjecting the sample to a moderate electrical field of 35 kV m^{-1} for 3600 s. The release of charge was then measured in 2 s intervals for about 1000 s. The current typically decays by two orders of magnitude in the time interval of interest. The results are thus given on a log–log scale. The log i against log t curves are nonlinear above 60 K, and virtually linear below 60 K. The approximation

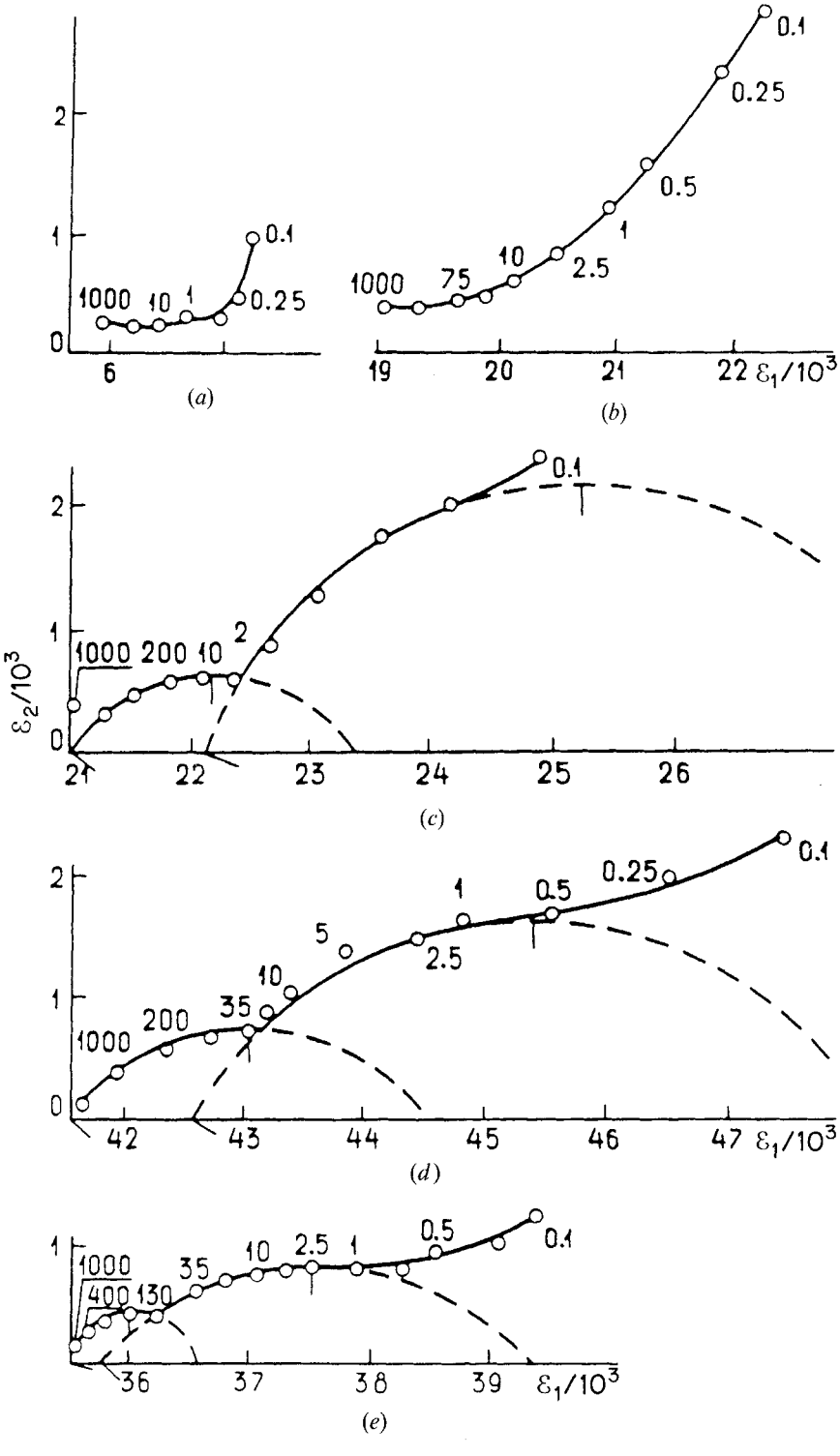

Figure 4.9. Cole–Cole plots for $x = 0{\cdot}10$: (*a*) $T = 78$ K; (*b*) 87 K; (*c*) 88 K; (*d*) 94 K; (*e*) 97 K. Frequencies are indicated next to the data points. From Smolensky *et al.* (1986).

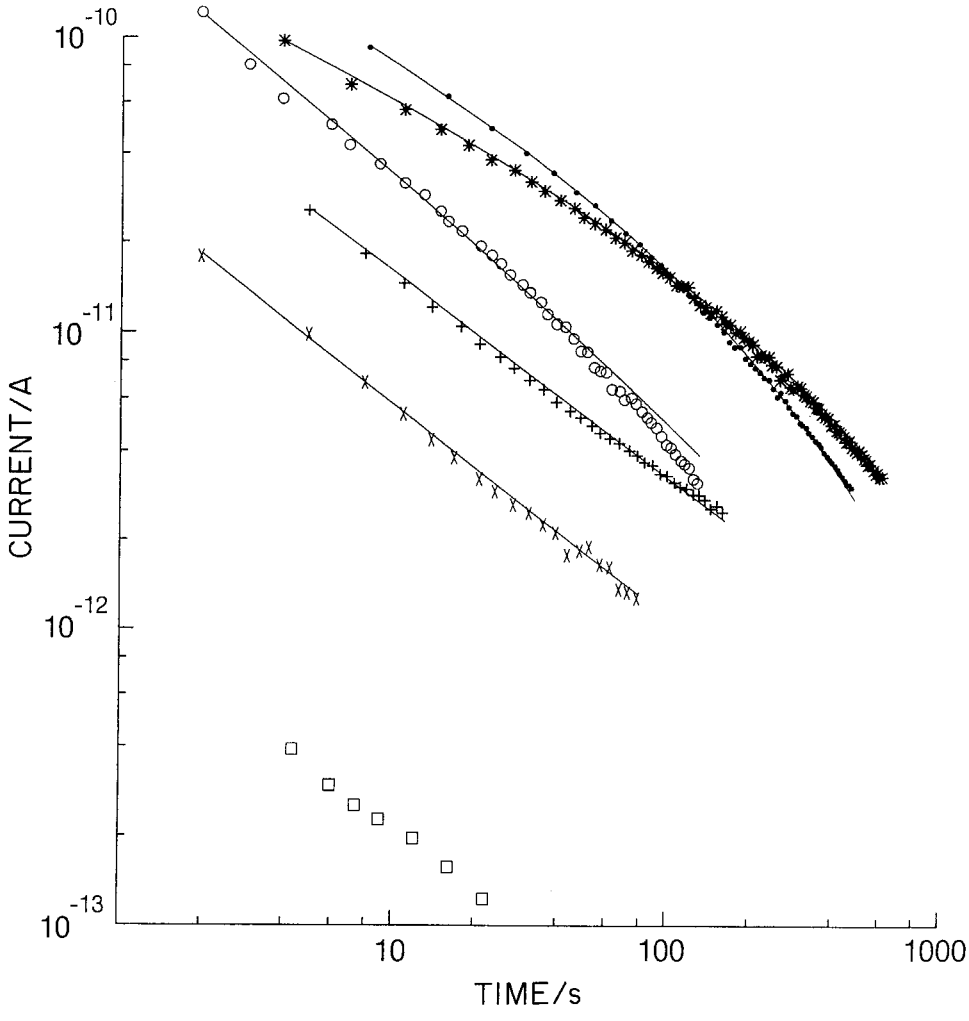

Figure 4.10. Polarization decay current and Kohlrausch–Williams–Watts fit to $\partial\Phi/\partial t$, where $\Phi = \Phi_0 \exp[-(\alpha t)^{\beta}]$ is the KWW function; sample is $K_{0.966}Li_{0.034}TaO_3$: (●), 65·9 K; (*), 63·9 K; (○), 60·0 K; (+), 55·5 K, (x), 48·0 K. For pure $KTaO_3$: (□), 48 K. From Höchli *et al.* (1990).

$\log i \approx \log t$ implies an arithmetical decay of i with t, which is compatible with the short-time behaviour resulting from the Kohlrausch–Williams–Watts (KWW) function $P(t) = \Phi \exp[-(t/\tau)^{\beta}]$, whose derivative contains the term $t^{\beta-1}$.

Evaluation of the KWW parameters yields the initial polarization $\Phi(T)$ and the stretched-exponential index $\beta(T)$. The first of these functions is given in figure 4.11. We note that $\Phi \approx 2{\cdot}5\,\mathrm{mC\,m^{-2}}$ is the maximum initial polarization in this experiment, while the saturation polarization amounts to $62\,\mathrm{mC\,m^{-2}}$. Since Φ depends linearly on E in this experiment, one obtains the true static value for the susceptibility $\varepsilon_s = \varepsilon_0^{-1}\,\partial\Phi/\partial E$ (see also figure 4.27 for analogous data for $KTaO_3$: Na). While a.c. susceptibilities show a cusp at $T_f(\omega)$, the static susceptibility rises sharply and becomes temperature-independent below $T_f(0)$, which may be associated with the true glass temperature, $T_f(0) \equiv T_g$. The stretched-exponential index decreases steadily, indicating growing deviation from exponential decay if T is reduced. This finding is

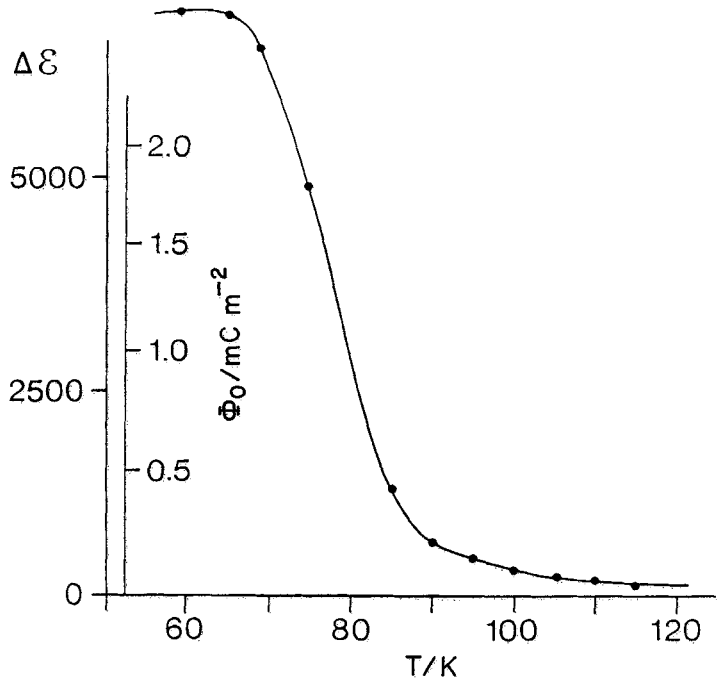

Figure 4.11. Polarization induced by field treatment with $E = 36\,\mathrm{kV\,m^{-1}}$, Kohlrausch–Williams–Watts (KWW) parameter Φ_0, and related dielectric step $\Delta\varepsilon$ ($\Phi_0 = \varepsilon_0 \Delta\varepsilon E$) against T. From Höchli *et al.* (1990).

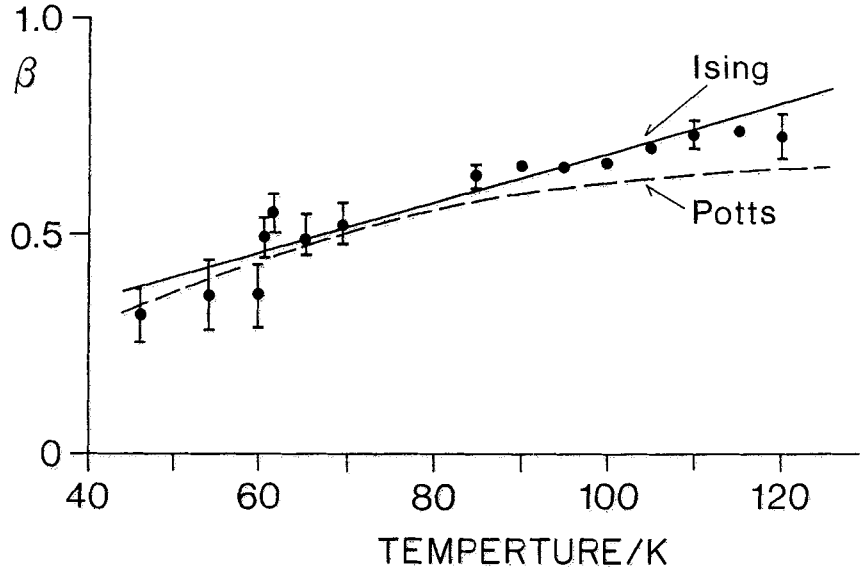

Figure 4.12. KWW parameter β, the stretched exponential index, against temperature (Höchli *et al.* 1990) and prediction by Carmesin and Binder (1988) using Ising and random-bond Potts models. From Höchli *et al.* (1990).

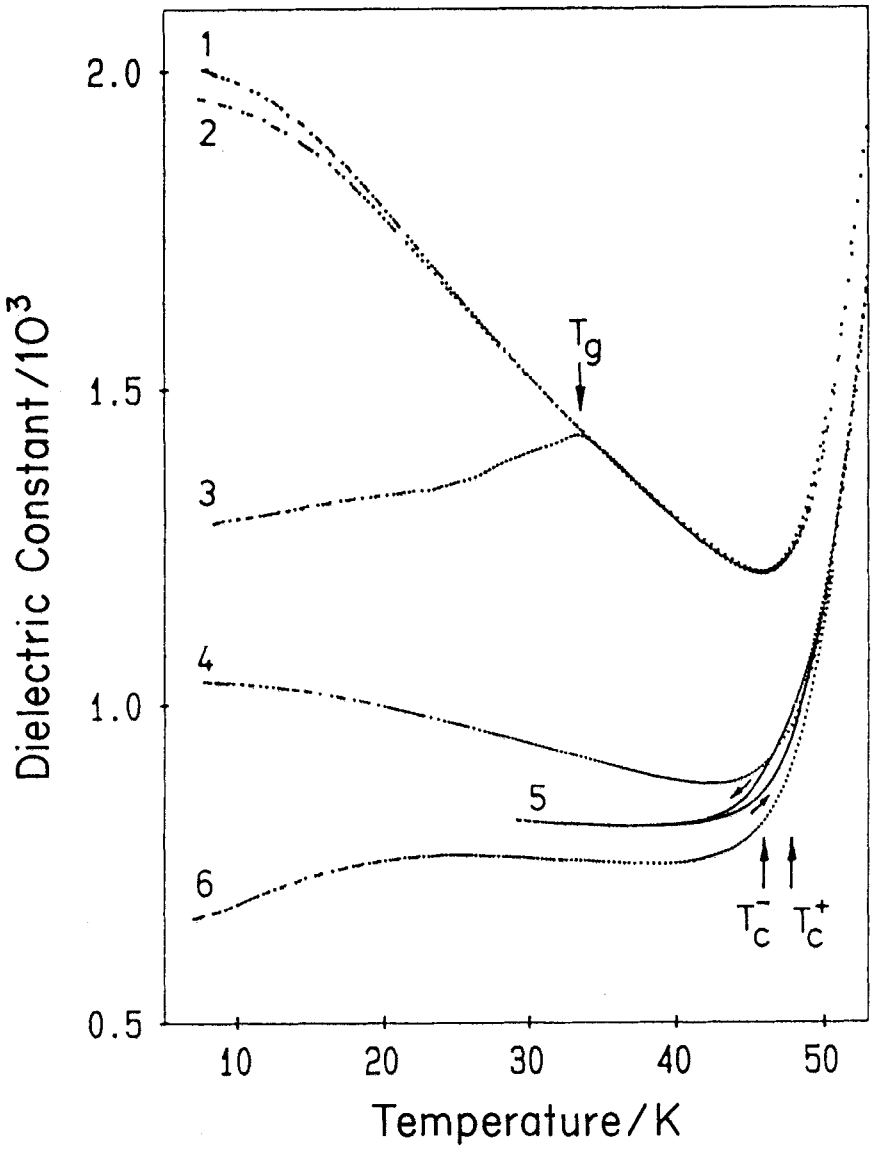

Figure 4.13. ε_1 against T measured in zero field on heating at 10 kHz on KTL with $x = 0{\cdot}011$ (curves 1–3) and 0·026 (curves 4–6), after rapid quenching (curves 1, 4), slow cooling (curves 2, 5), and field cooling with $E = 300\,\mathrm{kV\,m^{-1}}$ (curves 3, 6). Curve 5 also contains a cooling cycle; T_g and T_c^+ (T_c^-) as marked by arrows refer to $x = 0{\cdot}011$ and 0·026, respectively. From Kleemann *et al.* (1987).

reproduced in figure 4.12 together with a prediction from the random-bond Potts model (Carmesin and Binder (1988).

Kleemann *et al.* (1987) reported the variation of the dielectric constant at 1 kHz upon temperature cycling. There are unmistakable signs of hysteresis near T_f. The apparent hysteresis loops (figure 4.13), however, do not originate from jumps between the two states of the first-order ferroelectric scenario (Lines and Glass 1977). In fact, after a sudden change in T, ε_1(1 kHz) changes slowly, even at fixed T near T_f (see the inset in figure 4.6). This indicates the presence of a multitude of states participating

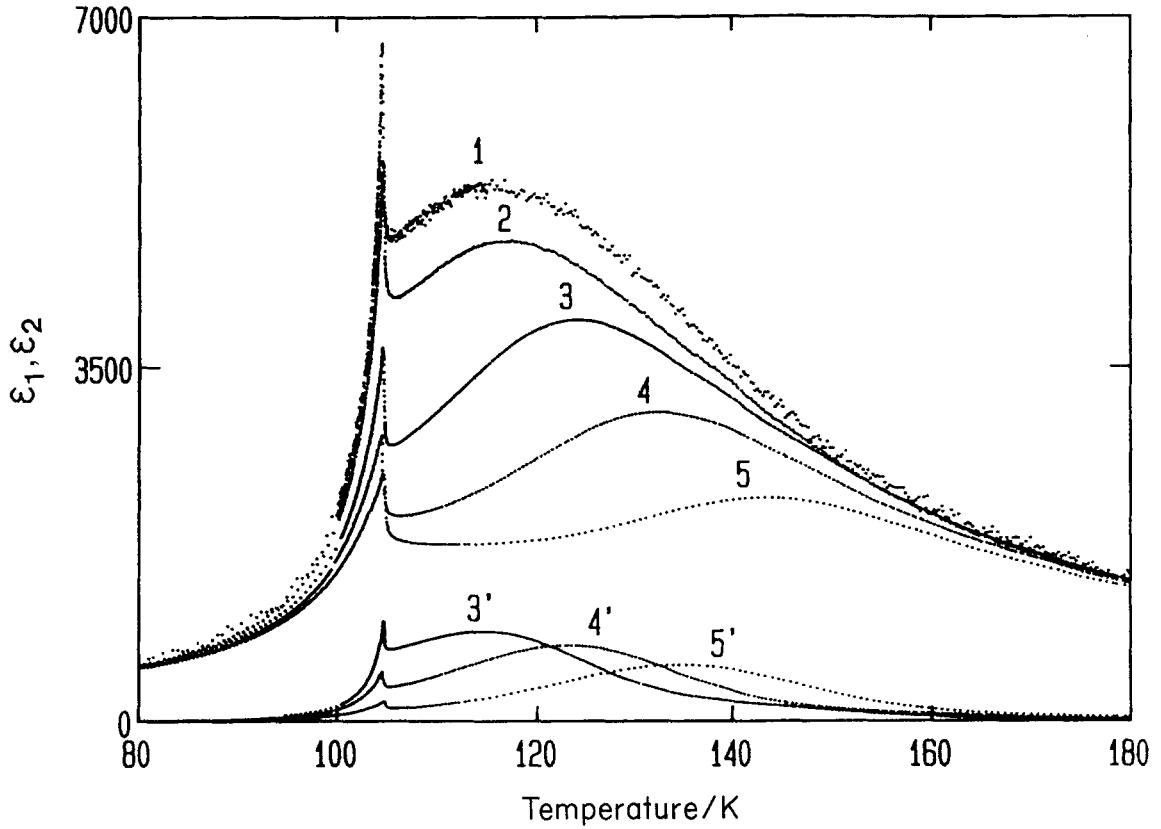

Figure 4.14. Temperature dependence of the real (curves 1–5) and imaginary (curves 3′–5′) parts of the dielectric permittivity measured on zero-field heating at various frequencies after field cooling under $E = 360\,\mathrm{kV\,m^{-1}}$: (1) 30 Hz; (2) 100 Hz; (3, 3′) 1 kHz; (4, 4′) 10 kHz; (5, 5′) 100 kHz. From Schremmer *et al.* (1989).

in relaxation (Höchli and Maglione 1989). Data on ε^* in *field-cooled* $K_{0.937}Li_{0.063}TaO_3$ found by Schremmer *et al.* (1989) are reproduced in figure 4.14: both $\varepsilon_1(\omega)$ and $\varepsilon_2(\omega)$ peaks appear narrow and occur at the same temperature. The authors conclude that narrow peaks are reminiscent of long-range order.

In summary, the a.c. dielectric susceptibility has cusp-like features near T_f, while its d.c. limit shows a plateau below T_f. All impurity-related relaxation branches are strongly polydispersive; the dispersion widths increase when T is lowered. Upon increasing the Li concentration, the dispersion width increases, a second dispersion branch appears near 4%, which outweighs the first one at 6·3%. Broad relaxation features are observed at 10% Li concentration.

4.1.2. *Static polarization; pyroelectric effect*

Upon cooling and with an electric field applied, a polarization can be induced that remains when the field is turned off at low T. It is not possible to induce the same polarization in a sample that has been cooled at zero field. The remanent polarization was measured by its pyroelectric current stored as charge in the electrometer while the sample was slowly heated from 4 K to T_f. Such results are shown in figure 4.15. Clearly, the curves $P(T)$ have an appearance similar to that of a ferroelectric, where $P \sim (T_c - T)^{1/2}$, but with two main differences. First, P is a *remanent* polarization, which cannot be measured by the hysteresis effect implemented by the Sawyer–Tower method, and, secondly, P_r depends on the cooling speed (Höchli *et al.* 1985, Maglione 1987). Reversibility was shown to be restricted (figure 4.16) to fields larger than those given by de Almeida and Thouless (1978):

$$E = A\left[\frac{T_f(0) - T_f(E)}{T_f(0)}\right]^{\gamma}. \tag{4.3}$$

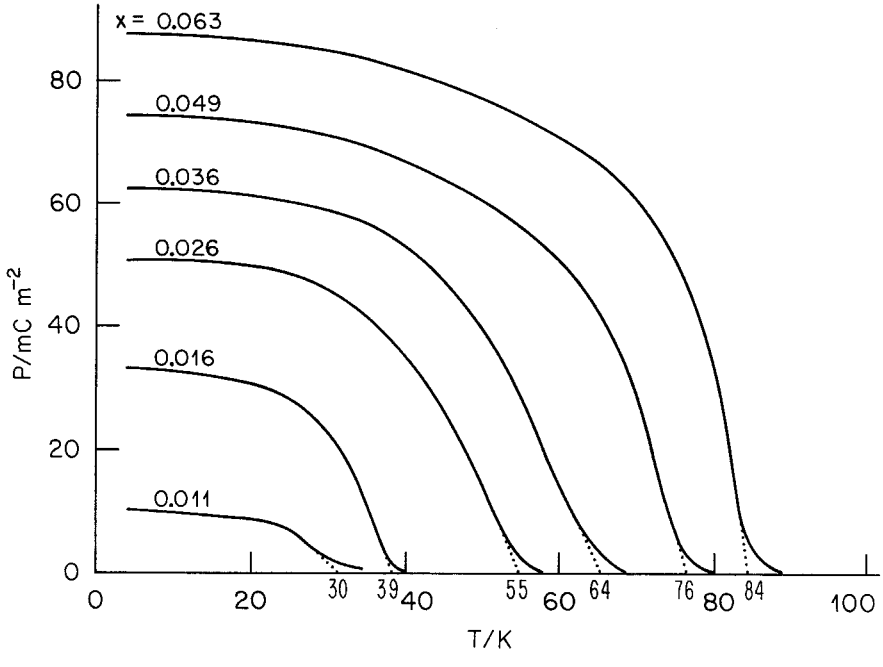

Figure 4.15. Remanent polarization and the thawing temperature in $K_{1-x}Li_xTaO_3$. From van der Klink *et al.* (1983).

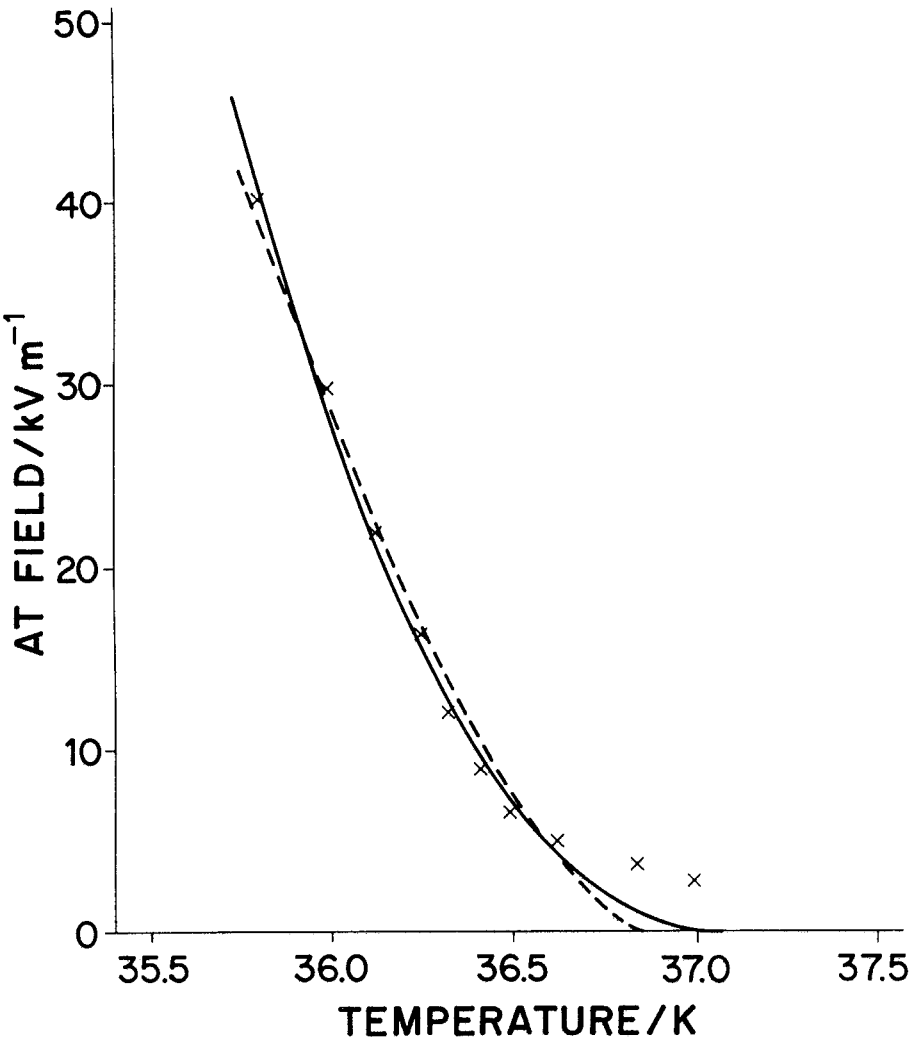

Figure 4.16. Limit of ergodicity ((x), experimental data); (– – –), de Almeida–Thouless line ($\gamma = 1{\cdot}5$); (——) best fit to a modification leaving γ adjustable, with $\gamma = 2{\cdot}1$. $x = 0{\cdot}016$; cooling speed 3 mK s^{-1}. The sample is $K_{0{\cdot}985}Li_{0{\cdot}015}TaO_3$. From Höchli *et al.* (1985).

The experimental value of $\gamma = 2{\cdot}1$ differed somewhat from the de Almeida–Thouless (1978) prediction of $\gamma = 1{\cdot}5$.

The value for the remanent polarization exceeds that of aligned Li atoms by a factor of about six, provided that the concentration is below about 4%. These findings have been attributed to the formation of a polarization cloud around the Li, consisting of displaced Ta^{5+} and O^{2-} lattice ions (Höchli *et al.* 1979). The polarization per Li atom should thus be $6e$Å and extend to about 25 unit cells to explain saturation of $P(x)$ for $x > 4\%$. A microscopic model involving nonlinear oxygen polarizability was able to account for the origin of ferroelectricity in perovskites (Migoni *et al.* 1976). Applying the same model to the Li-doped perovskite, Stacchiotti and Migoni (1990) were able to account for this polarization cloud almost quantitatively. The polarization cloud is presented in figure 4.17.

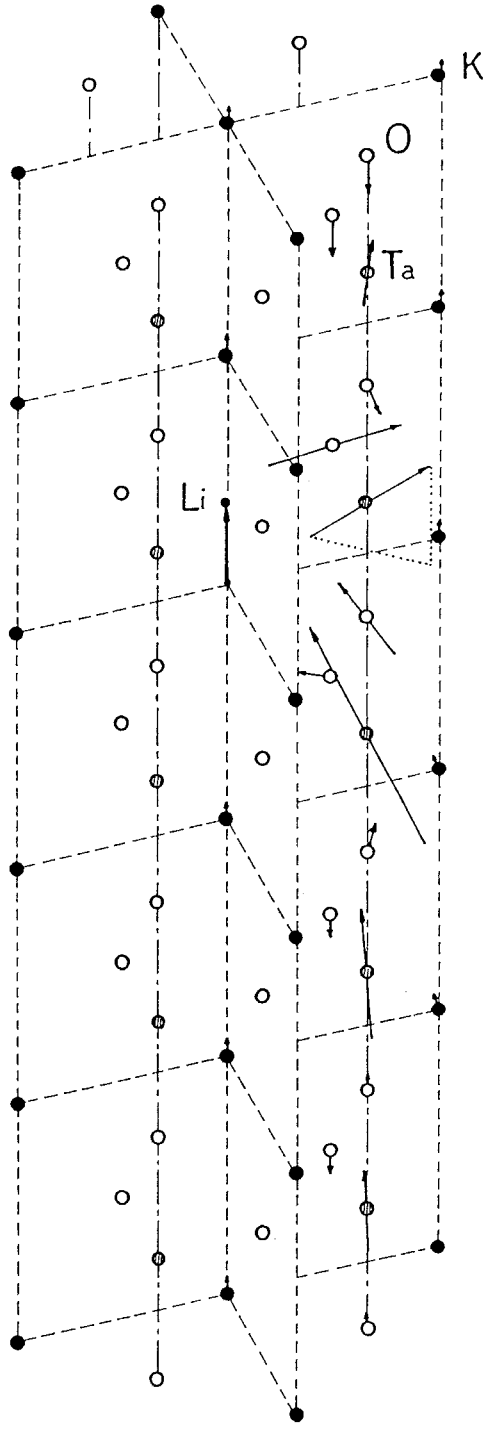

Figure 4.17. Polarization cloud around a displaced Li ion in $KTaO_3$. Arrows indicate ionic displacement of ligands. From Stacchiotti and Migoni (1990).

4.1.3. *Acoustic spectroscopy*

When Li is displaced with respect to its centrosymmetric site, it carries not only a dipole moment (ρ is the charge density)

$$P_\alpha = \int \rho(r) r_\alpha \, dr,$$

but also a quadrupole moment

$$Q_{\alpha\beta} = \int \rho(r) r_\alpha r_\beta \, dr,$$

α and β being Cartesian coordinates. Accordingly, it interacts with the strain of proper symmetry and may influence the propagation of sound. Application of very moderate electrical fields induces piezoelectricty (Rupprecht and Winter 1967) in these crystals. Making use of the mechanical resonances, the sound velocities were studied in several small ($< 10\,mm^3$) samples of various concentrations (Höchli *et al.* 1982). Up to a concentration of 3%, the low-temperature compliance $s_{11} = \rho_m^{-1} v^{-2}$ (ρ being the mass density and v the sound velocity) decreases in proportion to the impurity concentration. At high temperature, the compliances depend less on concentration. The transition from low-temperature to high-temperature behaviour can be approximately located at the polar transition. Strong ultrasonic loss, indicative of dispersion, does not permit detection of resonance near T_f. It was, however, shown that in the range of $x \lesssim 0{\cdot}03$ and up to a temperature of 100 K the change in elastic compliance with respect to pure $KTaO_3$ is proportional to the dielectric susceptibility. The dispersive nature of the elastic compliance is further shown by a comparison between resonance pulse-echo data at 30 MHz (figure 4.18). An evaluation of the parameters τ_∞ and ΔE in terms of a Debye model for acoustic relaxation (which is an oversimplification) provides practically identical values to those determined from dielectric relaxation. The quadrupole moment associated with the Li position thus follows the dipole moment adiabatically. For large concentrations and low temperatures, this association cannot be made, so the peculiar behaviour of $s_{11}(T)$ at large x remains unexplained. Sound propagation was also reported for $K_{0{\cdot}90}Li_{0{\cdot}10}TaO_3$ at 30 MHz. The data of Smolenski *et al.* (1986) are quite similar to earlier data by Höchli *et al.* (1982): a 5% drop in the rigidity of c_{11} following a Curie–Weiss law. In addition, Smolenski *et al.* (1986) reported a 2×10^{-3} jump in c_{44}, which should be forbidden by symmetry if the Li positions are along $\langle 100 \rangle$, and such a jump was indeed absent in $K_{0{\cdot}974}Li_{0{\cdot}026}TaO_3$ (Höchli *et al.* 1982). Smolenski attributes the weak jump in c_{44} to the sign of a ferroelectric phase transition, but leaves the twenty times stronger relaxation phenomenon unexplained.

Brillouin scattering reveals sound propagation at about 10^{11} Hz and, in view of the small wavelength (about $0{\cdot}5\,\mu m$) of sound at this frequency, it also provides insight into spatial resolution. Chase *et al.* (1982) found regular acoustic propagation in both zero-field-cooled (ZFC) and field-cooled samples containing 5·4% Li (figure 4.19). These samples showed a strong acoustic anisotropy below T_f, but no jump of any kind for c_{44}. Thus Chase *et al.* (1982) concluded that their sample had long-range quadrupolar order even when zero-field-cooled.

4.1.4. *Birefringence patterns revealing static strain*

Birefringence patterns of ZFC samples show domain-like structures (Cornaz *et al.* 1981). The domain boundaries are more irregular than for example in $BaTiO_3$, and they do not move when a field is applied below T_f; rather, at large fields, birefringence

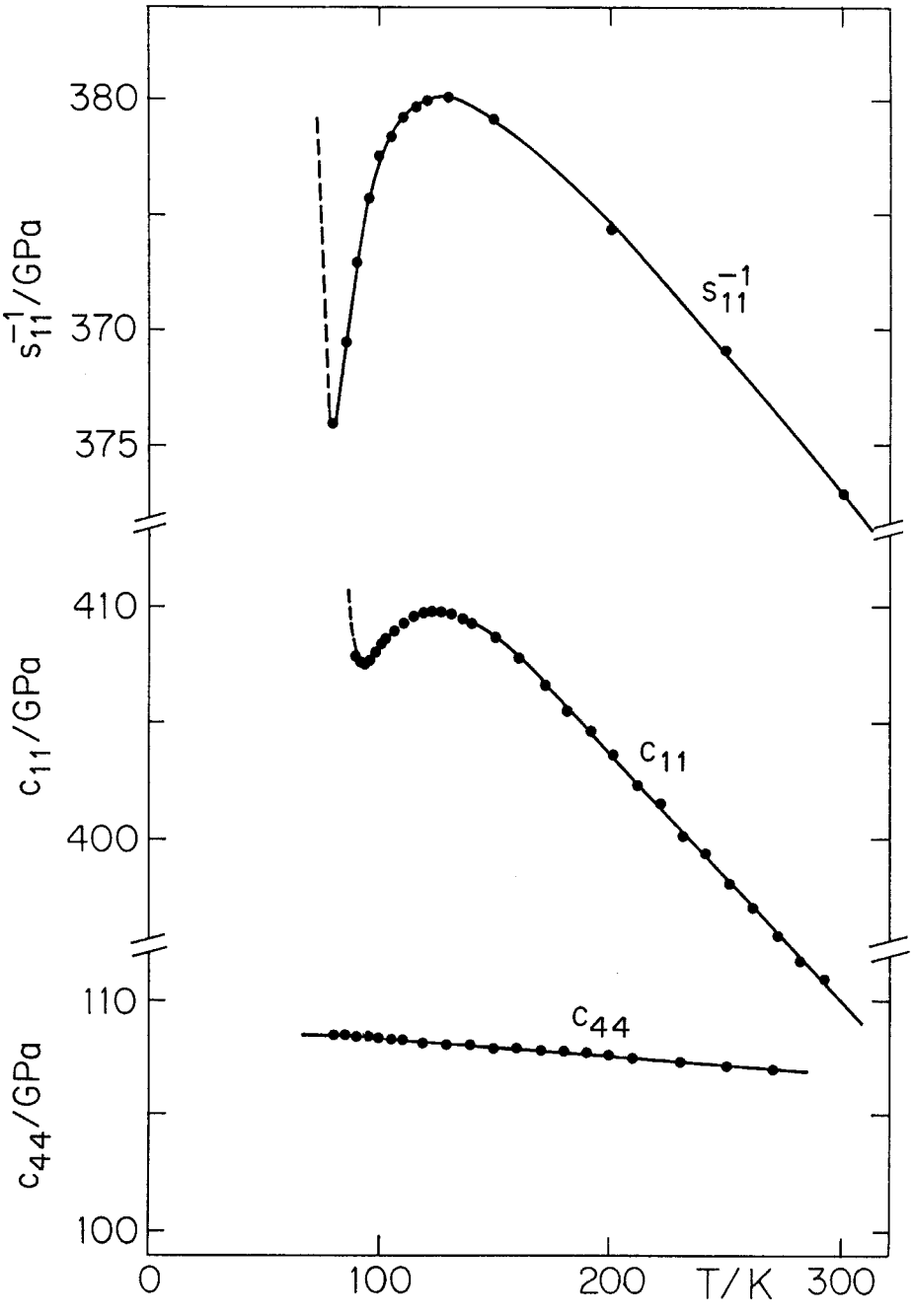

Figure 4.18. Inverse elastic compliance $1/s_{11}$ (at 300 kHz) and elastic stiffnesses c_{11} and c_{44} (at 15 MHz) of a sample with $x = 0{\cdot}026$. The curves represent a numerical fit to $c(\omega, T) = C^{\infty} - g^2\chi(0, T)/[1 + \omega^2\tau^2(T)]$, where $\chi(0, T) = n_D/3k_B(T - T_f)$, $\tau(T) = \text{Arrh}(T)$, $T_f = 68$ K, $g = 1{\cdot}1$ eV, $\tau = 0{\cdot}13$ ps, $\Delta E/k_B = 1100$ K. From Höchli *et al.* (1982).

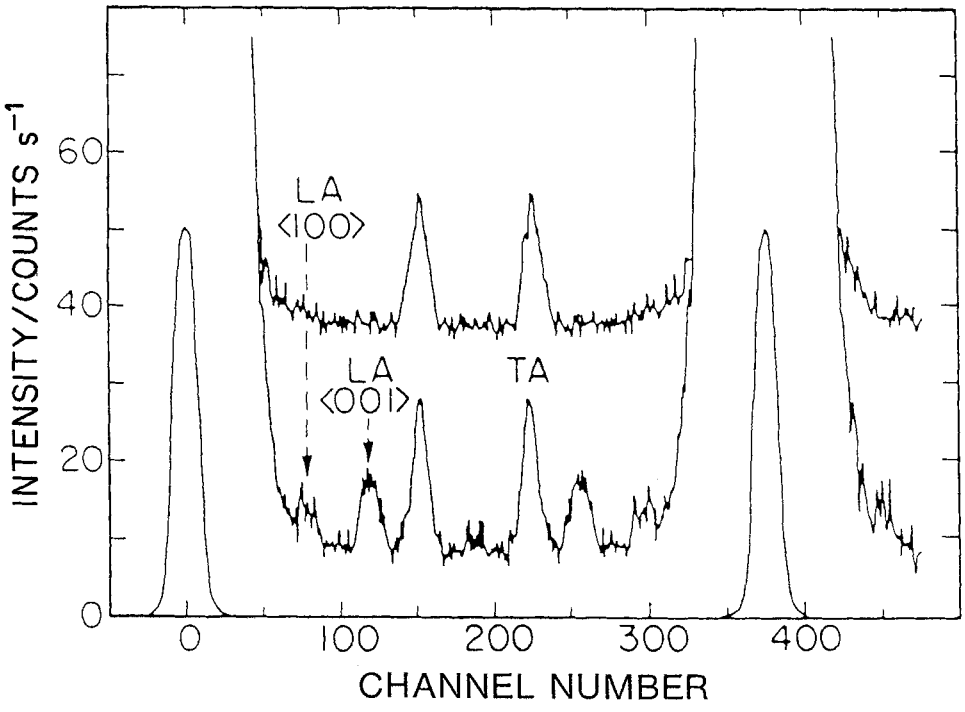

Figure 4.19. Brillouin spectra observed for an unpoled sample of $K_{1-x}Li_xTaO_3$, $x = 0{\cdot}054$, at $T = 35$ K. The upper and lower traces were obtained for two different regions of the sample, separated by about 1 mm. The polarizations selected are $HH + HV$. The free spectral range is 62·2 GHz, and the peaks labelled LA ⟨100⟩, LA ⟨001⟩ and TA are in the same order as the elastic peak in channel number 375. From Chase *et al.* (1982).

patterns appear much as in pure $KTaO_3$ (Höchli 1976), where they are attributed to space charge. Birefringence patterns of ZFC $K_{0{\cdot}974}Li_{0{\cdot}026}TaO_3$ have also been evaluated by Courtens (1981). Using the electro-optic coefficient for pure $KTaO_3$ (Landolt–Börnstein 1981), he found $(P_x^2 - P_y^2)^{1/2} \sim 40\,\mathrm{mC\,m^{-2}}$ for the magnitude of the polarization anisotropy, which is in substantial agreement with the remanent polarization of the field-cooled sample. The light transmitted through an apparently homogeneous region, however, is considerably depolarized (Cornaz *et al.* 1981, Chase *et al.* 1982). Early identifications of the birefringence pattern with a polar domain structure (Courtens 1981, Prater *et al.* 1981a) are incorrect, and Prater *et al.* (1981b), Chase *et al.* (1982) and Andrews (1985) have pointed out that homogeneous birefringent regions consisted of parallel and antiparallel-aligned dipoles.

Recently, Kleemann *et al.* (1987) presented an investigation of potassium lithium tantalate (KTL) crystals by means of birefringence and optical retardation. They found that low-concentration samples, $x \leqslant 0{\cdot}016$, have birefringence images with smooth contours, while heavily doped samples show signs of domain-like structure. Differences between ZFC and field-cooled birefringence were explained in terms of the presence or absence of domain walls that are optically inactive and reduce the effect activity of the bulk for geometrical reasons. Taking this model literally and inserting the layer thickness of some 200 Å found by Lehndorff (1986) and confirmed by Azzini *et al.* (1990), one finds that such a stack of regular layers would have frequency-dependent transmission (Liddell 1981). Such effects were not observed

(Azzini *et al.* 1990). We agree with Prater *et al.* (1986b, c) that birefringence patterns in ZFC samples do not have a straightforward interpretation. The birefringence patterns change with time after the sample is cooled to below T_f. Kleeman *et al.* 1988) reported that $\Delta n(t) \sim \ln \tau$ at fixed T and appear to have found an improved fit to $\exp[-(\alpha t)^{\beta}]$ (W. Kleeman, personal communication). They compared their results with the time-dependent Bragg intensity $I(t)$ reported by Kamikatahara *et al.* (1987), who deduced essentially two relaxation components for $I(t)$ (see also section 4.1.8). Kleemann *et al.* (1988) attributed the short-lived component in the Kamikatahara *et al.* (1987) data to an experimental artefact and claimed that there is only one relaxation time present. This claim, however, is not supported by their own data: the decomposition of either $\ln(t/t_0)$ or $\exp[-(t/t_0)^{\beta}]$, $\beta \neq 1$, by the inverse Laplace transform (2.2) produces a wide distribution of relaxation times. When properly evaluated, such decay function data are of great value in identifying glass formation.

4.1.5. *Heat capacity*

A search for a discontinuity of C at T_f by Strukov *et al.* (1986) had a negative result. Heat-capacity C data are sometimes used to reveal low-lying tunnel states in amorphous and glassy substances (Hunklinger and von Schickfus 1981). An attempt to detect a nearly linear (rather than the classical cubic) dependence of C on T produced negative results. Only a small additional contribution to C above T_f was measured (Lawless *et al.* 1981). The absence of tunnelling states concluded on the basis of these findings was later confirmed by ultrasonic experiments (Doussineau *et al.* 1989). It was argued that the enormous barrier height prevented tunneling at a rate detectable by ultrasound.

4.1.6. *Raman spectroscopy*

Prater *et al.* (1981c) found that the low-lying Raman line of transverse-optical character was split into two transverse-optical components of A_1 and E symmetry in a crystal of $K_{0.946}Li_{0.054}TaO_3$ that was field-cooled (figure 4.20). In the same crystal, the Raman phonon was isotropic when the crystal was cooled under zero-field conditions. Similar behaviour, but with smaller anisotropy, was found in $K_{0.986}Li_{0.014}TaO_3$. Prater *et al.* (1981c) estimated the density of vibrations of the low-lying split TO mode at all propagation directions and were able to fit the Raman intensity of the ZFC sample. They also noted that external stress was capable of further separating the two TO components. Comparison with Brillouin spectra obtained on the same ZFC crystals, however, confirmed that TA phonons did propagate and that, accordingly, correlation between even-parity displacements (distinguishing the x, y and z axes but not the polarization $\pm x$) extended further than λ. The Raman *efficiency*, however, is sensitive to inversion twinning. If no net polarization is present because of inversion twinning in volumes of order λ^3 then the Raman efficiency is greatly reduced for TO modes but unaffected for TA modes. The weak broad spectra Prater *et al.* (1981a) observed, together with a confrontation of birefringence with Raman data, allowed them to estimate the polar correlation length (distinguishing $\pm x$) between 100 and 1000 Å. Lack of macroscopic polar correlation was also observed in an ion-channelling study (Dubus *et al.* 1985).

4.1.7. *Second-harmonic generation and light mixing*

Lehndorff (1986) performed a light–microwave mixing experiment on the material

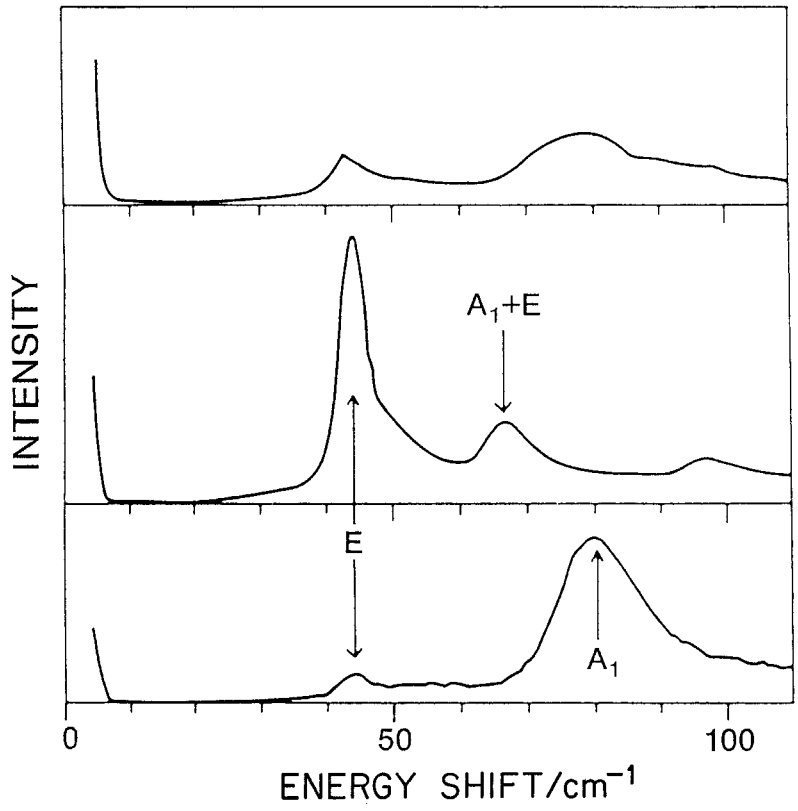

Figure 4.20. Raman spectra of $KTaO_3$ containing 5·4 mol % Li at 4·2 K: (*a*) unpoled with $\mathbf{k}_{phonon} \parallel \langle 110 \rangle$; (*b*) poled sample with $\mathbf{k}_{phonon} \parallel \langle 011 \rangle$; (*c*) poled sample with $\mathbf{k}_{phonon} \parallel \langle 110 \rangle$. Polarizations included at $Y(ZY)Z$ and $Y(ZZ)X$, where X, Y and Z are pseudocubic axes. From Prater *et al.* (1981c).

$K_{0.974}Li_{0.026}TaO_3$. He found that the polarization of light generated by two beams,

$$P(\omega_1 \pm \omega_2) = \chi_{12} E(\omega_1) E(\omega_2), \tag{4.4}$$

involved a susceptibility χ_{12} of *odd* parity. The second-harmonic efficiency thus depends on the structure of χ_{12}, which involves polar displacement of all species, including Li. In particular, if the local polarization, and thus χ_{12}, varies at a much shorter distance than λ, then the efficiency drops to 0 because of phase cancellation of $P(\omega_1 \pm \omega_2)$. Lehndorff's null result for ZFC crystals allowed an upper estimate for the correlation length to be given: $\xi \leqslant 200$ Å. A recent evaluation of χ on the basis of calibrated second-harmonic generation produced $\chi = 100$ Å (Azzini *et al.* 1990). Second-harmonic generation has also been reported by Voigt *et al.* (1990). Microwave-induced Brillouin scattering determined this correlation length to be 120 Å for $x = 0{\cdot}003$ (Sommer *et al.* 1989). These findings revise the estimates of Prater *et al.*

4.1.8. *X-ray and neutron diffraction*

A determination of the correlation lengths ξ of polar displacements is, in principle, afforded by studies of diffuse X-ray and neutron scattering as well. Andrews' (1985)

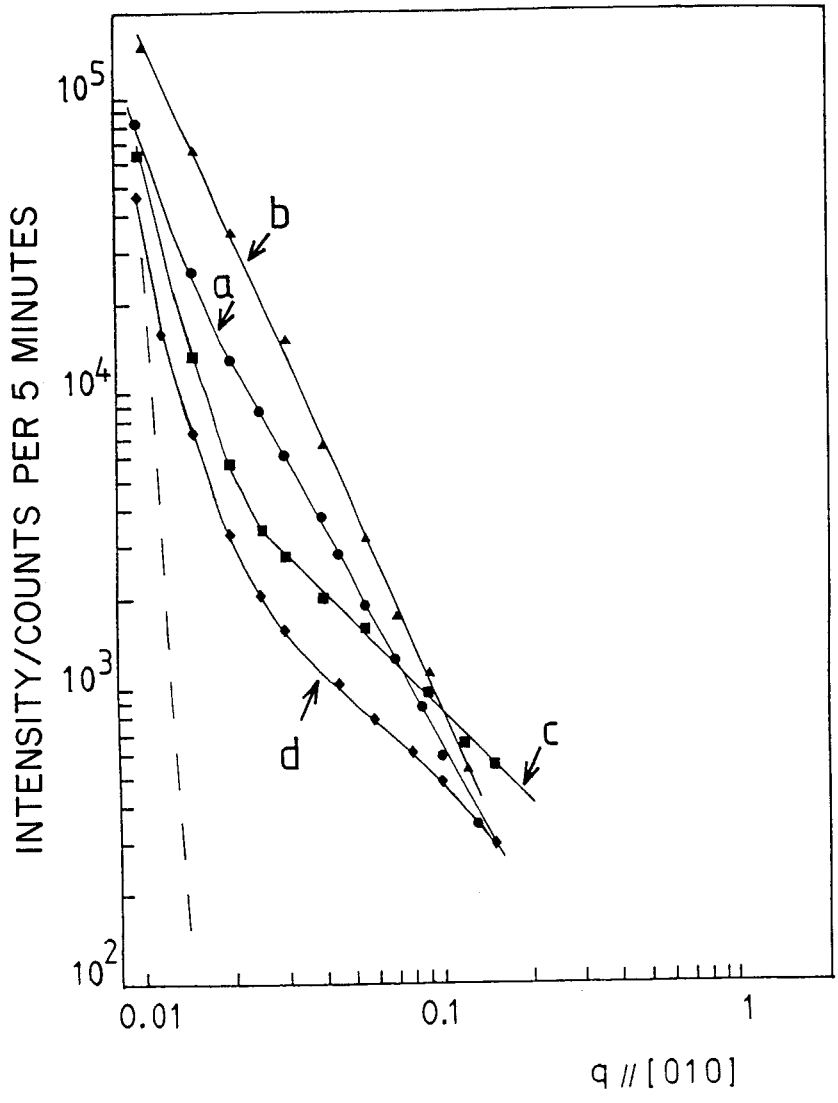

Figure 4.21. Scattered intensity, above background, in $KTaO_3$: 1·6% Li for $Q = (0, 1 + q, 3)$ with $E = 0$ at 11·4 K (curve a), 90 kV m^{-1} at 15·5 K (curve b) and 700 kV m^{-1} at 18 K (curve c). The scattering in zero field at 100 K, with intensity scaled to 11 K, is shown by curve d. Smooth curves are guides to the eye, and the broken line is the contribution to the scattering from the tail of the (0, 1, 3) Bragg peak calculated with the known instrumental resolution. Adapated from Andrews (1985).

study of X-ray diffraction revealed intensities that fit the well known expression $I = I_0(1 + q^2\xi^2)^{-1}$ (figure 4.21), where q denotes the distance from a Bragg peak in q space. He fitted ξ and found $\xi_\parallel \approx 100$ Å and $\xi_\perp \approx 1000$ Å, where $\parallel$ and $\perp$ refer to the surface normal. The $K_{0.984}Li_{0.016}TaO_3$ sample revealed no tetragonal splitting within $c/a - 1 = 10^{-4}$. In view of the nearly vanishing scattering efficiency of Li for X-rays, the polar displacement refers to that of Ta, not Li, which would be of primary interest. The fact that the two are quite different is revealed by a $c/a - 1$ parameter of $1{\cdot}4 \times 10^{-3}$ for $K_{0.946}Li_{0.054}TaO_3$, obtained from the splitting of the Bragg peak

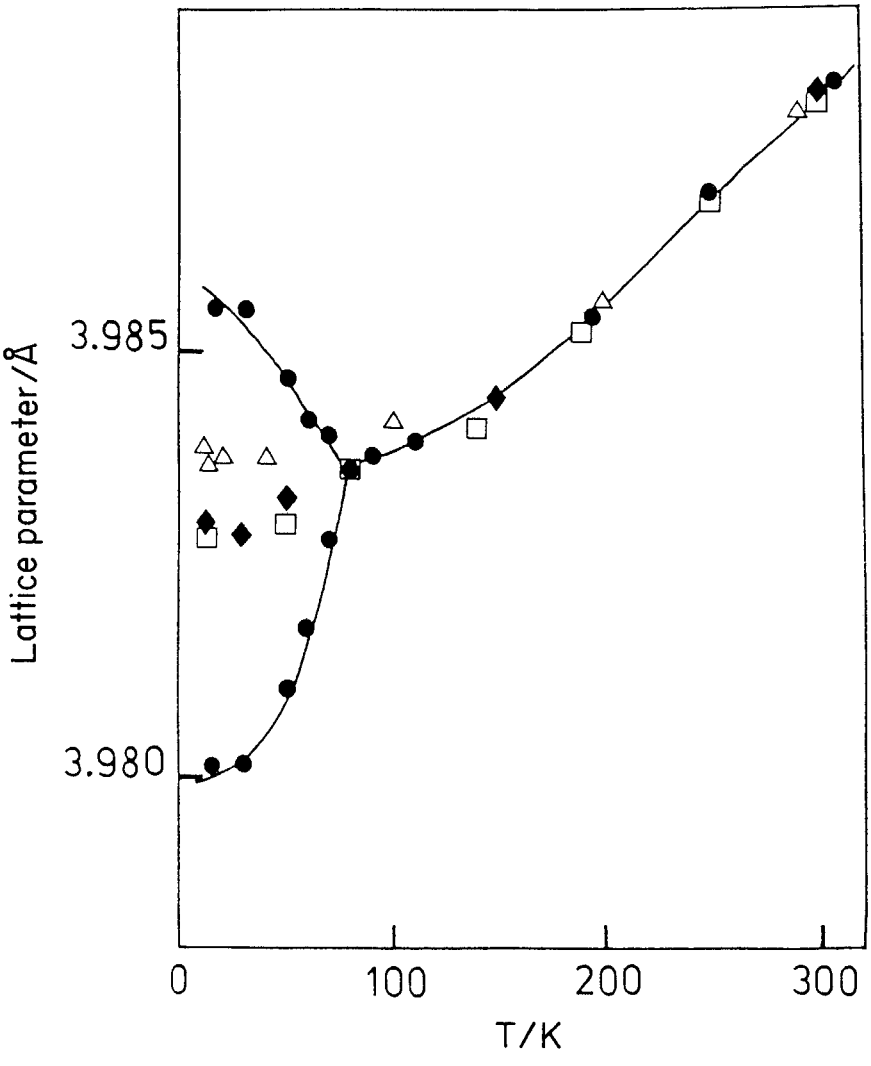

Figure 4.22. Lattice parameters of pure $KTaO_3$ (□), $KTaO_3$: 1·7% Nb (△), $KTaO_3$: 1·6% Li (◆) and $KTaO_3$: 5% Li (●) in zero electric field. Within experimental error, all materials remain cubic except for $KTaO_3$: 5% Li, which transforms into a tetragonal phase below T_c. Error bars are comparable in size to the symbols used, and the smooth curves are a guide to the eye. From Andrews (1985).

below T_f (figure 4.22). This splitting shows that the axial lattice distortion, to which X-rays are more sensitive, is much smaller than the Li displacement of 1 Å and that the Li and Ta displacements are only weakly coupled. The correlation length of these distortions in heavily doped KTL apparently exceeds the coherence length of the X-rays, which is estimated to be several thousand Ångström units, whereas no such estimate can be given for dilute samples. The two models considered by Andrews, cluster formation of length ξ or domain structure (Bruce 1981), confirm this estimate. Andrews rightfully questioned whether these characteristics pertain to the surface whose depth was estimated to be of the order of the penetration length of X-rays (Ansermet *et al.* 1981). Neutron studies, however, confirm the assignment of limited

correlation as a bulk property (Kamikatahara *et al.* 1987). Broken correlation of Ta ions appears to be limited to low-concentration KTL at $x = 0{\cdot}017$ (but not at $x = 0{\cdot}04$), and to depend on sample history. Associated with it is the generation of a mosaic-type grain structure with a grain size of 30 μm and an average tilt angle of about 3×10^{-4} (Maglione *et al.* 1989). Furthermore, inelastic-scattering data show an increase of the TO mode frequency of $KTaO_3$ upon Li doping (i.e. ω increases (Kamikatahara *et al.* 1987, Maglione *et al.* 1989)). On heavy doping, Li appears to induce a macroscopic distortion of order 10^{-3} to the lattice. This distortion is probably associated with Ta, not Li, displacement, whose off-centre position appears to be independent of x, as shown in the next section.

4.1.9. *Resonances probing local properties*

Magnetic spins of quantum number greater than or equal to one possess a nuclear quadrupole moment and interact with electric field gradients due to the surrounding lattice. Their spectrum can thus reveal interesting local properties. Both nuclear and electronic spins have been applied. The quadrupole moment of the $I = \frac{3}{2}$ spin of the ^{7}Li nucleus is an obvious candidate for such investigations. Borsa *et al.* (1980), van der Klink *et al.* (1983) and van der Klink and Borsa (1984) have presented detailed analyses: they evaluate this nuclear magnetic resonance spectrum (figure 4.23) in terms of an electric-field gradient ΔV at the site of the Li nucleus. For cubic symmetry (at $T = 54$ K), the field gradient vanishes. Accordingly, one unsplit magnetic resonance line is observed. Below 45 K, the spectrum is split and allows the electric-field gradient to be determined at the Li site. From its value, they deduce the displacements on the basis of a point-charge model. The displacement, 1·2 Å, nearly corresponds to the maximum displacement allowed for a hard-sphere Li ion in the [100] direction until it touches hard-sphere oxygen ions. Spin-relaxation data determine the hopping time of Li over barriers, in agreement with dielectric and acoustic experiments. Arrhenius-type behaviour is found, with $\nu_0 \approx 10^{13}$ Hz and $E_b/k_B \approx 1000$ K. The coincidence of the symmetry of the NMR displacement and the dynamics of the ^{7}Li nucleus with the corresponding findings by microscopic methods confirm the assignment of polar behaviour of Li ions beyond a doubt. Furthermore it is found that the spin–lattice relaxation of the constituents ^{7}Li, ^{39}K and ^{181}Ta lacks critical behaviour at T_f; in particular, there is no maximum at T_f, in contrast with findings in $KTaO_3$: Nb, where critical spin–lattice relaxation was considered a landmark of a true thermodynamic phase transition (Rigamonti 1984).

Paramagnetic ions Fe^{3+}, Mn^{2+} and Gd^{3+} have been introduced into KTL and their resonance studied by Geifman (1981) and Geifman *et al.* (1981). From the broadening of the resonances, it was concluded that isolated Li ions ($x = 0{\cdot}008$) formed a polar cluster containing some 26 unit cells, qualitatively confirming the origin of enhanced polarization.

Refined studies by Vugmeister *et al.* (1989) allowed a connection to be established between the ESR linewidth and the local polarization of Li ions. Similarly, indications on the local strain field were given by this method (Pechenyi *et al.* 1989). The quantitative analysis attempting to determine the local moments of Li was based on two assumptions: first, that the dipolar field can be described by the Lorentz correction at distances as close as a few lattice distances (Wang 1980), and, secondly, that the $3d^5$ wavefunction associated with Fe^{3+} is well localized. In view of double charge compensation, this second assumption might not be justified. Marked differences

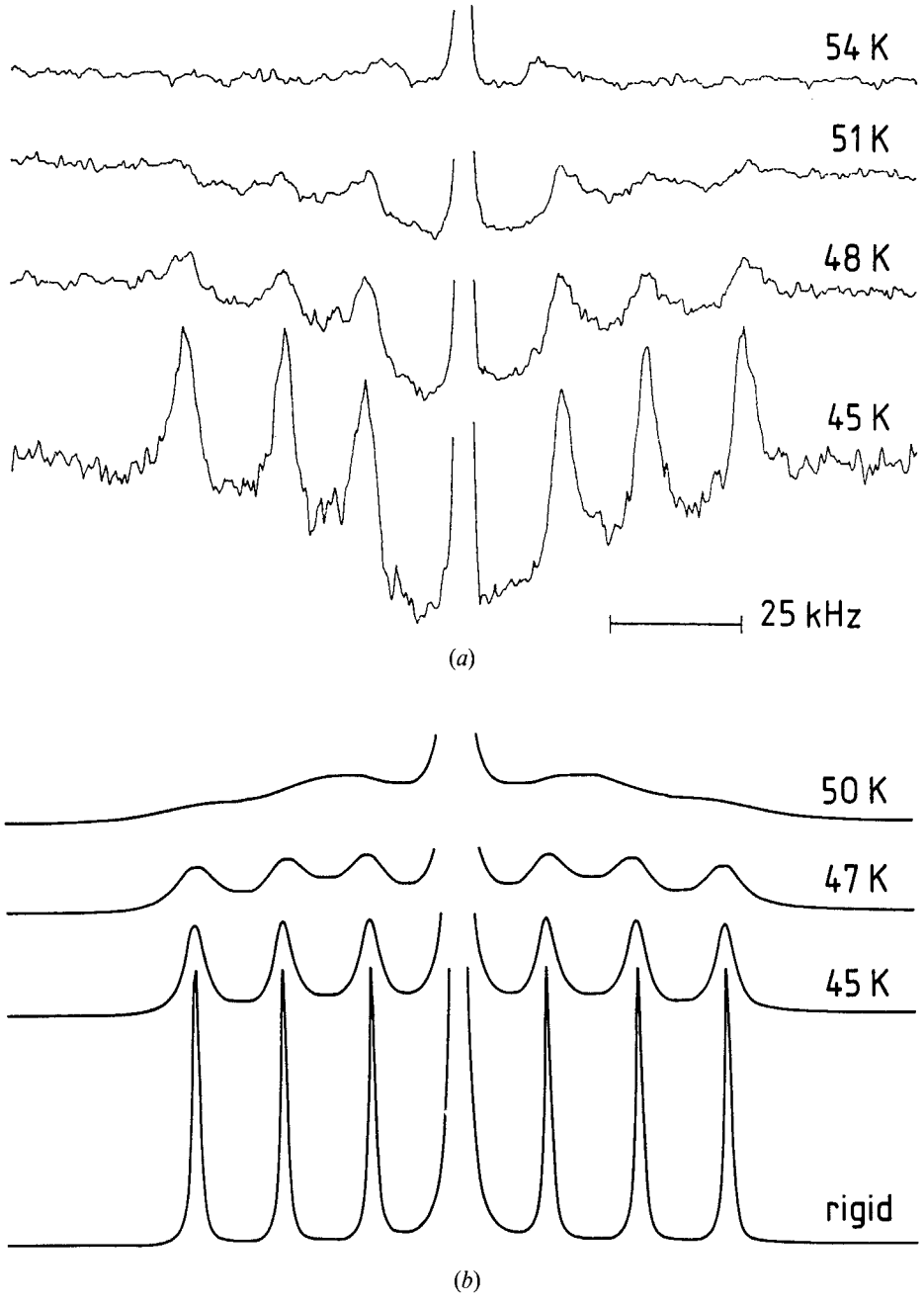

Figure 4.23. Evolution of the quadrupole-split NMR spectrum of ^{7}Li in $K_{1-x}Li_xTaO_3$ as a function of temperature for an orientation of $\mathbf{H}_0$ at 24° to the crystalline axis. (*a*) Experimental results for $x = 0{\cdot}016$. The 'hole' in which the lines lie is an experimental artefact. (*b*) Calculated results from a three-site chemical-exchange model using hopping rates derived from T_1 data for $x = 0{\cdot}016$. The bottom spectrum is the assumed 'rigid-lattice' spectrum. The agreement between the calculated and observed temperature ranges where the structure disappears, and its approximate independence of x (not shown), indicate that this is due to single-particle dynamics rather than to the polar properties of $KTaO_3$: Li. From van der Klink and Borsa (1984).

between the dynamical behaviours of Li and Nb are reported by this method (see Pechenyi *et al.* (1988), and references therein).

We believe that these studies give valuable circumstantial evidence of glass formation, but, in view of the complex impurity system, they present difficulties in interpreting electric fields quantitatively.

4.1.10. *Microscopic origin of polar configuration in $KTaO_3$: Li*

The idea of expressing the dipolar interaction of random-site dipoles in terms of probability distributions containing variance gave a correct order-of-magnitude estimate for the phase diagram in KCl : OH (section 3). This simple idea appears to give correct results for $KTaO_3$: Li, provided that the polar moment of Li is taken from the lattice-dynamical approach (confirmed by experiment), $p = 10^{-28}$ C m, and provided that the interaction is corrected by the Lorentz factor $\varepsilon_l = 10^3$. Equations (3.1) and (3.2) then predict $T_f \approx 2 \times 10^3 x$, which is roughly confirmed by experiment. This hybrid argumentation, however, fails badly for $KTaO_3$: Na, and this leaves open the question as to whether the coincidence between experiment and prediction is fortuitous. There are, in principle, three straightforward approaches to account for the polar configuration: lattice dynamics, effective interaction between dipoles as modified by coupling to soft modes, and probabilistic distributions of interactions. The first two were applied specifically to $KTaO_3$: Li and are treated below, the third is of general nature and is treated in section 10.

4.1.10.1. *Lattice-dynamical approach.* Migoni *et al.* (1976) argued that the lattice instability of $KTaO_3$ is a consequence of strong anharmonic coupling between the electronic shell of the oxygen ions and the Ta ligands. Their model accounted for the ferroelectric transition of $KTaO_3$ doped with Nb, but did not address the question of Li doping. Recently, Stacchiotti and Migoni (1990) extended the original lattice-dynamical model to Li sites and predicted an enhancement of the polar moment of Li by a factor of about 4·5 owing to a lattice contribution. This is in substantial agreement with experiment. It is plausible to assume that the effective Li–Li interaction will be enhanced by a factor of $(4{\cdot}5)^2$, and there is indeed order-of-magnitude agreement between this interaction energy and the energy associated with the transition temperature T_f,

$$\frac{xp^2}{\varepsilon\varepsilon_0 d} \approx k_B T_f(x), \tag{4.5}$$

where x is the Li concentration. The sign of the interaction depends on the relative Li positions and moments. Since these are random variables, the interactions are distributed. It remains to be shown whether these model interactions lead to a glassy, a mixed or a ferroelectric state.

4.1.10.2. *Effective interaction between moments associated with Li impurities.* Vikhnin and Borkovskaya (1978) considered this problem first and found that the range of interaction may be greatly enhanced by coupling Li displacements to soft modes. This is intuitively appealing: if a soft phonon mode is able to reorient a moment then it will align all moments along its path. These moments will thus be correlated. Vugmeister and Glinchuk (1979, 1980) subsequently applied this model to dipole moments on K sites in $KTaO_3$ and found an additional term of the form $\gamma^2 \varepsilon_0 r^{-1} \exp(-r/r_c)$, where γ is the field of the polar site excited from a soft-mode displacement of unit strength, ε_0 the susceptibility of the host and r the distance

between dipoles. This term has a tendency to order the dipoles. For uniform point-charge displacement in perovskites, $\gamma = 0$. Taking *ligand* polarizability into account, Slater (1950) established the value of this coupling with the result $\gamma = 0{\cdot}1$. The effective polar moment d^* is then given by $p^* = \frac{1}{3}p\gamma\varepsilon$. From measurements of the remanent polarization against concentration, one estimates $p^*/p \approx 6$ for both Li and Na dipoles, which leads to $\gamma \approx 0{\cdot}02$ for $KTaO_3$: Li and to 0·006 for $KTaO_3$: Na. The value of $p^*/p = 31$ for $KTaO_3$: Li quoted by Vugmeister and Glinchuk was obtained from ESR linewidths, and its quantitative reliability is difficult to assess (see sections 4 and 9). Thus it is unlikely that the VG model applied to the A sites of $KTaO_3$ gives correct dipole moments, and, according to Vugmeister and Antimirova (1990), it certainly does not apply to B sites.

A possible cause of this limitation was considered by Vugmeister (1985), who showed that anharmonicity qualitatively altered the conclusions. His considerations, however, should not influence the findings for the tiny Na displacements for which $\gamma_{exp}/\gamma_{Slater} \approx 1/20$, a feature that cannot be blamed on anharmonicity.

We believe that failure is associated with the breakdown of the soft-mode picture in the presence of large impurity concentrations: the Slater displacements are no longer plane waves, but are disturbed as well. They may be expressed in terms of Green functions obtained from the lattice dynamics with source terms at each impurity site. This picture has provided the correct enhancement factor for a single dipole and might prove to be applicable to larger lattice portions with several impurities (Stacchiotti and Migoni 1990). More recent attempts by Vugmeister and Stephanovich (1987) to construct a phase diagram—and to account for the dynamics (Vugmeister and Stephanovich 1988)—are probably fraught with the same difficulties. In addition, the virial expansion used for the latter approach is known to be limited to very small impurity concentrations (Matho 1979).

The idea of expressing local moments in terms of self-mode dressing is, however, intriguing, and our pessimism as to its applicability to $KTaO_3$ may well be unjustified for other systems.

It was pointed out by Vikhnin and Orlov (1983) that the major coupling between transverse-optical modes with moments on K sites was of quadrupolar nature, and that this makes a contribution to nuclear magnetic resonance. It may also give rise to a quadrupole ferroelastic phase, as Ivliev and Sakhenko (1986) postulated. Indeed, the coupling between a quadrupole at a K site and an ordered array of quadrupoles is allowed by symmetry, in contrast with the dipole analogue. As in the lattice-dynamical model, only detailed knowledge of the interaction forces allows one to judge whether this approach predicts condensation into an ordered or disordered state (see also Glinchuk and Smolyaninov (1990)).

Here we draw attention to two further explanations of the low-temperature configuration of $K_{1-x}Li_xTaO_3$. The first, by Vikhnin *et al.* (1988), suggests identification with an incommensurate phase; the second, by Bersuker (1988), implies the Jahn–Teller (1937) effect. Neither of these proposals presents quantitative results sufficient to assess their validity.

4.2. *Na doping*

The polar nature of $KTaO_3$: Na was first discussed by Davis (1972) and attributed to the off-centre position of Na by Yacoby and Just (1974). The ionic misfit of the Na ion in the $KTaO_3$ lattice, $(r_{Na} - r_K)/r_K = -0{\cdot}3$, is much smaller than that of Li. Accordingly, the position of Na at the K site is much less off-centre, and the associated

dipole moment is very small compared to that of Li, 0·04 eÅ for Na compared to 1 eÅ for Li (Höchli and Rigamonti 1983). As a consequence, single-ion dielectric response should be weaker by $(p_{Na}/p_{Li})^2 \approx 625$, and in fact it is not observed for Na by dielectric spectroscopy. The barrier for rotation is also dramatically reduced, enhancing the reorientation rate of Na with respect to that of Li. The weak dipoles entail weak interaction; large Na concentrations (13%) are required for collective behaviour to occur. The concentration range of interest thus extends from 13% Na upwards to where large homogeneous crystals are difficult to grow (Höchli and Boatner 1977). This proves to be a disadvantage for diffraction studies. On the other hand, fast relaxation of Na dipoles represents an advantage for dielectric spectroscopy: data taken below the relaxation branches at still finite frequencies are reasonable estimates of the static susceptibility, particularly for the nonlinear part $\partial\varepsilon/\partial(E^2)$, which in the magnetic analogue is the 'spin-glass susceptibility'.

4.2.1. *Dielectric susceptibility*

A plot of the real part of the dielectric susceptibility is given in figure 4.24 in terms of a Curie–Weiss diagram (Höchli and Boatner 1979). For concentrations up to about 20%, the data taken at 1 kHz were interpreted in terms of a modified Curie–Weiss law, $\varepsilon^{-1} \sim (T - T_c)^{\gamma}$, with $\gamma > 1$. For larger nominal concentrations, evident homogeneity problems prevent a quantitative analysis of $\varepsilon(T)$. These data together with acoustic data on the same sample (see section 4.2.3) produced a phase diagram (figure 4.25) for polar order. The curvature of the stability line near 0 K as well as the deviation of γ from 1 were attributed to quantum fluctuations of polar distributions. These phenomena have been reviewed by Höchli (1981) and are of no further concern here.

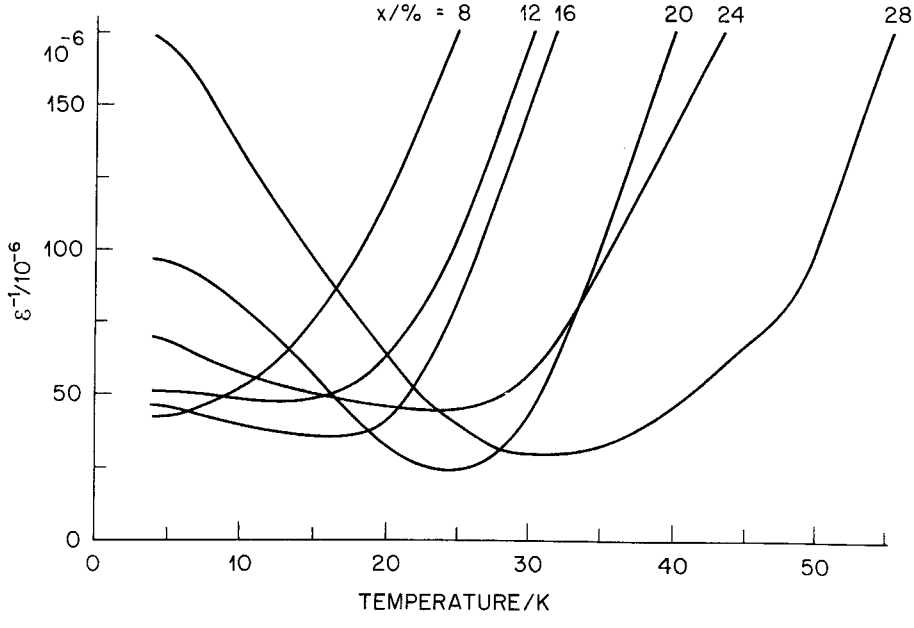

Figure 4.24. Inverse dielectric constant of $K_{1-x}Na_xTaO_3$ as a function of temperature for several values of x. The curves are labelled by the value of x in per cent. From Höchli and Boatner (1979).

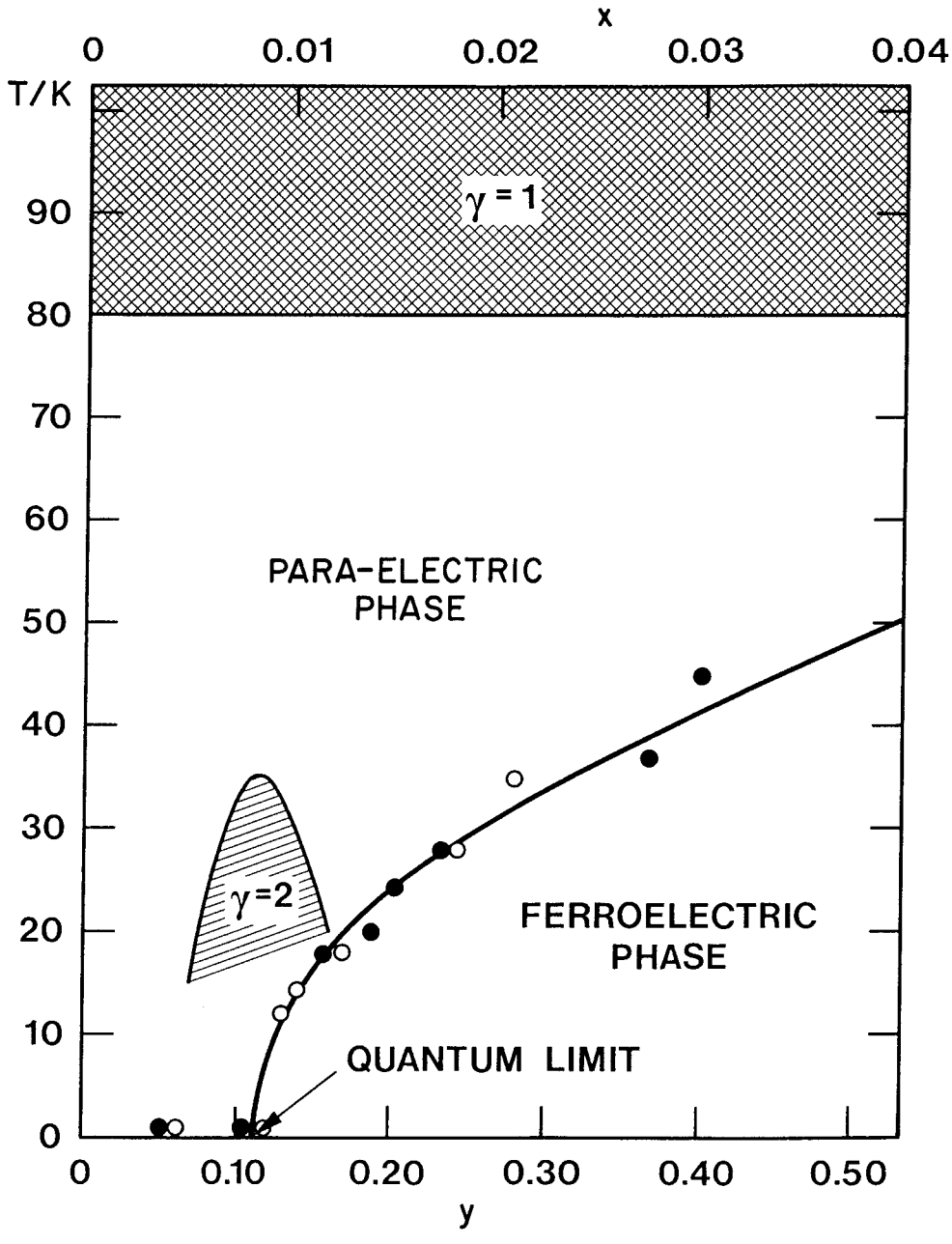

Figure 4.25. Phase diagram for $KTa_{1-x}Nb_xO_3$ (●, upper scale) and $K_{1-y}Na_yTaO_3$ (○, lower scale). The solid line is the transition line between para-electric and ferroelectric states. The cross-hatched and hatched areas indicate the temperature and concentration ranges where limiting behaviour $\varepsilon \sim (T - T_c)^{-\gamma}$, $\gamma = 1$ and $\gamma = 2$ respectively, is observed. From Rytz *et al.* (1980).

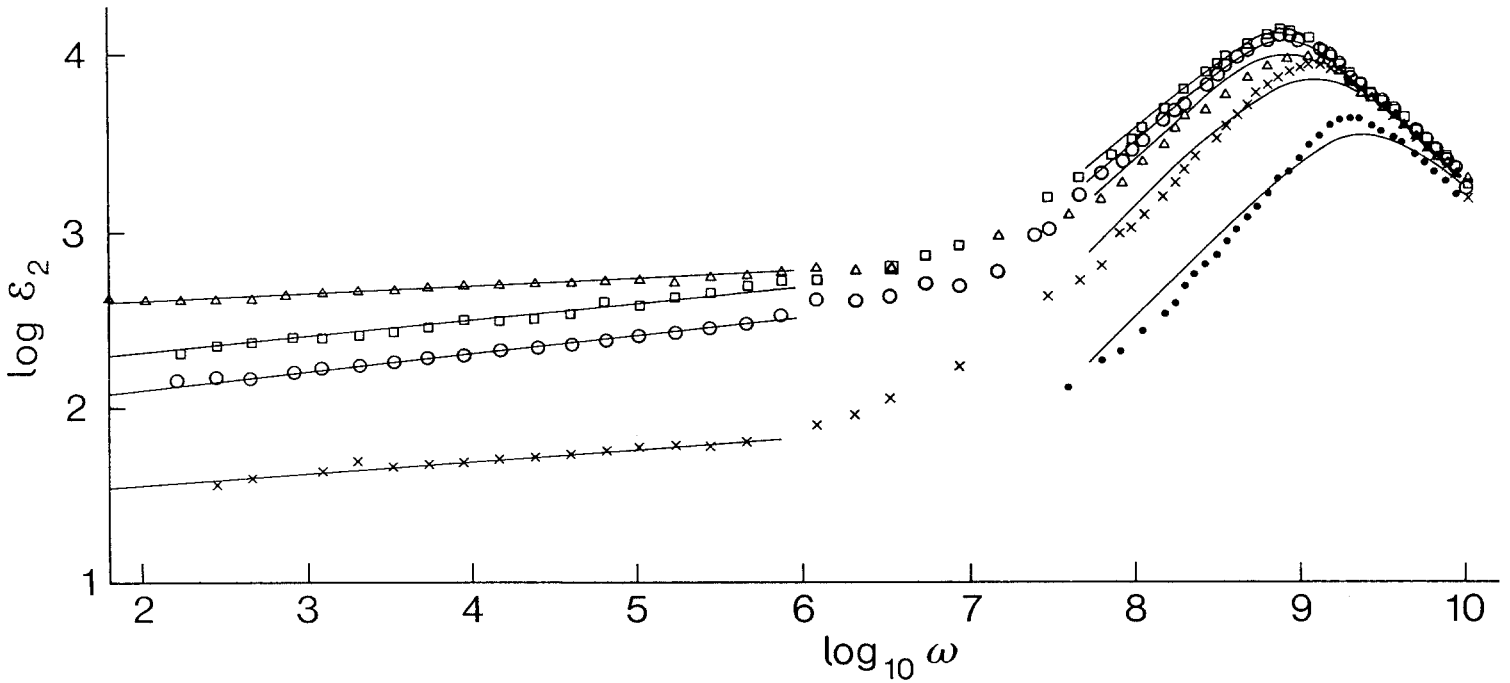

Figure 4.26. Imaginary part of the dielectric susceptibility ε_2 against log ω for $K_{0\cdot8}Na_{0\cdot2}TaO_3$. The parameter is temperature: △, 4·2 K; □, 17·5 K; ○, 20 K; x, 23 K; ●, 30 K. Solid lines for low frequency, $\varepsilon_2 \sim \omega^{\nu}$; solid lines for high frequency, $\varepsilon_2 = \Delta\varepsilon\,\omega\tau/(1 + \omega^2\tau^2)$. Parameters are $\Delta\varepsilon/10^3$ = 21, 27, 25, 18, 8, τ = 3·2, 3·9, 3·5, 3·0, 1·9 μs, and ν = 0·02, 0·09, 0·08, 0·08, 0·07 for the temperatures indicated above. From Maglione *et al.* (1986).

Owing to the lack of dispersion observed in the frequency range available at that time, the authors of these early investigations believed that the polar phase was truly ferroelectric. The discovery of properties beyond those of ferroelectricity by van der Klink and Rytz (1983) have since led to systematic investigations of the polar phase of $KTaO_3$: Na.

An observation of the susceptibility in a wide frequency range from 10 to 10^9 Hz (figure 4.26) revealed two dispersion phenomena (Maglione *et al.* 1986, 1988). The first, typically observed between 10 and 10^6 Hz, is described by an arithmetical dependence of ε_2 on ω. The exponent ν in $\varepsilon_2 = A\omega^{\nu}$ was found to depend linearly on T and to reach a maximum of about 0·1 at T_f. Such small exponents do not preclude evaluation in terms of $\varepsilon \sim \ln\omega$ except for the non-physical pole at $\omega = 0$. The amplitude of the dispersion step decreases dramatically above T_f. This phenomenon is observed only in crystals whose doping level is at least 12%, which therefore form a polar phase.

The real part of the susceptibility has been plotted in the 'conventional' representation: $\varepsilon(T)$ with ω as a parameter (figure 4.27) to underline the degree of analogy with spin glasses. At low frequencies, $\varepsilon(T)$ shows Curie–Weiss-type behaviour with $T_c < T_f$, while strong dispersion is found near T_f. Below T_f, an evaluation of $\varepsilon_1(0) = \varepsilon_s$ by means of the Kramers–Kronig relation, $\int \mathrm{d}(\ln\omega)\,\varepsilon_2(\ln\omega)$, gave evidence of T-independent behaviour, the so-called plateau located at a respectable value of 35 000. These phenomena are also restricted to above-critical Na concentrations, $x \geqslant 0{\cdot}12$. Inspection of figure 4.27 shows that the 1 kHz data are good approximations to ε_s at $T > T_f$, while at T_f they underestimate ε_s by about 10%. This has negligible consequences for the phase diagram in figure 4.25. The susceptibility was shown to depend on bias field: $\varepsilon(E) = \varepsilon(0) + \varepsilon_{NL}E^2 + O(E^4)$ (odd terms vanish by symmetry). The coefficient ε_{NL}, the nonlinear susceptibility, was evaluated as a function of temperature. It was shown to be critical in the sense of $\varepsilon_{NL} \sim (T - T_f)^{-\nu}$, with index ν substantially higher than the one that would result from mere ferroelectric behaviour. A renormalization of ε_{NL} in the spirit of Omary *et al.* (1983) yielded $\varepsilon_{NL} \approx T\varepsilon_s^4 a(T)$, with $a(T) \sim (T - T_f)^{\gamma}$, where $\gamma = 1{\cdot}7 \pm 0{\cdot}2$ (figure 4.28). On applying renormalization scenario of Pappa *et al.* (1985), γ becomes even higher. For $x < 0{\cdot}12$, no evidence for dispersion or critical nonlinearity is reported (figure 4.28).

A second relaxation mode is observed near 100 MHz (Maglione *et al.* 1986). It has nearly monodispersive (Debye-like) character for all Na concentrations $0 < x < 0{\cdot}2$. Its size *increases* with x and its rate decreases with x up to the critical concentration $x = 0{\cdot}12$. Above that concentration, this step behaves just like a relaxation mode of a conventional order–disorder transition to a ferroelectric. It has been associated with the Slater (1950) mode of the lattice, involving coherent Ta displacements.

4.2.2. *Static polarization*

As in $KTaO_3$: Li, the polarization obtained by hysteresis loops is vanishingly small. Instead, upon field cooling the sample, a sizeable remanent polarization of $12\,\mathrm{mC\,m^{-2}}$ has been obtained in $K_{0{\cdot}82}Na_{0{\cdot}18}TaO_3$. From its dependence on the applied field, it has been suggested that random fields of the order of $10\,\mathrm{kV\,m^{-1}}$ must be present in the lattice (Lanzi *et al.* 1987). An attempt was made to determine P_r from birefringence in a field-cooled sample (Banfi *et al.* 1988, 1989). The result for the optical anisotropy $\Delta n = 3 \times 10^{-5}$, when combined with the electro-optic coefficient of *pure* $KTaO_3$, yields $P_r = 45\,\mathrm{mC\,m^{-2}}$. The discrepancy between this value and that obtained by pyroelectricity suggests that the electro-optic coefficient depends on

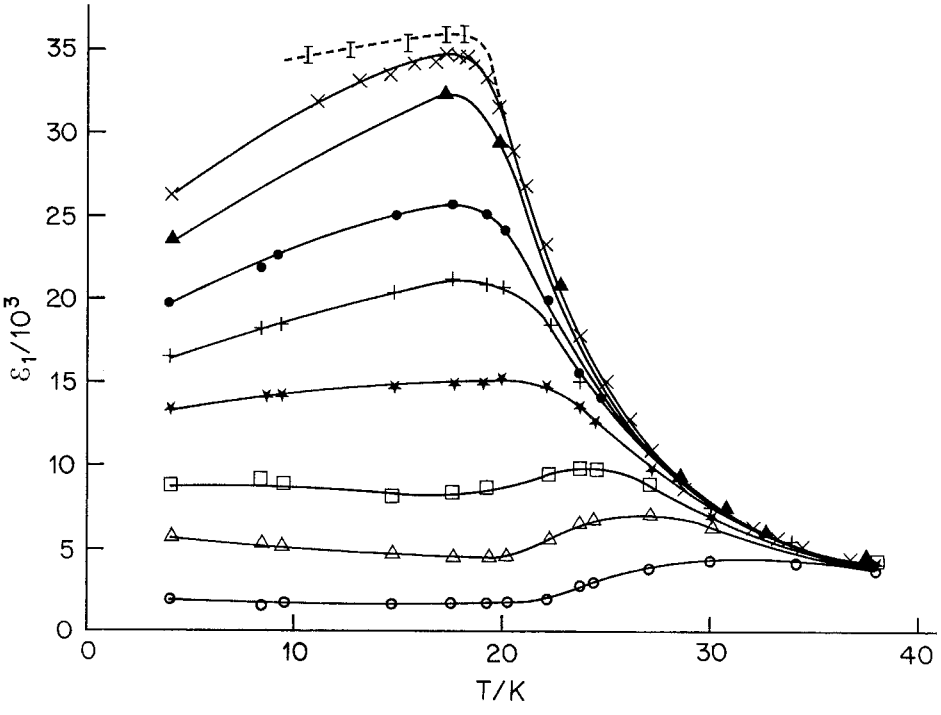

Figure 4.27. Temperature dependence of the real part of the dielectric susceptibility $\varepsilon_1(T)$ in $K_{0.8}Na_{0.2}TaO_3$. Parameter is frequency: x, 100 Hz; ▲, 1 kHz; ●, 1 MHz; +, 21 MHz; ★, 36 MHz; □, 55 MHz; △, 73 MHz; ○, 110 MHz. Note the frequency-dependent asymmetric maxima analogous to the so-called 'cusp' of spin glasses. Also shown is the static susceptibility from Kramers–Kronig analysis; note that ε_1 is nearly independent of T below T_c, in marked contrast with the Curie–Weiss prediction. From Maglione *et al.* (1986).

doping. Zero-field-cooled samples exhibit complex birefringence patterns (Lanzi *et al.* 1987) much like those in $KTaO_3$ with low Li doping (Kleeman *et al.* 1987), which do not allow an evaluation of P_r.

4.2.3. *Elasticity*

At the transition to the polar phase, the elastic compliance s_{11}, as measured by the resonance method at 300 kHz, rises by about a factor of two. The rise spreads over a considerable temperature range (figure 4.29). When expressed in terms of compositional inhomogeneity, this broad response of s_{11} accounts for a spread of the Na content in the sample, which amounts to 10% of the nominal doping. Brillouin spectra show only a small shift of elastic compliance at T_f (figure 4.30). The elastic dispersion has been evaluated in terms of a Debye function and found to yield relaxation rates of the strain that are practically identical with those of the lattice polarization for all temperatures. These relaxation rates are proportional to $T - T_c$ above T_c and roughly constant below T_c (figure 4.31).

An ultrasonic investigation was performed by Doussineau *et al.* (1989) at very low temperatures. The sound velocity v depends logarithmically on T up to 1 K and drops rapidly above this temperature. Strong anomalies were also found for the ultrasonic attenuation. Both effects are restricted to the polar phase, i.e. they occur only at

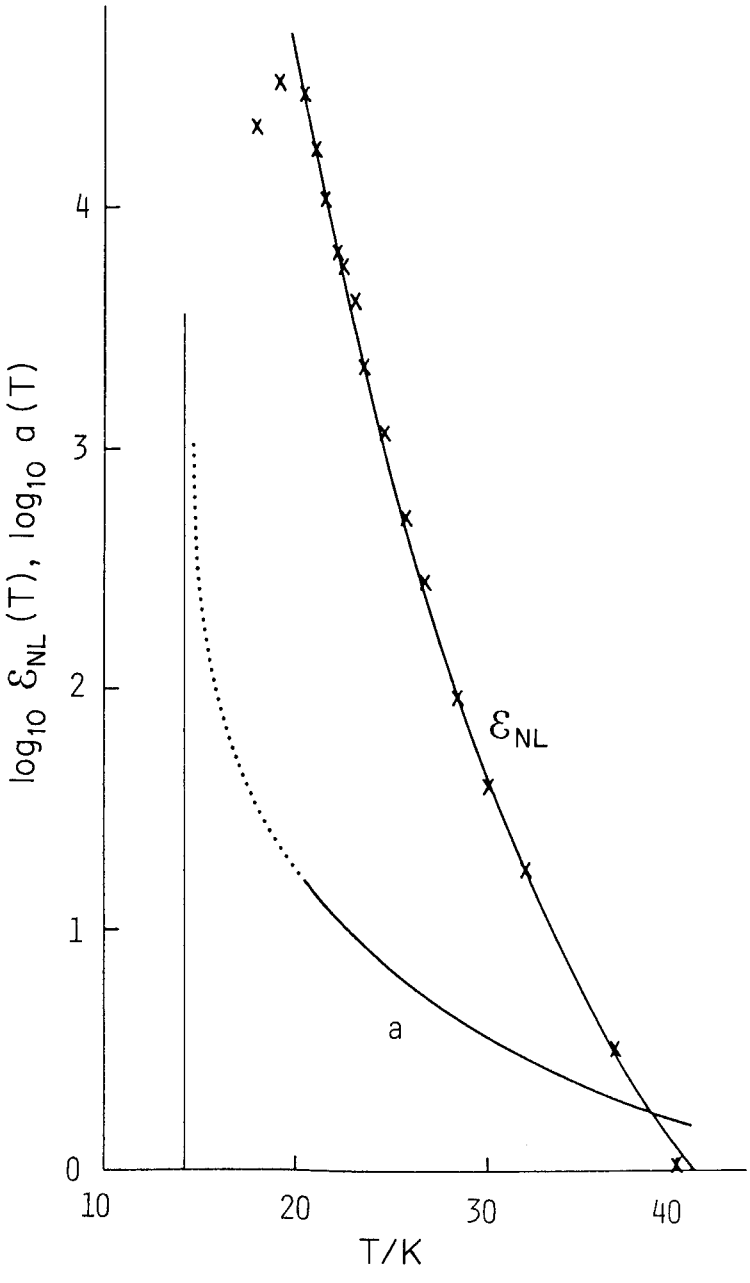

Figure 4.28. Nonlinear dielectric susceptibility $\varepsilon_{NL}(T)$ and critical coefficient $a(T)$. (——), best fits of ε_{NL} to $(T - T_f)^{-\nu}$; (· · · ·), extrapolation of $a(T) = \varepsilon_{NL}(T)/T\varepsilon_s^4$ to show critically. The sample is $K_{1-x}Na_xTaO_3$, $x = 0{\cdot}2$. From Maglione *et al.* (1986).

minimum Na concentration $x \geqslant 0{\cdot}12$ (figure 4.32). These findings are analogous to those for amorphous solids (Hunklinger and von Schickfus 1981), and were interpreted in terms of coupling between strain and two-level systems originating from local disorder. The coupling coefficient was found to be larger than that in the corresponding KBr : KCN systems (Berret *et al.* 1985, Sethna and Chow 1985), and the number of states involved in tunnelling was found to be very small.

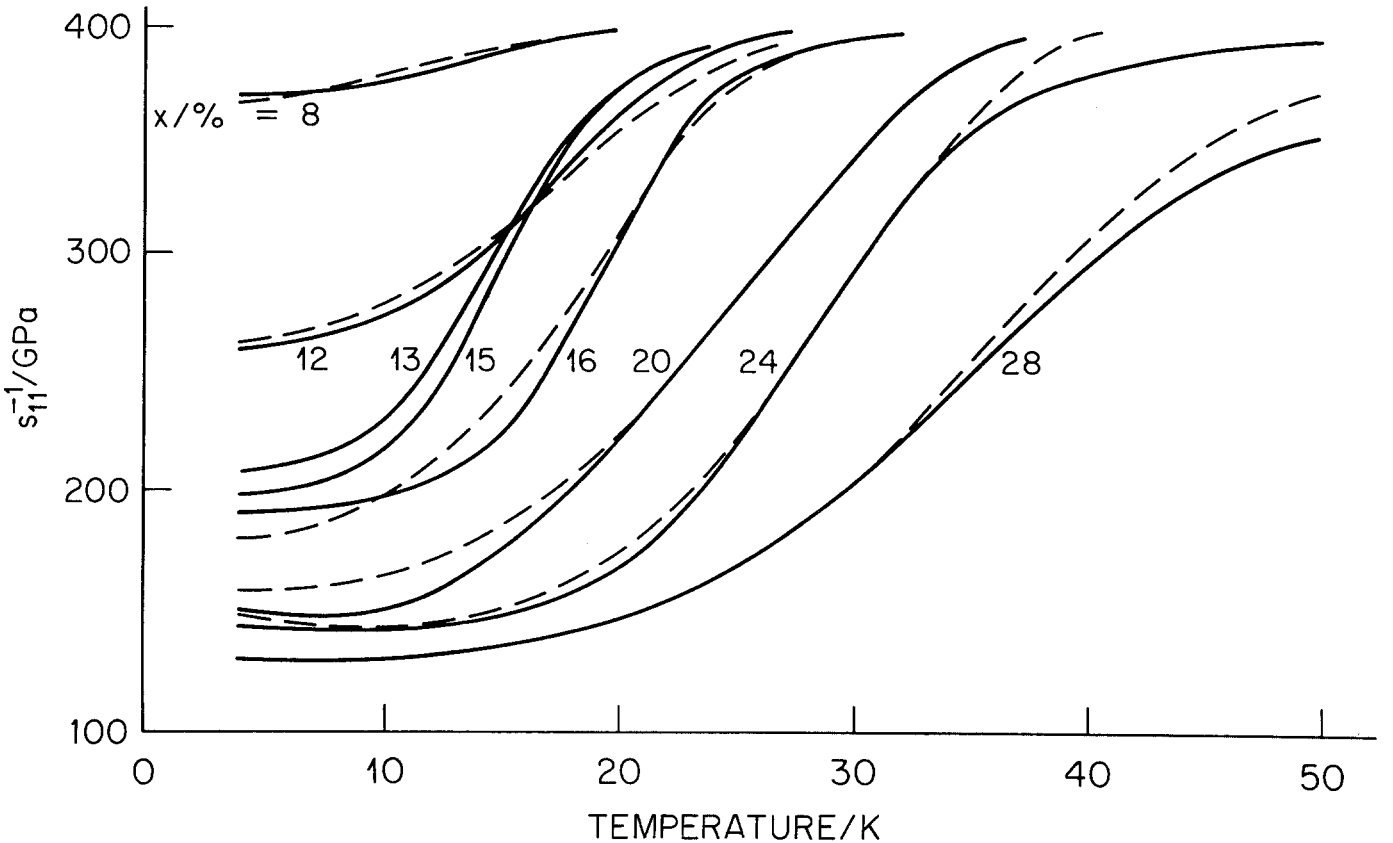

Figure 4.29. Inverse elastic compliance (——) and the fit to computed curves (– – –) for eight samples of $K_{1-x}Na_xTaO_3$. The curves are labelled by the sodium concentration x in per cent. The dashed curves were computed assuming that the transition was broadened by compositional inhomogeneity. From Höchli and Boatner (1979).

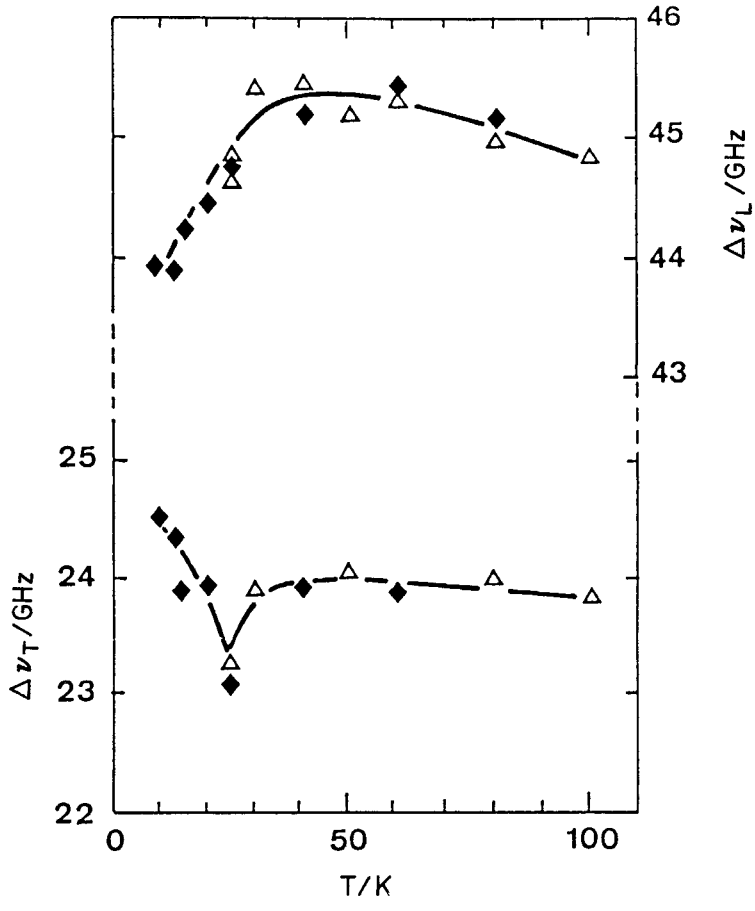

Figure 4.30. Brillouin shift in $(KTaO_3)_{0.82}Na_{0.18}$ due to longitudinal (upper curve) and transverse (lower curve) acoustic waves while lowering (△) and increasing (◆) T. From Maglione *et al.* (1988).

4.2.4. *Birefringence patterns*

In connection with second-harmonic generation experiments, Banfi *et al.* (1989) observed birefringence patterns of irregular shape in ZFC samples. Field cooling produced remanent patterns from which $P_r = 45\,\mathrm{mC\,m^{-2}}$ was deduced. This value is incompatible with the pyroelectric polarization of $12\,\mathrm{mC\,m^{-2}}$. Sources for errors are light scattering in the twinned crystal, the use of the electro-optic coefficient for pure $KTaO_3$ and generation of space charge. These patterns allowed an estimate of the quadrupolar correlation length $\xi_Q \approx 5000\,\text{Å}$ to be made.

4.2.5. *Heat capacity and conduction*

Wengenmayr (1988) found a low-temperature heat capacity in several crystals of $K_{1-x}Na_xTaO_3$, with x ranging from 0·08 to 0·24, that led to an unusually low Debye temperature. This and the long-range thermal relaxation observed in the 100 mK regime allowed low-lying tunnel states to be probed.

4.2.6. *Raman spectroscopy*

An investigation of $K_{0.82}Na_{0.18}TaO_3$ by Raman spectroscopy (Lanzi *et al.* 1987) revealed a softening of the TO mode at T_f, and a weak splitting of this mode into its

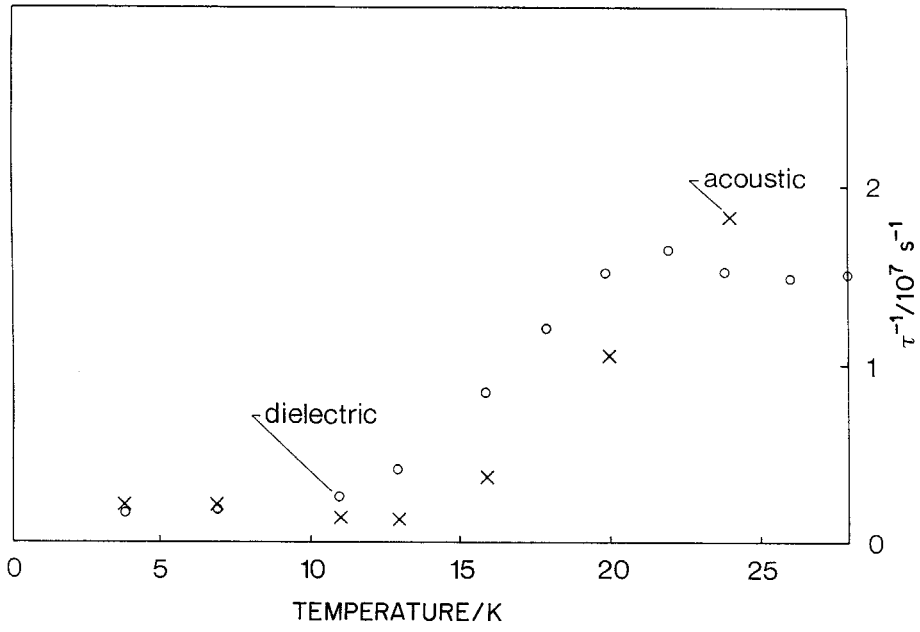

Figure 4.31. Dielectric and acoustic relaxation rates against temperature in $K_{0.8}Na_{0.2}TaO_3$. From Maglione *et al.* (1988).

A and E components. The spectra of poled and unpoled crystals were quite similar. This means that the local orientation of the crystal remained the same within at least the wavelength of light. Whereas the quadrupolar correlation length was thus given as several thousand Ångström units, correlation between $\pm$ polar order cannot be resolved by Raman spectroscopy (at least for this symmetry).

4.2.7. *Second-harmonic light generation*

Instead, an investigation on the basis of second-harmonic light generation resolves polar structure (Banfi *et al.* 1988, 1989). Evaluation of the linear optical retardation and of the efficiency of second-harmonic generation on the same sample, in connection with calibration of the apparatus with an ammonium dihydrogen phosphate crystal, allowed the polar correlation length to be determined (figure 4.33).

4.2.8. *X-ray and neutron diffraction*

Investigations by X-ray and neutron diffraction showed no sign of a transition (Maglione *et al.* 1989, K. Knorr and U. T. Höchli, unpublished data), either from the intensity of the scattered beam at the Bragg position or from diffuse scattering. In view of the resolution of the diffractometer used in the X-ray experiment, this sets a limit to the static displacement of Ta with respect to oxygen (the Slater (1950) displacement) at 10^{-3} Å in the polar phase.

4.2.9. *Local properties*

Following van der Klink and Rytz's (1983) discovery that the magnetic moment of the Na nucleus does not show critical relaxation at the polar transition (in contrast with Nb), more detailed investigations were aimed at detecting its role.

Höchli and Rigamonti (1983) found that the relaxation rate of ^{23}Na in $KTaO_3$ is equal to that in NaCl above 200 K. Below this temperature, the relaxation rate is

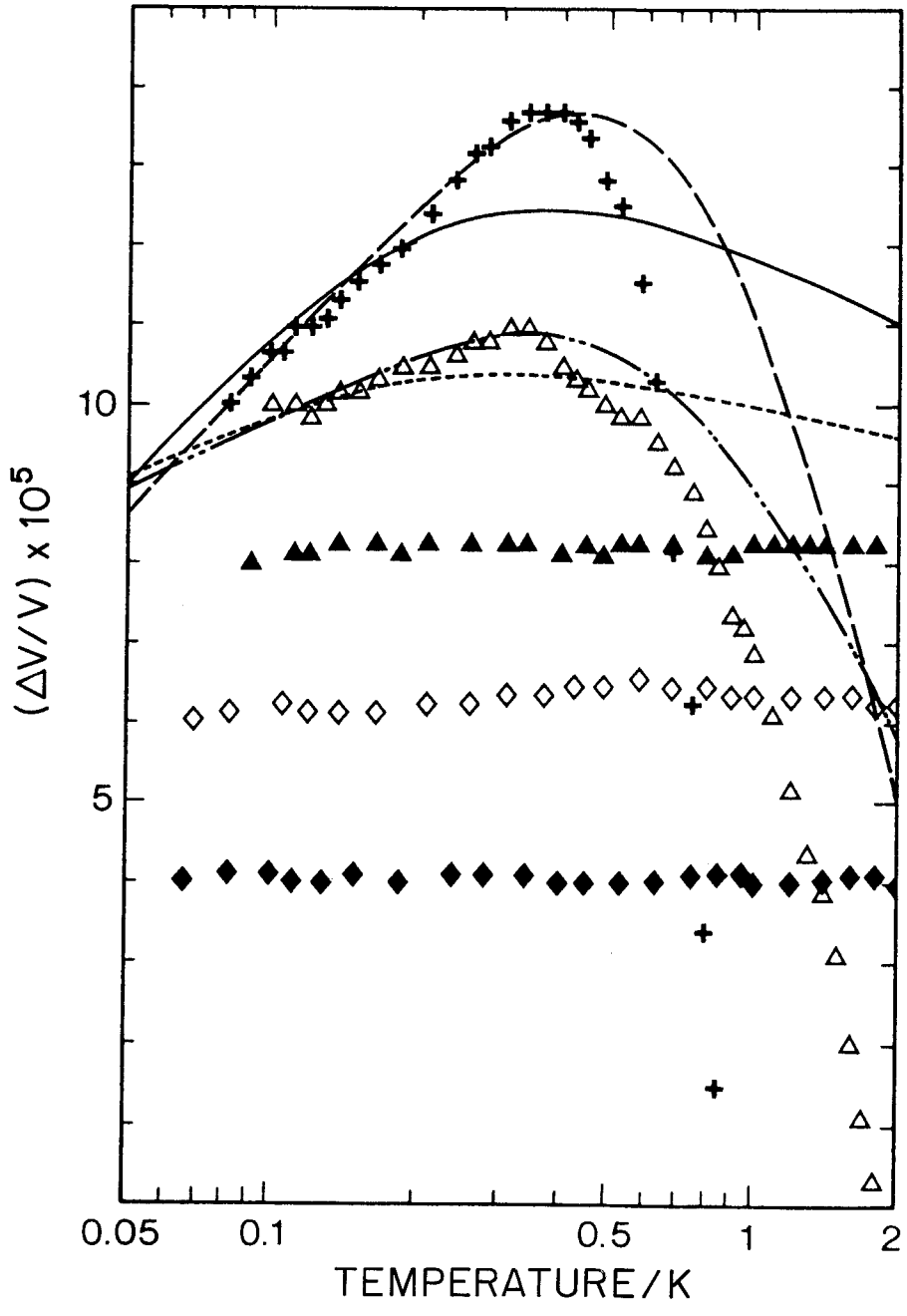

Figure 4.32. Relative change of sound velocity of longitudinal waves propagating along the [100] axis of five samples of $KTaO_3$ and Li- and Na-doped $KTaO_3$. The experimental sets of data are shifted arbitrarily relative to each other. Theoretical curves are from equations (20) and (28) of Hunklinger and von Schickfuss (1981). For the 22% Na sample: (——), flat distribution ($\mu = 0$); (– – –), modified distribution ($\mu = \frac{3}{2}$.) For the 15% Na sample: (· · ·), flat distribution ($\mu = 0$); (· · – · · –), modified distribution ($\mu = \frac{3}{2}$). +, $KTaO_3$: Na 22%, 445 MHz; △, $KTaO_3$: Na 15%, 349 MHz; ▲, $KTaO_3$, 435 MHz; ◇, $KTaO_3$: Li 2.5% 906 MHz; ◆, $KTaO_3$: Li 5%, 500 MHz. From Doussineau *et al.* (1989).

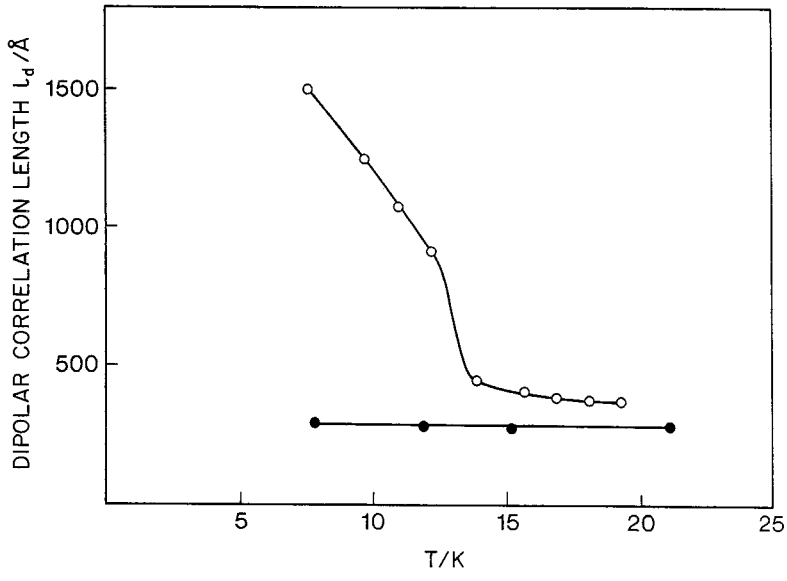

Figure 4.33. Polar coherence length of $KTaO_3$: Na against temperature: ●, 12% Na; ○, 15% Na. The 15% doped sample undergoes a transition to a polar phase when viewed with dielectric methods; the 12% doped one does not. From Banfi *et al.* (1989).

accelerated in $KTaO_3$: Na with respect to that in NaCl by several orders of magnitude and is also dependent on the Larmor frequency (Rigamonti and Torre 1985). Hence it was concluded that Na is centred above 200 K and displaced (by as little as 0·04 Å) below that temperature. This scenario confirms predictions by Höck *et al.* (1979).

Evidence for the metastability of $K_{1-x}Na_xTaO_3$ was provided by Rigamonti and Torre (1985, 1986) and Torre and Rigamonti (1987) on the basis of history-dependent NMR spectra. Interestingly, in the window from 10^4 to 10^6 s covered in this study, it is largely the low-doped samples that show hysteresis effects after quenching. A systematic evaluation of the relaxation rate as a function of Larmor frequency and temperature led to the determination of an effective barrier between equivalent Na positions, $E_b \approx 200$ K, and their distribution width or variance $\mathrm{Var}(E_b) \approx 150$ K. They also determined the tunnelling parameters for such potentials and found that not only Na was involved in the tunnelling process but also a portion of the lattice, some two orders of magnitude larger than the unit cell. On the other hand, only a few centres, about 1%, were involved in the NMR relaxation process. This view and that expressed by Doussineau *et al.* (1989) on the basis of ultrasonic propagation coincide at least qualitatively: tunnelling units are clusters containing many Na ions, and the number of such units is far below the number of Na ions in the crystal.

4.3. *Nb doping*

Unlike Li and Na, which replace K, the dopant Nb occupies the Ta site and has a negligible ionic misfit. The resulting mixed crystal of potassium tantalate niobate (KTN) was investigated using standard methods (Lines and Glass 1977, Rytz 1983) and regarded as an ordered ferroelectric until Samara (1984) discovered dielectric dispersion upon applying hydrostatic pressures. He attributed his observations to glass-like disorder effects and thus prompted a search for other evidence of disorder.

We review in particular recent experiments but also some early observations with a critical view to possible disorder effects that might have gone unnoticed at the time.

4.3.1. *Dielectric susceptibility*

Plots of ε^{-1} *versus* T (Höchli *et al.* 1977) revealed evidence for a transition to a polar phase for samples containing at least 0·8% Nb. The transition temperature T_c depends on x as shown in figure 4.25, and since no dispersion was detected, the low-temperature phase was considered ferroelectric. The particular form of the susceptibility curves $\varepsilon \sim (T - T_c)^{-\gamma}$, $\gamma > 1$, and of the phase diagram $T_c \sim (x - x_c)^{1/2}$ led Rytz *et al.* (1980) to assess the role of quantum fluctuations of the polarization in this compound. Dielectric dispersion was subsequently observed at 100 MHz. The fact that the relaxation mode was monodispersive and slowed down critically at T_c led to the conclusion that the transition was of order–disorder type (Höchli and Maglione 1989). Accordingly, the low-temperature phase should have long-range order (Lines and Glass 1977). This statement was contradicted by Samara (1984). He investigated the dielectric response at hydrostatic pressure and found dielectric dispersion at kilohertz frequencies (figure 4.34). He expressed his results in terms of an activation

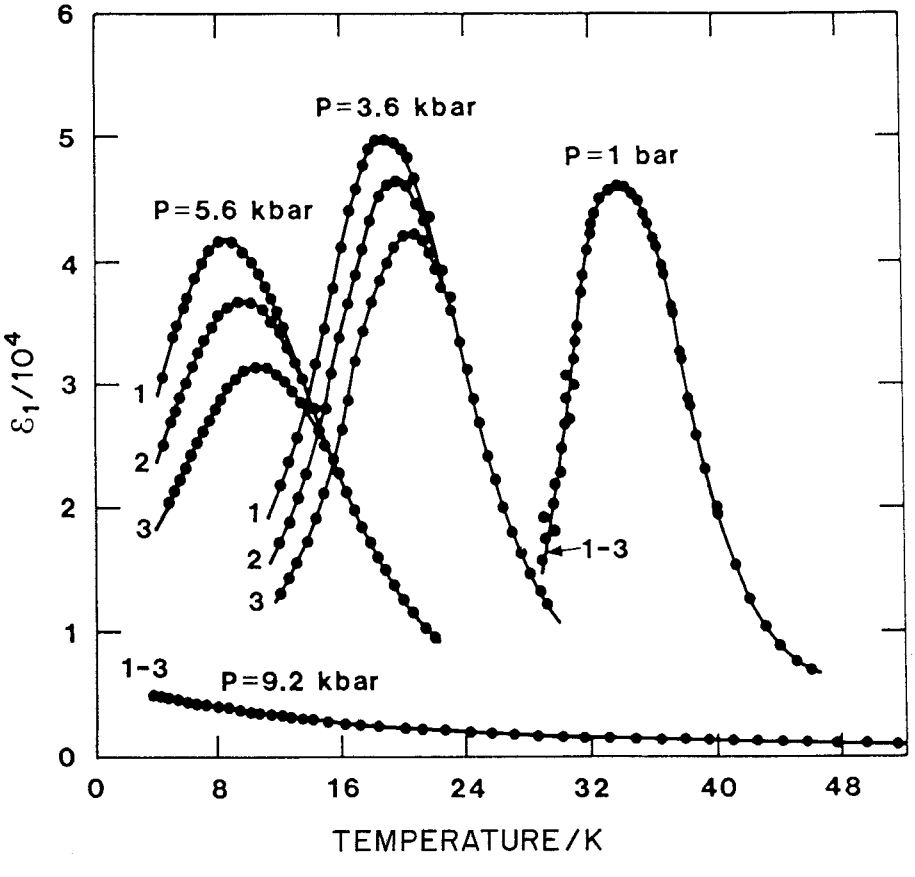

Figure 4.34. Isobars of the temperature dependence of the real part of the dielectric constant (ε_1) at different frequencies for a dilute KTN crystal ($KTa_{0.98}Nb_{0.02}O_3$): (1) 100 Hz; (2) 10 kHz; (3) 1 MHz. Note the pressure-induced frequency dispersion and the suppression of the $\varepsilon_1(T)$ anomaly at high pressure (9·2 kbar). From Samara (1988).

energy decreasing with pressure like $E_b \exp(-p/p_0)$, where $E_b \approx 1$ eV and $p_0 \approx 1$ kbar. The attempt frequencies necessary to fit the temperature-dependent relaxation times, however, are unphysically high, a deficiency that Samara (1985) tried to remedy by assuming distributions of relaxation times. His conclusion was that Nb ions under pressure were off-centre for times up to milliseconds and that they formed clusters with distributed relaxation characteristics. Extrapolating to zero pressure, Samara suggested that Nb stays off-centre for infinitely long times and that correlation was restricted to microscopic ranges. These are ingredients for a dipole glass.

Sommer *et al.* (1989) reported enormous dielectric dispersion in the kilohertz region in $KTaO_3$ doped with 0·6 and 2·1% Nb at ambient pressure and at all temperatures. The data are at variance with data by Samara (1984) and Höchli and Maglione (1989), who found that ε is essentially non-dispersive up to at least 100 kHz over a wide temperature range. Since the relaxation time from Sommer *et al.* (1989) varies by less than two orders of magnitude when T rises from $\frac{1}{2}T_c$ to $2T_c$, it follows from the Samara proposal that the polar clusters are destabilized by internal strain. Lyons *et al.* (1987) reported nonlinear behaviour near T_f in $KTa_{0.991}Nb_{0.009}O_3$. They found that the harmonics $P(v\omega)$, $v = 2, 3, \ldots$, generated by the field $E(\omega)$ depend in a non-trivial way on the strength of $E(\omega)$ and also reported a dependence of the polarization on time. They analysed the frequency-dependent polarization in terms of

$$P = \xi E + \operatorname{sign}(E)\beta E^2.$$

Nonlinear polarization behaviour was found, which Lyons *et al.* (1987) called 'non-analytical' because of apparent discrepancies with harmonic generation. Levi and Ogielski (1986) studied nonlinearity in the presence of dispersion for the spin glass Ag : Mn. They gave explicit results for dynamic scaling that imply that the length scale probed by spin–spin correlation changes with frequency. This behaviour might be connected with strongly field-dependent or field-induced dispersion (Höchli *et al.* 1984). In the presence of dispersion, the definition of the spin-glass susceptibilities in terms of

$$P_s = \sum_n a_n E^{2n+1}$$

is indeed non-unique. In view of the differences of the experimental set-up and evaluation techniques from those of Omary *et al.* (1983), Pappa *et al.* (1985) and Maglione *et al.* (1986), it remains to be shown to what extent the behaviour of KTN is qualitatively different to that of spin glasses.

4.3.2. *Static polarization*

Conventional hysteresis loops have been observed by Boatner *et al.* (1977a) in KTN at temperatures below T_f and at frequencies of order 0·1 Hz and fields of about 60 kV m^{-1} (figure 4.35). KTN is then the only compound on the $KTaO_3$ basis known so far that has a spontaneous (rather than just a remanent) polarization. Its size and its dependence on x and T are comparable to that of $K_{1-x}Li_xTaO_3$. Hysteresis loops taken at the more customary frequency of 50 Hz showed only partial polarization.

4.3.3. *Acoustic properties*

The low-frequency elastic compliance s_{11} measured in dilute KTN (Höchli *et al.* 1977, Rytz *et al.* 1983) shows a step reminiscent of a classical ferroelectric phase transition superimposed on a Curie–Weiss-type dip near T_f (figure 4.36). The

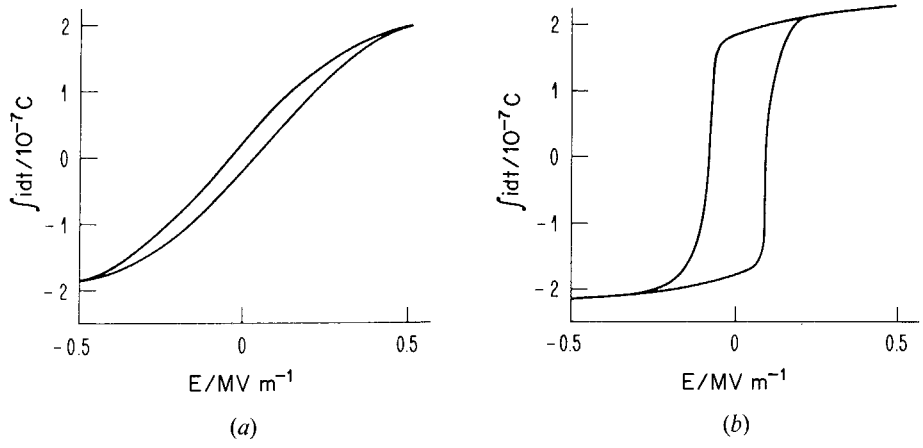

Figure 4.35. Hysteresis loops for $KTa_{0.98}Nb_{0.02}O_3$: (*a*) $f = 50$ Hz: (*b*) 2·5 mHz. Note that only the low-frequency hysteresis loop is reasonably square, such as to determine the spontaneous polarization. From Boatner *et al.* (1977a).

amplitude of this dip (the elastic analogue of the Curie constant) increases in proportion to T_c and has been regarded as evidence of a cross-over from quantum to classical ferroelectricity (Höchli 1981). Light scattering has been used to probe the gigahertz region of acoustic propagation (Lee *et al.* 1985).

Three phonon modes have been detected above T_f, which split into more modes below T_f unless an electric field is applied in the $\langle 111 \rangle$ direction. Except for splitting at $E = 0$, the modes do not depend appreciably on temperature (figure 4.37). Comparison of these findings with the behaviour of s_{11} at low frequencies leads to the conclusion that the elastic response is strongly dispersive between 10^5 and 10^{10} Hz. Furthermore, since phonon propagation is still possible below T_f, where multidomain or cluster structures form, one can safely conclude that quadrupolar correlation extends at least to the wavelength of light, 5000 Å.

4.3.4. *Birefringence patterns*

Birefringence patterns were also obtained, but, in view of the trigonal symmetry of the low-temperature phase, domain walls cannot be resolved properly (Rytz 1983). On the basis of birefringence measurements on selected quasi-homogeneous parts of the crystal, Kleeman *et al.* (1985) attempted to separate the fluctuating parts of the optical anisotropy from the static part. They state that for short-range ordered polarization with $\langle p_z \rangle = 0$ and $\langle p_z^2 \rangle \neq 0$, no linear birefringence is expected. As pointed out by Chase *et al.* (1982) and Andrews (1985), this is incorrect. Accordingly, their conclusion as to the range of order does not refer to polarization but to strain. They observe a striking drop in the refractive index below T_f. It is natural to associate this with the onset of light scattering at twin boundaries (Liddell 1981).

4.3.5. *Heat capacity*

Heat-capacity (Lawless *et al.* 1981) and heat-conduction data (Salce 1981) provided no evidence for an anomaly at T_f, but did reveal two terms, one linear and one quadratic in temperature. These terms are reminiscent of a distribution of two-level systems associated with glassy disorder. The absence of an anomaly in the specific-heat (Lawless *et al.* 1981) as well as in heat-conduction experiments is in

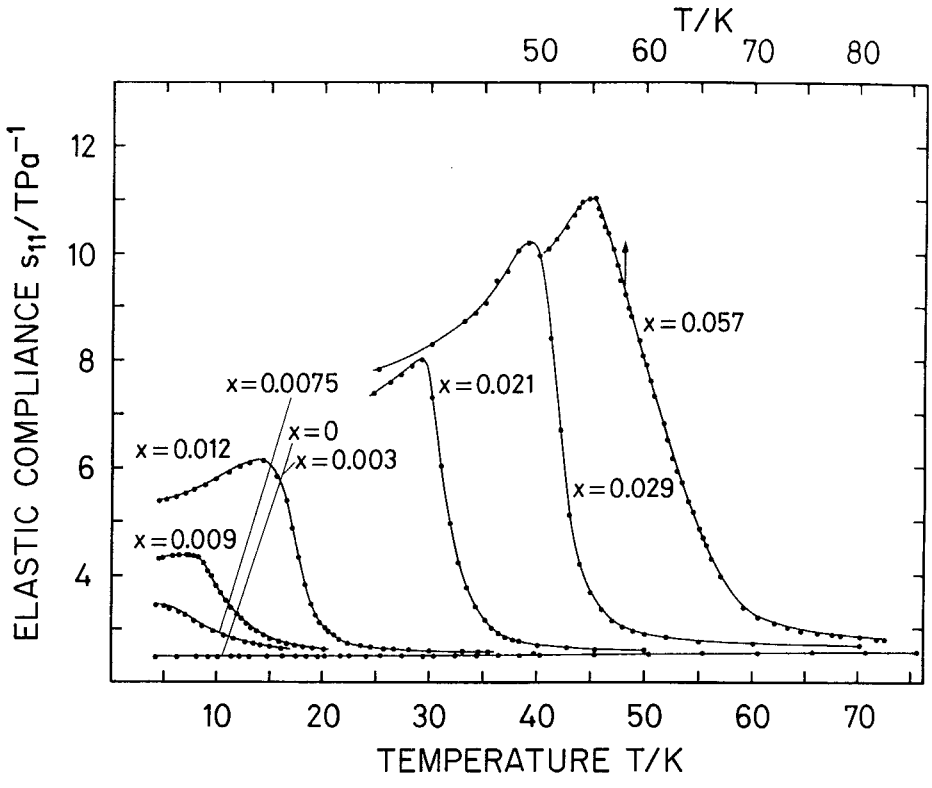

Figure 4.36. Temperature dependence of the elastic compliance s_{11} of $KTa_{1-x}Nb_xO_3$, with concentration x as a parameter. The data were obtained under a bias field $E_{dc} \approx 10\,kV\,m^{-1}$ applied after cooling. The temperature was changed at a rate of no more than $0{\cdot}5\,K\,min^{-1}$. Note the change of temperature scale for $x = 0{\cdot}057$. From Rytz *et al.* (1983).

contrast with the presence of two-level systems and remains unexplained (de Goër *et al.* 1980), as is also the case for spin glasses.

4.3.6. *Raman spectroscopy*

On the basis of Raman-scattering data, Yacoby (1978) suggested that correlated volumes of odd-symmetry distortions exist in KTN. A detailed analysis of Raman spectra by Uwe *et al.* (1986) in pure crystals led to a determination of correlated distortions as in KTN. The correlation volume was maximum at T_c, namely 4000 Å^3, and correlation persisted over at least 100 ps (figure 4.38). The presence of fluctuations was confirmed and evidence for disorder was provided by quasi-electric light-scattering observations (Prater *et al.* 1981a–c). They found a transverse-optical mode whose frequency decreases when $T \to T_c$ but remains non-zero at T_c. The value $\omega(T_c)$ grows with concentration. Lee *et al.* (1985) established these Nb fluctuations in detail and predicted that collective off-centre Nb modes would leave traces in the dielectric behaviour of KTN.

Lyons *et al.* (1986) reported similar behaviour in a sample doped with 0·9% Nb. They stated that the dielectric dispersion observed by Samara (1984) in the same sample pertains to the same relaxing polar entity, and from a plot of the leading relaxation rate against T they found an extrapolated temperature of 3 K (far below

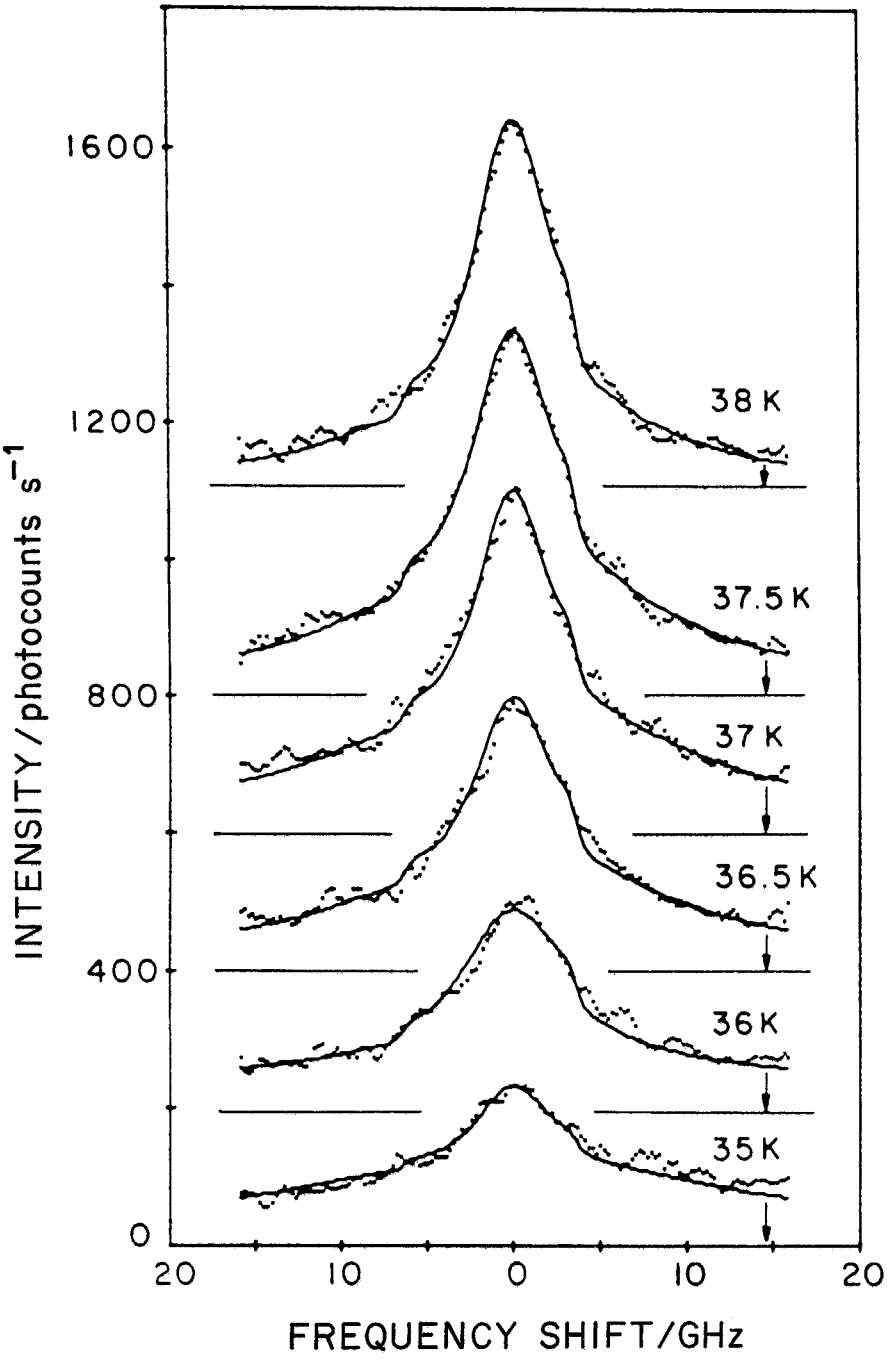

Figure 4.37. Reconstructed central-peak Raman spectra fitted to the sum of two Lorentzian functions. The value of T_c is 37·5 K. The width of the Lorentzians are T = 38 K, Γ_1 = 1·51 GHz, Γ_2 = 9·8 GHz; 37·5 K, 1·53 GHz, 10·3 GHz; 37 K, 1·33 GHz, 12·4 GHz; 36·5 K, 1·51 GHz, 12·4 GHz; 36 K, 2·53 GHz, 18·6 GHz; 35 K, 2·9 GHz, 41 GHz. The sample is KTN. From Lee *et al.* (1985).

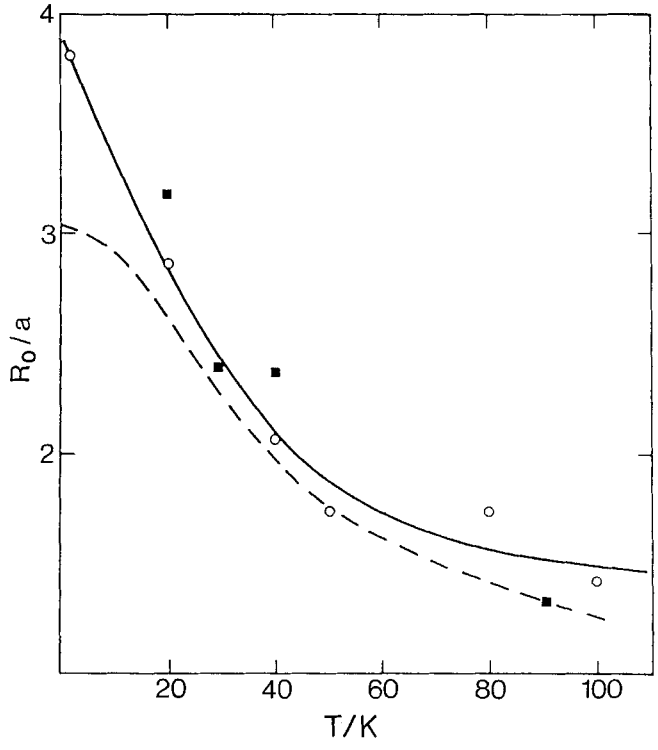

Figure 4.38. Size of the microscopic ferroelectric regions as a function of temperature, determined by experimental spectra. The open circles refer to nominally pure $KTaO_3$, for which the solid curve is a guide to the eye. The solid squares are determined by the same procedure for the 0·9% Nb-doped sample. The dashed curve is the result of the analysis of the KTN phase diagram. From Uwe *et al.* (1986).

the transition at 10 K) at which this polar entity freezes out. We believe that the central-peak phenomena observed at 1 GHz by Lee *et al.* (1985) and then by Lyons *et al.* (1986) are connected to the lattice-relaxation mode observed by Maglione *et al.* (1989) near 1 GHz, rather than to Samara's feature in the kilohertz region (figure 4.39). This feature, as proposed by Lyons *et al.* (1986), is in the frequency domain for polarization reversals (Boatner *et al.* 1977a) and might thus be due to domain-wall motion. A summary of these features, which leave some questions open, is given in figure 4.39.

Kugel *et al.* (1984) confirmed the existence of a soft TO mode by hyper-Raman experiments. In these experiments, phonon-induced scattering is observed off the second-harmonic of the light beam. In this way, they observed photons, whose generation is symmetry-forbidden for conventional Raman scattering. A detailed study of these spectra by Kugel *et al.* (1988) mainly served to establish the validity of the Migoni–Bilz–Bäuerle (1976) model of ferroelectricity. Of greater importance in the context of glasses is their statement that off-centre Nb (and we include Ta) freezes out above the transition, implying a time scale longer than Raman resolution, 1 ns, and correlation over at least $\lambda \approx 5000$ Å.

4.3.7. *Second-harmonic light generation*

Kugel *et al.* (1984) found an enormous increase in signal intensity for second-harmonic generation as they lowered the temperature from $T_f + 10$ K to T_f (figure 4.40).

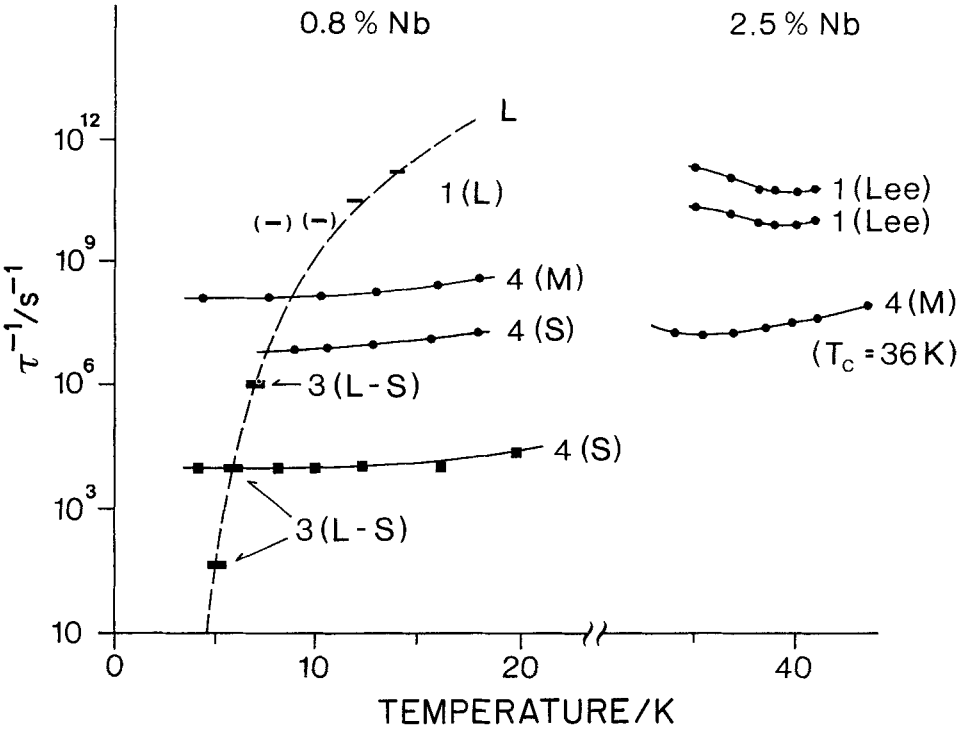

Figure 4.39. Relaxation modes in KTN. The first label gives the size of the relaxation step in decades (approximate); the second label gives the author (L, Lyons *et al.* (1986); S, Sommer *et al.* (1989); L, Lee *et al.* (1985); M, Maglione *et al.* (1989); L-S, interpretation by Lyons *et al.* (1986) of Samara's (1985) data). The dotted line is by Lyons *et al.* (1986); solid lines are guides to the eye. ●, monodispersive mode; ■, polydispersive mode. There appear to be some discrepancies, particularly between S and L-S data sets. It is unlikely that the L feature is involved in the freezing process. The dotted line proposed by L crosses (several) relaxation peaks three decades stronger than the L feature.

In this range, inversion symmetry breaks spontaneously at a scale that at T_f is at least comparable for $\lambda \approx 5000$ Å.

4.3.8. *Diffraction*

A study of X-ray diffraction on $K_{0\cdot983}Nb_{0\cdot017}TaO_3$ by Andrews (1985) revealed no distortion of the crystal (larger than $c/a - 1 = 10^{-4}$) below T_f (figure 4.22). On the other hand, critical inelastic scattering was detected with an intensity maximum at T_c. The findings were considered compatible with the standard domain-wall model for ferroelectrics. From extended X-ray absorption fine-structure (EXAFS) measurements, Hanskepetitpierre *et al.* (1986) concluded that the Nb position is off-centre along ⟨111⟩ by as much as 0·15 Å in a sample containing 9% Nb. The displacement was found to be independent of T up to room temperature; indications as to time scales are lacking. A study of KTN by scanning electron microscopy and X-ray topography has shown that the domain structure of KTN bears some resemblance to that of $BaTiO_3$, at least when $x > 0\cdot05$. In view of the shallow penetration depth of the source radiation, these findings were thought to be pertinent to the surface layer (Ansermet *et al.* 1981) rather than to the bulk (Buffat *et al.* 1986).

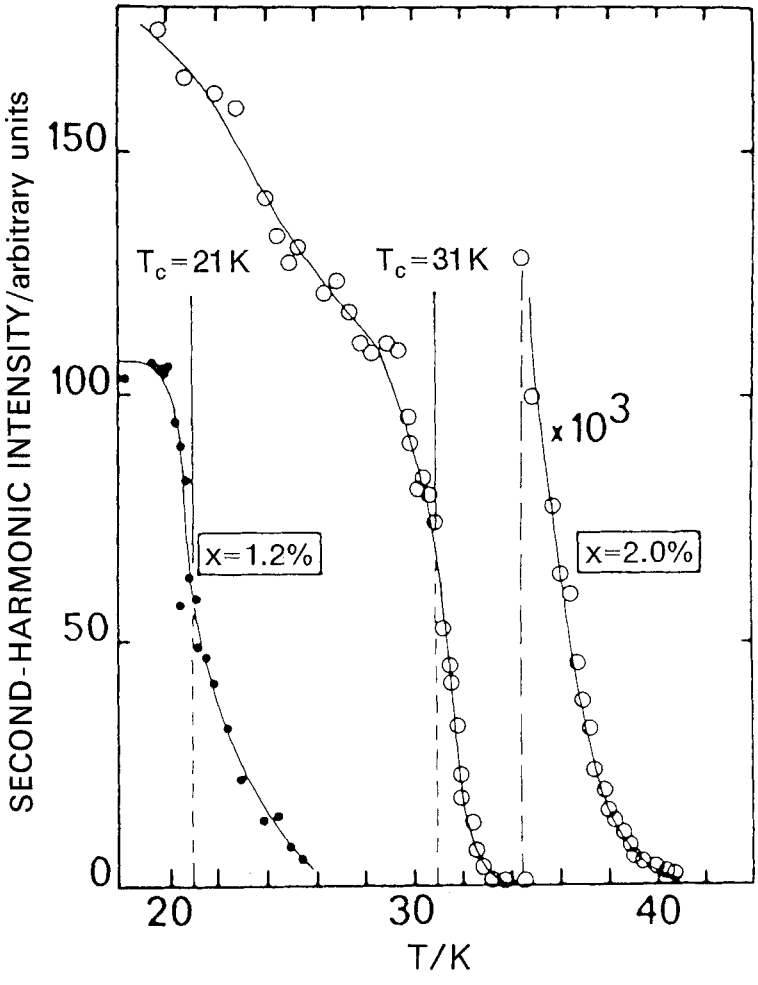

Figure 4.40. Second-harmonic-generation intensity in $KTa_{1-x}Nb_xO_3$ (x = 0·01 and 0·02) as a function of temperature. Note the enormous increase upon crossing T_c, providing evidence for the establishment of (reasonably) long-range order. From Kugel *et al.* (1984).

4.3.9. *Local properties; nuclear magnetic resonance*

van der Klink *et al.* (1986) followed the evolution of ^{39}K, ^{93}Nb and ^{181}Ta magnetic resonances through T_f. They found that magnetic transitions whose energies depend on the Nb position are wiped out below T_f, and concluded that Nb fluctuates around the centre position at a rate exceeding $10^4 s^{-1}$ above T_f, whereas it stays off-centre longer than that below T_f. Both ^{93}Nb and ^{39}K show critical relaxation (figure 4.41) as found in classical ferroelectrics. From the peculiar behaviour of the ^{181}Ta resonance, they arrived at the conclusion that Nb generates clouds of polarized regions that are about 100 lattice cells large. They attributed the critical relaxation to the low-temperature-phase ferroelectric order and argued that the fluctuation polarization clouds induce forced vibrations of the lattice at its soft-mode frequency. They set an upper limit of $\delta < 0{\cdot}15$ Å and stated that this shift was non-zero within a time interval

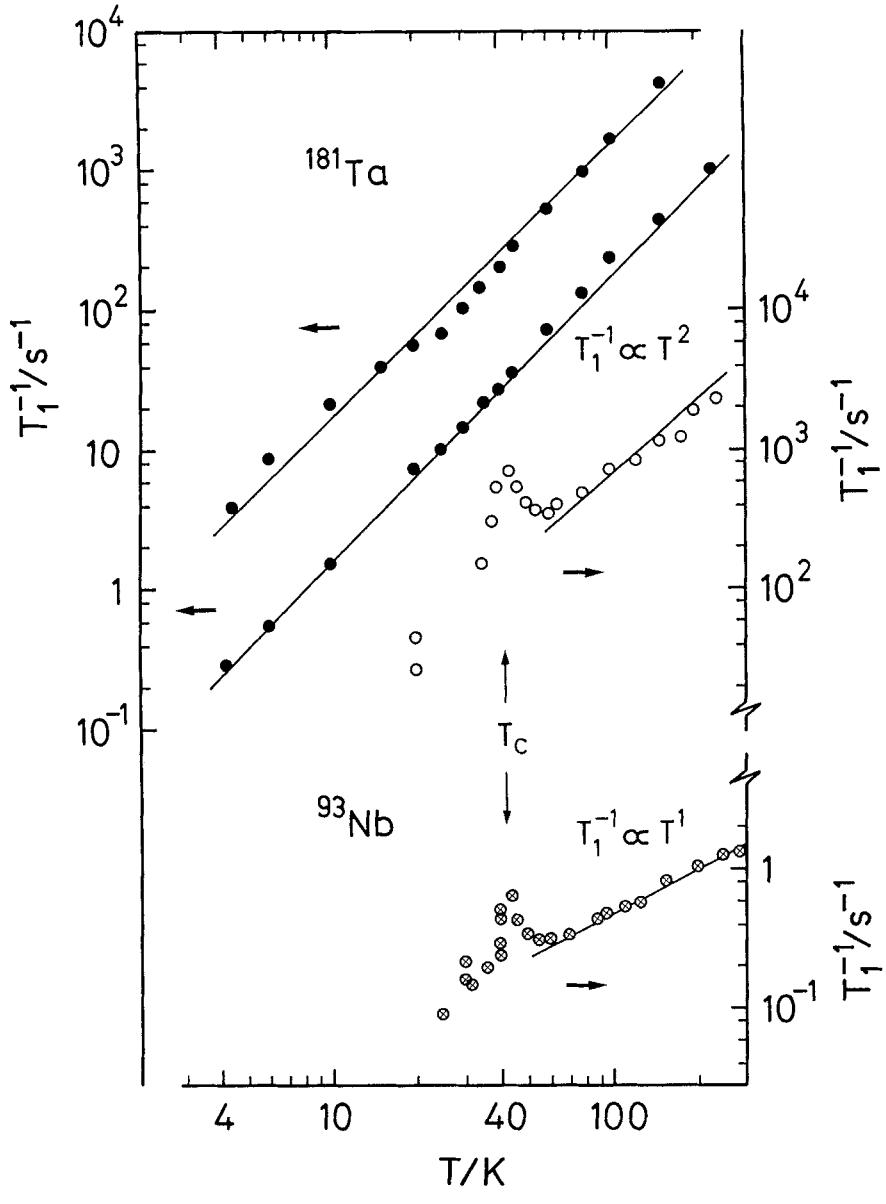

Figure 4.41. ^{181}Ta and ^{93}Nb spin–lattice relaxation rates in $KTa_{1-x}Nb_xO_3$ (sample KSK4, $x = 0{\cdot}029$) and $KTaO_3$–MIT as functions of temperature. ●, ^{181}Ta in $KTaO_3$ (at the Larmor frequency 40·7 MHz). Both time constants of the saturation recovery are represented. At all investigated temperatures the relaxation is due to phonon scattering (Raman relaxation). ○, ^{181}Ta in $KTa_{1-x}Nb_xO_3$ (at 40·7 MHz). Above 50 K, Raman relaxation is observed, as in pure $KTaO_3$. Around the transition temperature $T_c = 41$ K (indicated by a vertical arrow), an enhancement of the relaxation rate occurs, indicating a collective ordering transition. ⊗, ^{93}Nb in $KTa_{1-x}Nb_xO_3$ (at 83·1 MHz). The relaxation process is associated with the Nb dynamics. Around T_c, we observe similar behaviour to that in the ^{181}Ta nucleus. From Rod *et al.* (1988).

up to 100 ns (Rod *et al.* 1988). They also found that the relaxation rates of both ^{181}Ta and ^{93}Nb in KTN were maximal at the transition temperature $T_c = 41$ K. This implies a critical slowing down of the motion of Nb and Ta ions (as far as quadrupolar flips are concerned). Rod *et al.* (1988) related their findings to similar results from dielectric measurements. When expressed in terms of Debye relaxation of non-interacting ions, the displacement is indeed 0·27 Å as they stated, but, in view of the probable correlation of dipolar motion, this is an upper limit and therefore not incompatible with NMR results. On the other hand, the Debye relaxation rate is at least $10^8\,s^{-1}$, and this is too fast for the maximum permissible hopping rate to account for the data. A way to reconcile these two findings is to postulate that most of the ionic hopping motion is related to sites by inversion (i.e. 180° flips), and only a few 90° flips change the quadrupole symmetry by flipping between adjacent wells.

An ion-channelling study of KTN (Dubus *et al.* 1985) provided no evidence for Nb displacement from the centrosymmetric site. Upper limits and correlations are difficult to assess since this method is not widely used.

4.4. *$KTaO_3$ doped with both Nb and Li*

The principal roles of Li, namely cluster formation, 100 displacement and slow relaxation, and of Nb, namely 111 displacement and enhancement of the polarization, should lead to interesting competition effects on double doping. Prater *et al.* (1981a) performed a light-scattering analysis and found that the slowly relaxing defect, Li determines the structure of the compounds. This is true for Li concentrations as low as 0·025%, which in the presence of several per cent of Nb force the crystal into a tetragonal phase. Simultaneous observation of birefringence and light scattering in these samples made the authors aware of microscopic polar twinning of domains with quadrupolar order. Dielectric-susceptibility data on such crystals show the dominance of the slow relaxation process, as do elastic-compliance data (van der Klink *et al.* 1983). An attempt to evaluate the relaxation phenomena in terms of the Onsager theory did not produce quantitative agreement (Höchli *et al.* 1981).

4.5. *Summary of experimental results from doped $KTaO_3$*

In this section, we wish to establish the connection between the single-particle properties of dopants in $KTaO_3$ and the collective phenomena associated with the transition to a polar phase.

We start by summarizing the characteristics of the impurities Li, Na and Nb in the dilute limit, and refer in this context to table 4.1. These three dopants have ionic radii r_i that are smaller than those of the host, r_h, and that are expressed in terms of ionic misfits $(r_i - r_h)/r_h$. The magnitude of the misfit decreases in the order Li, Na, Nb; accordingly there is room for static displacements of the dopant ion, increasing in the same order. The static displacement of Nb in the dilute limit probably vanishes. The total polarization exceeds that of the dopant displacement by a factor of six; the enhancement is attributed to the formation of a lattice-polarization cloud extending several unit-cell distances around the dopant. The static susceptibility is enhanced proportionately. Dipolar reorientation implies crossing a barrier whose height decreases in same order as the polar moment (Li, Na, Nb). The dipole moments of the dopant interact with the lattice, so it is plausible that a static moment such as that of Li breaks long-range order and thus reduces the lattice polarizability. It has also been argued that Nb with zero static moment enhances the lattice susceptibility of

Table 4.1. Single-ion properties of Li, Na, and Nb in $KTaO_3$.

Dopant	Site	Ionic misfit $(r_i - r_h)/r_h$	Ionic displacement δ	Total moment/ local moment $P_r/\delta\bar{e}n$	Lattice dynamics $\partial\varepsilon_r/\partial x$, $\partial\tau/\partial x$
Li	K	−0·55	1·1 ± 0·1 Å [100]	6	<0
Na	K	−0·3	0·04 Å [100]	6	>0
Nb	Ta	−0·04	Unknown, [111] weak	Unknown	$\geqslant 0$

$KTaO_3$ for Nb since its affinity to oxygen is greater than that of Ta. In perovskites, the forces between an oxygen shell and B ions Ta (and Nb) are believed to be at the origin of ferroelectricity (Migoni *et al.* 1976). The Na ion is on an A site and does not have a direct influence on the oxygen shell. The reduction of occupied volume per unit cell, the dimension of which is nearly independent of doping, allows the lattice to relax. Under these conditions, the polarizability of the lattice is enhanced, but only moderately so.

Heavier doping entails collective effects, summarized in table 4.2. It is obvious that large interaction between impurities allows a low doping level to generate a polar phase. The nature of the phase appears to correspond to the characteristics of the dopant. Wherever static moments exist for Na and Li doping, the linear susceptibility follows the prediction made by Parisi (1979), see equations (3.6) and (3.7): the spin-glass susceptibility is critical, the polarization is irreversible at low T, the decay function is non-exponential, the polar correlation length remains small, and both heat capacity and spin–lattice relaxation are uncritical at T_f. The most probable relaxation rate deviates from pure Arrhenius behaviour. Extrapolation of $\tau^{-1}(T)$ in $K_{0\cdot974}Li_{0\cdot026}TaO_3$ by the Vogel–Fulcher expression yields $T_{VF} \approx 6\,K$, whereas $T_f \approx 50\,K$. The distribution of relaxation rates is nearly lognormal above T_f, and becomes asymmetric near and below T_f. At Li concentrations exceeding 4%, the quadrupolar correlation length starts to grow much more quickly with x than the dipolar correlation length. In $KTaO_3$: Nb, where static off-centre moments are absent and condensation is due to enhancement of bonds, Curie–Weiss behaviour is observed for the static susceptibility. Associated with the near-divergence of $\varepsilon_s(T)$ is a softening of the transverse-optical mode of vibration. Domain walls are mobile in view of the strain compatibility of domains (Fousek and Janovek 1968), and accordingly the polarization is reversible at all temperatures. Finally, spin–lattice relaxation of ^{181}Ta is critical at T_c. These are aspects of ferroelectricity. However, investigations of the dynamic susceptibility, the spin-glass susceptibility and the decay function suggest that $KTaO_3$: Nb is not quite as ordered as a classical ferroelectric.

We can imagine that random-site dipoles such as Li give rise to random forces with an average $\bar{J} = 0$ but $\mathrm{Var}(J) \neq 0$. On the other hand, for an impurity such as Nb, which is known to just enhance the interaction between the B ion and oxygen, we expect $\bar{J} \neq 0$ and $\mathrm{Var}(J) = 0$. Accordingly, we may attempt to classify our systems in terms of Toulouse's (1980) phase diagram (figure 4.42). $KTaO_3$: Li is located at the left and may move to the right for high concentrations; $KTaO_3$: Na is near $\bar{J}/\mathrm{Var}(J) = 1$, whereas $KTaO_3$: Nb is to the right and appears to move to the left if hydrostatic pressure is applied.

Table 4.2. Collective properties of dopants in $KTaO_3$.

	Lower critical doping	Static susceptibility	Spin-glass susceptibility	Ratio of impurity to total dispersion	Decay function near T_f	Dipolar correction length (Å)	Spin–lattice relaxation of nuclei
Li	0·01	Parisi (1979)[a]	No data	0·9	KWW[b]	300	Uncritical
Na	0·13	Parisi (1979)[a]	Critical	0·04	$t^{-\alpha}$	1500	Uncritical
Nb	0·008	Curie–Weiss	Uncertain	$<0·01$	$\ln t$, KWW[b]	5000	Critical

[a] See also Binder and Young (1986), p. 868.

[b] Kohlrausch (1847)–Williams–Watts (1970) function $\exp[-(\alpha t)^{\beta}]$, also known as 'stretched exponential'.

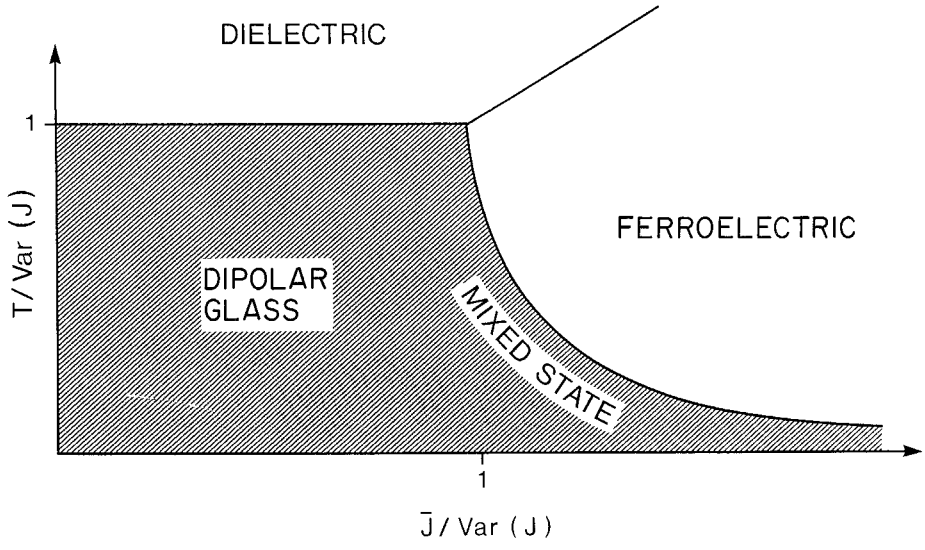

Figure 4.42. Phase diagram of random-interaction polar system (after Toulouse (1980)). $\bar{J}$ is the average interaction, Var (J) is the standard deviation and T is the temperature. The hatched region is the state with non-trivial degeneracy; the mixed state has non-zero polarization. Transitions experimentally accessible are dielectric-to-glass, and dielectric-to-ferroelectric-to-mixed state. From Höchli and Maglione (1989).

5. Mixed cyanides

5.1. *Background*

5.1.1. *Introduction*

The orientational-glass state of the mixed cyanides, in particular of $(KBr)_{0.5}(KCN)_{0.5}$, has been studied intensively. The popularity of these systems is due to the availability of good-quality single crystals and the applicability of most of the standard methods of solid-state science, but also arises from the long tradition of the study of defects, including CN, in alkali halides. $(KBr)_{1-x}(KCN)_x$, $(KCl)_{1-x}(KCN)_x$, $(NaCl)_{1-x}(NaCN)_x$ are the more prominent examples of the mixed alkali halide–cyanides, which are known to be miscible at all proportions x. A schematic phase diagram is shown in figure 1.1. To gain an understanding of the mixed crystals at intermediate concentrations, one can proceed either from the dilute case of a single substitutional CN^- impurity in the alkali halides or from the collective behaviour of the pure alkali cyanides. Both limiting cases are well understood. The crystallographic structures of the three solid phases of KCN are displayed in figure 5.1.

A second group of cyanide mixed crystals comprises the solid solutions of two alkali cyanides, the most prominent example being $(NaCN)_{1-x}(KCN)_x$. Here the orientational-glass state occurs at intermediate compositions, as shown schematically in figure 1.2. In such crystals the CN sublattice is undiluted, and the effects of the substitution on the cation sublattice on the CN orientations can be studied.

Reviews of the orientational-glass state of the mixed cyanides have been given by Lüty (1981), Loidl (1985, 1989) and Knorr (1987).

5.1.2. *Crystal growth*

Whenever the sizes of the substituents are not too different, complete series of mixed cyanides can be formed. Most of the series investigated so far have been grown

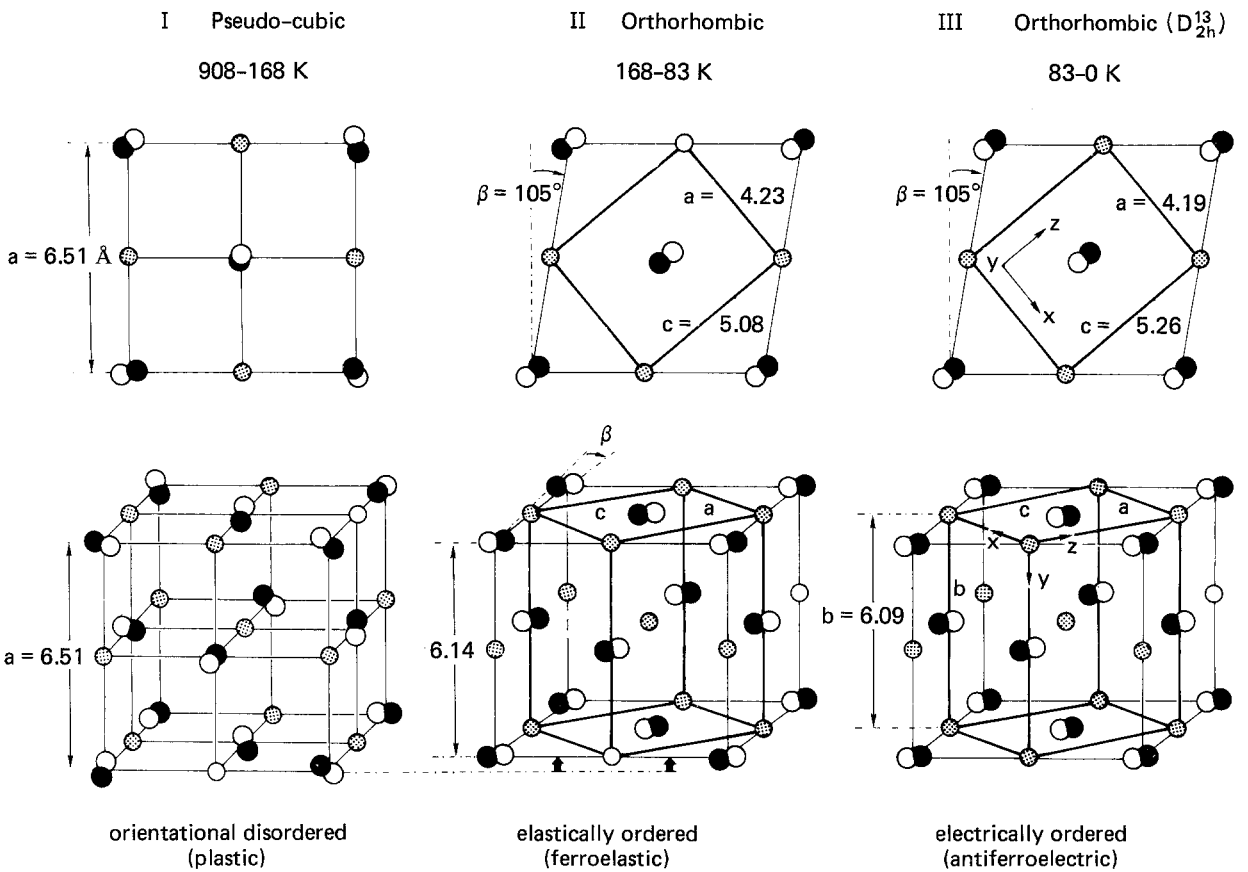

Figure 5.1. The three stable crystallographic phases of KCN and NaCN. The stability ranges and the cell parameters refer to KCN. ○, C; ●, N; ◎, K or Na. From Durand *et al.* (1980).

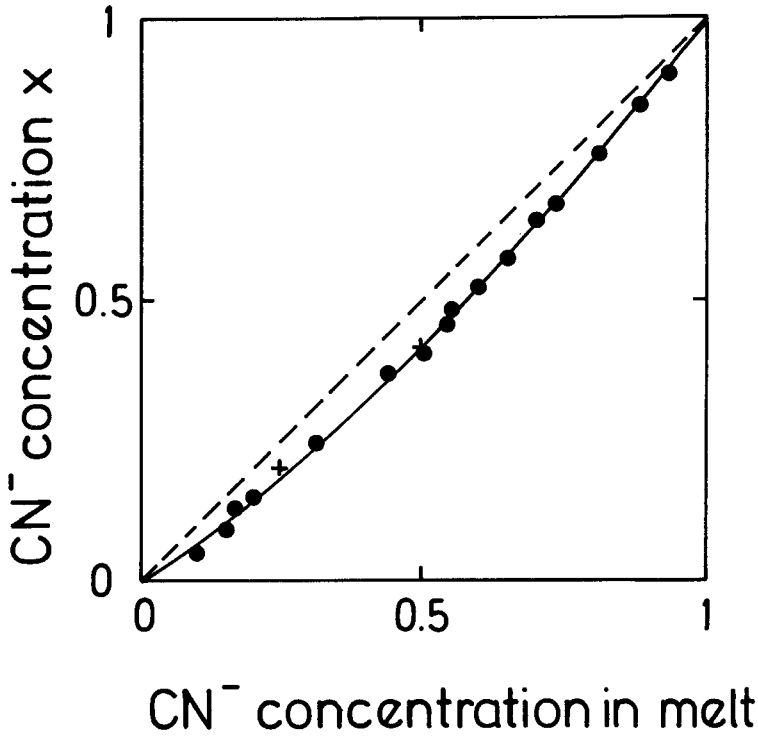

Figure 5.2. Molar concentration of $(KBr)_{1-x}(KCN)_x$ *versus* the concentration in the melt. From Loidl *et al.* (1989).

at (and can be purchased from) the Crystal Growth Laboratory of the University of Utah. Pure alkali cyanides and alkali halide–alkali cyanide mixed crystals were also supplied by S. Susman from the Argonne National Laboratory, by S. Haussühl from the Institut für Kristallographie at the Universität zu Köln and by J. Albers at the Universität des Saarlandes. To our knowledge, all of the crystals were seed-pulled from the melt under a protective atmosphere. Owing to the shapes of the liquidus–solidus boundaries, the actual CN concentrations can differ significantly from the concentrations in the melt. As an example, we show the dependence of the molar CN concentration in the solid state versus that in the melt for $(KBr)_{1-x}(KCN)_x$ in figure 5.2. The CN concentrations in the solid state have been determined gravimetrically (Loidl *et al.* 1989). The analogous plot for $(NaCN)_{1-x}(KCN)_x$ shows an S-shaped relation, which is due to a common minimum of the liquidus and solidus lines at intermediate concentrations. Other methods for determining the chemical composition are measurement of the lattice parameter (Schräder *et al.* 1989a) and atomic absorption spectrophotometry (Ortiz-Lopez 1983).

5.1.3. *CN defects in alkali halides*

Early work on CN defects in alkali halides has been reviewed by Narayanamurti and Pohl (1970). The first clear evidence that CN^- impurities lead to specific effects came from studies of the low-temperature ($0{\cdot}1\,K < T < 10\,K$) thermal conductivity, which strongly decreases with increasing CN concentration. This experiment showed

that discrete impurity states exist that are strongly coupled to the phonons and hence scatter them very effectively (Seward and Narayanamurti 1966). The first understanding of these states was obtained from interpretation of the infrared absorption studies (Seward and Narayanamurty 1966) of the stretching vibration of the CN^- ion and specific-heat measurements in terms of a linear rotator in a Devonshire crystal field (Devonshire 1936). The following conclusions were drawn from infrared measurements on $(KCl)_{1-x}(KCN)_x$. The characteristic double hump of the absorbtion line at higher temperatures (e.g. room temperature) is due to the simultaneous excitations of the stretching vibration and rotations of a freely rotating CN^- ion, analogous to results on diatomic molecules in the gaseous phase. The rotational constant is $B/hc = 1{\cdot}25\,\mathrm{cm}^{-1}$. Below 60 K, the stretching band shows satellites, a result that is consistent with the model of a coupling between the vibrational and librational modes. The librational frequency is $12\,\mathrm{cm}^{-1}$; the barriers of the Devonshire potential separating the easy directions were estimated to be $24\,\mathrm{cm}^{-1}$ (or equivalently 35 K). The finite width of the central line suggested a tunnel splitting of order $1\,\mathrm{cm}^{-1}$. The tunnel splitting has been deduced from low-temperature specific-heat measurements, where it leads to a Schottky-type anomaly slightly below 1 K.

Dielectric measurements on CN defects in KCl (Sack and Moriarty 1965) showed a Curie $1/T$ temperature dependence of the dielectric constant down to 2·5 K, indicating that the electric dipole moment carried by the CN^- ion can follow the oscillations ($\nu = 100\,\mathrm{Hz}$ and 100 kHz) of the external field even at 2·5 K. The dipole moment was determined to be 0·3 D. *Ab initio* molecular-orbital calculations by Klein *et al.* (1981) suggested a CN bond length of 1·154 Å and a charge distribution with $-0{\cdot}55e$ on the C site and $-0{\cdot}45e$ on the N site, yielding a dipole moment of $0{\cdot}058e$ Å or 0·29 D. The true value of the bond length was expected to be somewhat larger owing to electron correlations. Fowler and Klein (1986) calculated the molecular properties of the CN^- ion in alkali cyanide crystals. They found that, compared with the free ion, the electron cloud is more contracted, less anisotropic and less polarizable. The charge distribution depends sensitively on the host lattice and on the orientation of the CN^- ion with respect to the crystal axes.

An exhaustive study of the ultrasound velocity and attenuation of CN-doped alkali halides was carried out by Byer and Sack (1968). The fractional change $\mathrm{d}s/s$ of the compliance with respect to the compliance of the undoped sample was measured as a function of temperature, CN concentration, bias stress along [110] for several hosts and sound frequencies. For KCl : CN the following results were reported: $\Delta s/s$ of the T_{2g} mode, which is related to the elastic constant c_{44} in Voigt's notation, is proportional to $1/T$, with slight deviations below 5 K. The deviations are accompanied by the appearance of sound attenuation. The T dependence of $\Delta s/s$ for the E_g mode, which is related to $\frac{1}{2}(c_{11} - c_{12})$, shows two different Curie-like regimes, with a cross-over region around 10 K. The cross-over region also shows relaxational effects. The changes upon bias stress confirm the Curie-type nature of the elastic response. The complex compliance is evaluated in terms of the relation $\Delta s/s = C/T(1 - \mathrm{i}\omega\tau)$, with $\tau = \tau_0 \exp(E_\mathrm{b}/k_\mathrm{B}T)$. For the relaxation peak of the E_g mode, an inverse attempt frequency $\tau_0 = 8 \times 10^{-13}$ s and a barrier height $E_\mathrm{b} = 8{\cdot}2$ meV were derived. The results were interpreted in terms of coupling of the sound waves to the orientational excitations of the CN molecule in a cubic crystal field. At high temperatures, the CN^- ions are quasi-free rotors, giving rise to the Curie behaviour of $\Delta s/s$. The peculiar behaviour of the E_g mode is due to coupling to a librational excitation with

an energy of order 10 K. The T_{2g} shear mode interacts with a low-lying excitation, regarded as a tunnelling excitation at about 1 K.

Direct evidence for the coupling of the phonons with discrete orientational modes came from an inelastic neutron-scattering study where anticrossing of the acoustic E_g branch with the libration was observed (Walton *et al.* 1974, Rowe *et al.* 1980) (see figure 5.3). For the T_{2g} branch, resonant scattering of the phonons from a tunnelling transition at 0·174 meV was demonstrated in an experiment using a superconducting tunnel junction to generate monochromatic phonons (Windheim 1976).

Until then, it had been argued that the easy directions of the crystal field are along ⟨100⟩. Lüty (1974) reinvestigated the vibrational absorption band of KCl : CN under application of uniaxial stress along the main symmetry directions, and showed conclusively that the CN^- ions are preferentially aligned along ⟨111⟩, that the elastic and electric dipole moments of the ion are collinear and that accordingly models postulating that the electric dipole and the elastic dipole are at right-angles could be discarded.

Lüty's study was complemented by infrared measurements by Beyeler (1975), who also presented detailed level schemes for a linear rotor in a cubic field described by spherical harmonics of fourth and sixth order (Beyeler 1972), and by Raman measurements by Durand and Lüty (1977a). Seward *et al.* (1972) observed thermal transients in heat-pulse experiments on NaCl : CN and derived a $1/T$ dependence of the molecule–lattice relaxation time for $0{\cdot}2\,\mathrm{K} < T < 5\,\mathrm{K}$. Kerr-effect and birefringence measurements on CN in various alkali halides confirmed that ⟨111⟩ model for the K and Rb halides and brought clear evidence for a ⟨100⟩ orientation to the Na halides (Diaz-Gongora and Lüty 1978).

Following these studies, the general understanding of the CN defect in alkali halides was established: the free rotations of the CN molecule become increasingly impeded by the crystal field until at low temperatures only librations about and tunnelling between the easy directions are possible. The barriers between the easy directions are of order some tens of kelvin, corresponding to librational energies of typically 10 K and tunnelling splits of typically 1 K. The easy directions are ⟨111⟩ for K and Rb halides and ⟨100⟩ for Na halides.

5.1.4. *Concentrated cyanides*

Since there have been efforts to understand the orientational-glass state starting from the structural behaviour of the pure cyanides, we review some of the properties of these crystals.

NaCN, KCN and RbCN crystallize in the NaCl structure (figure 5.1). Information on the orientational distribution of the CN^- ions was obtained from neutron diffraction. The first measurements were interpreted in terms of free rotations (an isotropic distribution of the CN orientations (Elliott and Hastings 1961)); later the distribution was analysed in terms of symmetry-adapted spherical harmonics. Using fourth-order terms only, Atoji (1971) suggested a ⟨111⟩ model for KCN, which was confirmed by Price *et al.* (1972), who additionally considered sixth-order harmonics. For NaCN, Rowe *et al.* (1973) found a preference for ⟨100⟩ orientations. In both cyanides, ⟨110⟩ is the least likely direction of the CN axes. Thus the preferential orientations are the same as in the dilute case.

All cyanides undergo structural phase transitions at lower temperatures. X-ray diffraction work of Verweel and Bijvoet (1938) and Bijvoet and Lely (1940) revealed the low-temperature modification of KCN as orthorhombic Immm, where the CN^-

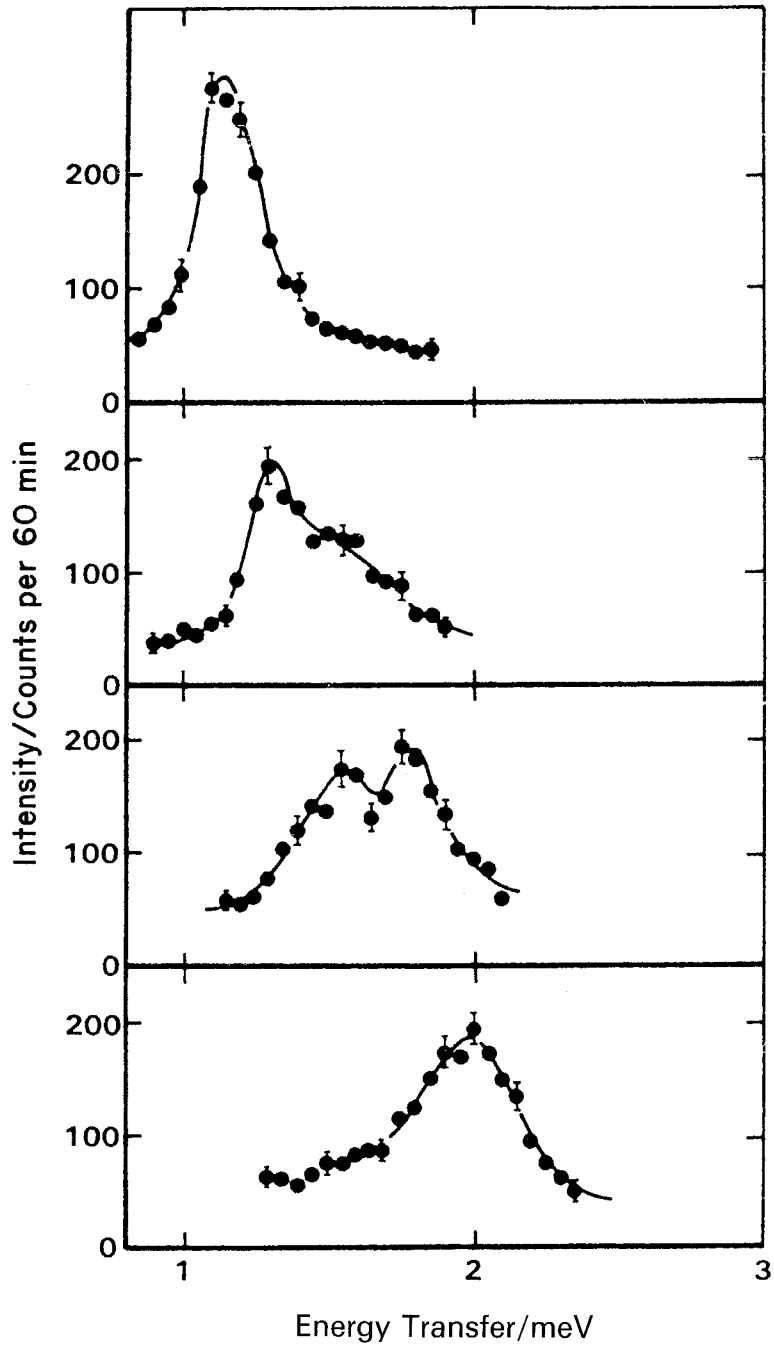

Figure 5.3. Neutron-scattering lineshapes for KBr doped with 0·0034 mole fraction KCN at 1·5 K for various values of the reduced wave-vector q measured around the (200) reciprocal lattice point: q = 0·055, 0·065, 0·075 and 0·085, from top to bottom. The E_g acoustic phonon branch anticrosses the librational excitation at approximately 1·6 meV. From Rowe *et al.* (1980).

ions are aligned along a former cubic [110] direction (figure 5.1). The changes of the cubic cell upon cubic-to-orthorhombic transition can be visualized as spontaneous shear of one of the cell angles, say β, by about 10° and uniaxial compression along the b direction. The alignment of the CN^- ions along [110] follows from steric considerations and was later verified by neutron diffraction (Rowe *et al.* 1977). The transition temperature T_c is 168 K. X-ray (Cimino *et al.* 1959) and heat-capacity (Suga *et al.* 1965) investigations established that the transition shows hysteresis and that a new monoclinic modification forms when the crystal is cycled through T_c. The monoclinic phase has an existence range of about 6 K. The orthorhombic and monoclinic phases exist in a multidomain state where the domains have well defined orientations of their crystallographic axes with respect to the cubic matrix (Cimino and Parry 1960, Parry 1962). This observation has been regarded as an indication that the transition is martensitic. Heat-capacity measurements by Messer and Ziegler (1941) and in particular by Suga *et al.* (1965, 1968) led to detection of a second phase transition at 83 K. The entropy changes at the transitions are $R \ln 4$ for the upper and $R \ln 2$ for the lower one. Hence the CN^- ion is assumed to reorient between the $\langle 111 \rangle$ directions in the cubic phase and is then confined to one direction, namely [110], in the intermediate phase, where it still has head–tail degeneracy. The transition into the phase at the lowest temperatures is of second order and involves an antiferroelectric ordering in the space group Pmnm (Rowe *et al.* 1977) (figure 5.1.).

NaCN is isomorphic to KCN in the three stable phases; the transitions occur at $T_{c1} = 288$ K and $T_{c2} = 172$ K. The metastable monoclinic phase has not been observed in NaCN.

RbCN shows a single first-order phase transition at 110 K (Sugisaki *et al.* 1968), from the cubic high-temperature phase into a monoclinic phase, isomorphic to the metastable phase of KCN. The monoclinic structure has a residual entropy due to head–tail disorder of the CN^- ions. This structure can be understood as a homogeneously deformed cubic lattice with additional staggering of the ionic positions and the elastic dipole moments of the CN^- ions (Rowe *et al.* 1984). More recent heat-capacity measurements have led to an adjustment of the value of the transition temperature to 132 K and the location of a feeble anomaly near 30 K, which is ascribed to a glass transition into a state with frozen-in dipolar disorder (Shimada *et al.* 1986). It has been argued that the herringbone arrangement of the CN axes characteristic of the monoclinic phase preempts the electric ordering that occurs in the orthorhombic low-temperature phases of KCN and NaCN.

CsCN has attracted little attention because it is extremely hygroscopic and difficult to prepare. It crystallizes in the CsCl structure, which is stabilized by rapid reorientations of the CN ion between the $\langle 111 \rangle$ directions. Around 190 K, CsCN undergoes a phase transition into a rhombohedral structure where the CN^- ions orient spontaneously along one of these directions. (Sugisaki *et al.* 1968, Knopp *et al.* 1983). There are no indications of any ordering of the CN dipole moments. CsCN and related mixed crystals would be an interesting alternative to the cyanides with NaCl structure. The cubic-to-rhombohedral transition is prototypic for a shear instability.

As revealed by Raman and diffraction studies, the cyanides show a rich variety of high-pressure modifications (Dultz *et al.* 1981, Dultz and Krause 1978, Dultz and Rehaber 1983).

The structural phase transitions of the cyanides from the cubic high-temperature into the orientationally ordered low-temperature phase are heralded by a decrease of

the elastic shear constant c_{44} with decreasing temperature. As shown in the pioneering work of Haussühl (1973), c_{44} of KCN decreases from a value of $2{\cdot}3 \times 10^{10}$ dyn cm^{-2} at 450 K to about 2×10^{9} dyn cm^{-2} at the transition temperature. Haussühl suggested that c_{44} follows a ln T dependence. The thermoelastic behaviour of the cyanides and of the mixed cyanides is now usually discussed in terms of the relation

$$c_{44} = c_{44}^{0}(T - T_0)/(T - \Theta),$$

which results from a mean-field treatment of a structural instability where the CN orientations are linearly coupled to the T_{2g} lattice strains. This relation can be written in the more transparent form

$$c_{44} = c_{44}^{0}(1 - g^2\chi(T)),$$

where c_{44}^{0} is the background elastic constant of a reference system without orientational degrees of freedom, i.e. a suitable alkali halide. $\chi(T)$ is the T_{2g} orientational susceptibility in a 'clamped' crystal, that is a crystal in which the mutual interaction of the CN orientations via T_{2g} deformations of the lattice is suppressed. Finally, g is the coefficient of the bilinear orientation–strain coupling. The original form is recovered by assuming that $\chi(T)$ obeys a Curie–Weiss law $\chi = C/(T - \Theta)$. Analogously to magnetic systems, Θ contains the $q = 0$ Fourier component of all orientational interactions between CN^- ions other than those mediated by T_{2g} lattice strains, for example the direct electrostatic interaction between electric quadrupoles. If these residual interactions were of the 'ferro' type then the "clamped" crystal would show a spontaneous quadrupolar polarization at the temperature $T = \Theta$. The instability of the free crystal is reached at the temperature T_0, where the crystal shows a spontaneous ferroelastic T_{2g} shear and simultaneously a spontaneous T_{2g} ferroquadrupolarization. In reality, the cyanides undergo first-order transitions at a T_c somewhat above T_0. For KCN, the extrapolation of $c_{44}(T)$ yields $T_0 \approx 155$ K, compared with $T_c = 168$ K. The cubic-to-orthorhombic transition of KCN and NaCN is strongly first-order, as can be seen from the jumps in the spontaneous lattice deformations at T_c (Yamamoto and Shinnaka 1981, Gruber and Knorr 1990). The deformation contains not only T_{2g} shears but also an E_g uniaxial compression and an A_{1g} volume collapse. For NaCN, the tensor of the spontaneous deformation at T_c is given by (Knorr 1990a)

$$\boldsymbol{S} = \begin{bmatrix} 0{\cdot}957 & 0 & 0 \\ 0 & 1{\cdot}020 & 0{\cdot}117 \\ 0 & 0{\cdot}117 & 1{\cdot}020 \end{bmatrix}.$$

The off-diagonal element describes the T_{2g} component and corresponds to a change in one of the cell angles by 11·5°. As mentioned above, the ferroelastic transition of the cyanides has a martensitic aspect. Several features of the transition can be accounted for satisfactorily by the model of Wechsler *et al.* (1953) of martensitic transformations (Gash 1983). This model assumes that the transformation is accomplished by the propagation of a transformation front at which the parent and the product phase are matched in a way that avoids the accumulation of macroscopic strains. Release of these transformation strains is achieved by the formation of transformation twins. The applicability of this model to NaCN has been demonstrated by a microscope study of domain formation (Gash and Lüty 1985) and by X-ray

studies of the relation between the cubic and orthorhombic crystal axes (Parry 1962, Gruber and Knorr 1990).

Following the work of Haussühl (1973) on KCN, the mean-field behaviour of the elastic constant c_{44} in other alkali cyanides was verified by several ultrasonic, Brillouin and neutron experiments, for example by Haussühl *et al.* (1977) for NaCN, Wang and Satija (1977) for NaCN and KCN, Haussühl (1979) for RbCN, and Loidl *et al.* (1983a) for CsCN.

The first determination of phonon dispersion curves for a cyanide by means of inelastic neutron scattering was reported by Rowe *et al.* (1975) for the cubic phases of KCN and NaCN. The T_{2g} branch showed an anomalous upward curvature. Signals from optical phonons have not been observed. Raman measurements (Dultz 1974) and inelastic neutron measurements (Nücker *et al.* 1978)—the latter performed on a powder—yield broad distributions of excitations covering an energy range up to about 30 meV. In the cubic phase these distributions fail to show van Hove-like singularities; this suggests that the phonons and the orientational modes overlap in energy and are strongly coupled, introducing strong orientational–translational relaxation. Better-defined phonon signals, including optical phonons, have been measured in RbCN and have led to a parametrization of the dispersion curves in terms of a Born–von Kármán model (Ehrhardt *et al.* 1983).

The microscopic foundation of the orientation-translation coupling was established by Michel and Naudts in a series of papers (Michel and Naudts 1977a, b, 1978). They basically showed that in the cubic phase of the cyanides the frequency and T-dependent orientational susceptibility is described approximately by a Curie–Deybe form:

$$\chi(T, \omega) = C/T(1 - i\omega\tau).$$

χ is incorporated into the phonon propagator that determines the scattering law for the neutron-scattering studies. The expression for the elastic constant given above is obtained in the limit $q \to 0$, $\tau \ll 1$ (the regime of rapid relaxation). This model explains quantitatively the results of inelastic neutron-scattering studies (Rowe *et al.* 1975, 1978a, b).

Landau theories for the upper phase transition of the cyanides have been developed (de Raedt *et al.* 1981, Sahu and Mahanti 1982a, b). The basic ingredient is bilinear coupling between orientations and strains. This coupling can be translated into an effective interaction of the CN quadrupoles which has the analytical form of a dipole–dipole interaction; that is, for a fixed orientation of a given CN^- ion, the second ion aligns parallel to field lines of a dipole—without, of course, differentiating head and tail. The anisotropy of this interaction led to the question of 'frustration' arising in the ordered phases of the pure cyanides. A further point is that lattice sums for this type of interaction are conditionally convergent: the value of the sum is different for needle-shaped infinite and plate-shaped infinite crystals (de Raedt *et al.* 1981). The cubic-to-orthorhombic transition of NaCN and KCN is due to the condensation of a coupled T_{2g} translational–orientational mode. c_{44} is the relevant inverse susceptibility in the cubic phase. Higher Landau-expansion coefficients couple the T_{2g} to the E_g and A_{1g} components. The most recent Landau model is that given by Michel and Theuns (1989), which also treats the cubic-to-rhombohedral transition of several mixed cyanides and the cubic-to-monoclinic transition. In the latter case, the primary mode is at the zone boundary, and condensation of this model leads to the staggering of the internal coordinates. Nevertheless, the

interaction of the primary mode with the long-wavelength T_{2g} modes, and hence with c_{44}, is strong.

In summary, the structural instability of the cyanides is due to the coupling of relaxational-type orientations and translational modes of the centre-of-mass lattice (i.e. phonons). T_{2g} modes play the most important role. At T_c, the lattice shears spontaneously and the CN orientational distribution acquires a spontaneous T_{2g} component.

The complex dielectric constant in KCN and NaCN has been investigated by Julian and Lüty (1977). In the pure cyanides, the structural phase transitions are indicated by steps in ε_1 (T). Below the antiferroelectric phase-transition temperature, the Debye-type dispersion signals a gradual freezing-in of the dipoles. The Debye loss was found to be almost monodispersive and the relaxation times followed by Arrhenius behaviour. Julian and Lüty (1977) noted the absence of any Curie or Curie–Weiss behaviour of the (static) susceptibility in the paraelectric phase. Dielectric investigations of KCN were extended to ultralow frequencies (10 mHz) by Ziemath and Aegerter (1986), and slight deviations from the standard Debye equation were detected. The width of the loss peaks varied from 1·36 decades at 68 K to 1·44 decades at 53 K, which should be compared with 1·144 decades of the pure Debye loss.

RbCN was investigated in detail by Kondo *et al.* (1979). In contrast to NaCN and KCN, RbCN undergoes no electric ordering transition. The temperature dependence of the dielectric constant exhibits the characteristic step at the structural phase transition and a dispersion step with the appearance of appreciable loss, which indicates freezing-in of the CN molecules. However, in RbCN, no long-range electric order can be established. This can be explained by the fact that in the elastically ordered phase, RbCN exhibits a monoclinic structure characterized by a quadrupolar order reminescent of a herringbone structure. In the orthorhombic structure, sheets of ferroelastically ordered molecules favour dipolar order. Obviously, this is not the case in the monoclinic structures, which have low (virtual) electric phase-transition temperatures. Thus, at the hypothetical ordering temperature, the relaxation processes are extremely slow and long-range electric order cannot be established. At low temperatures, RbCN is characterized by a residual entropy due to frozen-in dipolar orientations. The dielectric loss on a logarithmic frequency scale exhibits slightly broadened symmetric Debye curves of 1·32 decades. The static susceptibility, as defined by the area of the loss peaks when plotted against ln ω, follows a Curie law with an electric dipole moment of 0·115 D (under the assumption that the dipoles relax independently). Thus the dipole moment is approximately three times lower than the values determined experimentally for isolated CN ions in KCl (Sack and Moriarty 1965).

Dielectric results for CsCN were published by Knopp *et al.* (1983). CsCN crystallizes in the cubic CsCl structure. At 190 K, it transforms into an elastically ordered rhombohedral structure. Slowing down of the dipolar relaxation could be observed between 70 and 90 K. Again, the loss peaks behaved in an almost Debye-like function and the static susceptibility was constant as the reorientation rates passed the frequency window of the experiments. It was concluded that CsCN was on the borderline between dipole ordering and freezing into random CN orientations. The absence of long-range electric order became evident from heat-capacity experiments, where no anomaly due to an electric-order phase transition could be detected down to the lowest temperatures (Sugasaki *et al.* 1968).

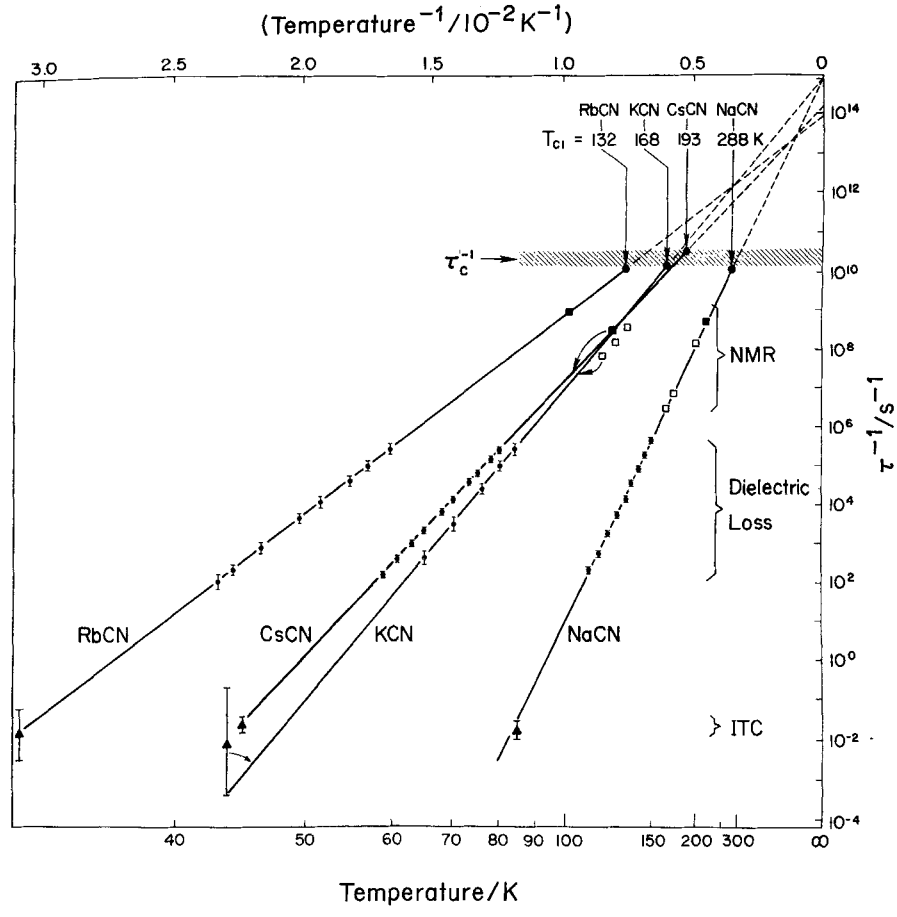

Figure 5.4. Arrhenius plots of the dipolar relaxation rates of four pure alkali cyanides measured with ionic thermal-conductivity, dielectric and NMR techniques. The critical relaxation rate where the crystals undergo phase transitions from orientationally ordered to plastic high-temperature phases is indicated by the shaded area. Taken from Lüty and Ortiz-Lopez (1983).

Finally, it was demonstrated by Lüty and Ortiz-Lopez (1983) that the elastic order–disorder transition in all pure cyanides is governed by a critical and universal relaxation rate $\Gamma_c \approx 2 \times 10^{10}\ s^{-1}$. For all cyanides, the extrapolated Arrhenius plots intersect the structural phase-transition temperature at approximately this critical frequency. Figure 5.4 shows the Arrhenius plots of the dipole reorientation rates of the pure alkali cyanides, including results from dielectric, NMR and ionic thermal-conductivity measurements (Lüty and Ortiz-Lopez 1983). The observation was interpreted by Sethna *et al.* (1984) in terms of a simple mean-field theory.

Electric-dipole ordering in NaCN and KCN was investigated theoretically by Pirc and Vilfan (1981) and Koiller *et al.* (1984). Good agreement with experimental results could be achieved by assuming dressed dipoles (i.e. dipole ordering accompanied by sublattice shifts of the centre-of-mass positions). These sublattice shifts in the electrically ordered phases have been investigated using neutron diffraction (Schräder *et al.* 1990a).

5.1.5. *First evidence for the orientational glass*

The first mixed crystals $(KBr)_{1-x}(KCN)_x$ and $(KCl)_{1-x}(KCN)_x$ with intermediate CN concentrations x were grown in the mid-1970s by Lüty and co-workers at the University of Utah and Haussühl at the Universität Köln. The Raman spectra of Durand and Lüty (1977) yielded the first evidence that the cubic-to-non-cubic phase transition known from KCN is suppressed upon chemical substitution (figure 5.5).

The pioneering experimental work on the glass-like state in the mixed cyanides is that of Rowe *et al.* (1979). Neutron-scattering results for $(KBr)_{0.5}(KCN)_{0.5}$ showed that this sample remains cubic down to the lowest temperatures. The T_{2g} transverse acoustic phonon frequencies (the square of the frequency is proportional to c_{44}) soften, pass through a minimum at a characteristic temperature T_f and stiffen again below T_f, where $T_f \approx 100\,K$ (figure 5.6). At the lowest temperatures, the room-temperature values are approximately recovered. The stiffening of the phonons is accompanied by the appearance and growth of diffuse scattered intensity that shows up as central peaks in constant-Q scans of the neutron experiment (figure 5.6). Central peaks occur in those scattering geometries that are sensitive to T_{2g} phonons (figure 5.7). The frequency width of the central peak is limited by resolution. Hence it was assumed to represent static disorder which can be understood as frozen-in T_{2g} phonons or, more precisely, as frozen-in coupled phonon–orientation modes of T_{2g} symmetry. Weak indications of the central-peak intensity appeared already well above T_f, at about 150 K (figure 5.6).

The minimum in c_{44} and the appearance of diffuse intensity are the fundamental characteristics of the freezing into the glass-like state. c_{44} describes the elastic response to shear stresses of T_{2g} symmetry. These stresses transform like a quadrupole moment. The quadrupolar character of the response is plausible: homogeneous distortions of the lattice can only orient the axis of the CN molecule (the principal axis of the quadrupole tensor), but cannot induce head–tail alignment. This is why the glass-like state of the cyanides is often called a quadrupolar glass.

The results of Rowe *et al.* have been interpreted by Michel and Rowe (1980) on the theoretical basis of the bilinear coupling between translations and rotations. They relate the minimum of c_{44} to a cusp of the orientational susceptibility and show that both the appearance of the diffuse scattering and the increase in c_{44} (the decrease in the orientational susceptibility) below T_f are connected with the appearance of a glass order parameter. The Q dependence of the diffuse intensity of the experiment is described well by their model. It should be pointed out that the glass order parameter was introduced in a purely heuristic manner.

5.2. *Mixed alkali halide–alkali cyanide crystals*

5.2.1. *Elastic properties*

The elastic properties of the mixed cyanides have been investigated by several research groups using a variety of techniques, namely ultrasonics, Brillouin and inelastic neutron scattering, torsion pendulum and quasi-static torque–shear measurements. The results are discussed in chronological order.

Rehwald and Rosinelli (1977) reported ultrasonic and Brillouin measurements of c_{11} and c_{44} for $(KCl)_{1-x}(KCN)_x$ with high CN concentrations x, $0{\cdot}94 < x < 1$. These samples undergo ferroelastic phase transitions at lower temperatures. The mean-field expression from above was fitted to the data on $c_{44}(T)$. $c_{44}(T)$ decreases

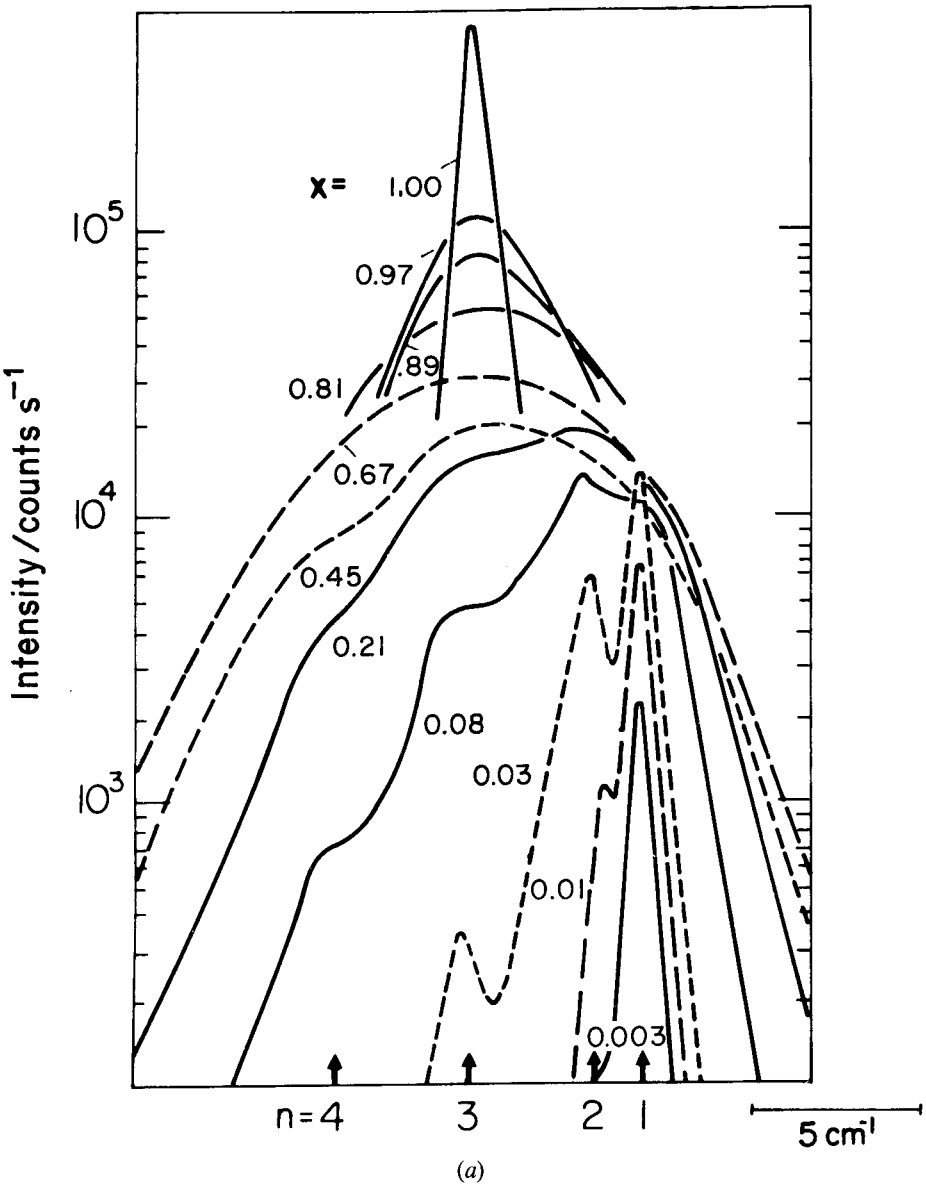

(*a*)

Figure 5.5. The Raman spectrum of $(KCl)_{1-x}(KCN)_x$ (*a*) and $(KBr)_{1-x}(KCN)_x$ (*b*) at 10 K, showing the frequency regime of the CN stretching vibration around 2090 cm^{-1}. Samples with $x > 0{\cdot}8$ (KCl) and $x > 0{\cdot}6$ (KBr) are in the ferroelastic multidomain state. At low CN concentrations, the features indicated by arrows are attributed individual CN defects, pairs and triples of CN defects in neighbouring sites on the anion sublattice. From Lüty (1981).

with temperature and extrapolates to zero at the temperature T_0, which decreases linearly with decreasing CN concentration. Θ is of the order of -200 K.

Satija and Wang (1978) presented Brillouin results on c_{44} for $(KBr)_{1-x}(KCN)_x$ with $x = 0{\cdot}19$, $0{\cdot}34$, $0{\cdot}56$, $0{\cdot}76$ and 1. The samples with $x = 0{\cdot}76$ and $x = 1$ order at lower temperatures; here $c_{44}(T)$ softens towards extrapolated ordering temperatures T_0.

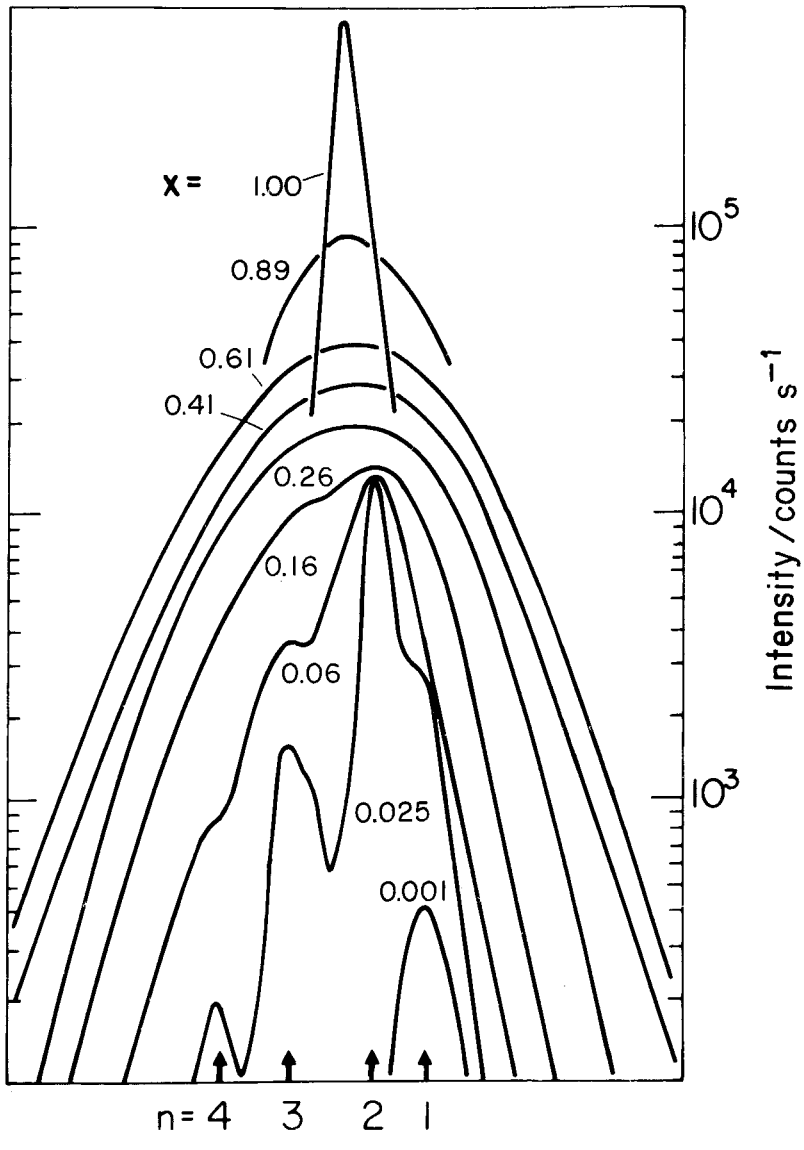

(*b*)

Figure 5.5. Continued.

The Brillouin signals were lost at temperatures considerably above these extrapolated temperatures. The samples with $x \leqslant 0{\cdot}56$ show no phase transition; here $c_{44}(T)$ passes through a minimum at T_f. Both T_f and T_0 depend linearly on the CN concentration x.

Ultrasonic data on $c_{11}(T)$ and $c_{44}(T)$ were obtained by Loidl *et al.* (1980) for $(KBr)_{1-x}(KCN)_x$ with $x = 0{\cdot}04$ and $0{\cdot}14$. These data suggest that both elastic constants pass through the minimum at the same temperature T_f (i.e. the E_g and T_{2g} strains freeze in at the same temperature), although the variation with temperature is much stronger for the T_{2g} mode.

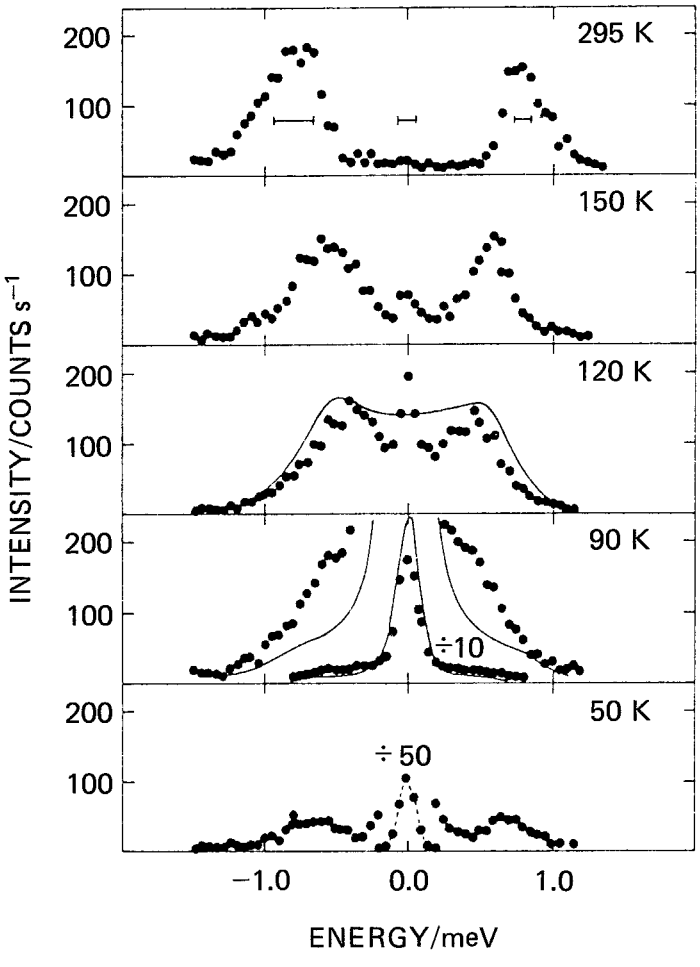

Figure 5.6. (*a*) Neutron-scattering lineshape of $(KBr)_{0\cdot5}(KCN)_{0\cdot5}$ at various temperatures. The peaks at finite energy transfer are due to the excitation and deexcitation of T_{2g} acoustic phonons. Note the growth of the 'central-peak' intensity. (*b*) Temperature dependence of the central-peak intensity and the squared phonon frequency (which is proportional to the elastic shear constant c_{44}). From Rowe *et al.* (1979).

Kwiecien *et al.* (1981) demonstrated in an ultrasonic study that $c_{44}(T)$ of $(KBr)_{1-x}(KCN)_x$ with $x = 0\cdot6$ and $0\cdot8$ and of $(KCl)_{1-x}(KCN)_x$ with $x = 0\cdot75$ and $0\cdot85$ follow the mean-field law at higher temperatures. c_{44} is practically independent of the hydrostatic pressure applied. As c_{44} softens on cooling, the ultrasonic echoes are eventually lost, as was already noted in the earlier studies. It was pointed out that the mean-field law holds down to the temperature where the signals are lost, regardless of whether the samples show the ferroelastic instability or stay cubic.

An ultrasonic study by Loidl *et al.* (1981) of various elastic constants $c_{ij}(T)$ of $(KBr)_{1-x}(KCN)_x$ with $x = 0\cdot04$ provided further evidence that the E_g and T_{2g} modes freeze at the same temperature T_f. The ultrasonic attenuation peaks slightly below T_f

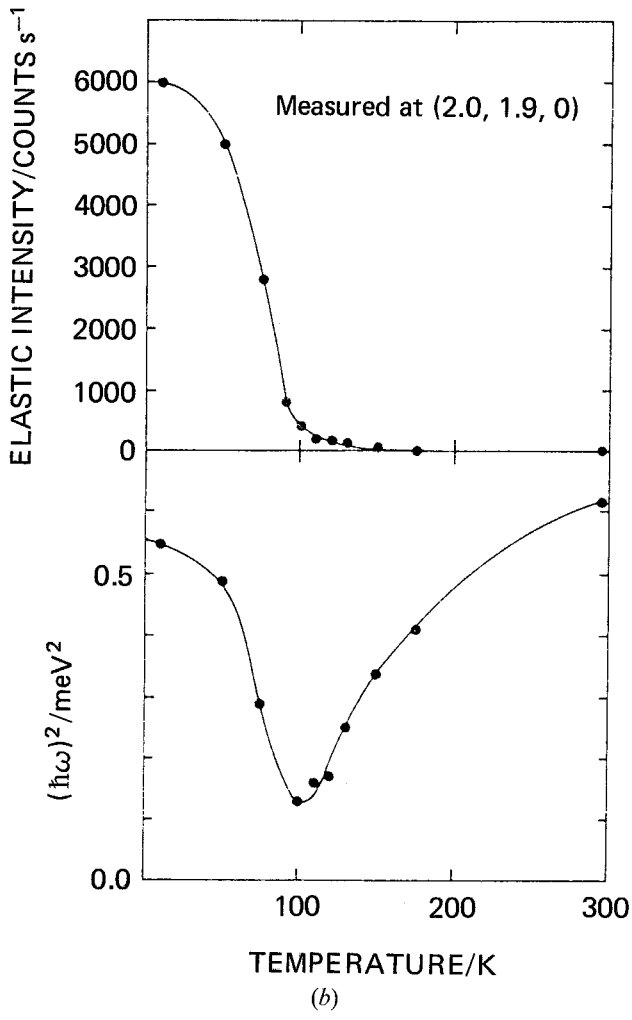

(*b*)

Figure 5.6. Continued.

(figure 5.8). The minimum of $c_{11}(T)$ shows dispersion: there is a small shift of T_f on comparing the 10 MHz with the 50 MHz data.

The work of Kwiecien *et al.* (1981) was complemented by further ultrasonic measurements by Garland *et al.* (1982) of samples with lower CN concentrations. Here $c_{44}(T)$ deviates at lower T from the mean-field law. The minimum could not be traced out. Dispersion effects were made evident by comparison with the Brillouin data of Satija and Wang (1978).

Loidl *et al.* (1982) discussed the frequency dependence of T_f in terms of a relaxational *Ansatz* for the rotational susceptibility. The quadrupolar and the dielectric freezing of $(KBr)_{1-x}(KCN)_x$ were treated on the same footing. It was assumed that the quadrupolar and the dipolar degrees freeze-in simultaneously, a view that was later proved to be incorrect. An Arrhenius law was derived for the orientational relaxation time.

Ultrasonic data on $c_{11}(T)$ and $c_{44}(T)$ for $(KBr)_{1-x}(KCN)_x$ with $0{\cdot}008 < x < 0{\cdot}20$ were reported by Feile *et al.* (1982).

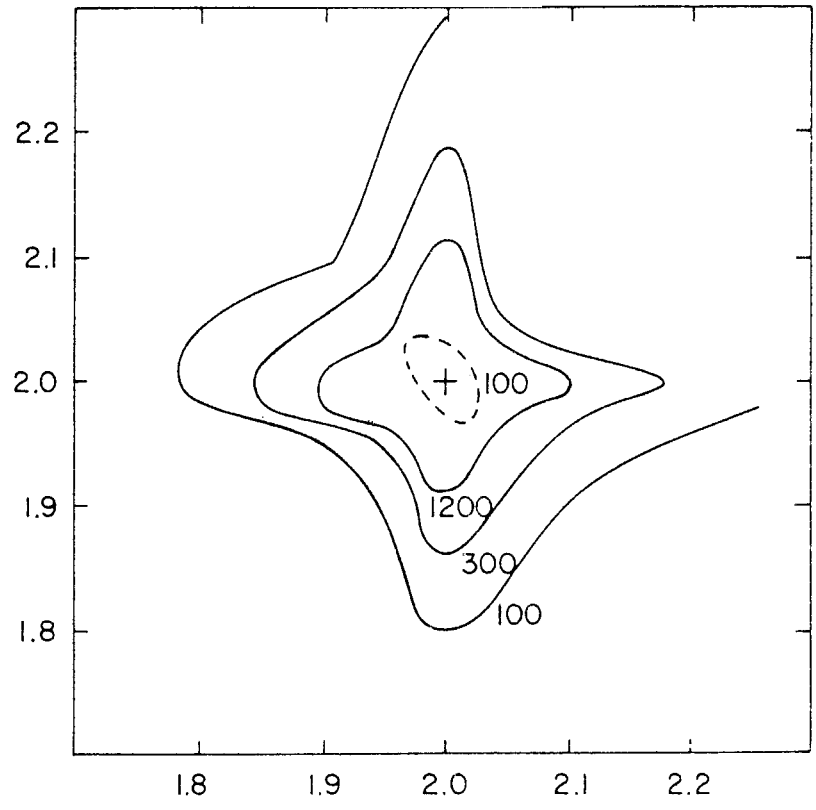

Figure 5.7. Contours of the central-peak intensity of $(KBr)_{0.5}(KCN)_{0.5}$ at 150 K (– – –) and 51 K (——) around the (220) reciprocal lattice point. The shapes of the contours at 51 K are consistent with the picture of frozen-in T_{2g} strains. From Rowe *et al.* (1979).

Low-frequency data on $c_{44}(T)$ for $(KBr)_{1-x}(KCN)_x$ with $x = 0{\cdot}2$, $0{\cdot}53$ and $0{\cdot}73$ were obtained from measurements using a miniature torsion pendulum (Knorr *et al.* 1986) (figure 5.9). This set-up has the advantage that the minimum of $c_{44}(T)$, where the ultrasonic signals are usually lost, can be traced out and that the imaginary part of the elastic shear response can be studied. The following points have been emphasized.

(i) The minimum is remarkably deep for $x = 0{\cdot}53$ and $0{\cdot}73$. For the ordering sample, $x = 0{\cdot}73$, which undergoes two phase transitions—namely cubic to rhombohedral and rhombohedral to monoclinic (see below)—the softening is almost complete and the shear constant remains low in the intermediate rhombohedral phase. The sample with $x = 0{\cdot}53$ must be close to a ferroelastic instability because the minimum value is only about 1/20 of the room-temperature value.

(ii) There is no elastic loss above T_f and T_c.

(iii) The elastic loss increases below T_f and below the rhombohedral-to-monoclinic transition temperature T_{c2} respectively, and shows a first maximum at a somewhat lower temperature.

(iv) A second loss peak and a corresponding dispersion step in the real part are observed for $x = 0{\cdot}53$ and $0{\cdot}73$ at temperatures well below T_f and T_{c2} respectively. The second loss peak occurs at about the temperature where dielectric loss was observed in measurements carried out with comparable frequencies. For $x = 0{\cdot}2$, there is only one elastic loss peak, which again coincides with the dielectric loss peak.

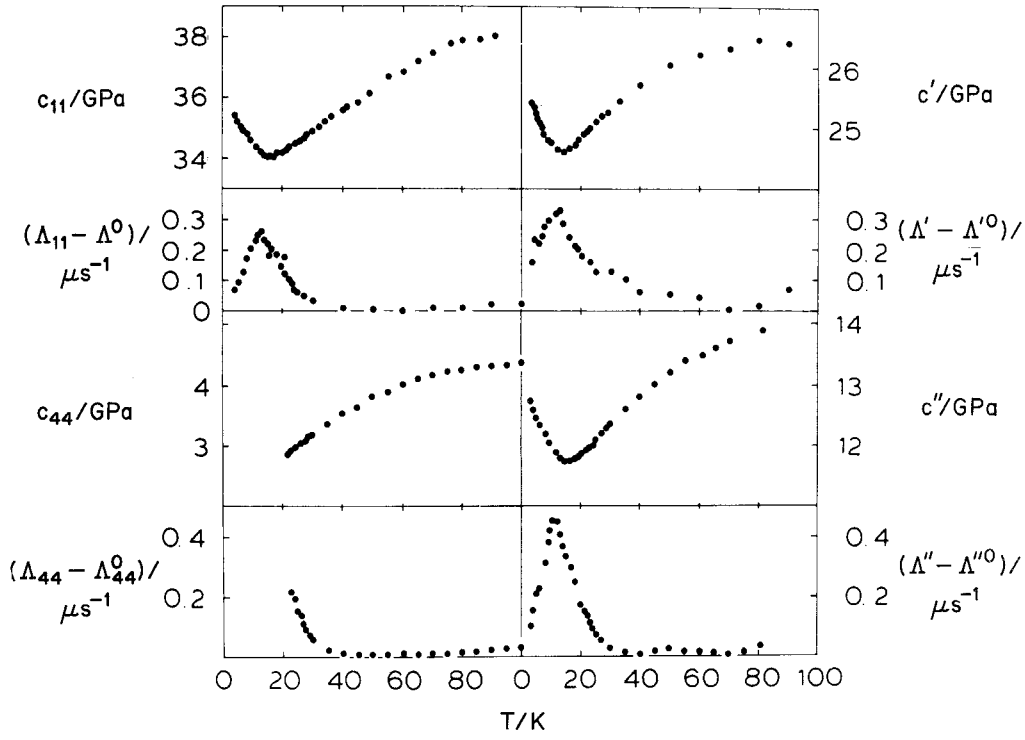

Figure 5.8. Temperature dependences of various elastic constants and corresponding attenuations in $(KBr)_{0.96}(KCN)_{0.94}$ as derived from ultrasonic 10 MHz measurements: c_{11} $[A_{1g} + \frac{4}{3}E_g]$, $\Lambda_{11} - \Lambda^0_{11}$, c_{44} $[T_{2g}]$, $\Lambda_{44} - \Lambda^0_{44}$, $c' = \frac{1}{2}(c_{11} + c_{12} + 2c_{44})$ $[A_{1g} + \frac{1}{3}E_g + T_{2g}]$, $\Lambda' - \Lambda'^0$, $c'' = \frac{1}{2}(c_{11} - c_{12})$ $[E_g]$ and $\Lambda'' - \Lambda''^0$. For the c_{44} modes, the echoes are lost at lower temperatures. c^0_{ij} is a T-independent background. From Loidl *et al.* (1981).

(v) The striking similarity of the elastic response for $x = 0{\cdot}53$ and $0{\cdot}73$ suggests that the interpretation of the elastic behaviour of the ordering and the 'glass-forming' mixed cyanides should be treated using the same framework. It has been suggested that the formation of the glass-like state is closely related to a ferroelastic transition, the long-range order of the ferroelastic phase being replaced by an equivalent short-range order in the glass state. The primary loss peak could be due to stress-induced domain motion, conventional ferroelastic domains and domain-like regions of uniform shear strain in the glass state (Ihm 1984, Galam 1990a, b). The torsion-pendulum measurements provided the basis for the concept that the primary freezing process of the mixed cyanides involves quadrupolar modes, namely coupled orientational–translational quadrupolar modes. The secondary process simultaneously involves quadrupolar and electric dipolar modes. Both freezing processes are accompanied by relaxation effects, as is evident from the frequency dependence of the loss peaks and the related cusps or steps in the real part of the response functions. The frequency dependence of the quadrupolar freezing temperature is evident from a comparison of inelastic neutron-scattering, Brillouin, ultrasonic and torsion-pendulum experiments on c_{44} (figure 5.10). $T_f(\omega)$ follows roughly an Arrhenius law with a hindering potential of the order of 6000 K for $x = 0{\cdot}5$ (figure 5.11; Volkmann *et al.* 1986).

The linewidth of the T_{2g} transverse acoustic phonons in $(KBr)_{1-x}(KCN)_x$ has been investigated by Brillouin scattering (Vanderwal *et al.* 1986, Hu *et al.* 1988a). The

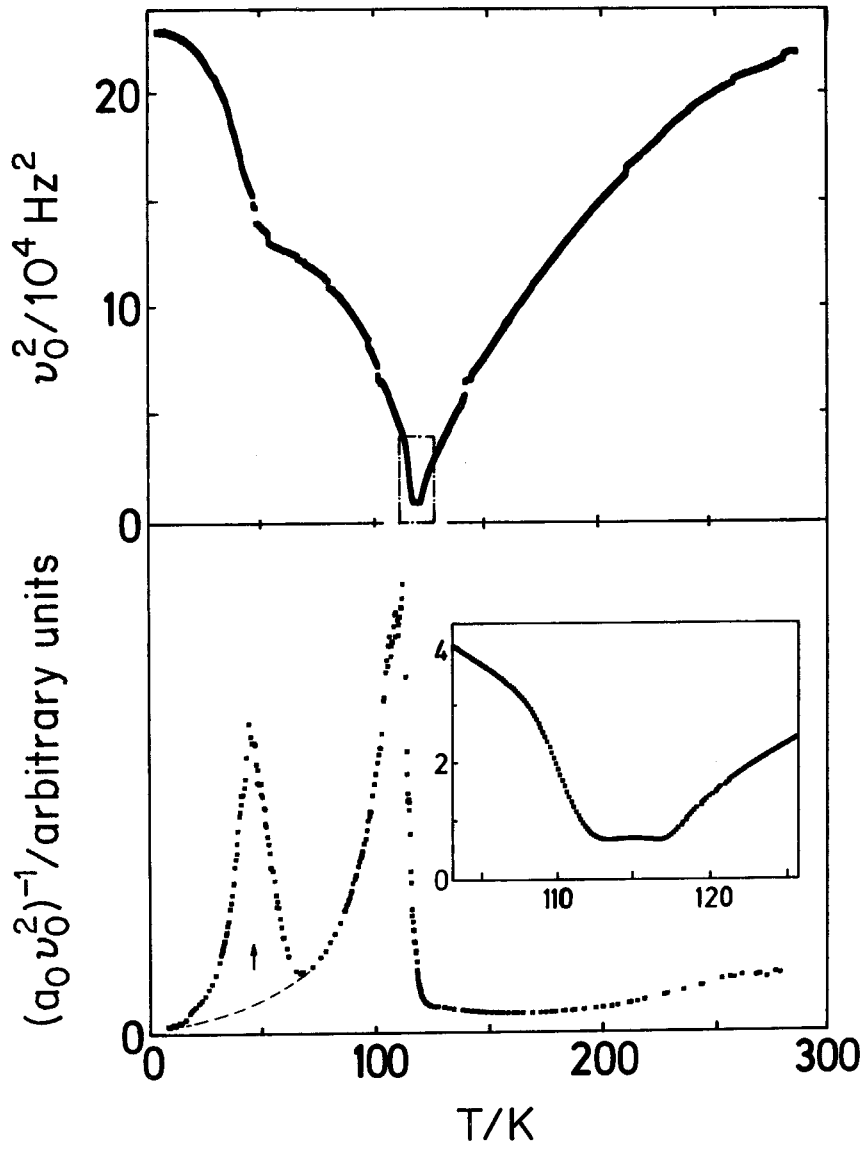

(*a*)

Figure 5.9. Temperature dependence of the elastic shear constant c_{44} and the related internal friction (lower plots) of $(KBr)_{1-x}(KCN)_x$ for $x = 0{\cdot}75$ (*a*) and $0{\cdot}5$ (*b*) as derived from the eigenfrequency ν_0 and the amplitude in resonance a_0 of a torsional oscillator. The sample with $x = 0{\cdot}75$ (later re-determined as $0{\cdot}73$) (*a*) undergoes two consecutive phase transitions at 117 and 112·5 K into orientationally ordered non-cubic low-temperature phases. The sample with $x = 0{\cdot}5$ (later redetermined as $0{\cdot}53$) (*b*) forms a glass-like state at low temperatures. Discontinuities are due to the anticrossing of parasitic resonances in the set-up. Arrows indicate the temperatures where the dielectric loss peaks when extrapolated to the frequencies of the torsional oscillator. From Knorr *et al.* (1986).

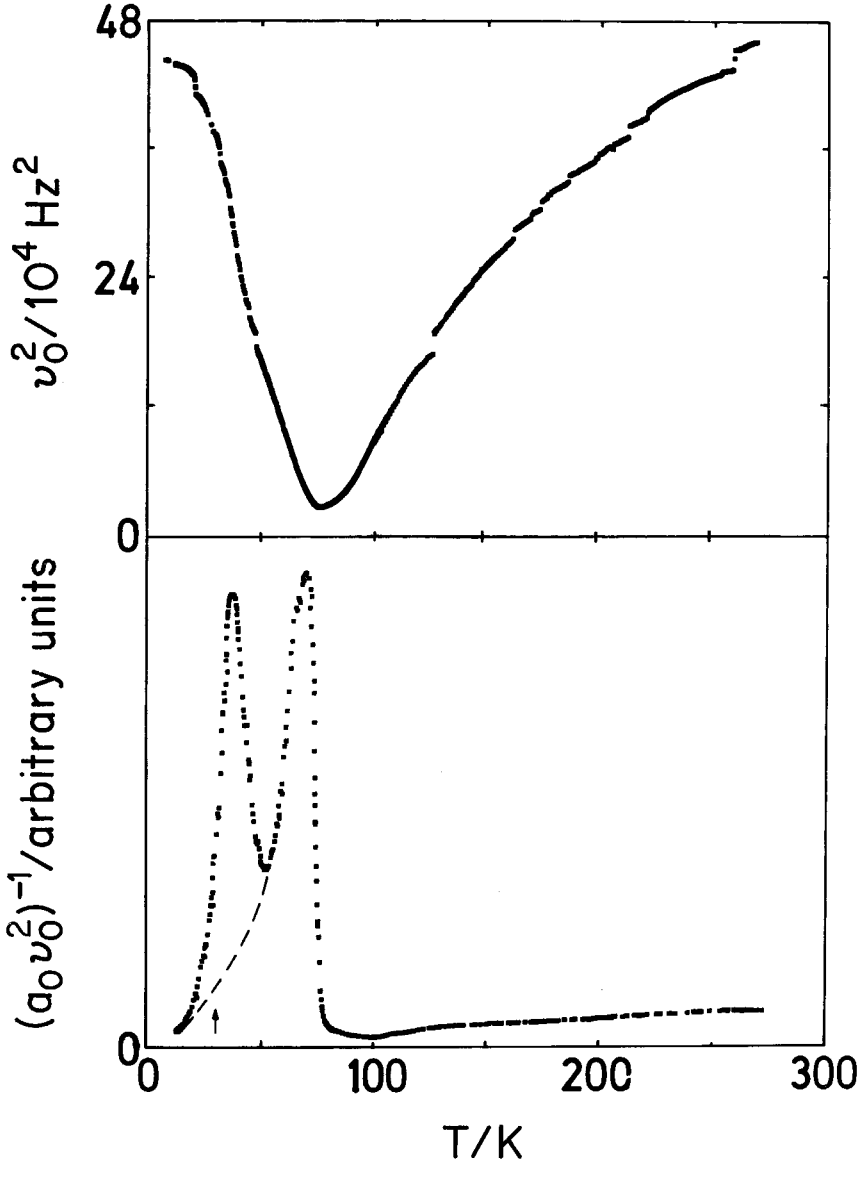

(*b*)

Figure 5.9. Continued.

phonon linewidth peaks at temperatures slightly below T_f; above T_f the width is proportional to $e^{-1/T}$. The results have been discussed by Walton (1990) in terms of a model of hierarchically constrained relaxations (Palmer *et al.* 1984). Hu *et al.* (1988b) showed that symmetry-forbidden Brillouin peaks appear in uniaxially stressed samples around T_f.

Michel's (1986, 1987a, b) random-strain-field model stimulated further studies of the elastic shear response of the mixed cyanides. Garland and co-workers have investigated $c_{44}(T)$ in $(KBr)_{1-x}(KCN)_x$, $(KCl)_{1-x}(KCN)_x$, $(RbBr)_{1-x}(RbCN)_x$ (Fossum

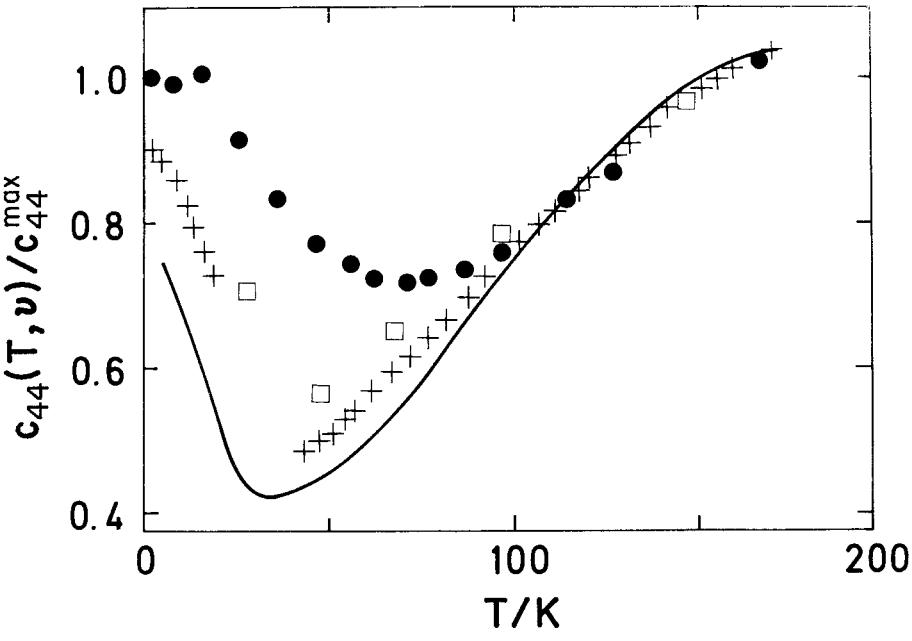

Figure 5.10. Normalized elastic constant c_{44} against temperature as determined in $(KBr)_{0\cdot8}(KCN)_{0\cdot2}$ for different measuring frequencies: (●), terahertz region, neutron-scattering studies; (□), gigahertz region, Brillouin data (x = 0·19) (Satija and Wang 1978); (+), 10 MHz region, ultrasonic results; (——), kilohertz region, torsion-pendulum measurements. From Volkmann *et al.* (1986).

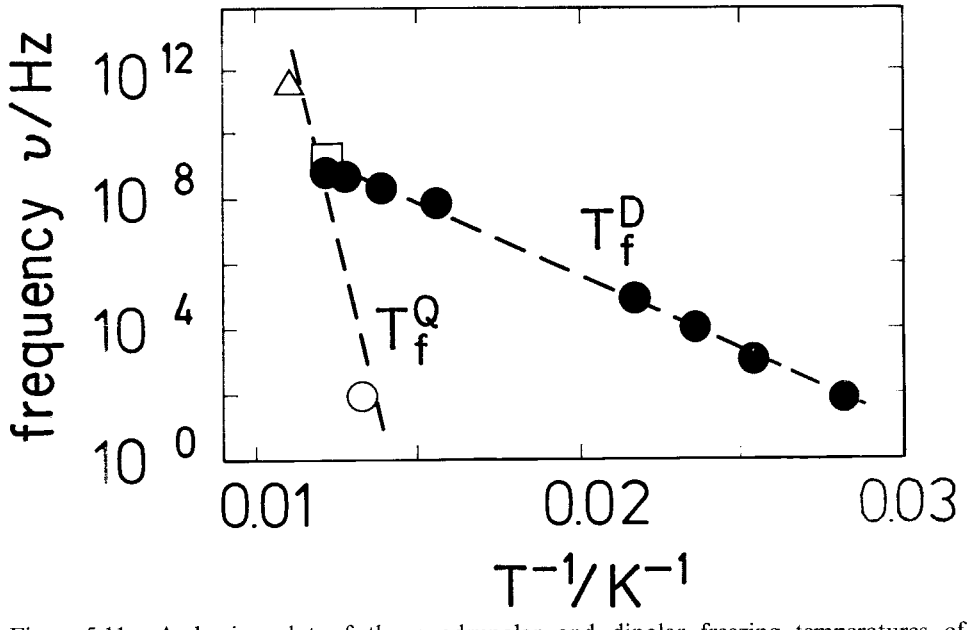

Figure 5.11. Arrhenius plot of the quadrupolar and dipolar freezing temperatures of $(KBr)_{0\cdot5}(KCN)_{0\cdot5}$. The freezing temperatures were determined by the maxima of the real parts of the dipolar and quadrupolar susceptibilities. From Volkmann *et al.* (1986).

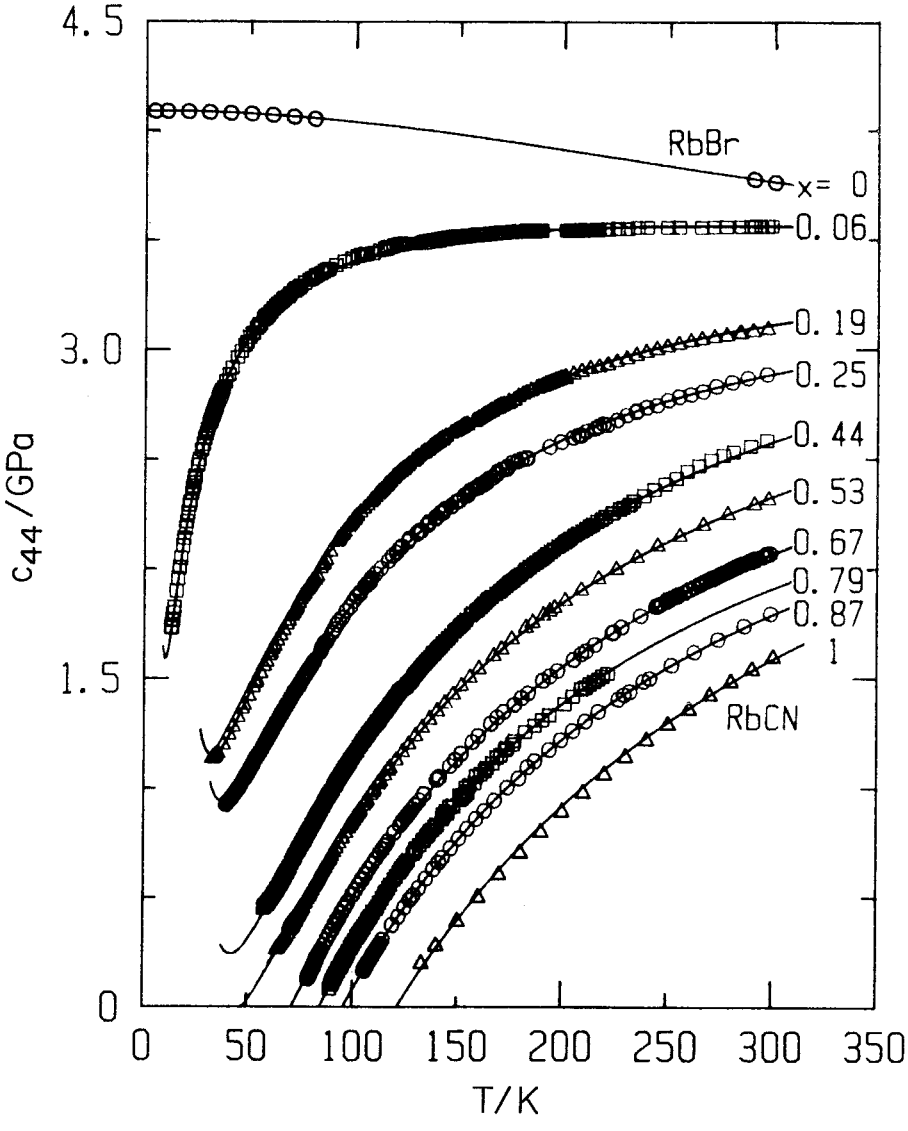

Figure 5.12. Temperature dependence of the elastic constant c_{44} of $(RbBr)_{1-x}(RbCN)_x$, obtained from ultrasonic measurements at megahertz frequencies. For $x = 0{\cdot}19$, the ultrasonic echoes are recovered at low temperatures. The solid lines are fits of the random-field model to the data. From Fossum *et al.* (1988).

and Garland 1988a, b, Fossum *et al.* 1988, Garland *et al.* 1988). The data for a series of mixed crystals of the latter type are displayed in figure 5.12. In the para-elastic regime (i.e. at temperatures above the prospective ordering or freezing temperature), $c_{44}(T)$ shows slight deviations from Curie–Weiss behaviour that are well described by the random-field model of Michel. From a pragmatic point of view, this means that in the para-elastic regime $c_{44}(T, x)$ for a given series of mixed crystals can be approximately described by just three parameters: a background elastic constant c_{44}^0, a translation–rotation coupling constant represented by $T_0(x = 1)$ and the variance of the random field distribution h_0^2, with $T_0(x) = xT_0(x = 1)$ and $h^2(x) = x(1 - x)h_0^2$.

According to Michel, the quantity $q(T) = h^2/T^2$ is regarded as the 'glass order parameter'. The fit of the model to the data becomes excellent when the Weiss parameter Θ is introduced. The fitted curves can be extrapolated to lower temperatures where no experimental data exist; here the curves predict a minimum of $c_{44}(T)$ at a temperature T_f. The relevance of these temperatures is open to question since the model was developed for the high-temperature limit only.

Occasionally, in particular in samples with low CN concentrations, Garland and co-workers could recover the ultrasonic echoes at low temperatures. They interpreted the results at these low temperature in terms of an analytical form for $q(T)$ taken from Ising random-field models.

Berret *et al.* (1988) investigated $(KCl)_{1-x}(KCN)_x$ by Brillouin scattering and presented data on $c_{44}(T)$, $c_{11}(T)$ and the attenuation α of the longitudinal (c_{11}) mode. They were able to trace the minimum of $c_{44}(T)$, and showed that the results are in good agreement with Michel's random-field model. It might be asked whether the upturn of $c_{44}(T)$ as measured at gigahertz frequencies is really characteristic of the static elastic properties, for which Michel's model was developed, and not of dispersion effects. It should also be realized that Michel treats the high-temperature limit, where $q(T) << 1$. It is an open question whether the model can be extrapolated down to temperatures where $q > \frac{1}{3}$.

Hessinger and Knorr (1989) investigated c_{44} for $(KBr)_{1-x}(KCN)_x$ with $x = 0{\cdot}41$, $0{\cdot}53$ and $0{\cdot}73$ in a quasi-static set-up with a sinusoidal variation of the shear stress with frequencies of $0{\cdot}1$ and 1 Hz, and alternatively by elastic transients in a time window from 5 ms to 5 s. The results basically show the same features as the torsion-pendulum study. In addition, it was shown that the shear response below T_c and T_f consists of a spontaneous and a relaxing component. The maximum relaxation time observed was $0{\cdot}8$ s. The T_f values are slightly lower than those from the torsion-pendulum study, and are consistent with the Arrhenius law cited above. The values of the elastic constant at the lowest temperatures are considerably lower than those from studies at higher measuring frequencies, where the low-T values are usually about equal to the room-temperature values. In addition these low-T values vary slightly from run to run. This observation suggests that the stiffening of $c_{44}(T)$ is a mainly dynamic effect (i.e. that the static elastic shear constant stays low in the glass-like state) and depends on the microstructure of the glass-like state, which may be different from cooling cycle to cooling cycle in the same sense as the domain pattern of the ordered phases depends on the details of the (usually badly controlled) experimental conditions at T_c, such as temperature gradients, residual external strains and lattice defects. Comparison with Michel's model shows that the increase of c_{44} below T_f is considerably weaker than predicted by the model.

Summarizing the elastic properties, we emphasize the following points. In the pure cyanides and in the case of dilute CN impurities in halides, the elastic constant c_{44} is linearly coupled to the T_{2g} quadrupolar orientational susceptibility. It is assumed that this linear relation also holds at intermediate CN concentrations. Thus c_{44} is the relevant susceptibility for the freezing into the quadrupolar-glass state. When measured at finite frequency, $c_{44}(T)$ shows a minimum at the so-called freezing temperature T_f. The elastic loss shows a maximum at a temperature slightly below T_f. The value of T_f is lower for lower measuring frequencies, roughly following an Arrhenius law. It is thus clear that the stiffening of c_{44} below T_f has to be regarded partly, if not completely, as a dispersion step. The quadrupolar relaxations, which are responsible for the elastic loss peak slightly below T_f, are called primary or α

relaxations. The T dependence of the static shear response below T_f is not known. There are initial indications that the static elastic constant c_{44} is independent of T and small below T_f. Michel's (high-T) random-field model is a valuable starting point and has been successfully applied at higher temperatures, but it should not be extrapolated to lower temperatures, where the condition $q << 1$ is necessarily violated.

Many questions on the elastic behaviour are left unanswered. There have been no measurements of either the nonlinear elastic susceptibility or on field-cooled samples, from which the remanent shear strain could be determined. Even the primary relaxations have not been investigated systematically. Here elastic studies suffer from the problem that large changes in the measuring frequency are not possible without a change in the experimental method.

5.2.2. *Phonon dispersion and neutron scattering*

In principle, inelastic neutron scattering can probe the frequencies and wavevectors of both the orientational and translational (phonon) excitations. In practice, mainly because of restrictions of the accessible momentum transfer, only the phonons have been investigated. The orientational modes are probed only indirectly, namely when they couple to the phonon susceptibility $D(Q, \omega)$. The coupling is apparent from modifications of the acoustic branches. A hybridization of the phonon branch with a well defined orientational mode could only be observed at low temperatures for relatively low CN concentrations. Neutron studies have not been performed in the ordered phases because of the formation of the multidomain state.

Measurements on $(KBr)_{1-x}(KCN)_x$ (Rowe *et al.* 1980, Loidl *et al.* 1980, 1983b) and $(KCl)_{1-x}(KCN)_x$ (Nicklow *et al.* 1980), on samples with x in the 1% range, basically confirm what was already known from the dilute case: E_g phonons couple to a librational mode in the 1 meV range, with a systematic shift to higher energies at higher CN concentrations. The T_{2g} phonons couple to a tunnelling excitation in the 0·1 meV range: 0·28 meV in the bromide with $x = 0{\cdot}00037$. Various data on bromides with higher concentrations exist for $x = 0{\cdot}5$ (Rowe *et al.* 1979) and $x = 0{\cdot}16$ and 0·20 (Loidl *et al.* 1984). The latter authors reported a shift of the librational mode from 1·7 meV to 2·4 meV and 4 meV for $x = 0{\cdot}008$, 0·035 and 0·16 respectively. The tunnelling mode could only be observed for $x = 0{\cdot}008$; for $x = 0{\cdot}16$ it is no longer detectable even at the lowest temperatures, presumably owing to a wide distribution of the tunnelling frequencies in the glass state. It was also shown that the coupling of the orientational modes to the phonons is significantly reduced on cooling through the freezing temperature—as if an increasing fraction of the CN^- ions no longer interact with the T_{2g} phonons. A comparison with ultrasonic data was made and the consistency of the results obtained with the two techniques was noted. In mixed cyanides with higher CN concentrations and/or higher temperatures, where discrete orientational modes are no longer observable, the orientational susceptibility can be approximated by a relaxational *Ansatz* $\chi(\omega) = C/(1 - i\omega\tau)$. In the initial part of an acoustic branch, the case of fast relaxation is realized. Here the phonon frequencies are renormalized to lower frequencies. It is this behaviour that leads to the softening of the elastic constant c_{44} in the cyanides. The case of slow relaxation is realized for the acoustic phonons of the outer part of the Brillouin zone. Here the phonon modes are practically unaffected, but an additional quasi-elastic component appears in the phonon response. The cross-over from one case to the other leads to a spectral response function Im $D(q, \omega)$, whose maxima with respect to q and ω yield an S-shaped dispersion relation of the T_{2g} branches. Pertinent neutron results have

been presented by Rowe *et al.* (1978a, b) for KCN, Loidl *et al.* (1984) for $(KBr)_{1-x}(KCN)_x$ and Elschner *et al.* (1987) for $(NaCl)_{1-x}(NaCN)_x$. This relaxational model does not predict the central peak at low q values, mentioned above as a measure of the glass order parameter.

5.2.3. *Molecular excitations and Raman spectroscopy*

Raman measurements on $(KBr)_{1-x}(KCN)_x$ and $(KCl)_{1-x}(KCN)_x$ performed at the University of Utah in the mid-1970s were the first investigations of mixed cyanides at intermediate CN concentrations (Durand and Lüty 1977, Lüty 1981). They showed that the phase transitions of pure KCN are eventually suppressed below a threshold concentration x_c. The idea of CN molecules coupled to clusters was formulated.

For $(KCl)_{1-x}(KCN)_x$ and $(KBr)_{1-x}(KCN)_x$, the Raman spectrum at low energies and in the vicinity of the CN stretching mode has been studied as a function of CN concentration x and temperature. Considering the spectrum at 10 K, one notes that it changes continuously with x on going from the dilute case to pure KCN (figure 5.5). Orientational modes are identified in the low-energy spectrum and as side bands of the stretching mode. The low-energy spectrum shows additionally a contribution from phonons, which become Raman-allowed because of the chemical disorder of the mixed crystals. The stretching band does not couple to phonons. Making use of the x dependence of the various features in the spectrum, the stretching mode and the orientational modes at lower x could be attributed to single CN defects, pairs, triples and quadrupoles of coupled CN molecules. At higher x, all lines merge into a broad, almost structureless, distribution. Above about $x = 0{\cdot}8$, this distribution narrows again into the sharp stretching band characteristic of the ordered phase of KCN. Both the dilute-CN-impurity and the orthorhombic low-T states of KCN show well defined resonances, whereas for intermediate concentrations the spectra are washed out. Qualitatively the same observations have been made for $(KBr)_{1-x}(KCN)_x$.

Grant and Klein (1985) studied the stretching region of the Raman spectrum of $(KCl)_{1-x}(KCN)_x$ with $x = 0{\cdot}06$, $0{\cdot}08$ and $0{\cdot}11$ as a function of temperature. Their data confirm those of Lüty and Durand. Grant and Klein suggested specific configurations of CN pairs and triplets. In the most probable pair configuration of the neighbouring CN ions, the CN axes point in different $\langle 111 \rangle$ directions, forming a T.

5.2.4. *Structures and diffraction*

5.2.4.1. *Phase diagrams* The (x, T) phase diagrams of the mixed cyanides (figure 5.13) have been determined mainly by optical-transmission experiments, X-ray and neutron diffraction and heat-capacity measurements.

Lüty and co-workers (Lüty 1981, Ortiz-Lopez 1983, Ortiz-Lopez and Lüty 1988) have determined the cubic–non-cubic phase boundary $T_c(x)$ of several mixed cyanides from optical-transmission experiments. Cubic single crystals are transparent, whereas in the non-cubic state the samples are opaque because of the formation of a multi-domain state. In some cases, a second fall in the transmission due to a second phase transition was observed. The dependence of $T_c(x)$ in $(KBr)_{1-x}(KCN)_x$ and $(KCl)_{1-x}(KCN)_x$ on hydrostatic pressure was determined. The results suggest that $(KCl)_{1-x}(KCN)_x$ samples with $x < x_c$ can be driven from the glass-like state into the ferroelastic state by the application of pressure, whereas for $(KBr)_{1-x}(KCN)_x$ pressure favours the glass-like state. In the glass like state, the crystals remain transparent,

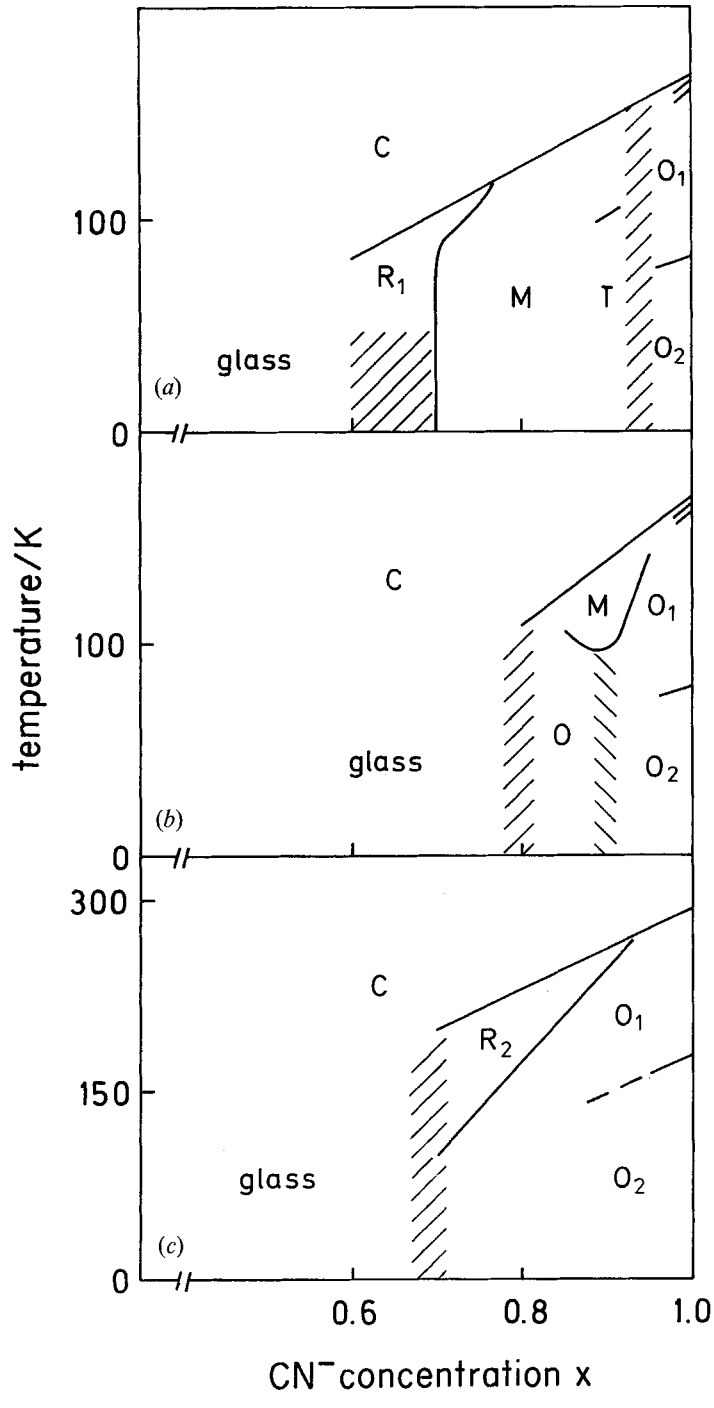

Figure 5.13. (x, T) phase diagrams of (*a*) $(KBr)_{1-x}(KCN)_x$ (based on Knorr and Loidl (1985), Mertz and Loidl (1987)), (*b*) $(KCl)_{1-x}(KCN)_x$ (Civera-Garcia *et al.* 1987, Bouillot *et al.* 1989) and (*c*) $(NaCl)_{1-x}(NaCN)_x$ (Elschner *et al.* 1985). Shaded areas indicate coexistence regions or states dependent on sample history. C, O, M, R and T stand for cubic, orthorhombic, monoclinic, rhombohedral and triclinic respectively.

indicating that possible quasidomains should have dimensions small compared with the wavelength of light.

The structures of the mixed cyanides were established by a long series of X-ray and neutron-diffraction studies. It was originally believed that one type of structural order exists in the low-T regime for all x with $x_c \leqslant x \leqslant 1$. Rowe *et al.* (1983) showed, however, that the non-cubic modification of $(KBr)_{1-x}(KCN)_x$ with $x = 0{\cdot}80$ is actually monoclinic rather than orthorhombic, and is isomorphic to the metastable form of thermally cycled KCN (and to the non-cubic state of RbCN, as verified later by Rowe *et al.* (1986). As mentioned above, the monoclinic structure results from homogeneous deformation of the cubic lattice and staggering of the internal positions.

A complete (x, T) phase diagram of $(KBr)_{1-x}(KCN)_x$ was derived from X-ray diffraction results by Knorr and Loidl (1985). An additional rhombohedral and a triclinic modification have been observed. Thus $(KBr)_{1-x}(KCN)_x$ shows five non-cubic modifications besides the cubic and glass-like states: two orthorhombic, a monoclinic, a rhombohedral and a triclinic phase.

$(NaCl)_{1-x}(NaCN)_x$ shows, besides the two orthorhombic forms known already from NaCN, a rhombohedral phase that results from homogeneous stretching of the cubic lattice along [111] (Elschner *et al.* 1985).

Various suggestions have been made for the structures of the non-cubic regime of $(KCl)_{1-x}(KCN)_x$. There is a consensus that for x close to unity the same sequence of phases as for KCN exists and that the threshold concentration x_c is around 0·8. Rowe *et al.* (1986) reported a phase with an unspecified non-cubic structure and orthorhombic–triclinic coexistence at low temperatures for $x = 0{\cdot}8$ and 0·9. Civera-Garcia *et al.* (1987), Bourson *et al.* (1987) and Bouillot *et al.* (1989) concluded that the low-T state is orthorhombic for all x, $x_c \leqslant x \leqslant 1$. For $x \approx 0{\cdot}9$, a monoclinic structure is observed at intermediate temperatures; the transformation from the monoclinic to the low-T orthorhombic state is incomplete. Civera *et al.* (1987) showed that for $x = 0{\cdot}8$ the orthorhombic state coexists with the glass-like state.

$(KI)_{1-x}(KCN)_x$ shows the orthorhombic low-T phase for $x > 0{\cdot}98$, the monoclinic state for $0{\cdot}85 < x < 0{\cdot}95$ and monoclinic–orthorhombic coexistence in between (Bourson *et al.* 1987).

The two orthorhombic and the monoclinic structures have already been described above in the section on pure cyanides. We recall that the orthorhombic phase at intermediate temperatures is elastically ordered but electrically disordered owing to head–tail degeneracy of the CN^- ions. The monoclinic phase is an antiferrodistortive variety of the cubic phase. It is electrically disordered. The rhombohedral phase results from ferroelastic distortion of the cubic parent phase, which can be visualized as stretching of the cubic lattice along [111] for $(NaCl)_{1-x}(NaCN)_x$ and compression for $(KBr)_{1-x}(KCN)_x$. In the latter situation, the CN^- ions are expected to conserve

Figure 5.14. The splitting of the (200) reflection of $(KBr)_{1-x}(KCN)_x$, $x = 1$, 0·73, 0·64, as seen in rocking scans as a function of temperature. The splitting is proportional to the spontaneous shear strain. The grey regions indicate the broadening of the reflection. The low-T phase of KCN is orthorhombic. The mixed crystal with $x = 0{\cdot}73$ is monoclinic at low T and rhombohedral at intermediate T. The low-T states for $x = 0{\cdot}64$ change upon thermal cycling. First cooling cycle (a) rhombohedral; third cycle (b) rhombohedral at intermediate T and monoclinic at low T; fifth cycle (c) glass-like at low T and a coexistence of glass-like and rhombohedral at intermediate T. In the 20th cycle (not shown) the rhombohedral component has practically vanished. From Knorr (1990b).

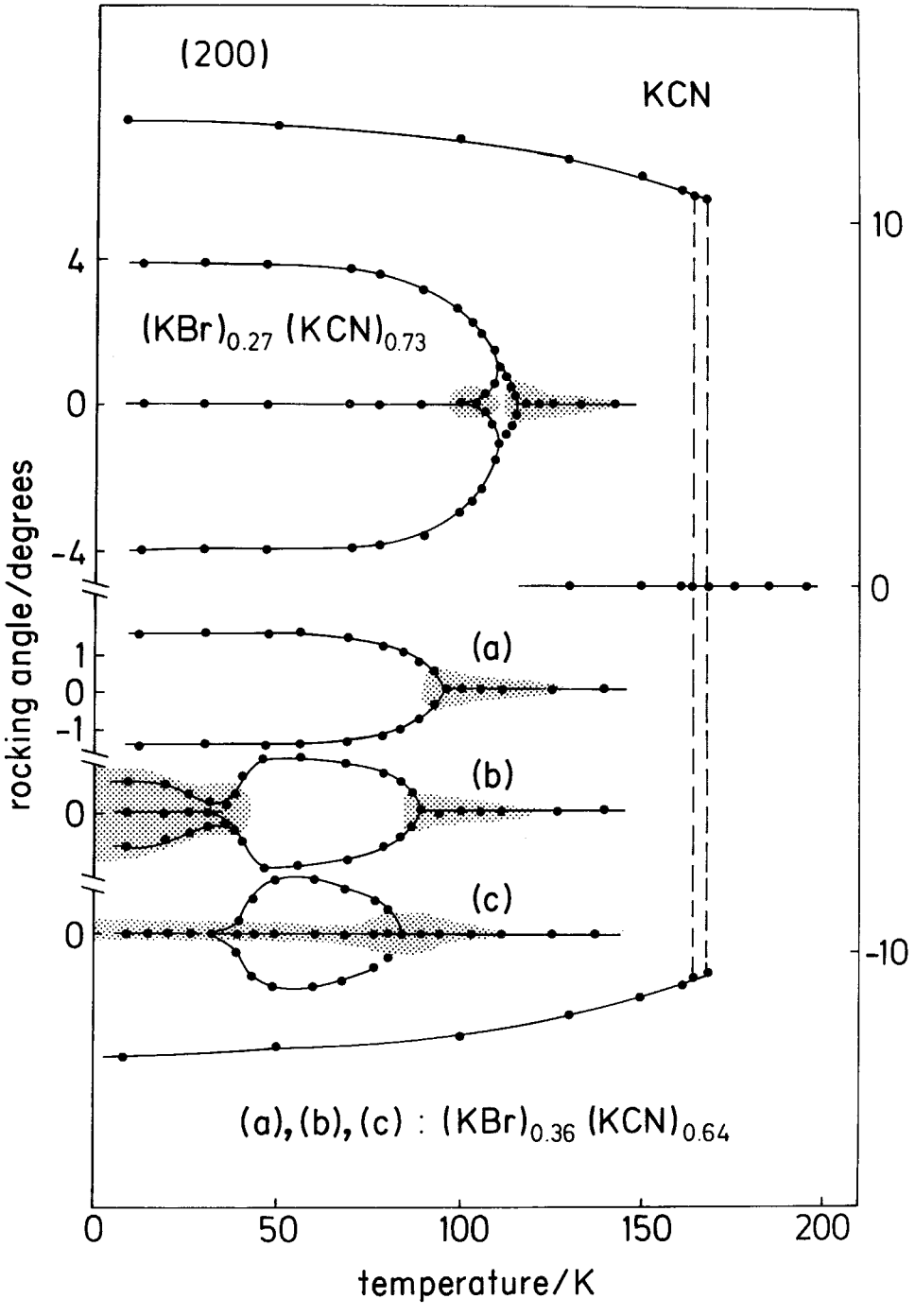
(200)
KCN
(KBr)0.27 (KCN)0.73
(a)
(b)
(c)
(a), (b), (c) : (KBr)0.36 (KCN)0.64
rocking angle/degrees
temperature/K
4
0
-4
1
0
-1
0
0
10
0
-10
0
50
100
150
200

their orientational disorder within the (111) plane. There are no indications of head–tail ordering in the rhombohedral state. The difference in the sign of the spontaneous shear between the rhombohedral state of $(NaCl)_{1-x}(NaCN)_x$ and that of $(KBr)_{1-x}(KCN)_x$ is surprising. Considering that the easy directions are along $\langle 111 \rangle$ for KCN and $\langle 100 \rangle$ for NaCN, one would have expected the signs to be opposite to what is observed. Clearly, expansion along [111] reduces the orientational entropy more effectively than compression.

The cubic-to-non-cubic transitions, with the exception of the cubic-to-rhombohedral transition of $(KBr)_{1-x}(KCN)_x$, are strongly discontinuous—as can be seen most clearly from the jump-like splitting of the diffraction lines at T_c (figure 5.14). For the cubic-to-rhombohedral transition of $(KBr)_{1-x}(KCN)_x$, which occurs for $0{\cdot}6 < x < 0{\cdot}75$, the splitting of the diffraction lines evolves continuously out of cubic lines that have already considerably broadened as T_c is approached. Thus, in $(KBr)_{1-x}(KCN)_x$, the character of the cubic-to-non-cubic transition changes from discontinuous to apparently continuous when x is reduced, until finally the phase transition is replaced by the evolution of the glass-like state. The corresponding decrease in the heat-capacity anomaly was observed by Lüty (1981) and more recently by Mertz and Loidl (1987). Already for the cubic-to-rhombohedral transition for $x = 0{\cdot}65$ the anomaly is hardly observable. Below x_c (here 0·6), the glass transition is not accompanied by heat-capacity anomaly.

The main element of pertinent Landau theories is the coupling of the orientations to the T_{2g} strains. The T_{2g} strain tensor has three components, which can be visualized as changes in the three cell angles of the cubic lattice. Condensation of all three components leads to the rhombohedral form, that of two components to the monoclinic form and that of one component to the orthorhombic form. How many components actually condense and whether there is an additional coupling to strains of other symmetry, like E_g strains for the cubic-to-orthorhombic or to a zone-boundary mode for the cubic-to-monoclinic transition, depends sensitively on the relationships between the expansion coefficients.

The cell parameters of the orthorhombic and monoclinic phases show remarkable degeneracies. For the monoclinic phase, for exmaple, with the parameters a, b, c and β, the relationship $c = 2b$ holds. It has been argued that these features are not so much manifestations of accidental relations between the Landau expansion coefficients but rather result from the principle of strain accommodation in a martensitic transformation (Knorr 1990a). The martensitic aspect of the transition has been pursued further, and it has been suggested that the change of the transition from cubic–orthorhombic to cubic–monoclinic to cubic–rhombohedral and eventually to cubic–glass-like, or more generally the polymorphism of the cyanides, is not so much a problem of the details of the microscopic interactions but primarily one of matching mesoscopic transformation strains. In fact, the appearance of the metastable monoclinic state in KCN shows that such problems occur already in a chemically well ordered cyanide.

5.2.4.2. *The planar ferroelastic instability* The ferroelastic instabilities have been classified by Cowley (1976) and Folk *et al.* (1976, 1979). For a cubic system, the soft T_{2g} modes form a two-dimensional manifold; they occur in planes of reciprocal space. Hence the structural instability is a planar one, belonging to the $m = 2$ class. On approaching a second-order phase transition, the amplitudes of the soft modes diverge. In contrast with the case of an individual soft mode ($m = 0$) or of a linear

instability ($m = 1$), a planar instability affects thermodynamic averages. In particular, the Debye–Waller factor is predicted to diverge when the critical temperature of an $m = 2$ system is approached; hence the Bragg intensities should disappear for $T \rightarrow T_c$. The crystal 'melts' for $T \rightarrow T_c$, in agreement with the popular idea that the disappearance of the shear rigidity signals melting. It has in fact been shown experimentally that in $(KBr)_{1-x}(KCN)_x$ with $x = 0{\cdot}73$ the Bragg peaks disappear and the T_{2g} phonon frequencies soften completely within the resolution of an inelastic neutron-scattering experiment (Knorr *et al.* 1985). Thus this compound appears to show the first example of a planar ferroelastic instability and its dramatic consequences. The objection can be made that the sample is a mixed crystal and that the phase transition is ultimately not due to the softening of c_{44} but rather to a divergence of the central peak. Analogously to the neutron results on the 'glass'-forming sample with $x = 0{\cdot}50$ (Rowe *et al.* 1979), the central peak develops below about 150 K, and eventually the soft phonons merge into it for $T \rightarrow T_c$. It is not clear whether the $m = 2$ aspect is essential for the formation of the glass-like state in the mixed cyanides, or whether this is just a peculiarity of $(KBr)_{1-x}(KCN)_x$, since in other mixed cyanides like, for example $(KCl)_{1-x}(KCN)_x$, the phase transition remains first-order for $x \rightarrow x_c$. However, in any case, the planar aspect of the low-lying T_{2g} modes—their abundance—has to be taken into account.

5.2.4.3. *Central peak* In their pioneering work, Rowe *et al.* (1979) showed that the glass-like state is characterized by static diffuse intensity, which is visible as central peaks in the constant-Q scans of neutron-scattering studies. The central-peak intensity can be regarded as the 'glass order parameter' $q(T)$. In Michel's random-field model, the central peak intensity is proportional to the random strains, which are again identified with the glass order parameter. Contour lines of the central-peak intensity in reciprocal space (figure 5.7) show that this intensity appears in those scattering geometries where T_{2g} phonons are also probed in an inelastic scattering experiment. This means that the diffuse intensity is due to a T_{2g} pattern of frozen-in phonons and orientations. The T and Q dependences of the diffuse pattern have been studied in several mixed cyanides. In X-ray powder diffraction, the growth of diffuse scattering leads to an apparent broadening of the powder lines in the glass state (with the exception of the $(h00)$ lines). This effect has been used to define a freezing temperature T_f in these studies (see Knorr and Loidl (1985) for $(KBr)_{1-x}(KCN)_x$; Elschner *et al.* (1985) for $(NaCl)_{1-x}(NaCN)_x$ (figure 5.15) and Civera-Garcia *et al.* (1987) for $(KCl)_{1-x}(KCN)_x$). In all of these studies, precursors of the line broadening were observed well above T_f, in agreement with the original work of Rowe *et al.* (1979).

More detailed information on the Q dependence of the diffuse intensity comes from single-crystal studies. Knorr and Loidl (1986) investigated the diffraction pattern of samples of $(KCl)_{1-x}(KCN)_x$ and $(KBr)_{1-x}(KCN)_x$. They showed that at room temperature, well into the cubic-phase region, the diffraction pattern consists of δ-function-like Bragg singularities and conventional diffuse intensity from acoustic phonons of a harmonic crystal: the diffuse intensity falls with the distance q from the Bragg point τ_{hkl} according to $I \sim q^{-2}$. With decreasing T, the diffuse intensity grows and the Bragg spikes decrease and merge into an anomalous diffraction profile. For $(KCl)_{1-x}(KCN)_x$ with $x = 0{\cdot}8$, a concentration that is close to if not identical with x_c, the low-temperature profiles measured in T_{2g} symmetry are described by $I \sim e^{-\alpha|q|}$ over three decades of intensity I (figure 5.16). Thus the δ-function-like singularity at $q = 0$ is replaced by a weaker cusp-shaped singularity. In the other samples, this

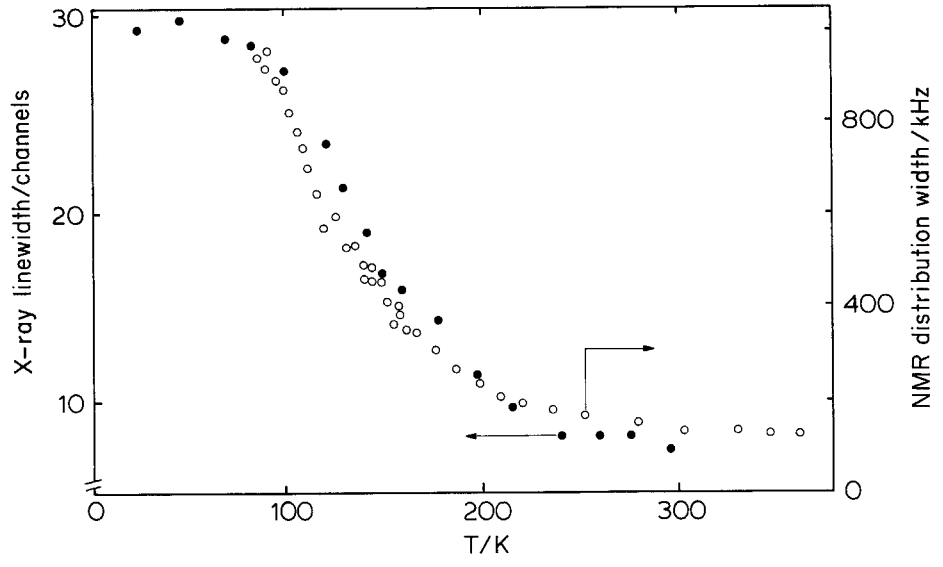

Figure 5.15. Temperature dependence of the width of the (220) powder line of the distribution of the electric-field gradient of $(NaCl)_{0.65}(NaCN)_{0.35}$. From Elschner *et al.* (1986).

peculiar shape is approached, but not completely realized. The decay parameter α depends on τ_{hkl}. Clearly, this is not the diffraction pattern of a harmonic crystal. It rather recalls that of a solid on the verge of crystallinity, such as a two-dimensional array or a liquid crystal. Nevertheless, the positions of cusp-like singularities of this profile still define the nodes of a cubic reciprocal lattice. The problem of the diffraction pattern of a crystal at a planar ferroelastic instability was treated theoretically by Mayer and Cowley (1988a), who found cusp-like singularities but a power law ($I \sim q^{-n}$, $n \neq 2$) rather than an exponential for $I(q)$.

Loidl *et al.* (1988) presented a detailed neutron-diffraction study of the diffraction profiles of $(KBr)_{1-x}(KCN)_x$ with $x = 0{\cdot}65$ and $0{\cdot}57$, concentrations that are just above and below x_c. They decomposed the profiles into Bragg and diffuse components and determined the weights and the T dependence of the components. The Bragg component decreases and the diffuse component increases with decreasing temperature. In the glass state, the Bragg component is virtually non-existent. The q width of the diffuse component scales approximately with $|\tau_{hkl}|$, suggesting that the random strains can be conceived as distributions of T_{2g} shear strains.

The q dependence of the diffuse intensity of a single crystal of $(KBr)_{1-x}(KCN)_x$ with $x = 0{\cdot}2$ was studied in detail by Wochner (1988). For this comparatively low CN concentration, the diffuse intensity is proportional to q^2 and was analysed in the framework of the local strain field induced by an aspherical defect (Huang scattering). It was suggested that in the glass state, two neighbouring CN^- ions are parallel. Wochner *et al.* (1989) also tried to resolve the frequency width of the central peak of $(KBr)_{0.8}(KCN)_{0.2}$. Their data suggest that well below and above T_f the width is limited by the experimental resolution (as in earlier studies), whereas around T_f it slightly exceeds the experimental resolution. At 50 K, they extracted an intrinsic width of 1·8 μeV, working with an experimental resolution of 8 μeV.

5.2.4.4. *Metastability* As already mentioned, the crystallographic structure of KCN just below T_c depends on the sample history.

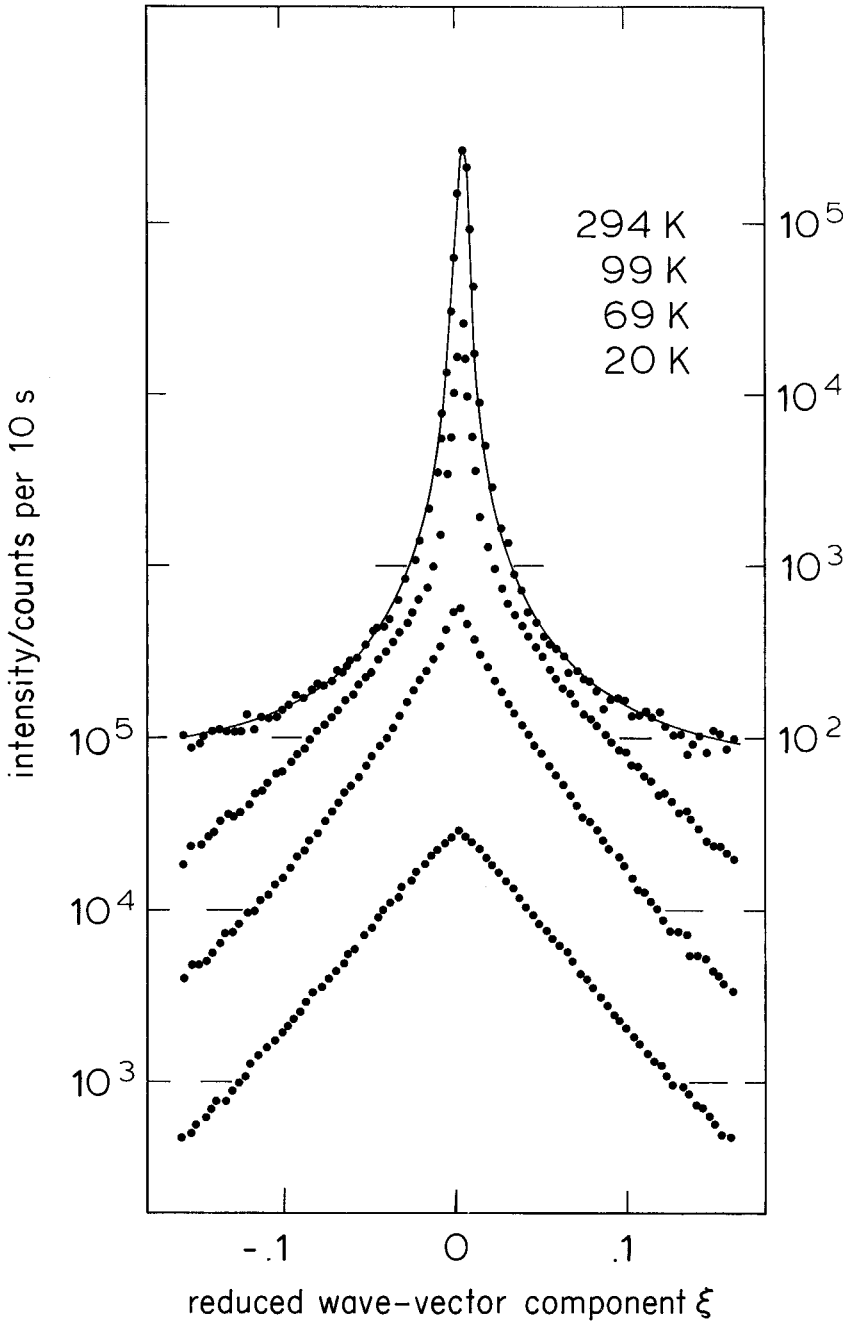

Figure 5.16. X-ray diffraction profile of $(KCl)_{0.2}(KCN)_{0.8}$ along $(2\xi\,0)$ at several temperatures. The intensity scale is logarithmic. The profiles are shifted by one order of magnitude with respect to each other. The 10^3 level is marked for each profile. The room-temperature profile is that of a harmonic crystal (solid line), consisting of a δ-function-like Bragg spike and thermal diffuse contributions ($I \sim q^{-2}$). The finite resolution has been taken into account. From Knorr and Loidl (1986).

$(KBr)_{1-x}(KCN)_x$ with $x = 0{\cdot}65$ has been investigated by X-ray powder diffraction. On the first cooling cycle, the sample undergoes a cubic-to-rhombohedral transition at about 85 K. After thermal cycling, the rhombohedral phase is conserved at intermediate temperatures, with a slight reduction of T_c of about 2 K. Below about 40 K, however, the structure changes to monoclinic, and the spontaneous deformations of the monoclinic phase are smaller than in the rhombohedral phase (figure 5.14). Upon further cycling, the monoclinic splitting of the diffraction narrows and becomes smeared out until it is eventually indistinguishable from the powder pattern of the orientational-glass state (Knorr *et al.* 1987).

In $(KCl)_{1-x}(KCN)_x$ with $x = 0{\cdot}80$, the powder lines broaden strongly upon cooling below 100 K. Hence, according to the criterion that broadened powder lines are characteristic of the glass state, it can be concluded that the sample has entered this state at $T_f = 100$ K. At 70 K, however, the linewidth saturates rather abruptly and sharp orthorhombic lines appear, superimposed on the broadened cubic lines. This profile suggests that the glass-like state coexists with the ordered orthorhombic state within the powder grains (Civera-Garcia *et al.* 1987). The observations may be related to Lüty's result on the different pressure dependences of the boundary of the ordered state in bromides and chlorides. If one assumes that both the formation of the rhombohedral phase in $(KBr)_{1-x}(KCN)_x$ and that of the glass-like state in $(KCl)_{1-x}(KCN)_x$ lead to the accumulation of pressure that increases with decreasing T then a release can be achieved according to Lüty's results by the formation of the glass state in $(KBr)_{1-x}(KCN)_x$ and of the ordered state in $(KCl)_{1-x}(KCN)_x$.

The rhombohedral structure of $(KBr)_{1-x}(KCN)_x$ with $0{\cdot}6 < x < 0{\cdot}75$ has been unambiguously identified in diffraction measurements on powders. A recent X-ray study of a single crystal with $x = 0{\cdot}65$ in the T range of the rhombohedral state, however, showed a pattern that is inconsistent with a rhombohedral lattice. It exhibits principal cubic reflections with additional satellites along the cubic axes (Knorr 1990a). Such a pattern suggests a cubic structure modulated by static shear modulations propagating independently along the cubic axes ('crest-riding periodon'). The wavelength of the modulation is about 25 lattice constants and the amplitude about 0·2 lattice constants. In a larger single crystal, these modulations cannot couple to a rhombohedral deformation. Knorr has suggested that this is because of transformation-strain accumulation—an effect that could be less serious in the smaller grains of a powdered specimen.

5.2.5. *Dielectric susceptibility*

5.2.5.1. *Low-temperature anomalies* We recall that the low-T dielectric properties of amorphous solids are fundamentally different from those of crystalline solids. The anomalous behaviour has been attributed to dipolar tunnelling transitions within a broad, almost constant, distribution of tunnelling states (two-level systems, TLS). The experimental manifestation of this scenario is as follows (Hunklinger 1977, von Schickfus 1982). The dielectric loss increases like T^3 and becomes temperature- and frequency-independent above T^* (T^* is related to a characteristic minimum relaxation time and is typically between 50 mK and 500 mK). For $T < T^*$, the real part of the dielectric constant exhibits a negative logarithmic temperature dependence. At T^*, ε_1 exhibits a minimum and increases for further increasing temperatures. The minimum in $\varepsilon_1(T)$ is frequency-dependent according to $T_{\min} \sim \omega^{1/3}$.

Low-temperature dielectric data for $(KBr)_{1-x}(KCN)_x$ were reported by Moy *et al.* (1984) for concentrations $x = 0{\cdot}01$, $0{\cdot}03$ and $0{\cdot}1$. Their general observation was

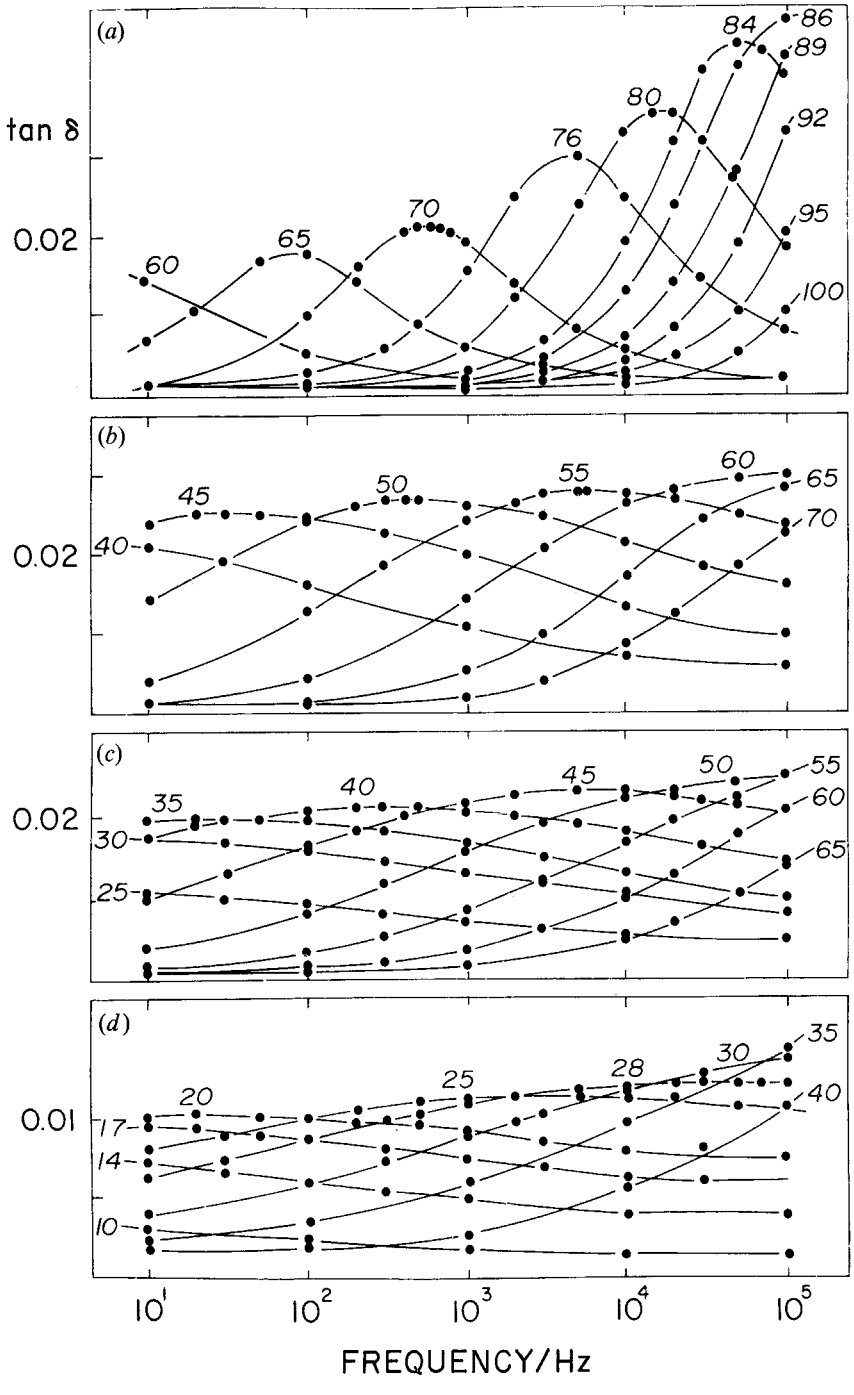

Figure 5.17. Dielectric loss (tangent of loss angle) against frequency in $(KBr)_{1-x}(KCN)_x$ for KCN concentrations $x = 1$ (*a*), 0·9 (*b*), 0·8 (*c*) and 0·5. (*d*) The number next to each curve gives the temperature in K. Note the dramatic increase of the frequency width of the loss from an almost-Debye-like behaviour ($x = 1$) to a wide distribution of relaxation times ($x = 0{\cdot}5$). From Lüty (1981).

that ε_1 passes through a minimum near 0·1 K. With increasing concentrations, this minimum becomes broad and smeared out. Moy *et al.* found $T_{\min} \approx \omega^{0.1}$ for $x = 0.03$ and $T_{\min} \approx \omega^{0.2}$ for $x = 0.1$, and concluded that the low-T dielectric behaviour of the mixed cyanides approaches that of the amorphous solids for higher CN concentrations.

Anomalous low-T dielectric properties of $(KBr)_{1-x}(KCN)_x$ mixed crystals with concentrations $x = 0.05$ and 0·08 have recently been reported by Baier *et al.* (1989), who found an increase of ε_1 with increasing temperature, while ε_2 remained almost constant. ε_1 and ε_2 depend strongly on the measuring frequency. Thus, although the relaxation behaviour is anomalous, it is fundamentally different from that observed in canonical glasses. Baier *et al.* (1989) analysed these results in the framework of a theory of collective dipolar relaxations (Janssen 1972). This model is only applicable if the defect concentration is so low that the tunnelling splitting is an almost fixed rather than a distributed value. Thus it appears that Janssen's view holds for low CN concentrations, whereas for higher CN concentrations the TLS behaviour is approached.

5.2.5.2. *Dielectric relaxation: dilute limit* Relaxation phenomena in dilute crystals ($x = 0.02$, 0·04 and 0·05) were described by Ortiz-Lopez (1983). An analysis in terms of an Arrhenius law yields an energy barrier $E_b = 32$ K and an attempt frequency $\nu_0 = 280$ MHz for $x = 0.05$. For a mixed crystal with a concentration $x = 0.02$, no loss peaks were observed down to 1·5 K.

5.2.5.3. *Dielectric relaxation at higher concentrations* A detailed and systematic investigation of the dielectric properties of $(KCl)_{1-x}(KCN)_x$ and $(KBr)_{1-x}(KCN)_x$ mixed crystals has been reported by Lüty and co-workers (Julian and Lüty 1977, Lüty 1981). Subsequently, $\varepsilon(\omega, T)$ data have been reported by Knorr and Loidl (1982), Loidl *et al.* (1982), Bhattacharya *et al.* (1982), Lüty and Ortiz-Lopez (1983), Ortiz-Lopez (1983), Birge *et al.* (1984) and Böhmer (1985). All mixed crystals investigated revealed clear dispersion effects. The relaxation phenomena were described by Arrhenius laws with energy barriers increasing almost linearly with concentration. The loss peaks of $\varepsilon_2(\omega)$ and dispersion steps of $\varepsilon_1(\omega)$ for the mixed cyanides are considerably broadened compared with the Debye case and can be described in terms of a wide distribution of relaxation times. The distribution is symmetric, and its width increases with decreasing concentration ($0.1 < x < 1$). In figure 5.17 the dielectric loss in $(KBr)_{1-x}(KCN)_x$ is plotted *versus* frequency for concentrations $x = 1$, 0·9, 0·8 and 0·5 (Lüty 1981).

The dielectric response of solid solutions of $(KBr)_{1-x}(KCN)_x$ was investigated by Knorr and Loidl (1982) for concentrations $0.01 > x > 0.5$. In order to explain the non-Debye behaviour of the complex dielectric susceptibility, they took additional random fields into account. A mean-random-field theory, which was originally

Figure 5.18. (*a*) Dielectric loss against logarithm of frequency for several temperatures in $(KBr)_{0.5}(KCN)_{0.5}$: ■, 19·7 K; ●, 25·9 K; ▲, 34·7 K. The solid lines indicate fits assuming a Gaussian distribution of hindering barriers. The dashed lines are the results of fits with a Kohlrausch–Williams–Watts function with $\beta = 0.16$. (*b*) Parameters of the Gaussian fits against inverse temperature: static dipolar susceptibility (■, ▲); mean relaxation time (●) and distribution width (□, △, ○). The inset shows a schematic diagram of the mean barrier heights and the distribution widths, which reveals a linear temperature dependence of the distribution width and of the mean height of the barriers. From Birge *et al.* (1984).

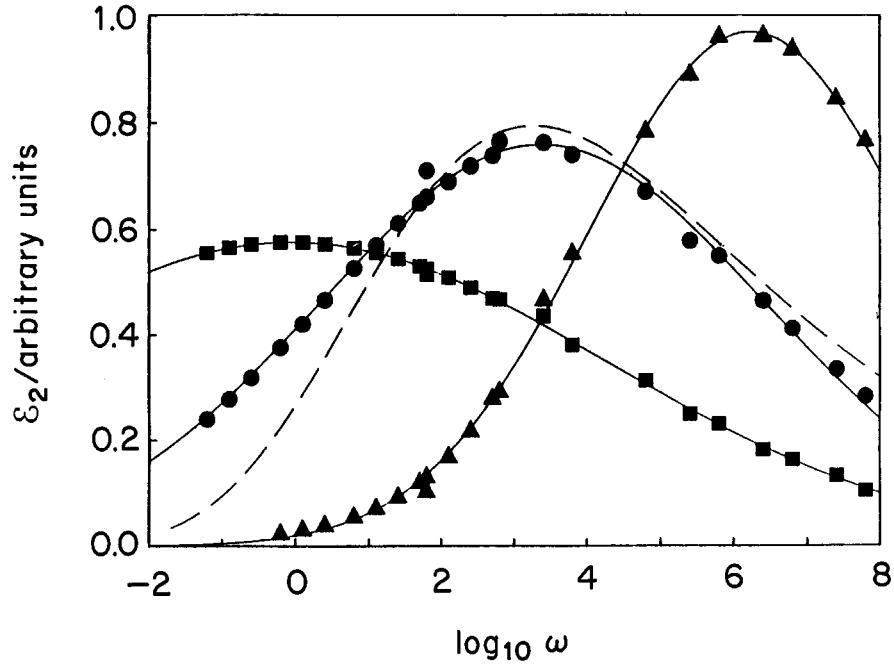

(*a*)

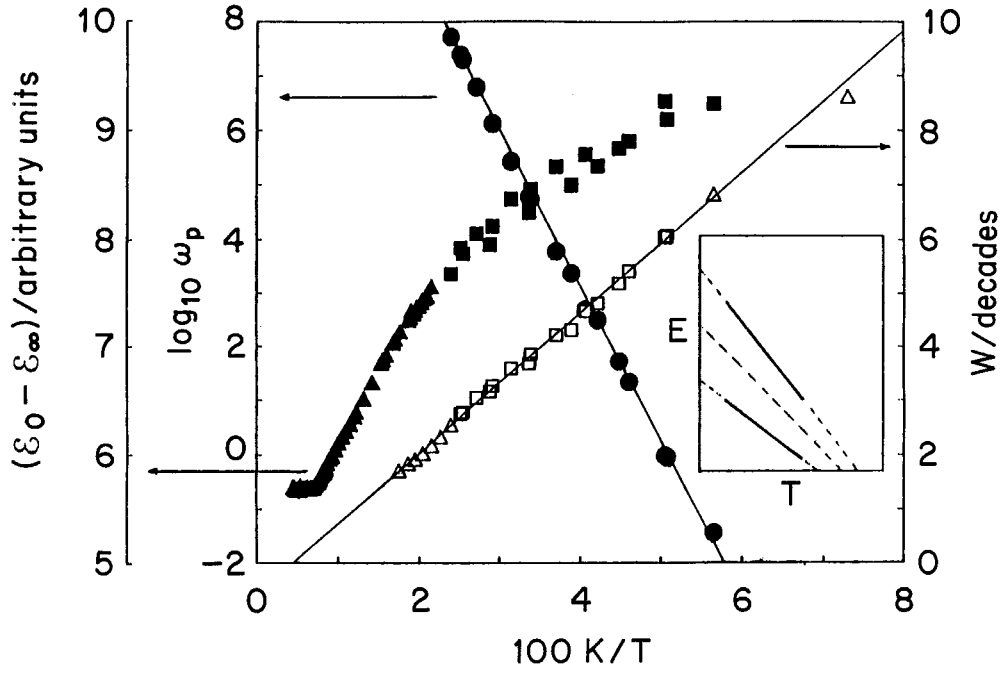

(*b*)

Figure 5.18. (Caption on previous page.)

developed by Fischer and Klein (1976) for OH^- ions in KCl at very low concentrations, accounted in a semiquantitative way for the concentration dependence of the dielectric constant. It did not, however, reproduce the observed dispersion. Later, the data of Knorr and Loidl (1982) were interpreted in terms of a distribution of energy barriers (Sekimoto *et al.* 1982).

Birge *et al.* (1984) reported the dielectric response of $(KBr)_{0.5}(KCN)_{0.5}$ covering approximately ten decades of frequency. They measured $\varepsilon(\nu)$ in the frequency range $10\,\text{mHz} < \nu < 100\,\text{MHz}$. For the slow time scales, the discharge current was investigated; it is proportional to the time derivative of the polarization. Figure 5.18 (*a*) shows ε_2 against log ν using combined frequency- and time-domain data (Birge *et al.* 1984). The results were interpreted in terms of a temperature-dependent Gaussian distribution of activation-energy barriers. The parameters of the fits are shown in figure 5.18 (*b*). The mean activation energies can be described by an ideal Arrhenius behaviour with a prefactor $\nu_0 = 50\,\text{THz}$ and an activation energy $E_b = 659\,\text{K}$. The static susceptibility increases for decreasing temperature, as does the width of the Gaussian fits.

Figure 5.19 shows $\varepsilon_1(T)$ for $(KCl)_{1-x}(KCN)_x$ with different concentrations x (Böhmer 1985). The drop in $\varepsilon_1(T)$ is accompanied by strong dispersion effects. It is interesting to note that, except for low concentrations ($x < 0{\cdot}3$), the dielectric data at high temperatures reveal no Curie or Curie–Weiss law. From the dielectric data, it is hard to decide whether or not the low-temperature state exhibits electric order: at high T, no paraelectric behaviour can be found, while at low T, in the region of dielectric dispersion, the static susceptibility (defined by the area of the loss peaks) is hard to determine because of the extremely broad distribution of relaxation times. For concentrations $x = 0{\cdot}91$ and $0{\cdot}81$, the elastic phase transitions show up as anomalies at high temperatures. For lower concentrations, the structural phase transitions are suppressed and the dielectric data give no evidence for the quadrupolar freezing as determined in the elastic experiments. The experimental evidence that only one freezing process is observable in the dipolar and in the quadrupolar susceptibilities was the starting point for some work concerned with the comparison of quadrupolar and dipolar freezing processes. In 1982 two groups noticed that the dispersion effects of the dipolar and quadrupolar susceptibilities followed a unique Arrhenius law (Loidl *et al.* 1982, Bhattacharya *et al.* 1982). Accordingly, dipoles and quadrupoles should be governed by the same relaxation process. More precise data lead to the opposite conclusion (see section 5.2.1 and below).

First hints that the dipolar and quadrupolar relaxation processes in $(KBr)_{1-x}(KCN)_x$ freeze out at different temperatures were given by Loidl (1985). However, the frequency range of the experiments was too limited to lead to conclusive results. Volkmann *et al.* (1986) presented data on the elastic and dielectric dispersions that covered a common frequency range of six decades ($100\,\text{Hz} < \nu < 1\,\text{GHz}$). Their results demonstrated unambiguously that dipolar and quadrupolar freezing are two different processes. For a quantitative comparison, the temperatures of the cusps of the dipolar and of the quadrupolar susceptibilities for $x = 0{\cdot}5$ are shown in an Arrhenius-type plot in figure 5.11 (Volkmann *et al.* 1986). The temperatures of both relaxation rates can be roughly described by an Arrhenius law (although significant deviations appear for quadrupolar freezing). The freezing temperatures coincide only at gigahertz frequencies. With decreasing temperature, the quadrupoles fall out of equilibrium much more rapidly, which results in an extremely steep slope of the relaxation rate in an Arrhenius representation. The hindering barriers and the attempt

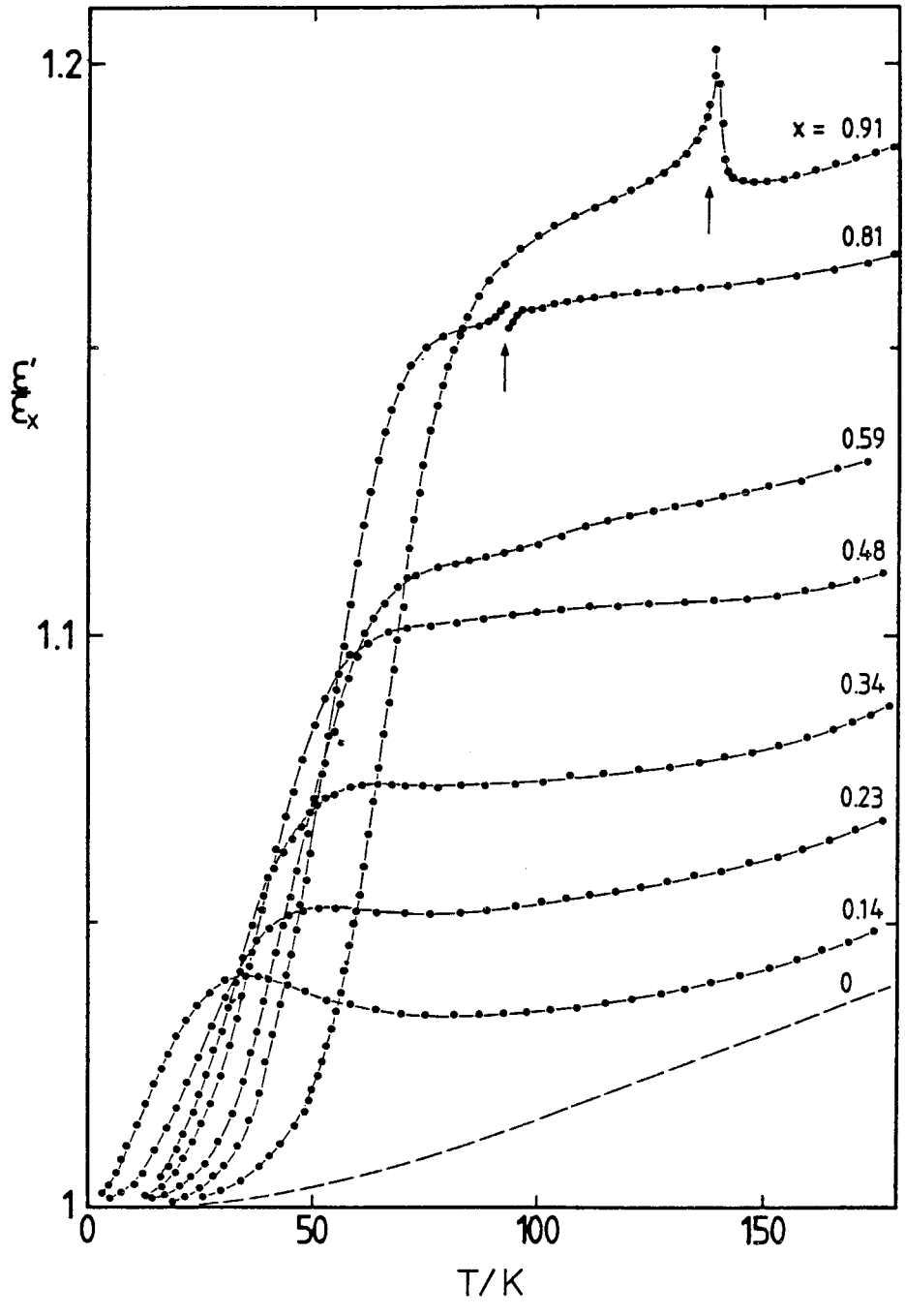

Figure 5.19. Dielectric constants of $(KCl)_{1-x}(KCN)_x$ at 100 kHz against temperature for concentrations x = 0·91, 0·81, 0·59, 0·48, 0·34, 0·23, 0·14 and 0. Arrows indicate structural-phase-transition temperatures. From Böhmer (1985).

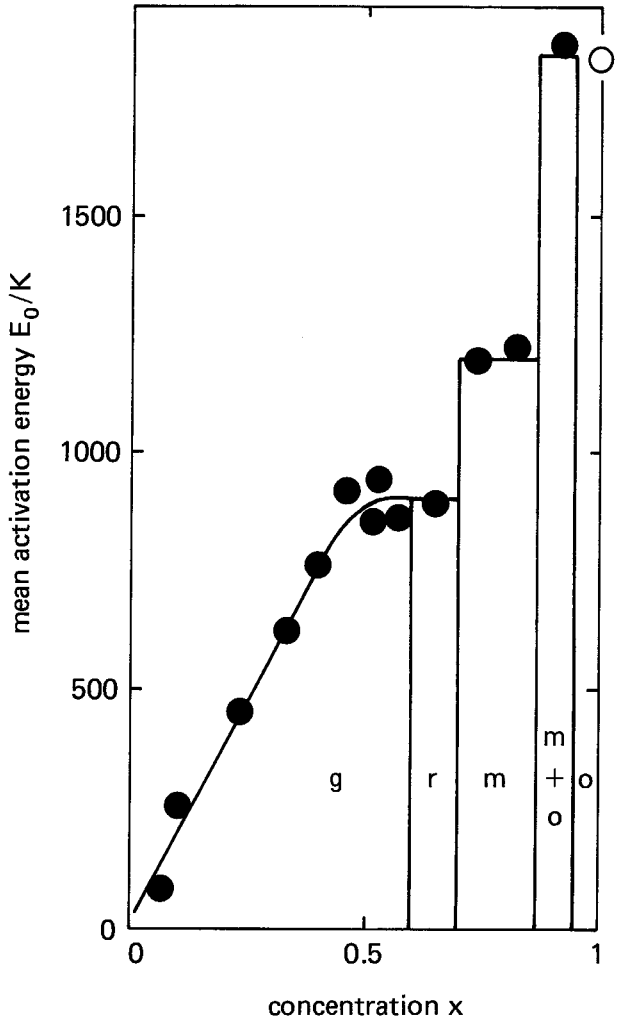

(*a*)

Figure 5.20. (*a*) Concentration dependence of the mean hindering barriers in $(KBr)_{1-x}(KCN)_x$. The vertical lines indicate the approximate phase boundaries. (*b*) Concentration dependence of the width of the Gaussian distribution of energy barriers in $(KBr)_{1-x}(KCN)_x$. Vertical lines indicate the phase boundaries between glassy (g), rhombohedral (r), monoclinic (m) and orthorhombic (o) phases. From Mertz *et al.* (1990a).

frequencies for quadrupolar relaxation are unphysically high and suggest a collective freezing process. These results reveal a striking similarity with relaxation dynamics in canonical glasses (Volkmann *et al.* 1986, Loidl and Knorr 1986): There are primary (α) relaxations of quadrupolar nature, which can be viewed as freezing-in of the quadrupole moments and local shear distortions. The secondary (β) relaxation is of dipolar and quadrupolar nature and probes the energy barriers as set up by the primary freezing.

Dielectric investigations have been extended up to frequencies of 10 GHz by Berret *et al.* (1988). The results of Volkmann *et al.* (1986) have essentially been confirmed.

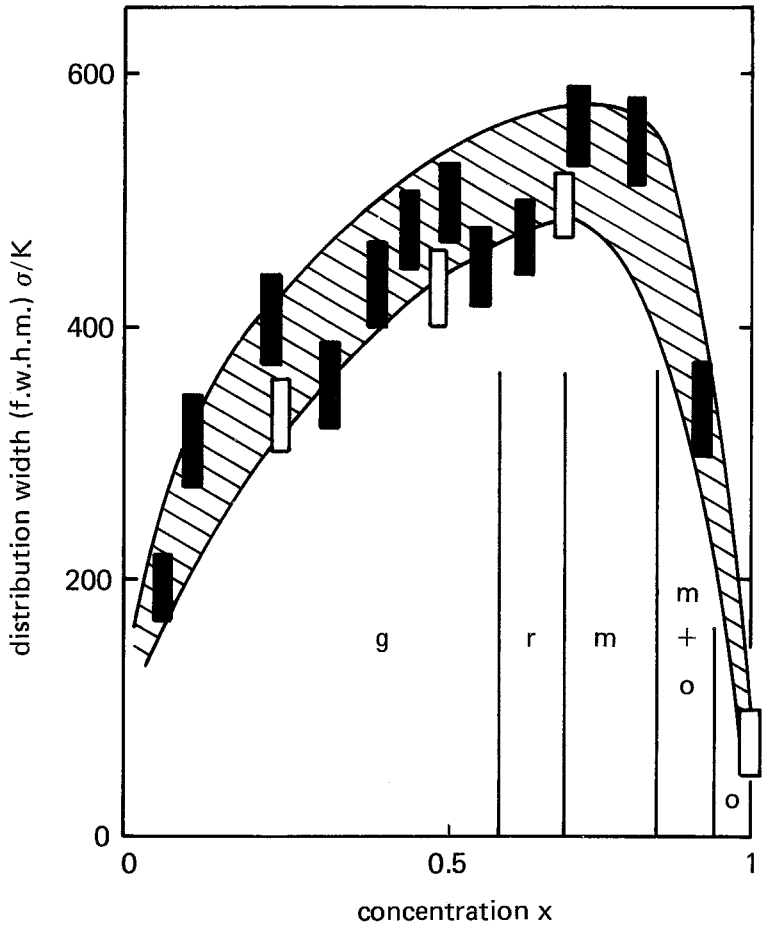

(*b*)

Figure 5.20. Continued.

The sequential freezing of dipolar and quadrupolar degrees of freedom has also been determined in nuclear magnetic resonance studies by Doverspike *et al.* (1986) (see section 5.2.7).

Sethna and co-workers proposed a microscopic model where the low-temperature thermodynamic behaviour has been related to the high-temperature dielectric relaxation phenomena (see section 5.2.6). To verify these model calculations experimentally, a number of dielectric investigations have been performed to determine the mean hindering barriers, their distribution widths and the attempt frequencies (Wu *et al.* 1988, Ernst *et al.* 1988, Mertz *et al.* 1990a). The concentration dependence of the attempt frequencies γ_0 is as follows: starting from the dilute limit, the attempt frequencies increase strongly with increasing CN concentration x and remain almost constant for concentrations $x > 0{\cdot}4$. The attempt frequencies for higher concentrations are approximately two decades higher than the lowest librational frequencies that one would regard as appropriate attempt frequencies. Under the assumption that the energy barriers increase linearly with T, τ_0 was shown to fall to reasonable values (Birge *et al.* 1984). At first glance, the mean activation energies shown in figure 5.20 (*a*) (Mertz *et al.* 1990a) grow linearly with increasing concentration. This suggests

that the hindering barriers to dipolar reorientations are set up by quadrupolar interaction forces (Sethna *et al.* 1984). Closer inspection shows that the energy barriers in crystals with orthorhombic or monoclinic low-temperature phases differ significantly from samples that exhibit a rhombohedral or a glassy (pseudocubic) phase. Thus the relaxation dynamics reflects the symmetry of the low-temperature state.

Finally, figure 5.20 (*b*) (Mertz *et al.* 1990a) shows the x dependence of the width σ of the Gaussian distribution of hindering barriers. The width of the distribution is largest in the monoclinic phases and decreases monotonically towards the pure compounds. It is a surprising result that the concentration dependence of σ does not exhibit any significant changes on the borderline between the disordered glassy state and the elastically ordered phases.

5.2.6. *Heat capacity and thermal conductivity*

5.2.6.1. *Heat capacity at phase and glass transitions* Pertinent heat-capacity measurements for $(KBr)_{1-x}(KCN)_x$ have been performed by Lüty (1981), Mertz and Loidl (1985, 1987), Moriya *et al.* (1984) and Matsuo *et al.* (1986).

The cubic-to-non-cubic phase transition shows up as anomalies in the temperature dependence of the heat capacity (figure 5.21). The measurements provide evidence of the first-order character of these structural phase transitions and help to establish the (x, T) phase diagram of $(KBr)_{1-x}(KCN)_x$. In particular, they allow specification of the (orthorhombic–monoclinic) coexistence region for $0{\cdot}90 < x < 0{\cdot}95$ (Mertz and Loidl 1987) and confirm the appearance of a metastable (monoclinic) phase in thermally cycled KCN (Suga *et al.* 1965).

The entropy changes at the structural phase transitions decrease dramatically with decreasing concentration x (Lüty 1981, Mertz and Loidl 1987) (figure 5.21). For $x = 0{\cdot}65$, the heat capacity as a function of T shows a change of slope only, which is located at the cubic-to-rhombohedral transition temperature. For concentrations $x < 0{\cdot}6$, the heat capacity varies smoothly with temperature. There is no anomaly at T_f. This observation has also been made in spin glasses (Mydosh and Nieuwenhuys 1980).

The antiferroelectric ordering of the CN dipoles at the Immm-to-Pmnm phase transition leads to a second anomaly in the heat capacity (figure 5.21); see Suga *et al.* (1965) and Mertz and Loidl (1987) and for $(KCl)_{1-x}(KCN)_x$ see also Ghivelder *et al.* (1985).

The freezing-in of the dipolar degrees of freedom in the monoclinic low-temperature phase of $(KBr)_{0{\cdot}3}(KCN)_{0{\cdot}7}$ is accompanied by relaxation effects in heat-capacity measurements (Matsuo *et al.* 1986).

5.2.6.2. *Low-temperature heat capacity and thermal conductivity* Amorphous solids are characterized by universal low-temperature properties. Zeller and Pohl (1971) found that the low-temperature specific heat in glasses can be described by

$$C = C_1 T^{\alpha} + C_{\text{exc}} + C_D T^3,$$

where the first term is time-dependent and nearly linear in temperature ($\alpha \approx 1$). $C_D T^3$ is the normal Debye specific heat, known from the crystalline state, and C_{exc} is an excess contribution of unknown origin, found only in amorphous solids. The linear term has been successfully interpreted in terms of a tunnelling model by Anderson *et al.* (1972) and Phillips (1972). With the assumption of a constant density of

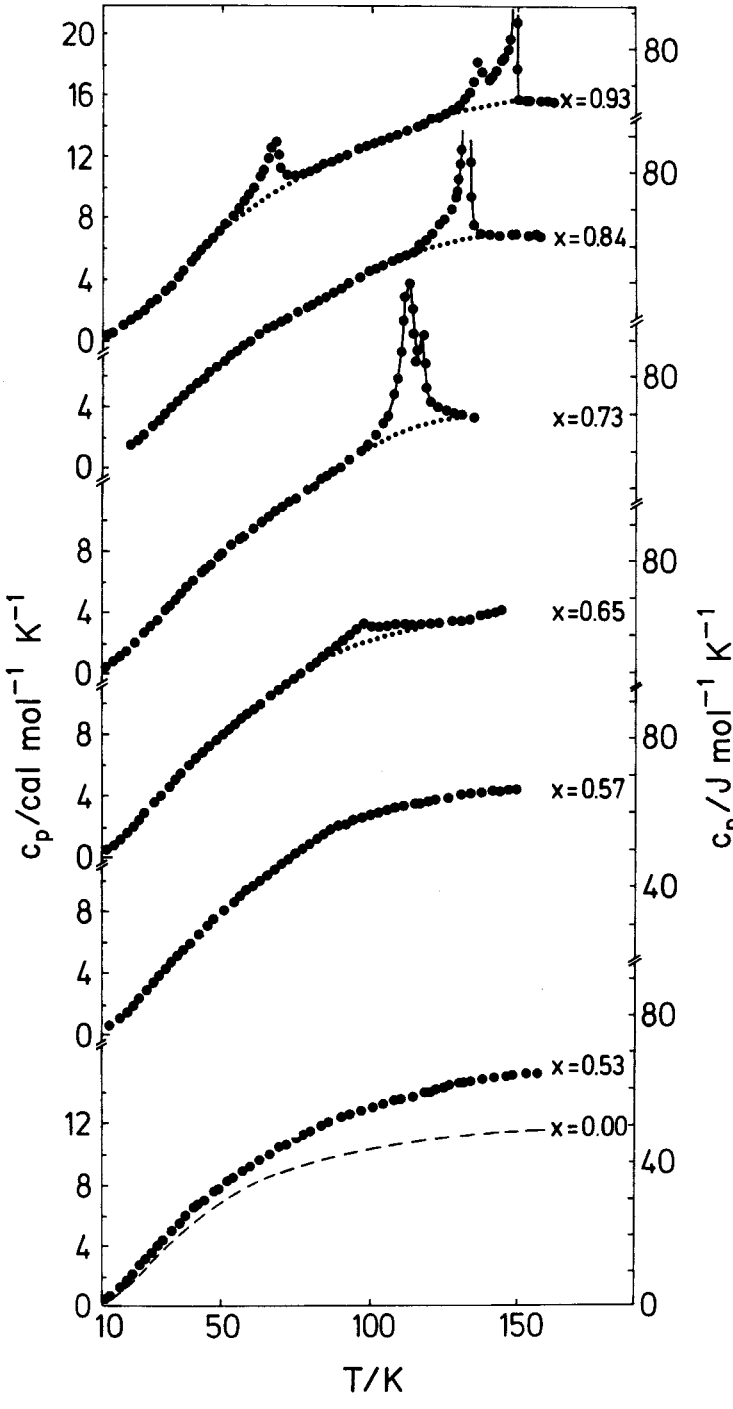

Figure 5.21. Heat capacity against temperature for $(KBr)_{1-x}(KCN)_x$ for concentrations x = 0·93, 0·84, 0·73, 0·65, 0·57, 0·53 and 0. From Mertz and Loidl (1987).

tunnelling states, these authors were able to calculate the experimentally observed time and temperature dependences. However, for most glassy materials, the tunnelling species remains unidentified.

De Yoreo *et al.* (1983, 1986) demonstrated that the heat capacity of $(KBr)_{1-x}(KCN)_x$ with $0{\cdot}25 < x < 0{\cdot}7$ varies linearly with temperature and logarithmically with measuring time. The results are shown in figure 5.22 (De Yoreo *et al.* 1986). For $x = 0{\cdot}25$, $0{\cdot}5$ and $0{\cdot}7$, the data can be fitted by the standard tunnelling model (solid lines in figure 5.22). For $x = 0{\cdot}05$, the time dependence is more pronounced and extends to higher temperatures. These data cannot be described by the tunnelling model (De Yoreo *et al.* 1986). The same authors investigated the thermal conductivity κ of $(KBr)_{1-x}(KCN)_x$. The results are shown in figure 5.23. Again the mixed cyanides with higher CN concentrations show TLS (i.e. $\kappa \sim T^2$) behaviour.

The excess term in the heat capcity has been observed in $(KBr)_{1-x}(KCN)_x$ over a wide concentration range. Some representative results reported by Mertz *et al.* (1990a) are shown in figure 5.24. The experimental results are plotted as C/T^3 against T. In this representation, the excess term appears as a well defined hump near 8 K. It is important to note that the excess term looks very similar for different concentrations and can be detected even in the elastically ordered phases (e.g. for $x = 0{\cdot}73$). However, the excess contribution almost vanishes for concentrations close to $x = 1$.

Sethna and co-workers (Sethna and Chow 1985, Meißner *et al.* 1985, Sethna 1986a, b, Randeria and Sethna 1986, unpublished work, 1988, Grannan *et al.* 1988) proposed a microscopic model in which the low-T TLS heat capacity was assumed to be due to 180° tunnelling flips of the cyanide molecules. The tunnelling takes place in a local non-cubic potential established by quadrupolar interaction forces at the quadrupolar freezing temperature. Dipolar relaxation at high T and tunnelling excitations for $T < 2\,\mathrm{K}$ probe the same distribution of barriers. Thus dielectric measurements can be employed to extract the distribution of tunnelling states. The model was later refined in order to explain the excess term of the heat capacity in terms of librational excitations (Randeria and Sethna 1986, unpublished work, Randeria 1987, Grannan *et al.* 1988). The plateau in the thermal conductivity was calculated within the framework of the same model, and good agreement with experimental results was achieved (Randeria and Sethna 1988). Consequently, $(KBr)_{1-x}(KCN)_x$ was assumed to be a unique model system in which it is possible to calculate the linear and the excess term of the specific heat from the parameters determined by the dielectric spectroscopy of the β relaxation.

Using dielectric data, Wu *et al.* (1988), Ernst *et al.* (1988) and Mertz *et al.* (1990a) calculated the linear heat-capacity term following this model and found good overall agreement with experimental results. On the basis of results from dielectric studies, it is possible to calculate the product of the density of tunnelling states P and the asymmetry parameter Δ. The results are shown in figure 5.25 (Mertz *et al.* 1990a), where $P\Delta$ is plotted and compared with experimental results. It is assumed here that the value of Δ taken for pure KCN, $\Delta = 314\,\mathrm{K}$ (Ernst *et al.* 1988), holds for all concentrations. The good agreement between the model calculation and experiment suggests that the microscopic picture proposed by Sethna and co-workers correctly describes the gross features of tunnelling motion in cyanide glasses.

On the other hand, we have some reservations about the explanation of the origin of the excess specific heat given by Randeria and Sethna (1986, unpublished work), Randeria (1987) and Grannan *et al.* (1988). Mertz *et al.* (1990a) showed that the bump in the excess term in the heat capacity is almost independent of concentration. They

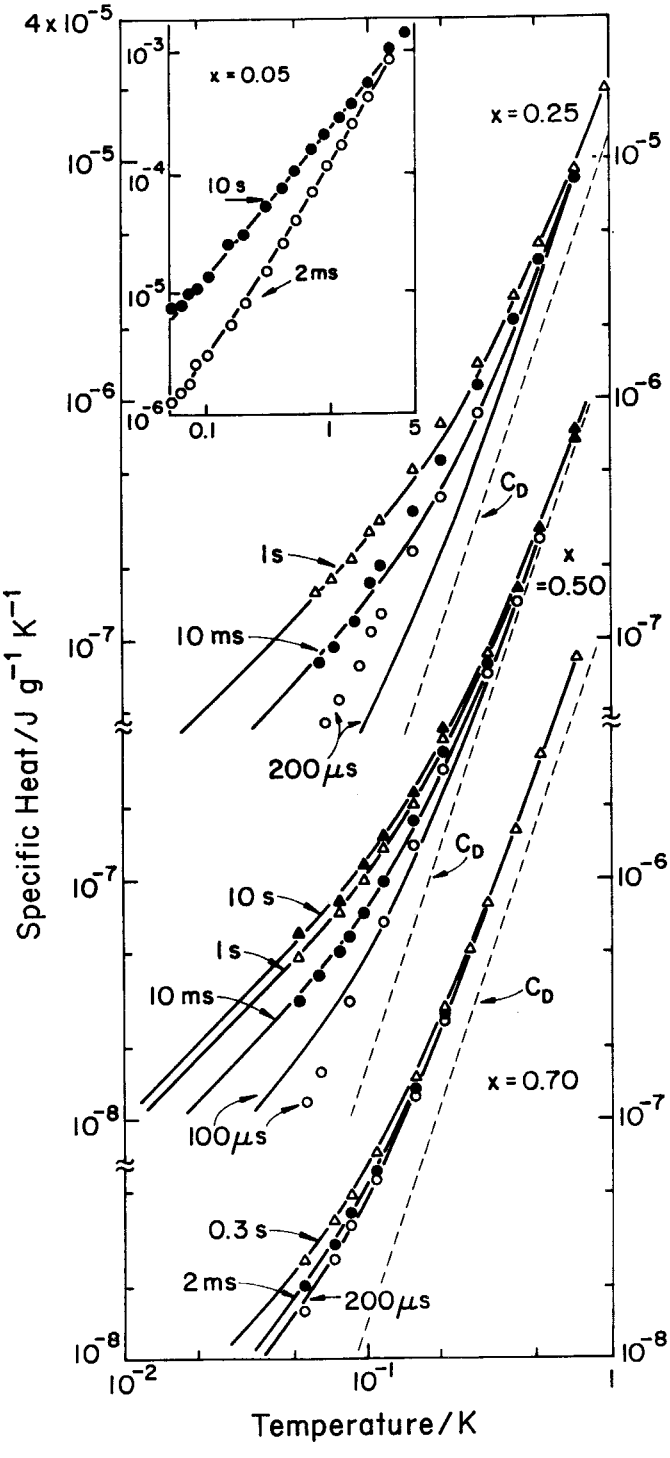

Figure 5.22. Low-temperature heat capacity of $(KBr)_{1-x}(KCN)_x$ for concentrations $x = 0{\cdot}05$ (inset), $0{\cdot}25$, $0{\cdot}5$ and $0{\cdot}7$ *versus* temperature at selected measuring times. For $x = 0{\cdot}25$, $0{\cdot}5$ and $0{\cdot}7$, the data were fitted within the framework of the standard tunnelling model (solid lines). The dashed lines represent the Debye specific heat c_D. The data for $x = 0{\cdot}05$ could not be fitted to the tunnelling model. The solid lines are fits to a power law. From De Yoreo *et al.* (1986).

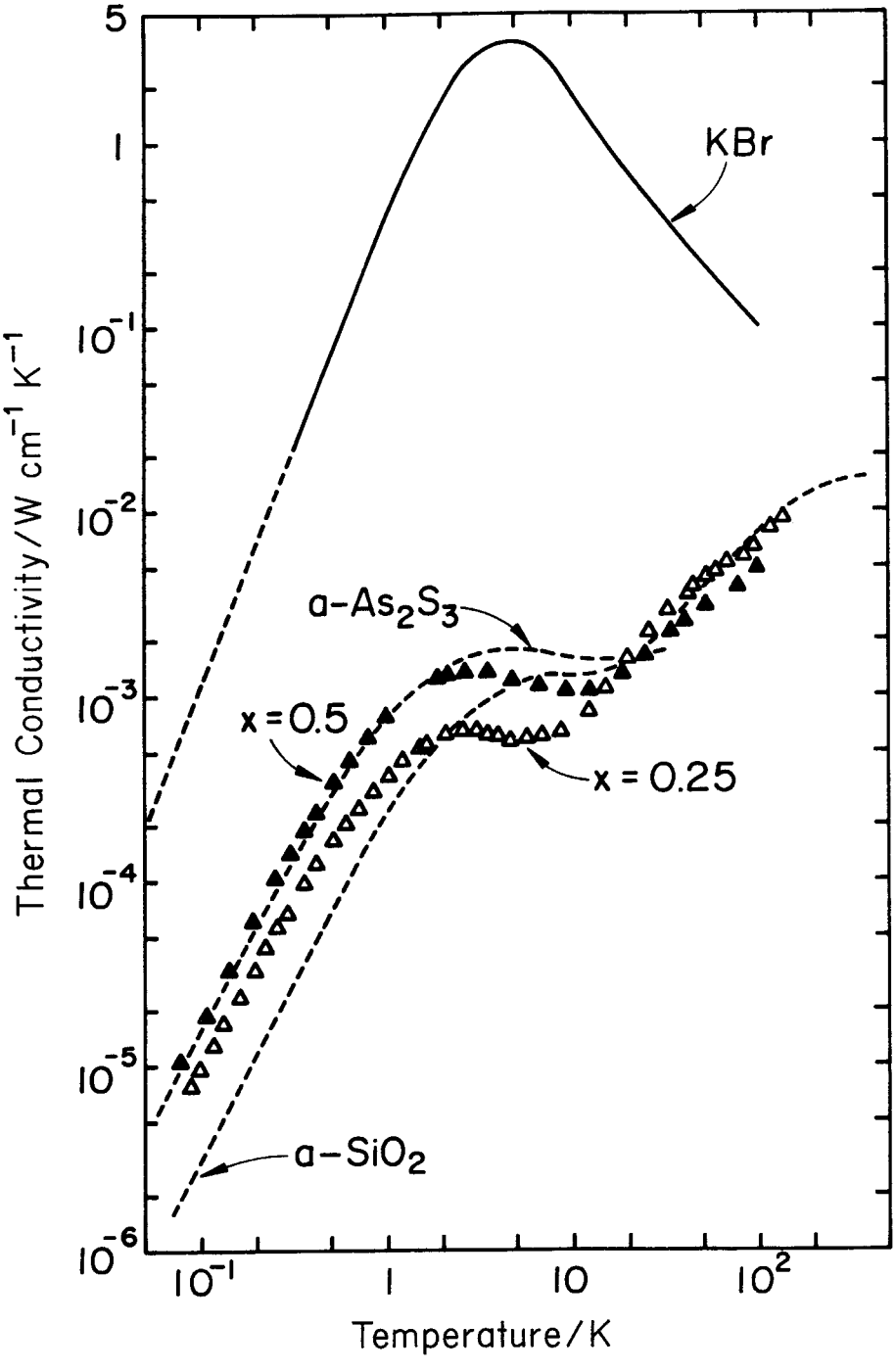

Figure 5.23. Thermal conductivity of $(KBr)_{1-x}(KCN)_x$ for $x = 0{\cdot}25$ and $x = 0{\cdot}5$ *versus* temperature compared with the thermal conductivity of amorphous SiO_2 and As_2O_3 and of pure KBr. From De Yoreo *et al.* (1986).

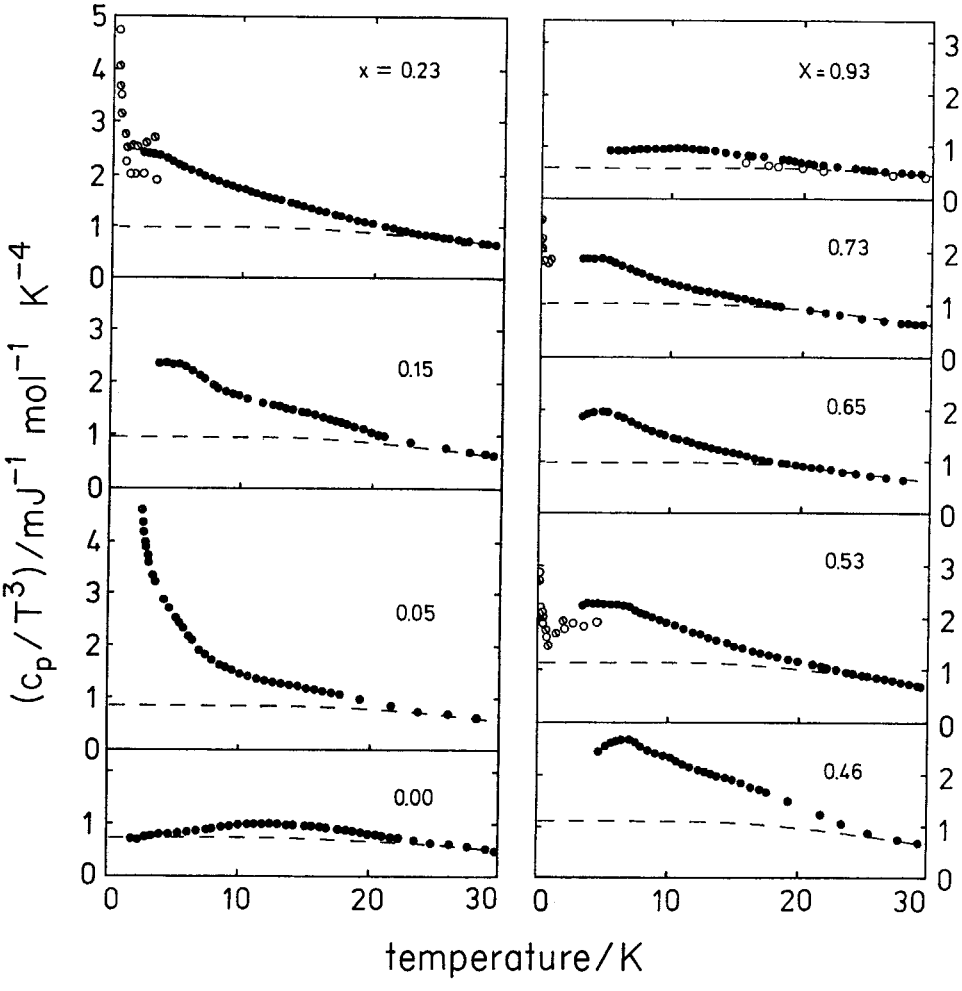

Figure 5.24. Heat capacity of $(KBr)_{1-x}(KCN)_x$ plotted as c/T^3 *versus* T. The Debye specific heat is represented by the dashed lines. From Mertz *et al.* (1990a).

argued that the energy of the librational modes should scale like the square root of the energy barrier of the hindering potential. It is known from dielectric measurements (Mertz *et al.* 1990a) that the barrier height for dipolar relaxation in alkali bromide–alkali cyanide mixtures increases almost linearly with CN concentration. Thus the excess contribution to the specific heat cannot result from librational excitation.

5.2.7. *Nuclear magnetic resonance*

^{23}Na and ^{35}Cl, ^{37}Cl NMR experiments have been carried out on single crystals of $(NaCl)_{1-x}(NaCN)_x$ (Elschner and Petersson 1986a, b, Elschner *et al.* 1985, 1987). NMR is essentially a local probe; thus collective effects like the structural phase transitions of the CN-rich mixed cyanides are probed in an indirect, but very sensitive, way. The ^{23}Na and Cl nuclei are sensitive to the local electric-field gradients. In pure NaCN, the static electric-field gradient vanishes in the cubic phase, but is finite in the

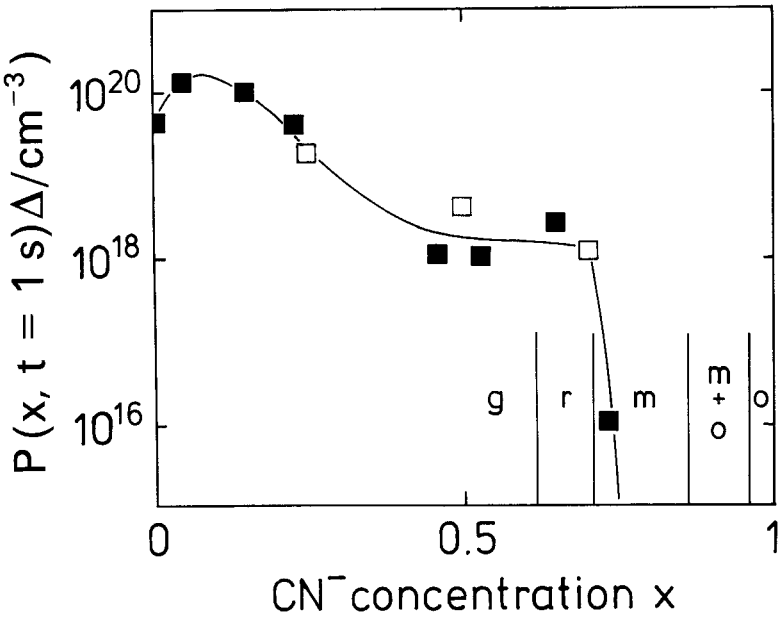

Figure 5.25. Concentration dependence of the density of tunnelling states $P(t = 1\,s)$ times the asymmetry Δ in $(KBr)_{1-x}(KCN)_x$. Values calculated from the parameters determined by dielectric spectroscopy (■) are compared with the calorimetric results (□). The solid line is drawn to guide the eye. The vertical lines indicate the different phases. From Mertz *et al.* (1990).

ferroelastic phase, where it is related in some monotonic way with the value of the spontaneous shear. In $(NaCl)_{1-x}(NaCN)_x$ mixed crystals the local environments of the Na and the Cl nuclei are non-cubic, and hence there is a static electric-field gradient (EFG).

The NMR lineshape can be explained by assuming that the principal axes of the EFG are along ⟨100⟩ and that the principal components of the EFG have a Gaussian distribution. The width of this distribution increases monotonically by about an order of magnitude between 300 K and 100 K for $(NaCl)_{1-x}(NaCN)_x$ with $x = 0{\cdot}65$, a concentration that is slightly below x_c. The steepest increase in the width occurs at about 130 K. Note that in an ordering sample like NaCN the width increases discontinuously at T_c (Albers *et al.* 1984). The results for the Na and the Cl resonance are analogous regardless of the fact that Cl is a second neighbour but Na a first neighbour to the CN^- ion. This suggests that the deviations of the local potential from cubic symmetry are not only due to the actual composition of the first-neighbour shell but also reflect lattice deformations over several lattice constants. This view is supported by the observation that the NMR width follows closely the width of X-ray powder lines (Elschner *et al.* 1985); see figure 5.15. It was also observed that the monotonic increase of the width with decreasing temperature is strongly reduced for lower CN concentrations. Already for $x = 0{\cdot}20$ the increase is practically absent.

Recently, Elschner *et al.* (1990) have interpreted the ^{23}Na and ^{35}Cl NMR data on $(NaCl)_{1-x}(NaCN)_x$ and the ^{23}Na data on $(NaCN)_{1-x}(KCN)_x$ in terms of a Edwards–Anderson-type order parameter q, given by the second moment of the CN

orientational distribution functions. They have shown that the second moment M_2 of the distribution of NMR resonance distribution is linearly related to q: $M_2 = A + Bq$, where A describes the residual contribution due to the substitutional disorder in a mixed crystal. The T dependence of q has been determined down to about 100 K. Elschner *et al.* (1990) have argued that q basically reflects a genuine (quadrupolar) glass transition due to random interactions at a temperature T_g, equal to 140 K and 146 K for $(NaCl)_{1-x}(NaCN)_x$ with $x = 0{\cdot}65$ and $0{\cdot}45$ respectively. Random fields are present, but small. They give rise to a high-T tail of $q(T)$ of the form $q \sim T^{-2}$ and to a smearing of the glass transition at T_g. The analysis is based on the random-bond–random-field Ising model. The question remains as to whether this model is applicable to the mixed cyanides.

The spin–lattice relaxation time T_1 of pure NaCN shows a thermally activated behaviour in the cubic phase, which is attributed to the fast reorientational motion of the CN^- ion in a cubic local environment (Elschner and Petersson 1986b). Below T_c, a so-called BPP-type behaviour is observed, with a minimum of T_1 at the cross-over from fast to slow motion, where the Larmor frequency is about equal to the inverse correlation time τ^{-1} of the CN reorientations, which below T_c are understood as 180° flips. τ follows approximately an Arrhenius law. Thus, at T_c, the slope of the log T_1 *versus* $1/T$ plot yields the activation energy E_b, which changes discontinuously at T_c. As x is reduced, this change of slope is smeared out, the BPP minimum shifts to lower T, broadens and approaches the minimum, which can be estimated from extrapolation of the high-temperature behaviour (figure 5.26). The activation energy at room temperature is independent of x and is about 60 meV. The qualitative picture that has been suggested by Elschner and Petersson (1986b) is as follows: there are two thermally activated reorientation processes of the CN^- ion: one between the six [100] directions of the non-perturbed cubic site, and the 180° flip in the locally distorted environment. For the ordering samples, the two processes are well separated, the first occurring above and the second below T_c. For CN concentrations slightly below x_c, the distinction between the two processes can be maintained. The cross-over signals the change in the local potential. It should, however, be noted that the cross-over is rather gradual; nevertheless, it can be used to define a characteristic temperature T_f. As x is further reduced, the distinction is blurred, which means that 90° reorientations become allowed even at lower temperatures. Around T_f, the reorientations are fast with respect to the NMR time scale. Extra-slow motions have not been observed.

^{13}C and ^{15}N NMR studies of an isotopically enriched powder sample of $(KBr)_{1-x}(KCN)_x$ with $x = 0{\cdot}5$ have been reported by Doverspike *et al.* (1986). These nuclei do not carry a quadrupole moment. Here the line broadening is not due to EFG distributions but rather to anisotropies of the chemical shift and to ^{13}C–^{15}N intramolecular coupling. The lineshapes of the two resonances have been measured as functions of T and compared with the shapes expected for a randomly oriented nonrotating CN^- ion. The experimental lines are sharp at high temperatures, broaden continuously as T is decreased, and approach the calculated profiles at low temperatures. At about 40 K, the low-T situation is reached. Since at this temperature the dielectric constant still shows Curie-type behaviour, it can be concluded that the quadrupolar modes, to which NMR is sensitive, freeze at higher temperatures than the dipolar ones. The same conclusion has been drawn from the comparison of $c_{44}(T)$ and the dielectric constant $\varepsilon(T)$ (see above). The decay time T_2 of spin echoes and the time T_2^* of the free-induction decay have also been investigated. From the static and dynamic results, Doverspike *et al.* (1986) concluded (in agreement with Elschner and Petersson (1986b))

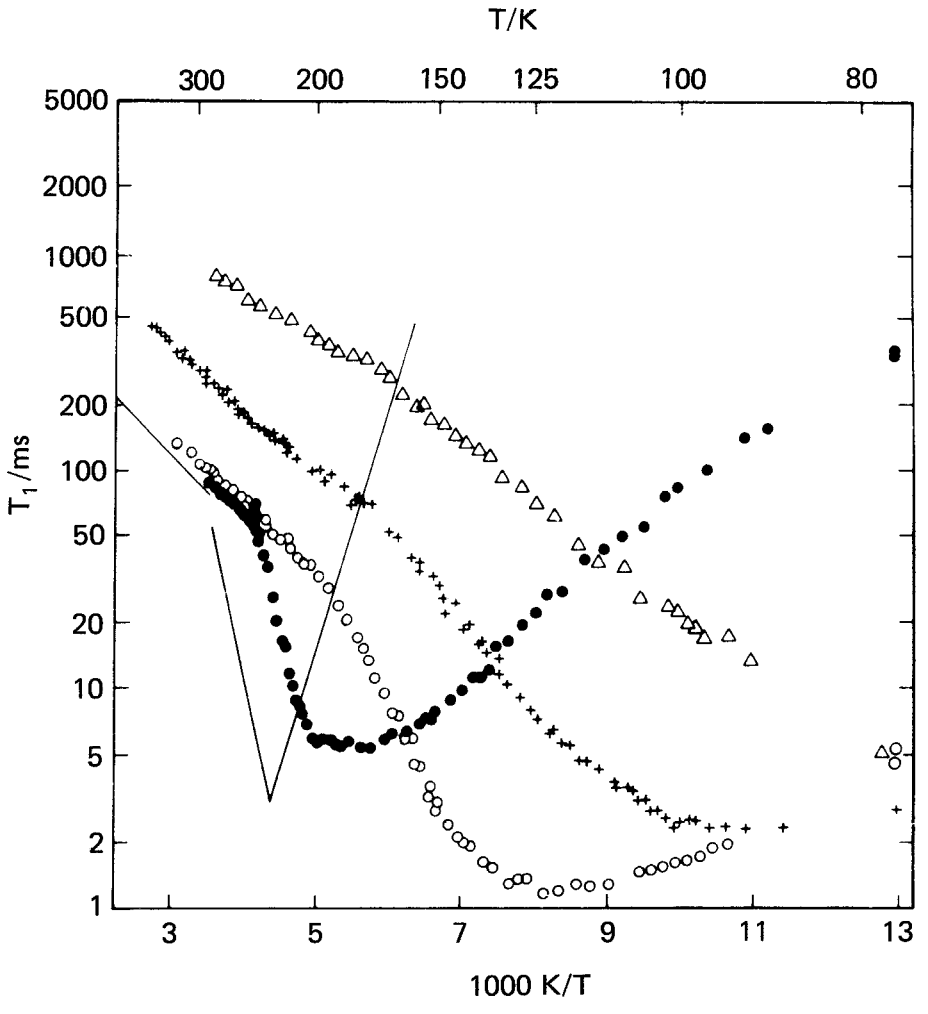

Figure 5.26. Arrhenius plot of the ^{23}Na spin–lattice relaxation time T_1 of $(NaCl)_{1-x}(NaCN)_x$: △, x = 0·2; +, 0·4; 0·7; ●, 0·9; ——, 1·0. From Elschner and Petersson (1986b).

that the model of favoured orientations is appropriate. Each molecule samples all orientations. It is the static shape of the orientational single ion distribution that changes with decreasing T, going from a nearly spherical one at high T to a strongly peaked one at low T.

5.3. *Alkali A—alkali B mixed cyanides* $(ACN)_{1-x}(BCN)_x$

5.3.1. *Introduction*

Truthe (1912) investigated mixtures of NaCN and KCN. Lüty and co-workers (Lüty 1981, Lüty and Ortiz-Lopez 1983, Ortiz-Lopez 1983) showed that $(NaCN)_{1-x}(KCN)_x$ and $(RbCN)_{1-x}(KCN)_x$ mixed crystals can be grown at any concentration. In $(NaCN)_{1-x}(KCN)_x$ the structural phase transitions are suppressed over a wide range of intermediate concentrations, whereas $(RbCN)_{1-x}(KCN)_x$ shows non-cubic low-T phases for all x, although the phase-transition temperatures are dramatically reduced

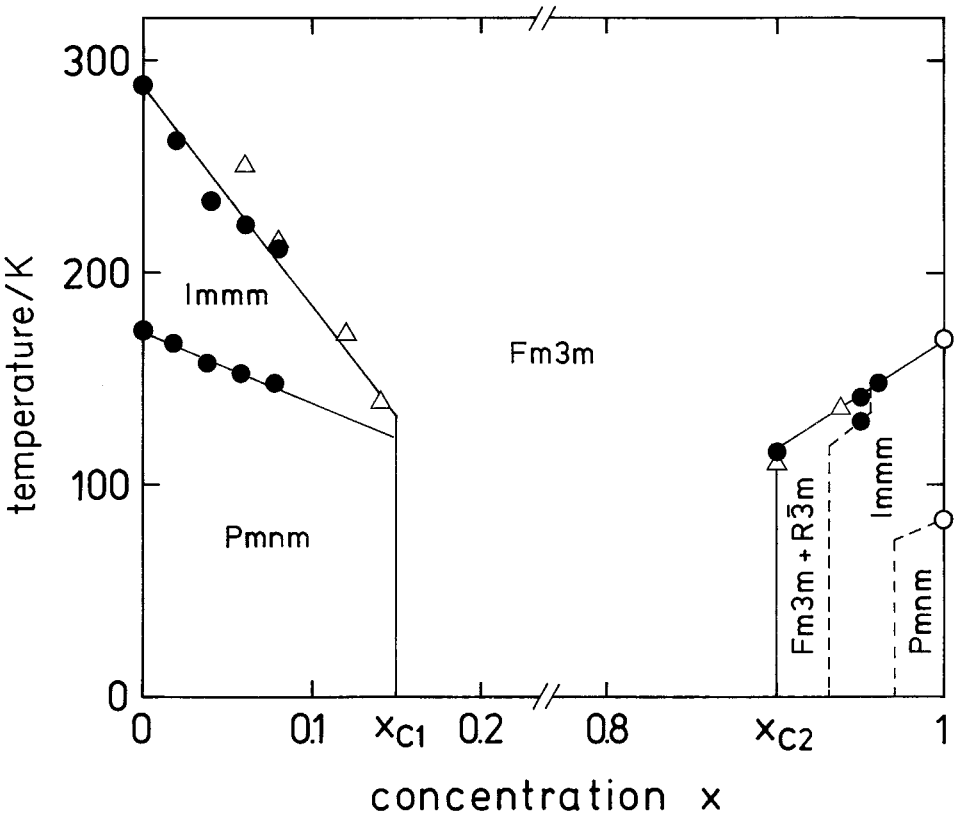

Figure 5.27. (x, T) phase diagram of $(NaCN)_{1-x}(KCN)_x$. From Schräder *et al.* (1990b).

at intermediate concentrations. A phase diagram of $(NaCN)_{1-x}(KCN)_x$ is shown in figure 5.27 (Lüty and Ortiz-Lopez 1983, Schräder *et al.* 1989b, 1990b). The occurrence of frozen-in orientational disorder for $0{\cdot}15 < x < 0{\cdot}9$ suggests that a glassy low-temperature state exists in $(NaCN)_{1-x}(KCN)_x$, a system with a fully concentrated molecular sublattice. In $(KBr)_{1-x}(KCN)_x$ mixtures and analogous solid solutions, the CN sublattice is diluted. Hence, in the latter compounds, site disorder and anisotropic interactions between the CN quadrupoles are thought to be responsible for the frustrated ground state. The analogy with random interactions in spin glasses is straightforward. In contrast, in $(NaCN)_{1-x}(KCN)_x$ the ferroelastic and antiferroelectric phase transitions are suppressed, despite an undiluted sublattice of quadrupoles. Clearly, the substitution of the large K ions ($r = 1{\cdot}33$ Å) by the much smaller Na ions ($r = 0{\cdot}98$ Å) introduces a strong disturbance of the crystalline field, thereby affecting the rotation–translation coupling and the dipolar and quadrupolar relaxation kinetics. Thus $(NaCN)_{1-x}(KCN)_x$ could be an example of a random-field system that has its analogues in the spin-glass varieties as well (Fisher and Huse 1986).

Focusing on the random-field problem, Michel (1986, 1987a, b) proposed a microscopic model in which the orientations are bilinearly coupled to the random strains generated by the substitutional disorder. Later, Michel and Bostoen extended this theory by including a collective freezing transition that results in a non-ergodic instability (Michel 1987c, Bostoen and Michel 1988). In $(NaCN)_{1-x}(KCN)_x$ it seems plausible that frustrated interactions play only a minor role and that the

low-temperature state is almost determined by the strength of the random fields: in $(NaCN)_{1-x}(KCN)_x$, random stresses are introduced by the volume difference of the impurity atoms, which cause (quenched) elastic displacements of the neighbouring ions. Hence these systems seem to be ideal for testing the role played by random strains in orientational glasses.

5.3.2. *Elastic properties*

Inelastic neutron-scattering studies focusing on the temperature dependence of transverse sound waves along [100] with a velocity proportional to the elastic constant $(c_{44})^{1/2}$ were performed by Loidl *et al.* (1986) and Schräder *et al.* (1985, 1989b, c, 1990b). The results were similar to those reported for $(KBr)_{1-x}(KCN)_x$—with decreasing temperature, the phonon side bands undergo considerable softening, pass through a minimum, and increase again on further cooling. With decreasing temperature, a central component evolves in addition to the side bands. Its width is resolution-limited at all temperatures. The temperature dependence of the elastic constant c_{44} as observed for glassy crystals with concentrations $x = 0{\cdot}19$, $0{\cdot}59$ and $0{\cdot}85$ is shown in figure 5.28. The behaviour of $c_{44}(T)$ varies considerably for the different concentrations investigated: the softening of the shear stiffness is rather strong for $x = 0{\cdot}85$, moderate for $x = 0{\cdot}19$ and weak for $x = 0{\cdot}59$. The temperature dependences of the concomitant central peak intensities behave similarly: a strong increase below the temperature of the minimum elastic constant was reported for $x = 0{\cdot}85$ (Loidl *et al.* 1986, Schräder *et al.* 1989c). For $x = 0{\cdot}19$ and $0{\cdot}59$, the central peak intensities grow much more gradually with decreasing T; for $x = 0{\cdot}59$ the intensity is in fact very weak.

Ultrasonic results have been reported by Schräder *et al.* (1989c) and Hu *et al.* (1990). Figure 5.28 shows the elastic constant c_{44} as a function of temperature as obtained by ultrasonic transmission and the values from inelastic neutron-scattering experiments (Schräder *et al.* 1989c). The elastic shear constant decreases with decreasing temperatures. However, in the ultrasonic measurements the signals could not be followed through the freezing temperatures owing to high attenuation. In these experiments, T_f was determined by the minimum in $c_{11}(T)$ (and is indicated by arrows in figure 5.28). The ultrasonic results are compared with the elastic constants as measured by inelastic neutron scattering at much higher frequencies. At high temperatures, dispersion effects are absent, since both measuring frequencies are expected to be smaller than the inverse relaxation time of quadrupolar reorientations. Clear dispersion effects become apparent near T_f. These ultrasonic results were analysed by Schräder *et al.* (1989c) in the pure random-strain model proposed by Michel (1986, 1987a, b). The results of these fits are shown as solid lines in figure 5.28.

The concentration dependence of the relevant fitting parameters, namely the characteristic temperatures T_s and T_f were determined by Schräder *et al.* (1989c) and Hu *et al.* (1990). T_s is the temperature at which the elastic constants would vanish in the absence of random strains, and is a direct measure of the rotation–translation coupling. The freezing temperature T_f is directly related to the strength of the random fields. T_f roughly follows the expected temperature behaviour of the random fields and scales approximately like $[x(1 - x)]^{1/2}$. T_s, on the other hand, deviates dramatically from a linear interpolation of the values for the pure cyanides (Schräder *et al.* 1989c, Hu *et al.* 1990). Clearly, the rotation–translation coupling is affected by the static random strain fields—an effect that is not predicted by the random-field theory of Michel (1986, 1987a, b).

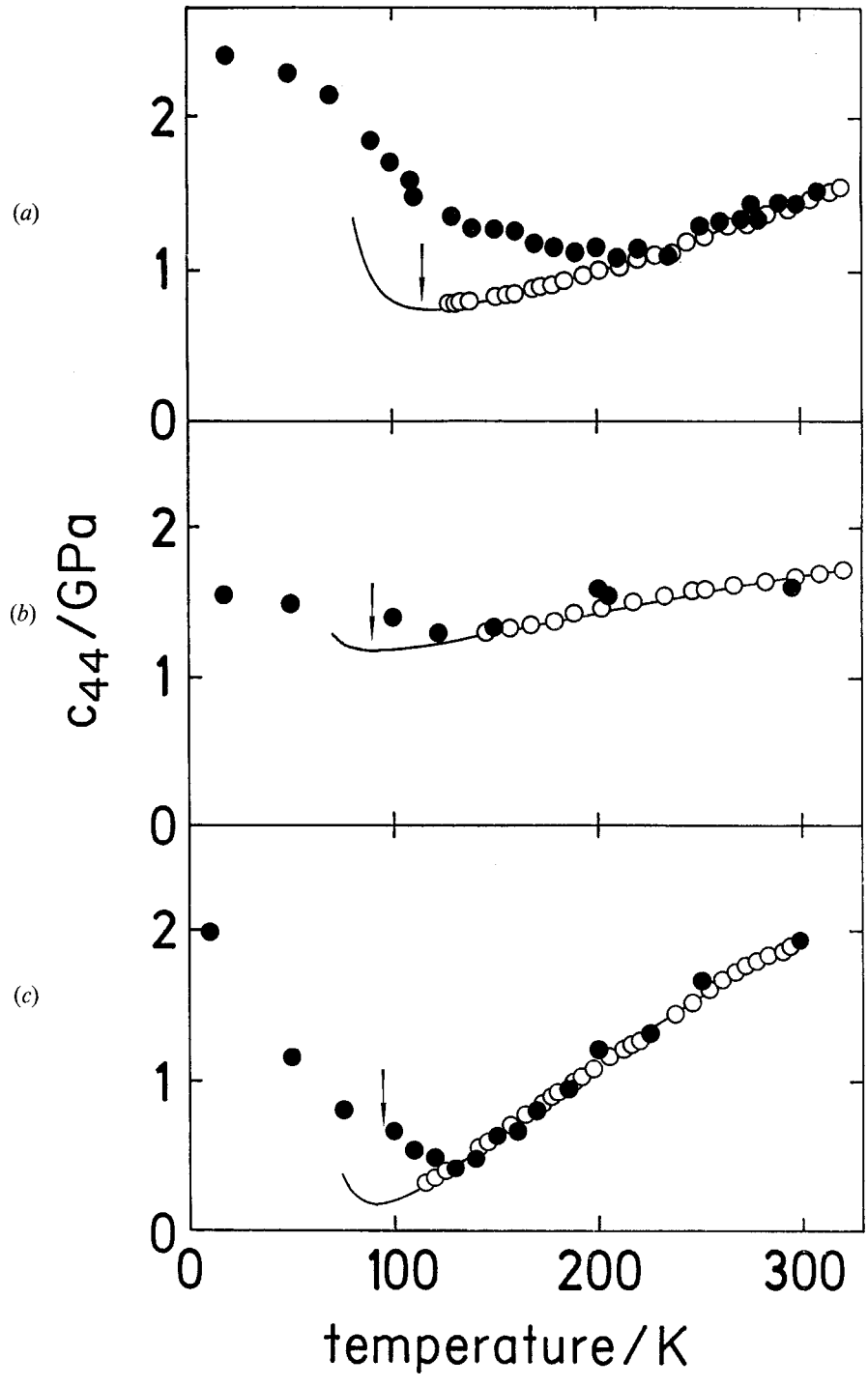

Figure 5.28. Temperature dependence of the elastic constant c_{44} of $(NaCN)_{1-x}(KCN)_x$ for KCN concentrations $x = 0{\cdot}19$ (*a*), $0{\cdot}59$ (*b*) and $0{\cdot}85$ (*c*). Ultrasonic results (10 MHz region, ○) are compared with neutron-scattering results (THz region ●). The solid lines are calculated using the random-strain model. The arrows indicate the position of the minimum in $c_{11}(T)$ as determined by ultrasonic techniques. From Schräder *et al.* (1989c).

Low-frequency (0·1 Hz) results on the elastic shear constant c_{44} of $(NaCN)_{1-x}(KCN)_x$ with $x = 0{\cdot}07$, 0·59 and 0·85 were reported by Hessinger and Knorr (1989) (figure 5.29). For $x = 0{\cdot}07$, $c_{44}(T)$ shows a linear T dependence between room temperature and the cubic-to-orthorhombic transition temperature $T_c = 220$ K. c_{44} extrapolates to zero at 180 K. Below T_c, the elastic shear constant shows an increase accompanied by elastic loss. A second step-like increase, again accompanied by an elastic-loss peak, is observed below the antiferroelectric-ordering temperature $T_E = 150$ K. The two other samples stay cubic down to the lowest temperatures; they show a rather broad minimum in $c_{44}(T)$. The minimum for $x = 0{\cdot}59$ is shallow, with Min $(c_{44})/c_{44}$ (300 K) = 0·4, whereas it is considerably deeper for $x = 0{\cdot}85$: Min $(c_{44})/c_{44}(300\,\text{K}) = 0{\cdot}2$. For the solid solution with $x = 0{\cdot}85$, the elastic loss could be measured; it peaks around 50 K.

For $x = 0{\cdot}85$, $c_{44}(T)$ starts to deviate from the para-elastic Curie–Weiss background behaviour below 130 K and is almost T-independent between 110 and 70 K. Below 70 K, $c_{44}(T)$ again increases until it finally saturates below 20 K. Hessinger and Knorr (1989) came to the following conclusions. The increase below 70 K and the loss peak at 50 K were interpreted as dispersion effects due to reorientations that are also dipole-active. It was suggested that the static elastic shear constant c_{44} stays low and T-independent throughout the orientational-glass state. Hessinger and Knorr abandonned the idea of a minimum static elastic constant defining a characteristic transition temperature into the glass-like state, traditionally called T_f. Of course, T_f may alternatively be defined as the temperature where the para-elastic behaviour crosses over into the T independence. This recipe yields about 120 K, which is in fact the T range where the central peak intensity starts to increase strongly. In summary, Hessinger and Knorr (1989) suggested that (i) the minimum of $c_{44}(T)$ as observed in finite-frequency measurements is a purely relaxational effect; (ii) the application of Michel's initial version of the random-field model, which was developed for static elastic behaviour, to finite-frequency measurements is incorrect, and (iii) the high-T limit of $q(T)$ should not be extrapolated down to low temperatures at which the model predicts an upturn in $c_{44}(T)$.

The shear elasticity of $(RbCN)_{1-x}(KCN)_x$ mixed crystals was investigated in the high-temperature cubic phase by Garland *et al.* (1988), using ultrasonic techniques. $c_{44}(T)$ was fitted with a simple Curie–Weiss law and with a modified Curie–Weiss law including random fields as proposed by Michel (1986, 1987a, b). Both models yielded satisfactory fits, and, on the basis of these results, it was impossible to favour one of them. Obviously, the rotation—translation coupling in $(RbCN)_{1-x}(KCN)_x$ is strong and dominates the rotation–random-field coupling. However, the critical temperatures, where c_{44} extrapolates to zero, deviate significantly from a linear interpolation between the values of KCN and RbCN. The reduction of the critical temperatures demonstrates that the random strain fields weaken the rotation–translation couplings.

5.3.3. *X-ray and neutron diffraction*

The phase diagram of $(NaCN)_{1-x}(KCN)_x$ was investigated by Lüty and Ortiz-Lopez (1983) using optical-transmission experiments and dielectric techniques. They found no phase transitions for concentrations $0{\cdot}15 < x < 0{\cdot}85$. The low-temperature phases were investigated by Schräder *et al.* (1989a, 1990b), using neutron-diffraction techniques. The phase diagram determined by these authors is shown in figure 5.27. Only for concentrations close to the pure cyanides is elastic and electric order established at low temperatures. Already 2% sodium diluted in KCN and 15%

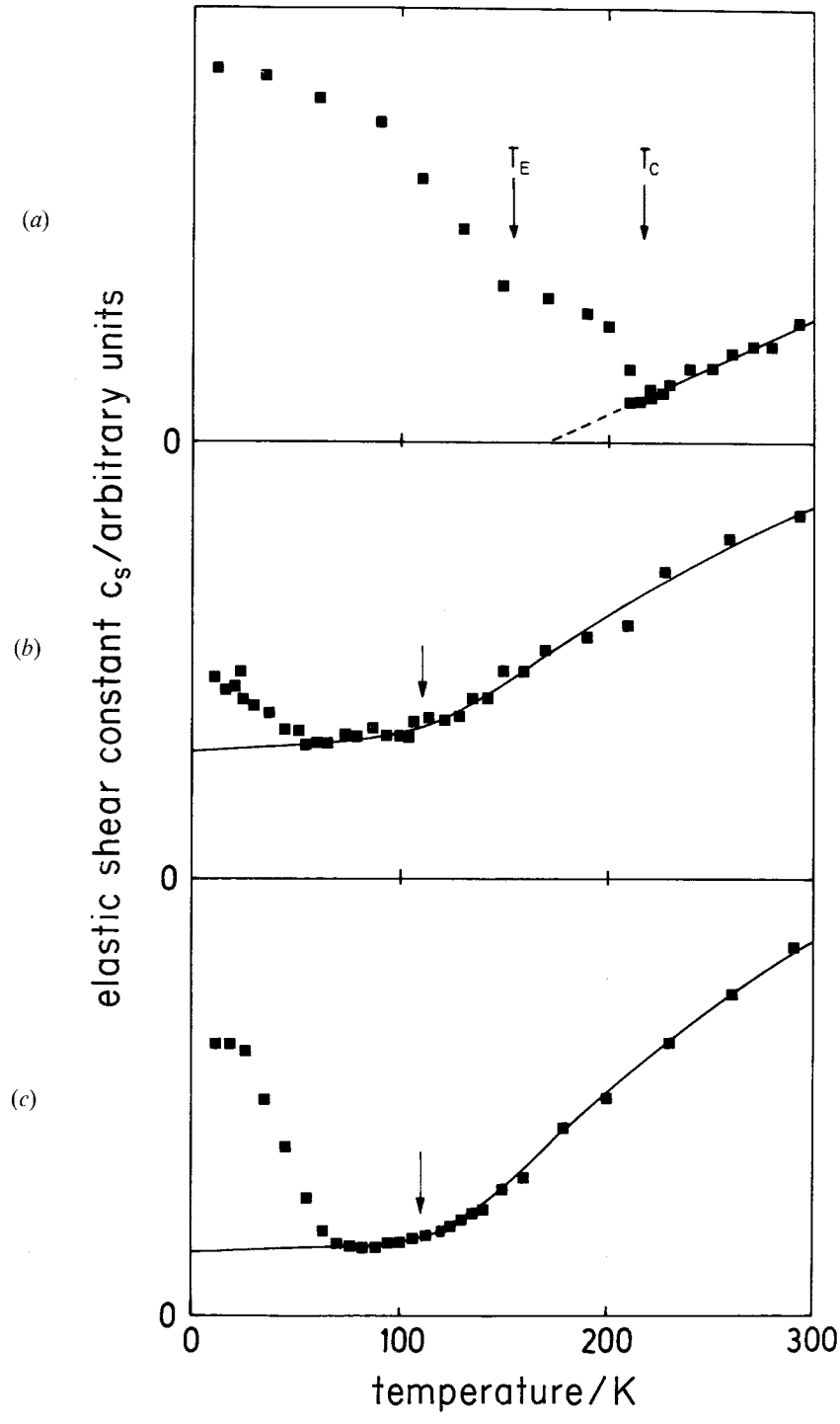

Figure 5.29. The elastic shear constant of $(NaCN)_{1-x}(KCN)_x$ as a function of temperature, obtained from shear-torque experiments at a measuring frequency of approximately 0·1 Hz: (*a*) $x = 0{\cdot}07$; (*b*) 0·59; (*c*) 0·85. From Hessinger and Knorr (1990).

potassium diluted in NaCN suppress the transition into the antiferroelectric phase. A frozen-in elastically disordered state appears for concentrations $x_{c1} = 0{\cdot}15 < x < x_{c2} = 0{\cdot}9$. In this concentration range, the overall cubic symmetry is maintained down to the lowest temperatures. However, the appearance of diffuse scattered intensities points towards frozen-in lattice strains. X-ray powder-diffraction patterns for mixed crystals with a potassium concentration of $x = 0{\cdot}85$ revealed an enormous broadening of Bragg reflections at low temperatures (Loidl *et al.* 1986).

As in all alkali halide–alkali cyanide mixed systems, the structural polymorphism is an interesting feature and is reminiscent of the polymorphism in a number of parent structures of canonical glasses (like SiO_2). It is, however, still an open question as to whether the tendency to form different structural phases is directly related to the tendency to form a glassy state (Jäckle 1986).

Schräder *et al.* (1990a) determined the structure of the antiferroelectric ground state in $(NaCN)_{1-x}(KCN)_x$. They found that the electric order is stabilized by a static sublattice shift of the cations, in agreement with theoretical predictions (Koiller *et al.* 1984).

5.3.4. *Inelastic neutron scattering (central peak)*

The quadrupolar freezing process in cyanide glasses is characterized by a freezing-in of orientational correlations and of lattice strains. Related to this freezing transition are the following phenomena, which can be explained by a disturbance of the long-range translational order: the appearance of a central line in inelastic neutron-scattering experiments, the linewidth-broadening in X-ray- and neutron-diffraction studies and the increase in the distribution width of the electric-field gradient in NMR experiments.

The appropriate way to characterize the low-temperature state in disordered systems is to study the temperature dependence of the order parameter. In cyanide glasses the order parameter is given by $q \approx \overline{\langle Y_\alpha(n)\rangle^2}$, where $Y(n)$ is the orientational coordinate at lattice site n and α labels the modes of T_{2g} symmetry. The angular brackets $\langle\ \rangle$ denote the thermal average and the overbar the configurational average. Owing to rotation–translation coupling, the order parameter is also proportional to $\langle s_i(n)\rangle^2$, where $s_i(n)$ is a displacement coordinate at site n. It is this latter quantity that leads to the existence of a static central peak in addition to the dynamic-scattering law. According to the model of Michel (1986, 1987a–c) and Bostoen and Michel (1988), the role of the static random strain is twofold: (i) it couples linearly to the orientations, and (ii) through anharmonic coupling with the dynamic modes, it leads to scattering of the internal modes and thus to internal friction. Frictional processes become dominant if the restoring forces are weak. This is the essence of the non-ergodic instability, which can only occur if the neighbourhood of a second-order phase transition.

Hence two contributions to the order parameter have to be taken into account: $q = q_1 + q_2$. The first term results solely from the response to the static random strain field h and is a smooth function of temperature, namely $q_1 = h^2/T^2$. q_2 accounts for the non-ergodic transition and exists only below the transition temperature.

To test the predictions of Michel's theory, Schräder *et al.* (1989b, c, 1990c) performed detailed inelastic neutron-scattering studies of $(NaCN)_{1-x}(KCN)_x$ in the glassy regime. The temperature and wave-vector dependences of the central-peak intensities were studied for crystals with concentrations with $x = 0{\cdot}19, 0{\cdot}31, 0{\cdot}59$ and $0{\cdot}85$. At concentrations $x = 0{\cdot}19$, $0{\cdot}31$ and $0{\cdot}59$, the central-peak intensities were

found to be smooth functions of temperature, indicative of a pure random-field effect. Anomalous increases in the central-peak intensities appeared for $x = 0{\cdot}85$ below $T = 130\,\mathrm{K}$. Representative results for central-peak intensities for $x = 0{\cdot}31$ and $0{\cdot}85$ as measured at different phonon wavenumbers are plotted in figure 5.30 (Schräder *et al.* 1990c). For $x = 0{\cdot}31$, the measured intensities increase smoothly until, at low T, saturation effects become dominant. The behaviour is different for $x = 0{\cdot}85$, where, close to $T = 130\,\mathrm{K}$, an additional contribution to the glassy-state order parameter occurs. This additional contribution has been interpreted as being due to a non-ergodic instability (Schräder *et al.* 1990c). 130 K is close to the temperature where there is a minimum in the elastic shear constant as measured at neutron frequencies. The wave-vector and temperature dependences of the order parameter q_2, as shown in the insert in figure 5.30, are in qualitative agreement with the predictions of Bostoen and Michel (1988). However, it must be kept in mind that the loss peak in the torsion-pendulum experiments shows up at 50 K (Hessinger and Knorr (1990); see figure 5.29).

5.3.5. *Dielectric susceptibility*

Detailed dielectric investigations of $(NaCN)_{1-x}(KCN)_x$ were performed by Ortiz-Lopez (1983) and Lüty and Ortiz-Lopez (1983). Dielectric results for $x = 0{\cdot}59$ and $0{\cdot}85$ were published by Loidl *et al.* (1986). Similarly to the dipolar relaxations in $(KBr)_{1-x}(KCN)_x$ and $(KCl)_{1-x}(KCN)_x$ solid solutions, the dipolar relaxation is characterized by an extremely broad distribution of relaxation times. The width of the distribution function increases with decreasing temperatures, reaching approximately ten decades at 50 K (Loidl *et al.* 1986).

The slowing down of the dipolar degrees of freedom (essentially 180° jumps) can be described in terms of an Arrhenius law with energy barriers of approximately 1500 K for mixed crystals in the glassy regime (Ortiz-Lopez 1983, Loidl *et al.* 1986).

5.3.6. *Heat capacity*

Mertz *et al.* (1990a, b) investigated the low-temperature specific heat in the glassy regime of $(NaCN)_{1-x}(KCN)_x$. Below 2 K, they used a transient heat pulse technique to measure the time dependence of the heat capacity within a quasi-adiabatic time window $0{\cdot}1\,\mathrm{ms} < t < 0{\cdot}1\,\mathrm{s}$. For temperatures $T > 2\,\mathrm{K}$, the specific heat was recorded using standard adiabatic calorimetry. The long-time low-temperature data increase almost linearly with temperature, as predicted by the standard tunnelling model (Anderson *et al.* 1972, Phillips 1972). Significant deviations appear for crystals with concentrations $x = 0{\cdot}19$ and $0{\cdot}85$ at temperatures $T > 0{\cdot}5\,\mathrm{K}$ (Mertz *et al.* 1990b).

The temperature dependence of the long-time specific heat is shown in figure 5.31 (Mertz *et al.* 1990b), where C/T^3 is plotted against T. There are three characteristic features: (i) a term that is almost linear in temperature for $T > 1\,\mathrm{K}$; (ii) a specific-heat plateau for $T > 5\,\mathrm{K}$; and (iii) extra contributions to the specific heat around $0{\cdot}5\,\mathrm{K}$, which could possibly be due to localized excitations (Löhneysen and Platte 1979). The origin of these modes is unknown.

5.3.7. *Nuclear magnetic resonance*

Quadrupolar freezing in $(NaCN)_{1-x}(KCN)_x$ was investigated by Wiotte *et al.* (1986) using NMR. From analysis of the ^{23}Na lineshapes, they concluded that at high temperatures, where the line is sharp, the time average of the quadrupole moment of the CN molecules vanishes because of the fast orientational motion. Thus the sodium

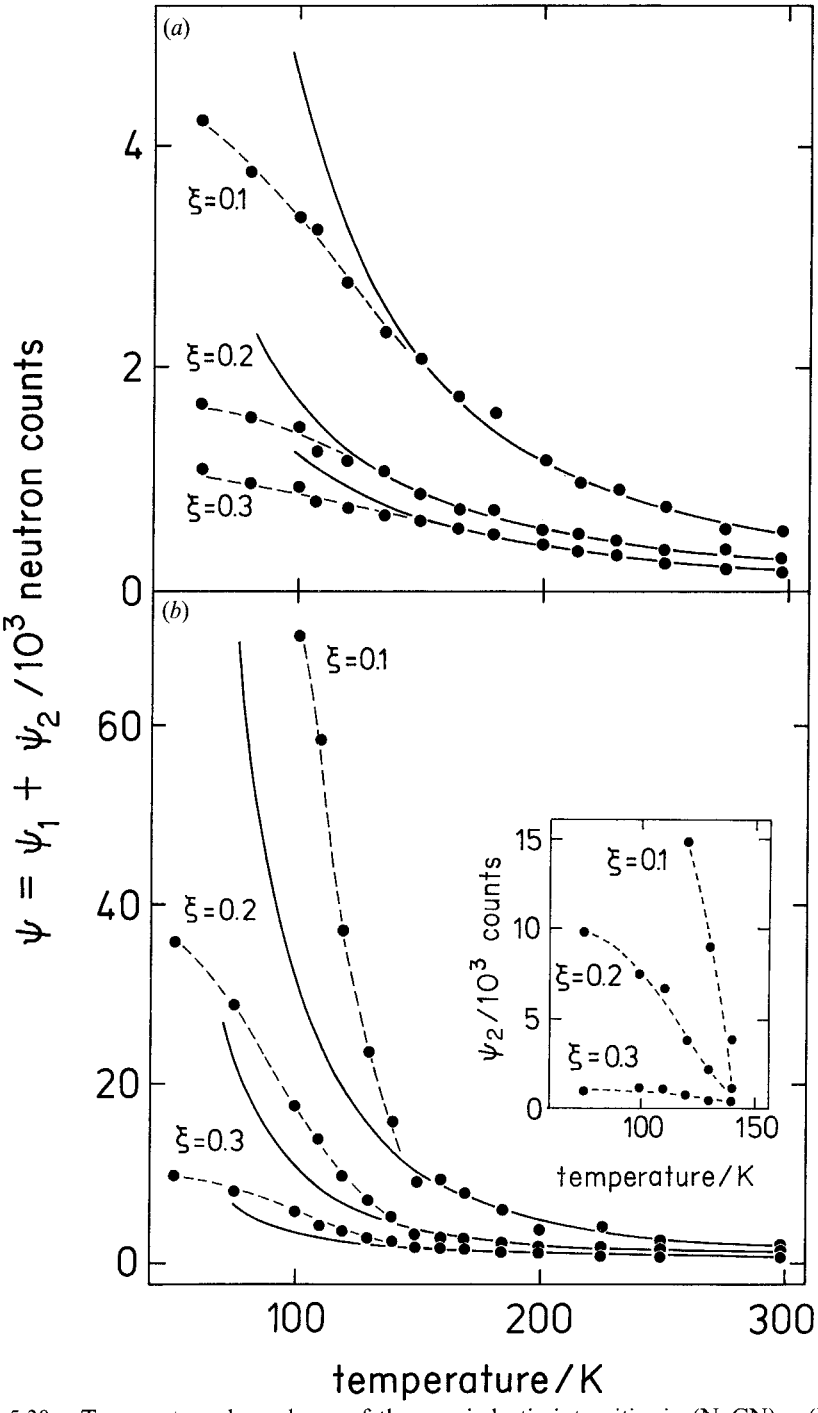

Figure 5.30. Temperature dependence of the quasi-elastic intensities in $(NaCN)_{1-x}(KCN)_x$ for $x = 0{\cdot}31$ (*a*) and $0{\cdot}85$. (*b*) The measurements were performed around the (111) Bragg reflection for different phonon wave-vectors: $Q = (1 + \xi, 1, 1)$. The solid lines are calculated within the framework of a pure random-strain model. The inset for $x = 0{\cdot}85$ shows extra contributions to the order parameter for $T < 140$ K. From Schräder *et al.* (1990c).

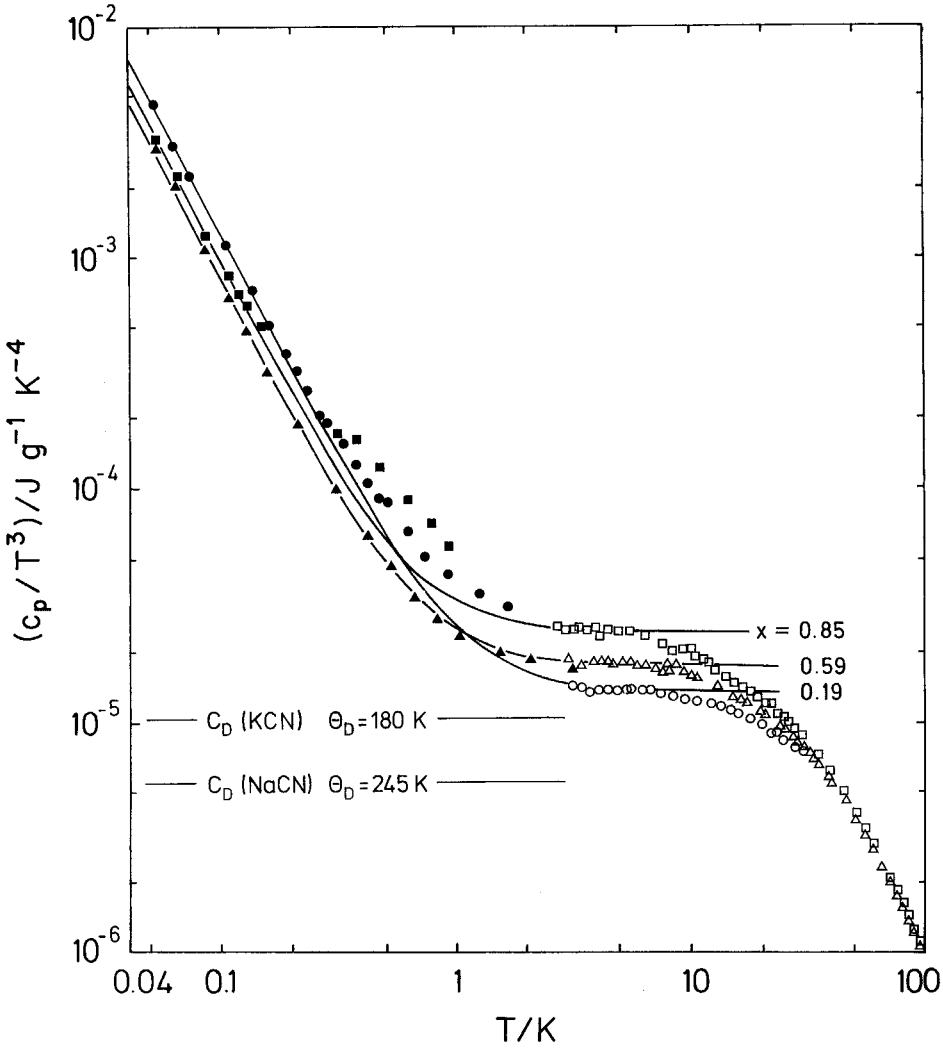

Figure 5.31. Temperature dependence of the heat capacity of $(NaCN)_{1-x}(KCN)_x$ for $x = 0{\cdot}19$ (●, ○), $0{\cdot}59$ (▲, △) and $0{\cdot}85$ (■, □). The data are shown as a log–log plot of c/T^3 *versus* T. The low-temperature data were obtained from time-resolved heat-capacity measurements (filled symbols) and the high-temperature data by standard quasi-adiabatic techniques (open symbols). From Mertz *et al.* (1990).

nuclei see an almost-cubic symmetry. At low T, the line is broad and asymmetric owing to the fact that the CN molecules are oriented randomly along one of the cube axes.

The ^{23}Na spin–lattice relaxation time T_1 was investigated for a number of concentrations. For $x = 0{\cdot}3$ and $0{\cdot}5$, broadened BPP minima were observed, reflecting the reorientational motion in highly asymmetric potentials with a broad distribution of relaxation times. It was concluded by Wiotte *et al.* (1986) that in the glassy state of $(NaCN)_{1-x}(KCN)_x$ there is only partial freezing: at higher temperatures, the distribution of quadrupole moments shows that there is coexistence of 180° and 90° flips, whereas only 180° flips exist at low T.

Elschner *et al.* (1990) recently attempted to interpret the electric-field-gradient (EFG) distribution at the Na sites in terms of a random-bond–random-field model as developed by Pirc *et al.* (1987). Their results showed that neither a pure random-bond model nor a pure random-field model, but possibly a contribution of both, could adequately describe the T dependence of the width of the distribution of the electric-field gradient.

5.4. *Models*

There have been several theoretical studies on the dynamics of an individual CN defect (Mahanti *et al.* 1985, de Raedt and Michel 1979) and on the lattice dynamics of pure cyanides (Michel and Naudts 1977a, b, 1978, Sahu and Mahanti 1982a, b). Here we concentrate on models developed specifically for the glass-like state of cyanide mixed crystals.

Michel and Rowe (1980) pointed out that a freezing in of the CN orientations leads to a freezing in of lattice strains, which in turn becomes observable in diffraction studies through the appearance of a central peak. The central-peak intensity is regarded as the glass order parameter. This parameter was added to the theory of orientation–phonon coupling in a heuristic way. The minimum in $c_{44}(T)$ is related to a cusp in the T dependence of the orientational susceptibility. Michel and Rowe (1980) also pointed out that the effective strain-mediated CN–CN interaction changes sign, depending on how the molecular axes are tilted with respect to the vector connecting the molecular centres. The analogy with magnetic interactions was mentioned and it was suggested that this type of interaction should lead to frustration in the presence of substitutional disorder.

Lewis and Klein (1986, 1987a, b, 1989a, b) performed constant-pressure molecular-dynamics simulations of the mixed cyanides based on realistic assumptions regarding the interatomic interactions and the dipole and quadrupole moments of the CN^- ion. The calculations were very successful in reproducing the (x, T) phase diagram, including the order parameters of the polymorphic phases in the ordered regime and the glass transition as a function of x and T. This is an interesting point, since the model starts out from a relatively small number of particles, typically $4 \times 4 \times 4$ unit cells, and hence cannot describe the long-range effects that are considered to be important in the structural and elastic effects. For the orientational-glass state, these simulations yield, among other details, the T dependence of the orientational distribution, the single-ion orientational relaxation time and the orientational correlation of neighbouring CN^- ions. Wherever comparison with experiment has been possible, excellent agreement has been found. The result that neighbouring ions are preferentially parallel supports the idea of ferroelastic-type quasidomains.

Quantitative predictions of $c_{44}(x, T)$ and hence of the $T_c(x)$ and $T_f(x)$ boundary of the (x, T) phase diagram were made using Michel's random-field model (Michel 1986, 1987a). In the model, Michel's theory of orientation–phonon coupling is merged with the concept of random strains. The coupling leads to a ferroelastic instability, which was treated in the mean-field virtual-crystal approximation. The random stresses are introduced by the size (not the shape) difference of CN and Br. The random stresses are temperature-independent, and lead to inhomogeneous T-dependent strain distributions. The variance of the strain distribution is $q(T) = h^2/T^2$, where h^2 is assumed to vary with the CN/Br mixing ratio as $h^2 = x(1 - x)h_0^2$. The temperature dependence of c_{44} is obtained as

$$c_{44}(T) = c_{44}^0[1 - g^2\chi(T)(1 - q(T)],$$

where g is the orientation–phonon coupling coefficient, χ the orientational susceptibility, and c_{44}^0 the background constant of a CN-free reference system like KBr. The simplest choice for χ is a Curie-law form (a Curie–Weiss form can be chosen alternatively). g is proportional to x. The model treats the high-temperature limit, where $q(T) \ll 1$. Michel derives from his model the boundaries $T_0(x)$ and $T_f(x)$. At T_f, $c_{44}(T)$ is a minimum, with $q(T_f) = \frac{1}{3}$ (which is no longer small compared with unity).

In subsequent work, Michel (1987b) dealt with dynamic effects and presented theoretical results on the phonon linewidth and the q and T dependences of the central peak intensity.

The model has been further extended to include a special type of dynamic process (Michel 1987c, Bostoen and Michel 1988, 1990), where a phonon is scattered by the random strains and converted into an orientational mode. The process sets in at a characteristic temperature T_g when the elastic shear constant $c_{44}(T)$ of the para-elastic phase softens below a threshold value. Below T_g, the system is non-ergodic. The non-ergodic instability at T_g might be regarded as the 'true glass transition temperature' of the mixed cyanides. It is important to realize that, within this concept, the 'broken symmetry' occurs through the appearance of a new process in the dynamic response, whereas for conventional phase transitions and for the spin-glass transition, one refers to static properties. This extended treatment is set up in close analogy with the mode–mode-coupling theory of liquids approaching a glass transition.

In Michel's theory, the random fields reduce the local orientational susceptibility, which in turn appears in $c_{44}(T)$. Mayer and Cowley (1988b) investigated a ferroelastic instability with soft c_{44} in the presence of random stresses (without specifying by what microscopic interaction this instability is actually driven). Within a mean-field approximation, they derived a self-consistent expression for the elastic coherence length and correspondingly for $c_{44}(T)$. They showed that the divergence of the coherence length at the prospective transition temperature can be suppressed by sufficiently large random stresses. The resulting structure can be understood as the short-range version of a ferroelastic phase. As far as we can see, the most important difference with Michel's model is that the random stresses of Mayer and Cowley have shear components interfering directly with the ferroelastic shears, which mathematically leads to a self-consistency condition on $c_{44}(T)$.

Galam (1990a) considered a compressible ferroelastic system including anharmonic terms that are introduced by the random-site occupation. He derived a reduced spin Hamiltonian and showed that the problem reduces to a site percolation problem (on an f.c.c. lattice). In order to reconcile the f.c.c. site percolation threshold $x_p = 0{\cdot}20$ with the experimentally observed threshold concentration $x_c = 0{\cdot}60$ (for $(KBr)_{1-x}(KCN)_x$), Galam (1990b) rescaled x in terms of the number of CN^- ions blocked by a neighbouring Br^- ion. This number is unity for the mixed bromide. He suggested that the x range of the orientational-glass state is divided into subregimes: the single-ion regime for $x < x_p$; the collective glass for $x_p < x < 0{\cdot}50$; and the glass with domain-like ordered regions for $0{\cdot}50 < x < x_c$. Such distinctions have been made in some experimental studies.

The models mentioned above deal with the formation of the quadrupolar state. A second direction of theoretical effort concentrates on the low-temperature (TLS) properties of the mixed cyanides. These models start out from the idea that—in contrast with the complex situation in amorphous solids—the microscopic degrees of freedom responsible for the TLS effects can be specified in dilute mixed crystals. The model of Sethna and co-workers has already been discussed in sections 5.2.5 and 5.2.6.

Earlier work along this line was performed by Fischer and Klein (1979), who started out from an individual CN strain dipole in an alkali halide host having a number of fixed discrete orientations, such as ⟨100⟩ or ⟨111⟩. The strain interaction with the other CN^- ions was considered in terms of a distribution of random strain fields of Gaussian or Lorentzian shape. Via the distribution of tunnelling splittings, the heat capacity and the thermal conductivity were calculated. The results suggest a close analogy with real glasses. An analogous model for electric dipoles due to the same authors has already been mentioned in section 3. This was re-investigated by Klein for electric dipoles (1989) and for strain dipoles (1985, 1990) in terms of a microscopic model, that is, without reference to the mean-random-field approach. On the basis of two microscopic parameters, the near-neighbour dipole–dipole interaction and the single-ion tunnelling matrix element, Klein calculated the density of excitations, heat capacity, thermal conductivity and frequency-dependent dipolar response function.

5.5. *Summary*

Over the last decade, relatively detailed experimental information has been collected on mixed cyanides; nevertheless understanding of the glass-like state is still incomplete. In the following, we comment on points that we consider particularly important.

The quadrupolar-glass state is, in principle, described by the distribution of local quadrupolar orientational polarizations and strains. In contrast with the quadrupolar-glass states of o–p-H_2 and $Ar_{1-x}(N_2)_x$, the quadrupolar susceptibility of mixed cyanides is measurable via the phonon response function. The $q = 0$, infinite-wavelength limit of this response function is commonly known as the elastic shear constant c_{44}. This, or to be more precise c_{44}^{-1}, plays a role analogous to the magnetic susceptibility of spin glasses and the dipolar susceptibility of dipole glasses. At the freezing temperature T_f, $c_{44}(T)$ as measured using finite-frequency techniques is a minimum. This minimum is considered as being equivalent to the cusp of the magnetic susceptibility in spin glasses. There are indications that extrapolation to zero frequency would yield a temperature-independent response function (Parisi-type T dependence) in the glass state. The nature of the primary, quadrupolar relaxations is still under discussion. Collective reorientations of CN quadrupoles accompanied by local shear–strain relaxations are involved in these processes. Two specific topological pictures have been cited: the dissipative motion of the walls of ferroelastic quasi-domains and the unbinding of pairs of screw dislocations. From NMR measurements, it is clear that the local quadrupolar polarizations that freeze in at T_f are small. The individual CN quadrupoles can still reorient rapidly, even well below T_f.

The cyanides are understood as model glass systems as far as secondary relaxations and TLS anomalies and the connection between these two phenomena are concerned. The pertinent model of Sethna may be oversimplified and even incorrect, but nevertheless has had an impact on the glass science in general, since it suggests a simple microscopic picture: the secondary relaxations are due to thermally activated head–tail flips of CN moieties in a double-well potential showing a broad distribution of barrier heights. Head–tail tunnelling in the same potential gives rise to the TLS anomalies at low temperatures. The model has yet to explain why head–tail flips should lead to secondary elastic loss. Furthermore, the extrapolation from high to low temperatures is not free from arbitrariness.

For the formation of the glass-like state, two different routes have been followed. The first starts from the well understood behaviour of an isolated CN defect in the

halide matrix. As the CN concentration is increased, larger and larger clusters of coupled CN orientations are formed. Clusters containing three or even four CN molecules can be identified in the Raman spectrum. The approach breaks down for $x > 0{\cdot}1$, where the spectrum broadens so that individual lines can longer be separated. The other approach starts from the ferroelastic transitions of pure cyanides. When the CN concentration is reduced, the ferroelastic transition temperature decreases, and finally, below the threshold concentration x_c, the long-range ferroelastic order is suppressed in favour of local ferroelastic and ferroquadrupolar ordering. The glass-like state is here a short-range-ordered variety of the ferroelastic phases. This approach is based on the observation that many experimental quantities (such as heat capacity and elasticity) render the distinction of samples with x slightly above x_c and those with x slightly below x_c impossible. Noticeable differences exist in optical transmission and X-ray and neutron diffraction only. Thus it is likely that the ferroelastic multidomain state differs from the glass-like state only in the size of the ordered regions. The size of the ferroelastic domains is of the order of the wavelength of visible light; the coherence length in the glass-like state, the size of the quasi-domains, is presumably around 100 Å.

It is not clear so far how and at what CN concentration the two approaches must be matched. It has even been suggested that there are two different glass states: a low-x glass between say $x = 0{\cdot}05$ and $0{\cdot}20$ (for $(KBr)_{1-x}(KCN)_x$), and a high-x 'ferroelastic' glass for $0{\cdot}20 < x < x_c$.

When modelled on a microscopic level, the glass-like state calls for randomness either of the bonds between the CN moieties or of the fields trying to break up the long-range ferroelastic order known from pure KCN. The experimental result strongly suggest that random strains exist in mixed cyanides. These fields preclude the existence of a sharp transition temperature to the glass state. The symmetry is broken, so to say, at any finite temperature. On the other hand, it is still an open question as to whether random bonds can be ignored completely. The relative importance of random bonds relative to random fields depends on the actual compound. $(KBr)_{1-x}(KCN)_x$ is the best candidate for realization of the random-bond picture, while random fields seem to dominate in $(NaCN)_{1-x}(KCN)_x$.

A new approach to the glass transition of the cyanides is Michel's 'non-ergodic instability'. Here extra relaxational channels are opened below a characteristic temperature.

The glass order parameter has been extracted from the NMR linewidth, the diffuse intensity of the diffraction experiment and the elastic shear response. Some of these procedures lack a clear conceptual basis and are to a large extent heuristic. Nevertheless, it is clear that q grows very gradually with decreasing temperature. Hence there is no doubt that the glass transition—if it exists at all—is smeared out, presumably by random-field effects.

Two pecularities of mixed cyanides must be considered: the ferroelastic and ferroquadrupolar polarization is a tensor quantity, and the instabilities are two-dimensional. The polymorphism of the ordered phases is intimately connected with the tensor character. Polymorphism in turn favours the appearance of a glassy state.

The $m = 2$ nature of the ferroelastic instability raises the possibility that the translational invariance of the lattice is lost at the transition temperature. A definite conclusion regarding this has not yet been reached. Nevertheless, it is appealing to think of a non-crystalline state where tensor properties still show the anisotropy of a cubic solid.

The analogy between real glasses (obtained from supercooled liquids) and spin and orientational glasses is traditionally based on the rather academic statement that the orientational degrees of freedom of the orientational subsystem behave above and below the freezing temperature very much like the positional degrees of freedom of real glasses. In cyanides, the analogy is deeper and involves the translational degrees of freedom too. At the ferroelastic transition temperature on the one hand, at the freezing temperature on the other, the elastic shear constant is small—almost zero —and the Bragg peaks have almost disappeared. Thus the cyanides are close to a liquid-like state. Upon further cooling, the elastic shear constant and the viscosity (internal friction) increase strongly—very much as for liquids solidifying in the glass state.

6. Rubidium ammonium dihydrogen phosphates: solid solutions of hydrogen-bonded ferroelectric and antiferroelectric compounds

At room temperature, the hydrogen-bonded phosphates (MH_2PO_4) and arsenates (MH_2AsO_4) (M = Na, K, Rb, Cs, Ag, Tl and NH_4) form a class of isostructural crystals of tetragonal symmetry. When M is an alkali ion, the low-temperature state is ferroelectric. However, the ammonium compounds exhibit a paraelectric-to-antiferroelectric phase transition. Mixtures of ferroelectric and antiferroelectric compounds show a broad regime in which the long-range electric order is suppressed owing to frustration effects, and these systems have been treated as dipolar analogues of spin glasses. Mixtures of $Rb_{1-x}(NH_4)_xH_2PO_4$ (RADP: $100x$) are the most prominent examples to have been studied in full detail. There exist a number of reviews dealing with this system (Courtens 1983, 1987a,b, Terauchi 1985a, 1986, Schmidt 1987). Glassy behaviour has also been reported for the mixed crystals $Rb_{1-x}(NH_4)_xH_2AsO_4$ (Trybula *et al.* 1988) and $K_{1-x}(NH_4)_xH_2PO_4$ (Ono *et al.* 1988). Here we focus on the most relevant results on solid solutions of RbH_2PO_4 and $NH_4H_2PO_4$. For further details, the reader is referred to the original papers.

RbH_2PO_4 (RDP), with a unit-cell volume $V = 422{\cdot}3\ \text{Å}^3$ and a c/a ratio of 0·959, undergoes a second-order ferroelectric (FE) phase transition at 146 K. $NH_4H_2PO_4$ (ADP), characterized by $V = 424{\cdot}7\ \text{Å}^3$ and $c/a = 1{\cdot}0067$, becomes antiferroelectric (AFE) near 148 K. This AFE transition is strongly first-order. The ordering of the acid protons in 'up–down' Slater configurations (Slater 1941) produces the ferroelectric transition in RDP, while in ADP the antiferroelectric phase is generated by lateral ordering. The difference is due to the formation of competetive hydrogen bonds by the NH_4 cations (Courtens 1982).

Since the rubidium and ammonium ions are a nearly perfect match in size, high-quality and strain-free mixed single crystals of $Rb_{1-x}(NH_4)_xH_2PO_4$ can be grown at all concentrations x (Courtens 1983, 1987b). Starting from the pure systems, the electric phase transitions are rapidly suppressed with increasing defect concentrations, and at intermediate concentrations ($0{\cdot}23 < x < 0{\cdot}74$) the mixed crystals freeze into configurations devoid of long-range dipolar order. Obviously, the competing interactions between different types of proton ordering lead to a frustrated ground state and suppress long-range electric order. A schematic phase diagram of RADP is shown in figure 6.1 (Courtens 1987a).

The deuterated isomorphs show enhanced electric-ordering temperatures (D-RDP $T_{FE} = 218$ K; D-ADP $T_{AFE} = 237$ K). It should be noted that deuterated RDP can be grown in either a tetragonal or a monoclinic structure (Kennedy and Nelmes 1980). However, small amounts of ammonium admixtures are sufficient to stabilize the

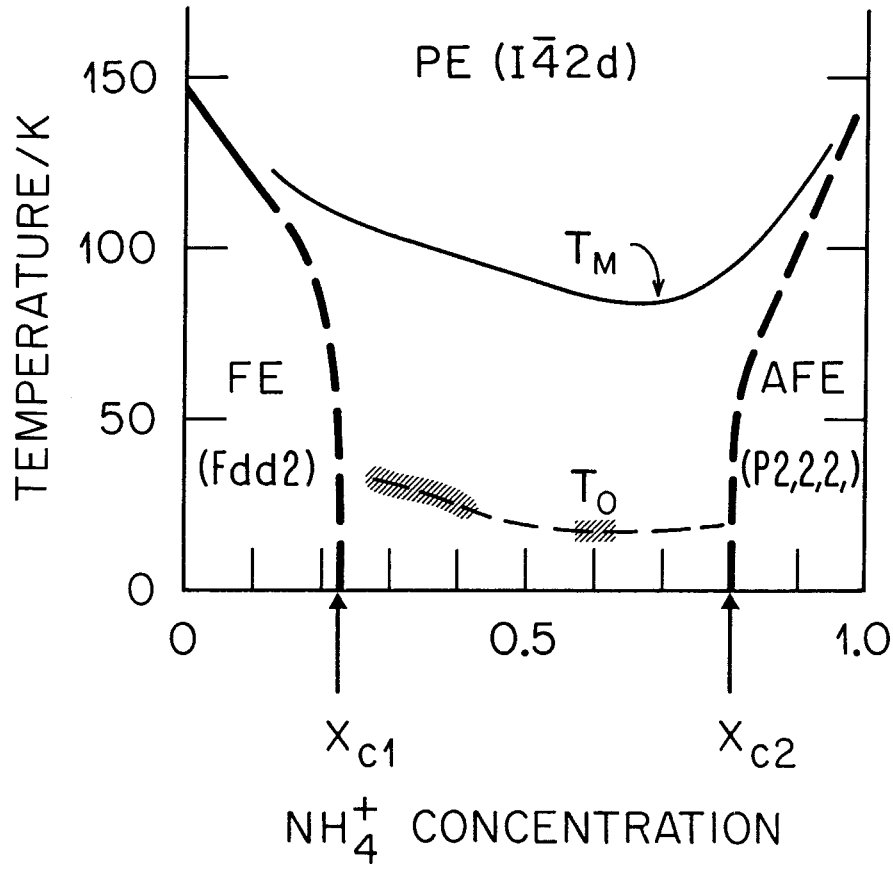

Figure 6.1. Schematic phase diagram of RADP. The solid line indicates the appearance of anomalies near T_M and the dashed lines the appearance of dielectric loss, which extrapolates to a static freezing temperature T_{VF}. After Courtens (1983).

tetragonal structure (Grimm *et al.* 1986). From the experimental results so far available it seems that the glassy regime of D-RADP is somewhat narrower than that of RADP ($0{\cdot}3 \leqslant x \leqslant 0{\cdot}7$).

The pioneering work in RADP mixed crystals was performed by Courtens (1982) using dielectric and birefringence techniques for concentrations $0 < x < 0{\cdot}35$. The results in solutions with ammonium concentrations $x > x_{c1}$ were interpreted as a freezing process into a glassy low-temperature state. The results for the real and the imaginary parts of the transverse dielectric constant ε_{11} in RADP : 34, as measured at 1 kHz are shown in figure 6.2. A broad maximum appears in $\varepsilon'_{11}(T)$ near 80 K, followed by a strong decrease below 30 K accompanied by an appreciable dielectric loss. The low-temperature dispersion has been interpreted in terms of relaxational processes compatible with a 'random ferroelectric type of ordering' (Courtens 1982), which is connected with the dynamics of the O–H···O bonds. This freezing process shows a striking similarity with the relaxation phenomena observed in spin glasses. At higher temperatures, ε'_{11} exhibits an inflexion point, which is better seen in the derivative plotted in figure 6.2. T_m as defined via the minimum value of $d\varepsilon'_{11}/dT$

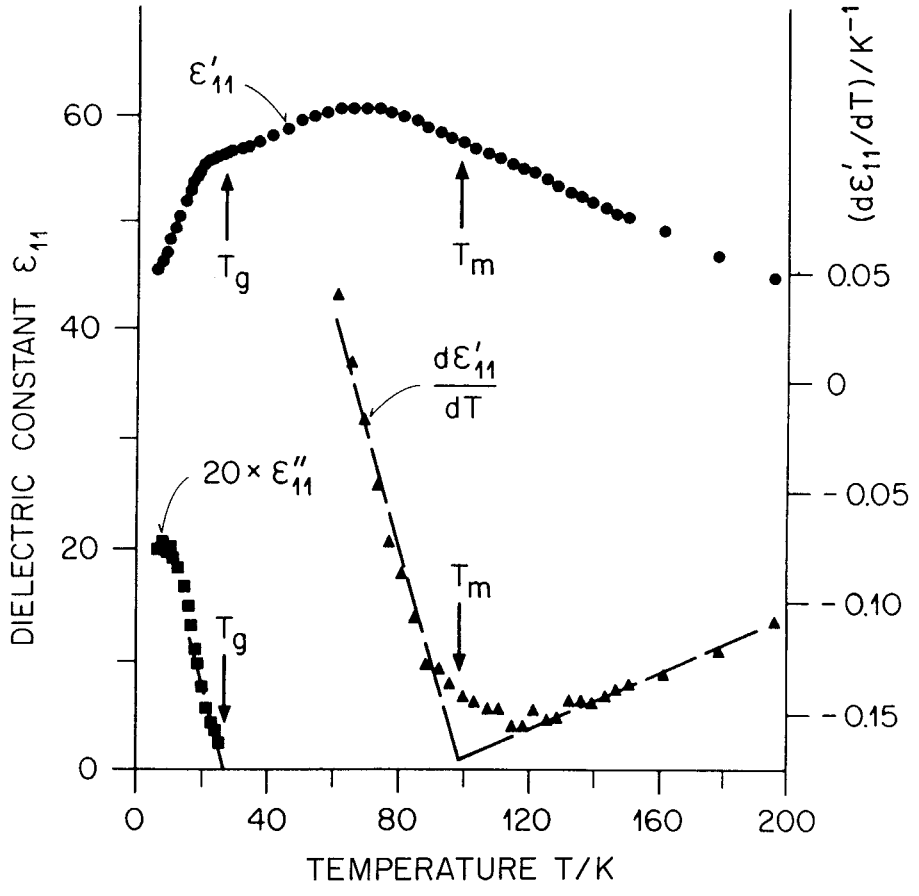

Figure 6.2. Temperature dependences of the real and imaginary parts of the transverse dielectric constant at 1 kHz for $x = 0{\cdot}34$ and temperature dependence of the derivative of the dielectric constant $d\varepsilon'_{11}/dT$. From Courtens (1982).

corresponds to the temperature where the dielectric constant along the ferroelectric axis, ε_{33}, deviates from Curie–Weiss behaviour. This high-temperature anomaly around 100 K was thought to correspond to the onset of short-range antiferroelectric order due to the freezing-in of the NH_4 reorientations, and this interpretation is supported by the appearance of birefringence anomalies near 80 K (Courtens 1982, 1983).

6.1. *Dielectric susceptibility*

6.1.1. *Protonated compounds*

The dielectric measurements by Courtens (1982) have been extended by Iida and Terauchi (1983) and Takashige *et al.* (1985a,b) to the complete concentration range of RDP and ADP solid solutions. A summary of their results is given in figure 6.3 (Takashige *et al.* 1985b), where the real and imaginary parts of the dielectric constant ε_{11} are shown *versus* temperature. For concentrations $0{\cdot}25 < x < 0{\cdot}75$, the mixed crystals are characterized by dispersion effects at low temperatures, which were again attributed to the slowing down of the proton dynamics. The dielectric constant is

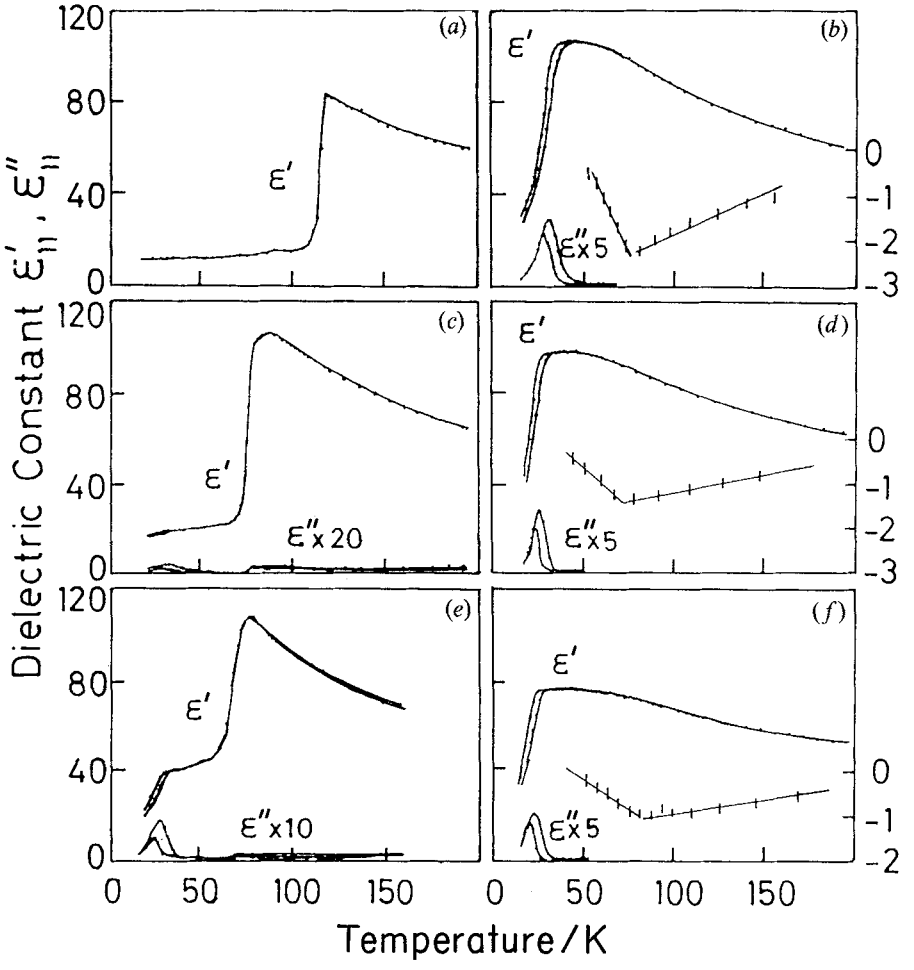

Figure 6.3. Real and imaginary parts of the dielectric constants *versus* temperature for concentrations $x = 0{\cdot}9$ (*a*), 0·8 (*b*), 0·75 (*c*), 0·7 (*d*), 0·6 (*e*) and 0·5 (*f*). The two curves in the dispersion regime in (*b*)–(*f*) correspond to frequencies of 300 Hz and 100 kHz respectively. In (*d*)–(*f*), the derivative $d\varepsilon_{11}/dT$ is also shown. From Takashige *et al.* (1985b).

frequency-independent for $0{\cdot}8 < x < 1$ and exhibits a discontinuous drop at the AFE phase transition. For concentrations $0{\cdot}75 < x < 0{\cdot}8$, both glass-like dispersion and an anomaly due to the antiferroelectric phase transition appear. This behaviour was interpreted as a re-entrant glass transition (Takashige *et al.* 1985a,b). The temperature dependence of the derivative of the dielectric constant $d\varepsilon_{11}/dT$ is indicated by vertical bars in figure 6.3. The temperature T_m of its minimum value was interpreted as the onset of local AFE order in the ammonium network. This interpretation was substantiated by results of diffuse X-ray scattering (Iida and Terauchi 1983, Terauchi *et al.* 1984): here diffuse scattered intensities around the (810) AFE-superstructure reflection have been observed, which signal the onset of short-range antiferroelectric order. The characteristic temperatures as observed in these experiments agree with those indicated in figure 6.1 (Takashige *et al.* 1985b). Besides the para-electric (PE), ferroelectric (FE) and antiferroelectric phases (AF), figure 6.1 also

shows an intermediate phase, which has been characterized by a frozen network of NH_4 molecules, while in the low-temperature glass state the O–H···O disorder is frozen in.

The dielectric susceptibility in $Rb_{0\cdot65}(NH_4)_{0\cdot35}H_2PO_4$ (RADP : 35) has been measured from 10 Hz to 100 kHz (Courtens 1984). The complex dielectric constant could be described well by a Vogel–Fulcher law with a 'static' freezing temperature $T_{VF} = 10$ K, an attempt frequency $\nu_0 = 6{\cdot}3$ THz and a distribution of relaxation times (Courtens 1984). The distribution broadened considerably with decreasing temperature, and an extrapolation suggested an infinitely broad distribution width near T_{VF}. Under the assumption of a temperature-independent distribution of hindering barriers, it has been possible to scale the ε'' data to a single curve. The dielectric measurements were later extended into the gigahertz regime (Brückner *et al.* 1988). Scaling works in the microwave region for frequencies $f < 100$ MHz. For higher frequencies, an additional relaxation mode contributes to the dielectric response and scaling fails. Figure 6.4 shows a Cole–Cole representation of the high-frequency dielectric data for RADP with $x = 0{\cdot}35$ (Brückner *et al.* 1988). These data give a clear impression of how the width of ε'' progressively broadens with decreasing temperatures. At 21·5 K, the dielectric loss is nearly independent of the measuring frequency f, indicating an extremely broad distribution of relaxation times.

Considerable efforts have been made to study the dipolar relaxation over an extremely broad range of frequencies. Figure 6.5 shows the Vogel–Fulcher law in RADP : 35 as observed over 17 orders of magnitude in frequency. Results are included from Brillouin and Raman investigations, as well as those derived from measurements of the saturation of electric polarization (Courtens and Vogt 1986). Specifically, it has been possible to study the attempt frequency directly by using Raman-scattering techniques. Details of the Raman and Brillouin investigations will be given later. A best fit to the experimental results yielded $T_{VF} = 8{\cdot}74$ K, $E_b = 268$ K and $\nu_0 = 3{\cdot}2$ THz. Since a theoretical justification of the Vogel–Fulcher law is still lacking, attempts were made to parametrize the experimental results of figure 6.5 using either a scaling law or a Binder–Young law as have been developed for spin–glass systems. However, the phenomenological Vogel–Fulcher law gave a significantly better fit (Courtens and Vogt 1986).

The low-temperature dielectric properties in RADP-75 were studied by Miura *et al.* (1985, 1987), who reported the temperature dependence of the complex dielectric constant for temperatures $0{\cdot}02\text{ K} < T < 1$ K. The temperature dependent variation of the real part of the dielectric constant, as measured along the a axis at different frequencies, is shown in figure 6.6 (Miura 1985). $\varepsilon_1(T)$ exhibits frequency-dependent minima that roughly follow $T_{min} \approx f^{1/3}$. This result was interpreted as evidence of a constant density of tunnelling states, the characteristic feature of dielectric glasses (Miura *et al.* 1985, 1987).

6.1.2. *Deuterated compounds*

The dielectric permittivity in partly deuterated RADP was studied at audio-frequencies by Schmidt *et al.* (1984), who measured ε_1 in $Rb_{0\cdot52}(ND_4)_{0\cdot48}D_2PO_4$ (D-RADP : 48) at 1 kHz from 4 K to 300 K. The dielectric constant showed a rounded maximum near 70 K. Deviations from the Curie–Weiss law appeared near $T = 150$ K. The experiments in this sample were extended to the microwave region by Stankowski *et al.* (1988).

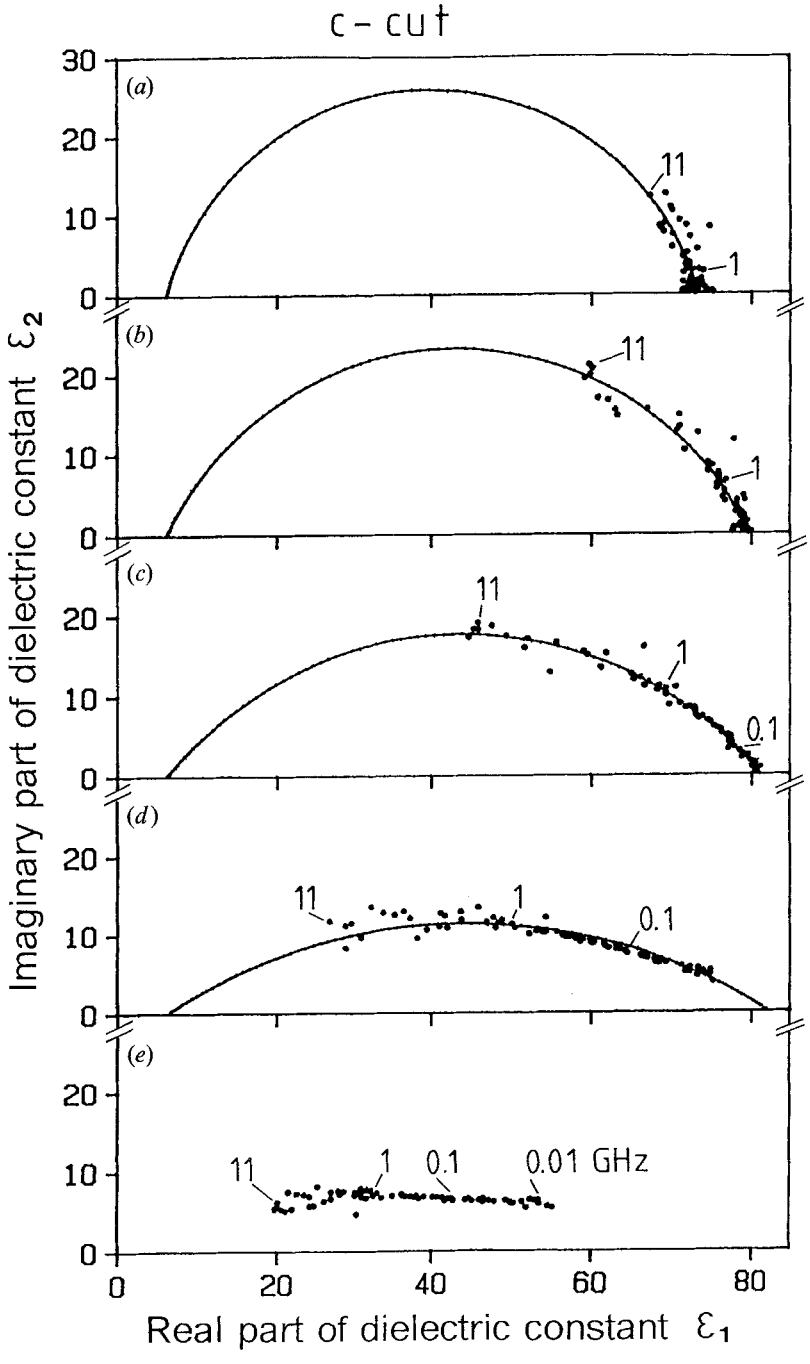

Figure 6.4. Cole–Cole representation of the complex dielectric constant in RADP:35 at temperatures 60 K (*a*), 45·4 K (*b*), 37·3 K (*c*) 28·9 K (*e*) and 21·5 K (*f*). The solid curves are Cole–Cole fits. From Brückner *et al.* (1988).

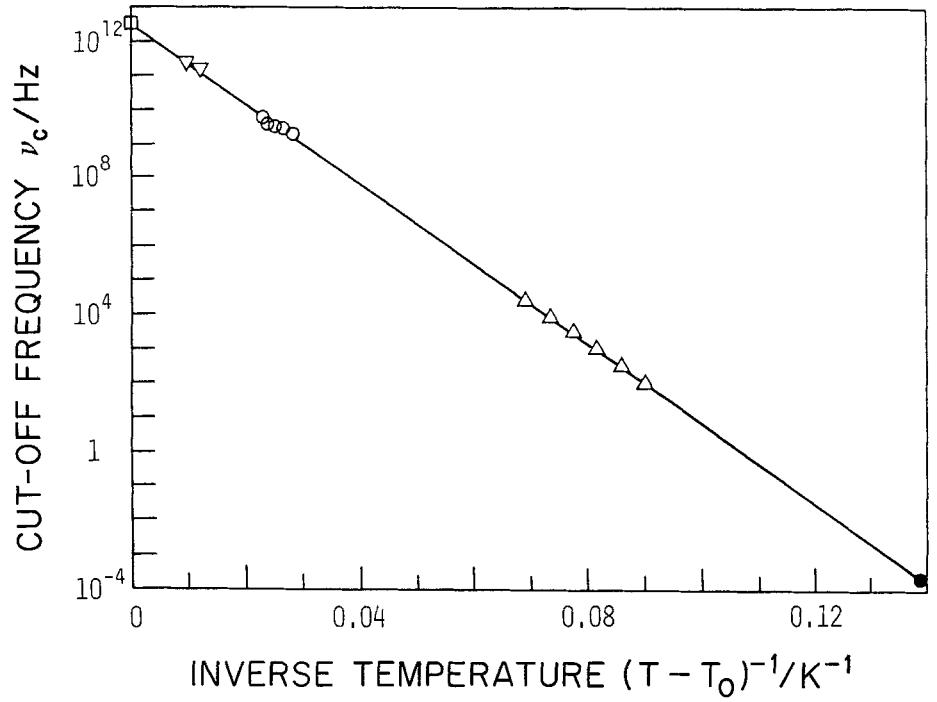

Figure 6.5. Cut-off frequency *versus* inverse reduced temperature $(T - T_0)^{-1}$ (Vogel–Fulcher representation) in RADP: 35: □, Raman attempt frequency; □, Raman central mode; Brillouin coupled modes; △, dielectric dispersion; ●, polarization saturation; (——), the best Vogel–Fulcher fit with $T_0 = 8{\cdot}7$ and $\nu_0 = 3{\cdot}5$ THz. From Courtens and Vogt (1986).

Dielectric measurements in the audiofrequency region were also performed on well deuterated RADP (D-RADP: 62) (Courtens 1986). A best-fit Vogel–Fulcher law yielded a Vogel–Fulcher temperature $T_{VF} = 30{\cdot}3$ K, a mean activation energy $E = 700$ K and an attempt frequency $\nu_0 = 2{\cdot}4$ THz. The distribution of energy barriers was found to be almost Gaussian. However, the scaling is not as perfect as in RADP. We return to more recent results in section 6.5.

6.1.3. *Pressure dependence of dielectric constants*

Pressure-dependent measurements of the dielectric constants in RADP: 35 were performed by Samara and Terauchi (1987). These experiments revealed a shift to lower temperatures of the maximum loss ε''_{max} with increasing pressure. The increasing relaxation rate was thought to result from the influence of pressure on the H-bond potential: on freezing into the glass state, the protons freeze into one of the potential minima, a process that leads to elongated asymmetric H bonds. Pressure opposes this tendency and yields shorter symmetric O–H···O bonds, thus leading to a reduction of the effective hindering barriers. Similar experiments were performed by Samara and Schmidt (1986) on deuterated samples of RADP (D-RADP: 65). Again, with increasing pressure, the loss peaks are shifted to lower temperatures. A linear extrapolation yielded a suppression of the freezing-in at 10 kbar, compared with a value of 4·5 kbar as obtained for RADP: 35. At these critical pressures, the glass transition is suppressed and reorientations occur even at the lowest temperatures.

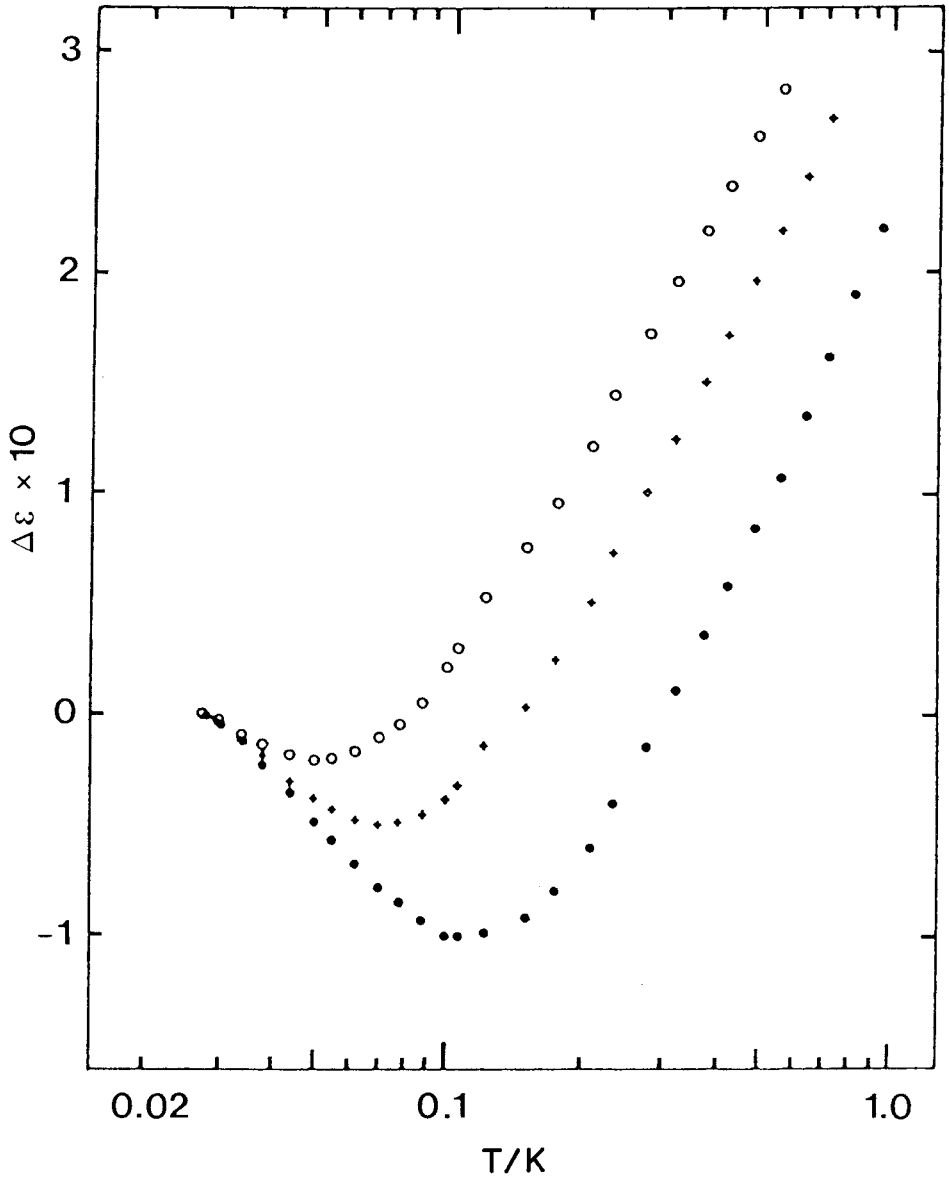

Figure 6.6. Low-temperature dielectric constant ε_1 in RADP:75 as measured at different frequencies along the *a* axis: (○), 10 kHz; (◆), 30 kHz; (●) 100 kHz. From Miura *et al.* (1985).

6.2. *Specific heat and thermal conductivity*

Specific-heat and thermal-conductivity measurements in D-RADP:48 were reported by Lawless and Schmidt (1985) for temperatures $1{\cdot}5\,\mathrm{K} < T < 30\,\mathrm{K}$. We turn to the specific-heat results first: a maximum in $C/T^3(T)$ was detected at 13·5 K and interpreted as being due to an Einstein-type mode. A similar Einstein mode has been found in pure KDP and is a characteristic feature of ferroelectric and antiferroelectric materials (Lawless 1976). An interesting feature of the specific heat in D-RADP:48 is the rapid rise in C/T^3 below 5 K. In this temperature range, the

specific heat follows a linear T dependence. Consequently, the results were interpreted as a glass-like behaviour due to a constant density of tunnelling states. However, it must be noted that the linear term in the temperature dependence of the specific heat is usually studied for $T < 1$ K, while in this specific-heat investigation the data were reported for $T > 1{\cdot}5$ K. Thus evidence for glass-like excitations in these specific-heat measurements must be viewed with some caution. De Yoreo *et al.* (1985) demonstrated that generally those electrically 'ordered' crystals that display a diffuse transition into a 'glassy polarization phase' exhibit glass-like thermal properties at low T.

For increasing temperatures, the thermal conductivity in D-RADP : 48 increases proportionally to $T^{1{\cdot}3}$, passes through a maximum at 12·5 K, and decreases for further increasing temperatures. These data do not reflect glass-like behaviour. In detail, the thermal conductivity exhibits no plateau and is approximately 30 times larger than in typical glasses (Lawless and Schmidt 1985).

Low-temperature specific-heat and thermal-conductivity data have recently been presented by Berret *et al.* (1989). The long-time (1 s) specific heat as determined by these authors is shown in figure 6.7, where c/T^3 is plotted against temperature for RADP crystals with concentrations $x = 0{\cdot}17$, 0·35 and 0·72. The data for vitreous silica are also shown for comparison. An almost-linear term is observed for $x = 0{\cdot}35$ and 0·72. The ferroelectrically ordered crystal ($x = 0{\cdot}17$) exhibits a slightly lower slope, and c varies like $T^{1{\cdot}5}$ for this crystal.

Berret *et al.* (1989) have also investigated the thermal conductivity of RADP. The results for $x = 0{\cdot}17$, 0·35 and 0·72 are shown in figure 6.8, together with the results for the thermal conductivity in ADP and RDP and for vitreous silica. The glassy RADP crystals with concentrations $x = 0{\cdot}35$ and 0·72 show almost identical thermal conductivities that follow a $T^{1{\cdot}8}$ behaviour at low temperatures and exhibit a plateau above 2 K. In the plateau regime, the thermal conductivity is enhanced in comparison with vitreous silica. The ferroelectrically ordered crystal exhibits very similar low-temperature behaviour and shows an increased thermal conductivity in the plateau region, similar to what is observed in polycrystalline materials.

Heat capacities in solid solutions of RADP with NH_4 concentrations $x = 0$, 0·7, 0·74, 0·79 and 0·89 were investigated by Moriya *et al.* (1985) using adiabatic calorimetry. In these experiments, the authors focused on the specific-heat anomalies at the glass and phase transitions. It is interesting to note that for the ordering compounds with $x = 0$, 0·79 and 0·89 two successive phase transitions were found. The anomaly at high T is due to the para-electric-to-antiferroelectric phase transition. The second specific-heat anomaly seems to signal a further structural phase transition, which has not yet been reported in the literature. The two crystals with $x = 0{\cdot}7$ and 0·74, which undergo transitions into a glassy low-temperature state, exhibit no distinct anomalies but rather a broad excess specific heat ranging from $20\,\text{K} < T < 100\,\text{K}$. As in other orientational glasses, the progressive freezing of local order takes place over a large temperature range, so that the specific heat looks smooth at all temperatures, see for example Mertz and Loidl (1987).

6.3. *Brillouin scattering*

Crystals of the KDP family are already piezoelectric in the paraelectric phase. Hence it is important to consider dielectric and elastic responses simultaneously. Brillouin spectra of transverse phonon modes coupled linearly to the polarization were reported for RADP : 35 by Courtens *et al.* (1986) and Courtens and Vacher (1987). Measurements of the xy shear mode revealed that, with decreasing temperature,

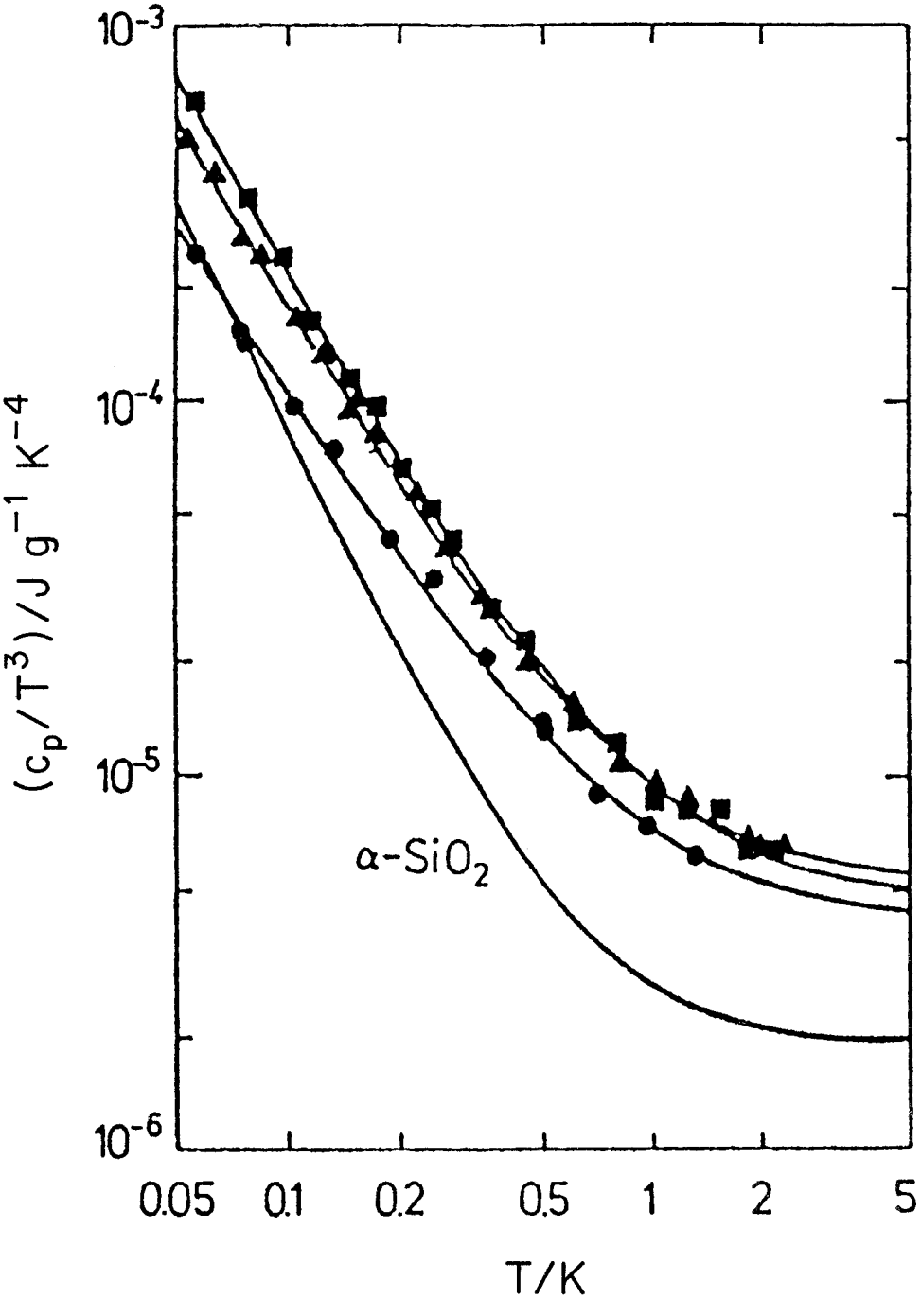

Figure 6.7. Low-temperature specific heat of RADP mixed crystals $Rb_{1-x}(NH_4)_xH_2PO_4$, plotted as c_p/T^3: ●, x = 0·17, ×, 0·35; ■, 0·72. Data for vitreous silica are shown for comparison. From Berret *et al.* (1989a).

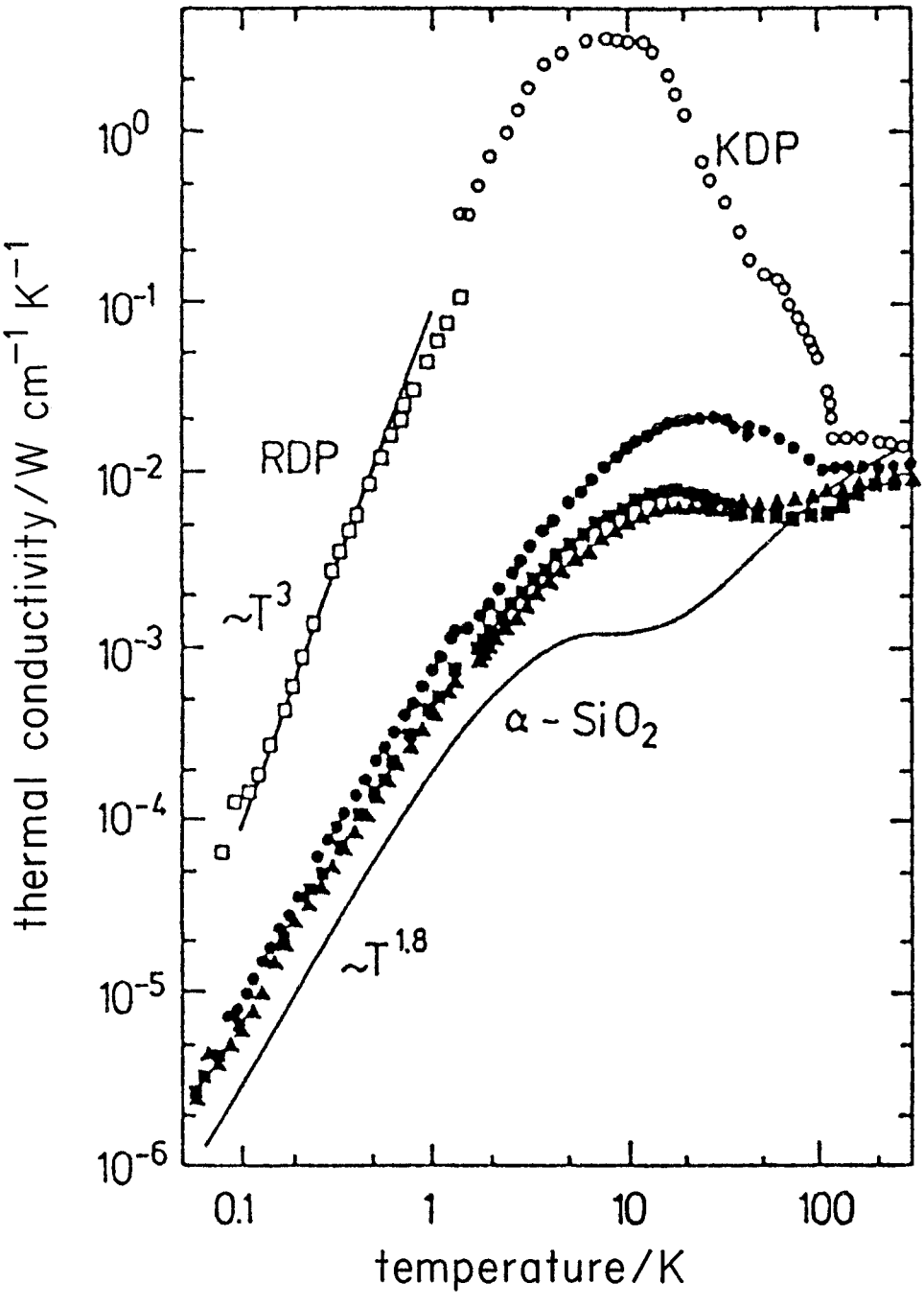

Figure 6.8. Thermal conductivity of RADP mixed crystals $Rb_{1-x}(NH_4)_xH_2PO_4$: ●, $x = 0{\cdot}17$; ▲, 0·35; ■, 0·72. Results for RDP, ADP and vitreous silica are shown for comparison. From Berret *et al.* (1989a).

the frequency of the Brillouin line softens, passes through a minimum near 50 K, and increases again as the temperature is lowered further. In addition, a distinct broadening of the inelastic line and a dynamic central peak were found. In this early work, the peak profile of the central line was fitted assuming a rectangular distribution of relaxation times with high- and low-frequency cut-offs. The main fitting parameters are then the bare phonon frequency, the low-frequency cut-off of the distribution of relaxation times, the piezoelectric coupling constant and the relative strength of the electro-optic and piezoelectric coupling coefficients. It should be noted that the main part of the central peak was masked by the strong Rayleigh scattering, and hence only the tails of the dynamic central line could be considered in the fitting procedure. The results of this analysis were that (i) the broad distribution of relaxation times is in agreement with values derived from the dielectric measurements, and (ii) the temperature dependence of the low-lying cut-off of the relaxation times was compatible with the Vogel–Fulcher fit derived from Raman and dielectric measurements of the relaxation dynamics (see figure 6.5).

In addition, Courtens *et al.* (1985) investigated phonon modes that were coupled electrostrictively to the square of the polarization fluctuations $(\delta P)^2$, with the linear couplings forbidden by symmetry. In this way, they were able to observe correlations of fourth order in the fluctuations of the polarization, a quantity that is believed to be directly related to the glass order parameter. Longitudinal sound waves with $q \parallel [100]$ were measured in RADP : 35. The temperature dependence of the Brillouin shift showed the behaviour of a normal anharmonic mode plus a dip in the mode frequency. There is a corresponding strong increase in linewidth near 50 K. The experimental data were analysed assuming two contributions to the sound velocity, namely from the coupling to dynamic and static (space-dependent only) polarization fluctuations. This analysis led for the first time to the conclusion that a static (Edwards–Anderson-like) order parameter must already exist far above the glass temperature as defined by the Vogel–Fulcher temperature T_{VF}. Courtens *et al.* (1985) concluded that the NH_4 network, which freezes-in at high T, is responsible for this observation. The broad and T-independent distribution of activation energies, found in the dipolar relaxation, was traced back to this process. This analysis has been vindicated by inelastic neutron-scattering experiments as explained in section 6.5.2.

Both types of experiments were extended to crystals with concentrations $x = 0{\cdot}15, 0{\cdot}25, 0{\cdot}72, 0{\cdot}75$ and $0{\cdot}78$ (Courtens *et al.* 1987). The main conclusions were that the spread of activation energies is larger for Rb-rich samples and that the quadratic coupling of the longitudinal acoustic (LA) modes to polarization fluctuations via electrostriction increases with NH_4 concentration x. These findings support the interpretations given above.

6.4. *Raman scattering*

Raman-scattering studies have been performed on protonated and deuterated RADP crystals from room temperature down to liquid-He temperatures. All vibrational modes that are involved in the phase transition are already Raman-active in the para-electric phase. The internal modes of the phosphate and ammonium molecular groups have been studied in detail. In the notation of Herzberg (1966), the internal modes of PO_4 and NH_4 are labelled $\nu_1, \ldots, \nu_4$: ν_1 is a symmetric stretching mode with A_1 symmetry, ν_2 a symmetric deformation of A_1 and B_2 symmetry, and ν_3 and ν_4 correspond to antisymmetric stretching and deformation modes respectively. Special attention has been paid to the symmetric deformation mode of PO_4 and to the

librations of the ammonium molecules. Both modes are sensitive to the ordering of the protons.

6.4.1. *Protonated compounds*

A detailed Raman study of RADP mixed crystals with concentrations $x = 0{\cdot}35$ and 0·66 was performed by Courtens and Vogt (1985, 1986). The transition into the glassy state affects the internal vibrations. The effect was studied by following the T dependence of the ν_2 (PO_4) lines. As the protons are attached to a given PO_4 tetrahedron, the effective moment of inertia of the vibrating entity becomes larger and consequently the frequency decreases. For both concentrations investigated, deviations from the normal anharmonic T dependence of the ν_2 modes appear for $T \leqslant 100\,\mathrm{K}$. These additional lineshifts saturate at $T \approx 30\,\mathrm{K}$.

Similar results were reported by Hattori *et al.* (1987, 1988) for a series of concentrations $0 < x < 1$. They monitored the temperature dependence of the ν_1 and ν_2 (PO_4) modes. In addition, the observed asymmetric lineshape of the symmetric deformation mode in the glass state was interpreted as the appearance of ferroelectric and antiferroelectric clusters below T_M.

Courtens and Vogt (1985) also monitored the T dependence of the NH_4 libration. The results are shown in figure 6.9. At room temperature, this mode is broad and heavily damped. With decreasing temperature, the linewidth decreases, and below 100 K a well defined librational mode can be observed. For $T \leqslant 60\,\mathrm{K}$, the linewidth remains constant. This behaviour is related to the freezing-in of the ammonia ions. As relaxation processes slow down, a defined librational mode within the frozen network becomes apparent. It is important to note that the freezing of the NH_4 ions definitely appears at higher temperatures than the slowing down of the acid-proton relaxation.

Using Raman-scattering techniques, Courtens and Vogt (1986) tried to extend the region of accessible measuring frequencies of the dipolar relaxation dynamics. The polarization-fluctuation mode in RDP is correlated with an in-phase motion of the protons in the (001) plane coupled with ionic displacements perpendicular to the plane. The in-phase motion corresponds to the ferroelectric soft mode; the out-of-phase motion of the protons is the main mechanism by which the proton excitations can change their phase. This out-of-phase mode is Raman-active and has been studied in detail. Thus in RADP it has been possible to measure the attempt frequency of the dipolar relaxation directly.

In addition, the central line was investigated using high-resolution multipass tandem interferometry (Courtens and Vogt 1986). The width of the central line was interpreted as the characteristic relaxation rate. The Raman results allowed the determination of the high-frequency end of the dipolar relaxation spectrum in RADP. They were directly plotted in the Vogel–Fulcher representation of figure 6.5 and yielded a precise determination of the relaxation dynamics over 17 decades of measuring frequencies.

6.4.2. *Deuterated compounds*

D-RADP:48 was investigated by Martinez *et al.* (1987). They followed the temperature dependence of the PO_4 ν_1 and ν_2 modes and the NH_4 librational mode. The observed splitting of the ν_1 mode at low T is interpreted by the different environments of the PO_4 groups in the mixed systems. Analogously to the results for the protonated samples, deviations from normal anharmonic behaviour were found

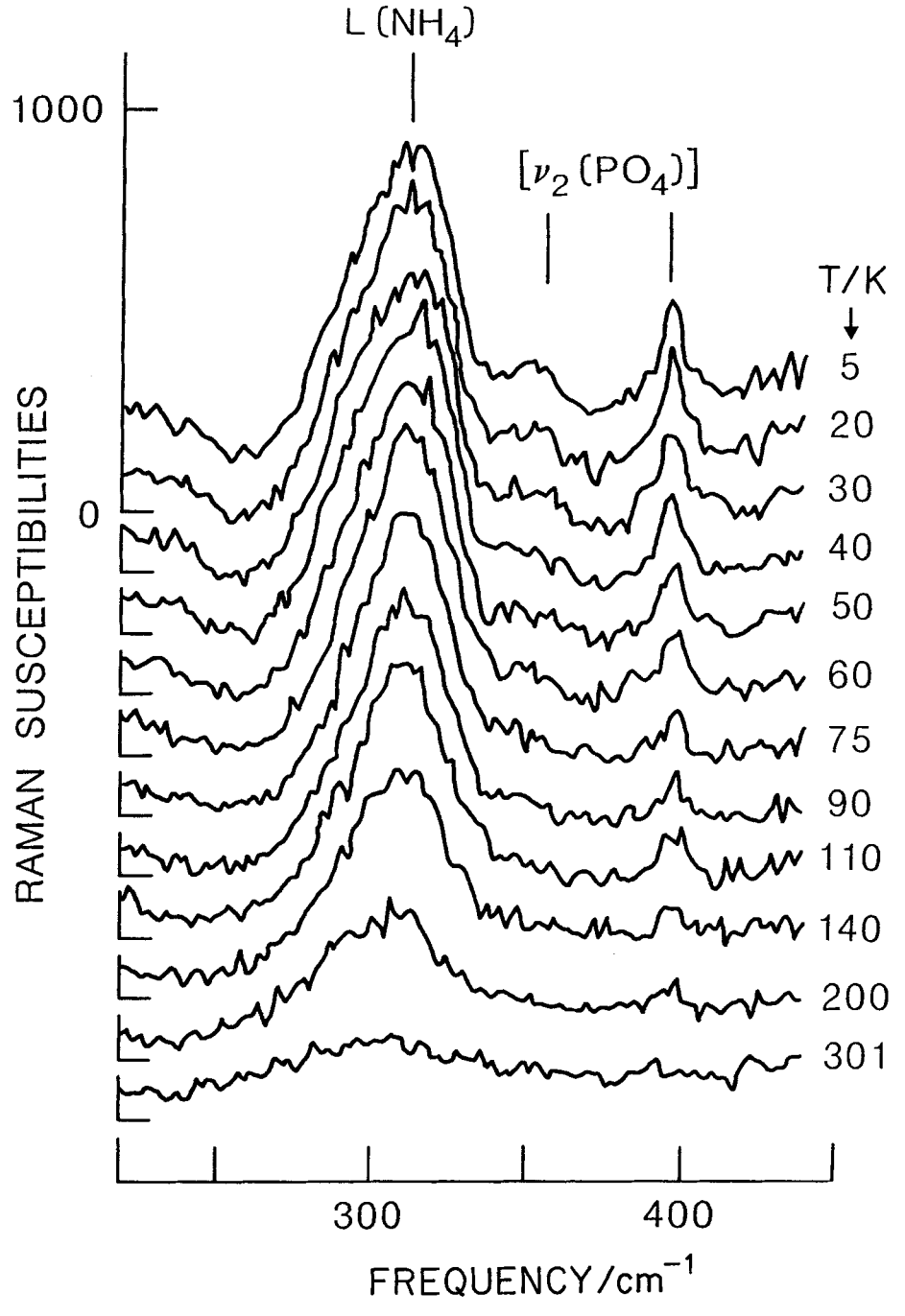

Figure 6.9. Raman spectra of RADP : 35, showing the NH_4 librational mode and two internal vibrations of the phosphate molecule as measured at different temperatures. Each curve is to be referred to a shifted baseline indicated on the ordinate axis. From Courtens and Vogt (1985).

in the T dependence of the ν_2 mode. However, in comparison with the protonated samples, the characteristic temperature T_M was shifted to 200 K. A well defined librational mode was detected below 200 K and ascribed to NH_4 librations in an almost rigid lattice.

6.5. *X-ray and neutron scattering*

6.5.1. *Protonated compounds*

X-ray-scattering techniques have been used to study the low-temperature structures of RADP mixed crystals covering the entire concentration range. Spectral attention has been given to the appearance of diffuse-scattering contributions characteristic of short-range incommensurate order and to an anomalous temperature dependence of the lattice constants in the glassy regime, first observed by Courtens *et al.* (1984).

In the glassy regime of RADP mixed crystals, two characteristic patterns of diffuse-scattered intensities appear that point towards the absence of macroscopic symmetry breaking:

(i) For concentrations $x \geqslant x_{c1}$, close to the ferroelectric regime, short-range incommensurate (IC) order with a modulation wave-vector q_0 along [100] and a magnitude of approximately $0{\cdot}15a^*$ has been detected (Amin *et al.* 1987, Hyase *et al.* 1987). Short-range IC order develops for concentrations $0{\cdot}2 < x < 0{\cdot}75$, and for temperatures $T < 100$ K (Courtens *et al.* 1984, Hayase *et al.* 1985a, 1987, Cowley *et al.* 1985). With increasing ammonium concentration, q_0 exhibits a shift from $0{\cdot}15a^*$ ($x = 0{\cdot}2$) to $0{\cdot}35a^*$ ($x = 0{\cdot}75$). The broad diffuse peaks are strongest near $x = 0{\cdot}5$ and almost disappear for $x = 0{\cdot}75$. Figure 6·10 shows the wave-vector dependence of the diffuse scattering along $(h, 0, -2)$ for concentrations $0{\cdot}49 \leqslant x \leqslant 0{\cdot}78$ at 7 K (Cowley *et al.* 1985).

(ii) The genuine antiferroelectric phase of ADP is characterized by the appearance of sharp superstructure reflections (e.g. (810)). These intensities are a direct measure of the spontaneous sublattice polarization. All mixed crystals with $0{\cdot}7 < x < x_{c2}$ show patterns of diffuse scattered intensities at the reciprocal lattice points, where superstructure reflections appear in the AFE phase (Iida and Terauchi 1983, Terauchi *et al.* 1984, Hayase *et al.* 1985a,b, 1986, 1987, Cowley *et al.* 1985). In figure 6.10, evidence for AFE correlations is provided by the appearance of *broad* peaks at $(7, 0, -2)$ for concentrations $x > 0{\cdot}7$ (Cowley *et al.* 1985). The T dependence of the intensities of the diffuse scattering near (810) is shown in figure 6.11 and compared with the appearance of well defined Bragg peaks in the antiferroelectrically ordered state (RADP : 80) (Terauchi *et al.* 1984). These diffraction patterns were interpreted by Hayase *et al.* (1985b) as being due to antiferroelectric clusters in a frustrated RDP–ADP medium. Both diffuse patterns show up for $T < 100$ K, which is the temperature T_M where the static dipolar susceptibilities start to deviate from a pure Curie–Weiss behaviour. The temperature dependence of the diffuse intensities near the AFE superstructure reciprocal lattice points is shown in figure 6.12 (the T dependence of the deviations of the lattice constant from normal anharmonic behaviour is also shown for comparison). In the glassy state of RADP, the onset of incommensurate or antiferroelectric long-range order is suppressed through a disordered RDP–ADP network with

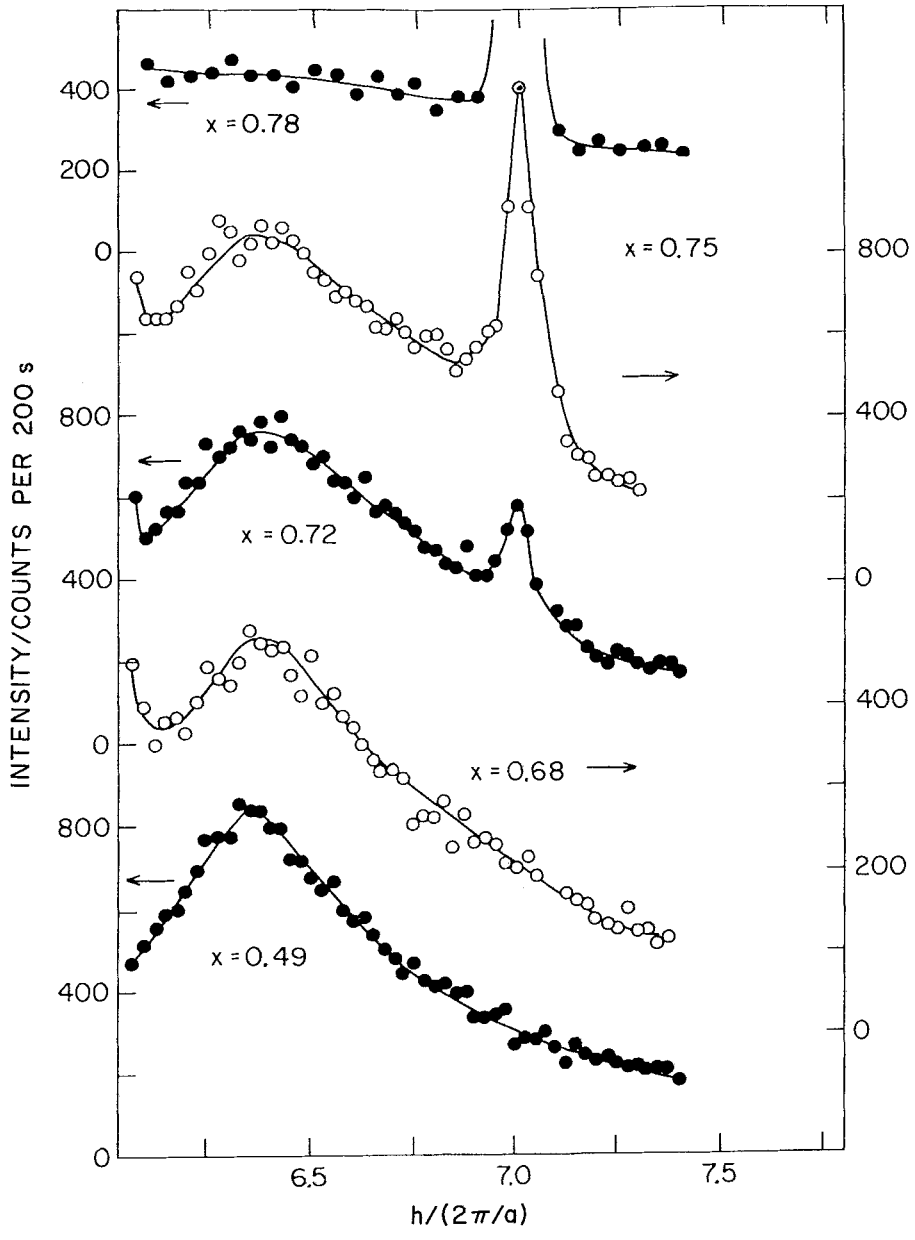

Figure 6.10. Wave-vector dependence of the diffuse scattered intensities in RADP: x as measured along $(h, 0, -2)$ for concentrations $x = 0{\cdot}78, 0{\cdot}75, 0{\cdot}72, 0{\cdot}67$ and $0{\cdot}49$ at 7 K. From Cowley *et al.* (1985).

competing FE and AFE interactions. A summary of the observed ordering wave-vectors q_0 in RADP is shown in figure 6.13 (Hayase *et al.* 1987): here q_0 is plotted against the ammonium concentration x. For $x < 0{\cdot}7$, short-range IC order dominates, while for $x > 0{\cdot}7$, short-range AFE order dominates. The coexistance regions near $x = 0{\cdot}3$ and $0{\cdot}7$ may indicate an inhomogeneous structure of the mixed crystals investigated in these experiments.

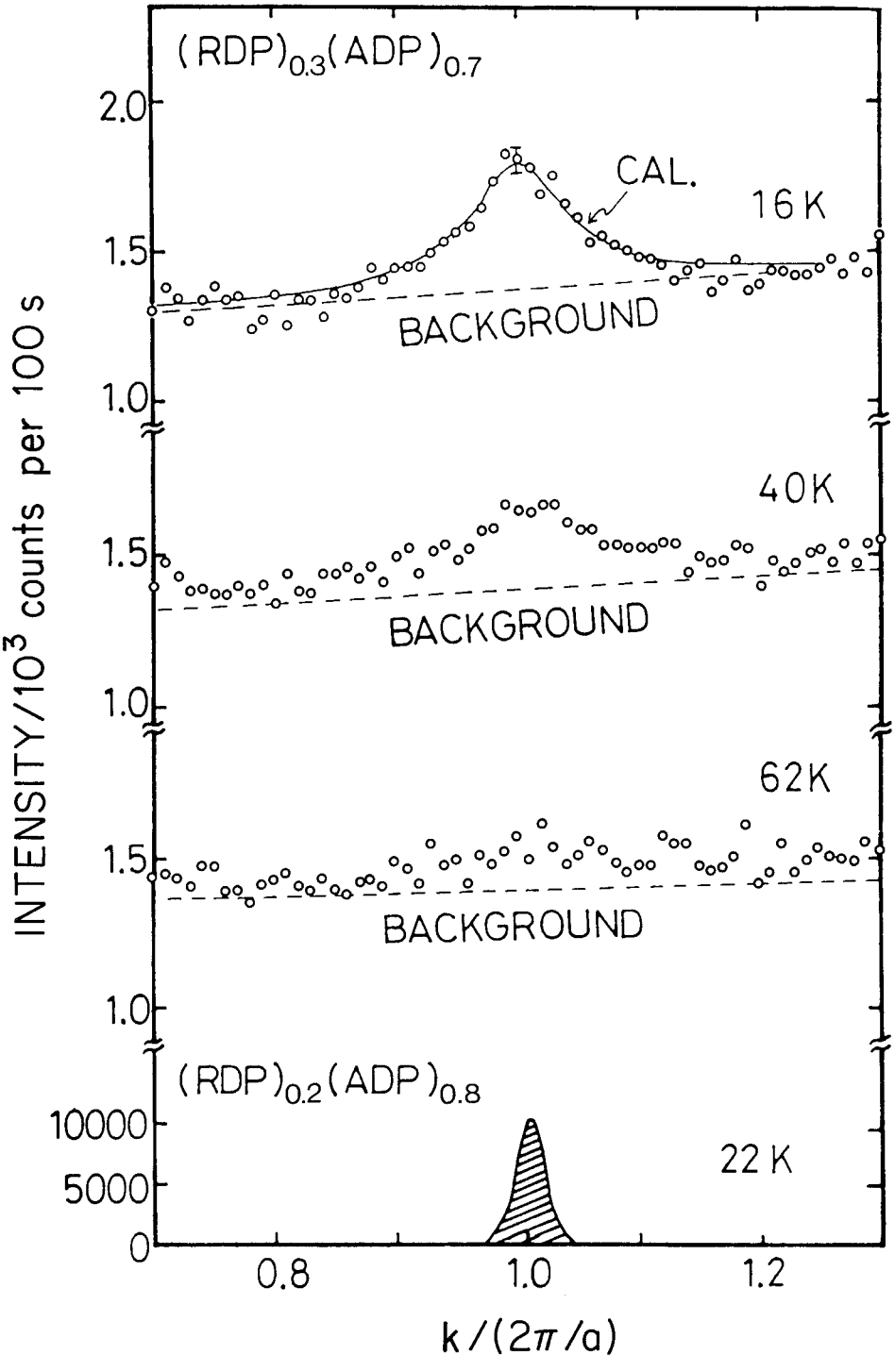

Figure 6.11. Diffuse-scattered intensities in RADP: 70 at the (810) reciprocal lattice point at different temperatures. The superstructure reflection in AFE RADP: 80 is shown for comparison. From Terauchi *et al.* (1984).

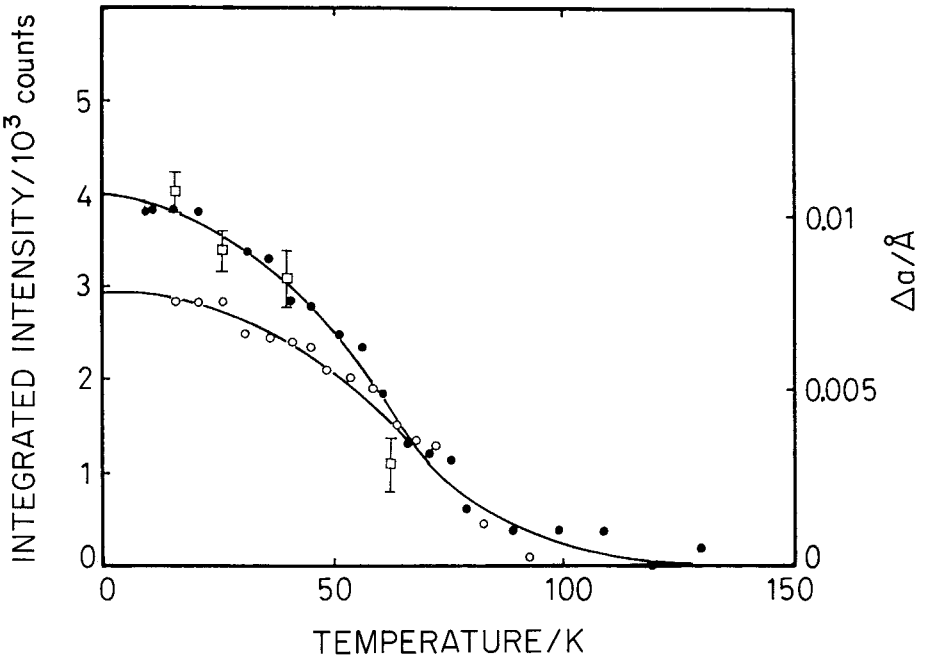

Figure 6.12. Temperature dependence of the integrated intensities (⌶) in RADP:70 as measured around the (810) reciprocal lattice point. The temperature dependence of the integrated intensities is compared with the deviations of the lattice constant Δa from normal anharmonic behaviour in RADP:60 (○) and RADP:70 (●). From Terauchi *et al.* (1984).

Anomalies in the temperature dependence of the lattice constants have been studied in RADP for all concentrations. The electrically ordered compounds exhibit abrupt changes in the lattice constants at the polar phase-transition temperatures. In the glassy crystals, a smooth but anomalous temperature dependence as compared with normal anharmonic Debye behaviour has been detected (Courtens 1984, Terauchi *et al.* 1984, Hayase *et al.* 1985a, 1986). An anomalous elongation along a and an anomalous contraction along c have been observed. Significant effects have been detected for temperatures $T < 100$ K, in a regime where short-range order is established (see figure 6.12).

The long-time relaxation of the intensities of the incommensurate modulations has been measured by Amin (1989) under applied electric fields.

EXAFS studies of the rubidium edge were reported by Nishihata *et al.* (1985) for concentrations $x = 0, 0{\cdot}3, 0{\cdot}5, 0{\cdot}7$ and $0{\cdot}9$. The main result was that in the glassy state the local structure was of RDP type for concentrations $x = 0{\cdot}3$ and $0{\cdot}5$, while the local structure was of ADP type for $x = 0{\cdot}7$. Hence FE clusters dominate for $x < 0{\cdot}5$, while AFE clusters dominate for higher ADP concentrations.

6.5.2. *Deuterated compounds*

Using X-ray techniques, the diffuse scattering from D-RADP:65 has also been studied (Cowley *et al.* 1986). Analogously to the findings in the protonated samples, the diffuse scattering shows maxima along [100] near $0{\cdot}3a^*$. The glassy state of D-RADP is a short-range incommensurate phase too, with local order persisting to about four lattice constants. The diffusive scattering that appears along the Σ line in

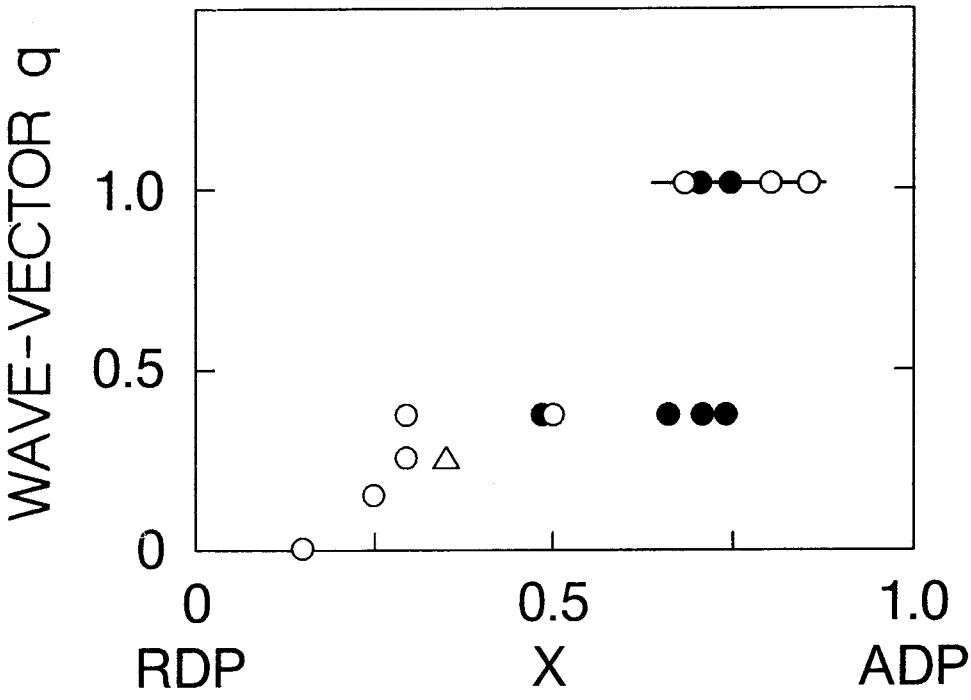

Figure 6.13. Concentration dependence of the wave-vector q_0 at which diffuse-scattered intensities appear in RADP: x: (○), Hayase *et al.* (1987); (△), Courtens *et al.* (1984); (●), Cowley *et al.* (1985). After Hayase *et al.* (1987).

reciprocal space has been explained within the framework of a simple pseudospin model for the D-bonding, taking into account ferroelectric displacements along c and b and their coupling with transverse acoustic modes (Cowley *et al.* 1986).

The X-ray measurements give no answer to the question of whether the short-range incommensurate correlations are of static or dynamic nature. Thus a number of neutron-scattering experiments have focused particularly on this point. The diffuse scattering along Σ lines has been studied in detail by elastic and quasi-elastic neutron scattering (Grimm *et al.* 1986, Grimm and Martinez 1986, Xhonneux *et al.* 1988, Grimm 1989). Energy scans at different temperatures are presented in figure 6.14 (Xhonneux *et al.* 1988). The profile of the scattered neutron intensities consists of an elastic and a quasi-elastic component. The truly elastic line (central peak) grows rapidly on cooling and reaches its saturation value at $T = 80\,\mathrm{K}$ (figure 6.15). The temperature dependence of the central peak cannot be explained by a high-frequency extrapolation of the relaxational spectrum as observed by dielectric and Brillouin measurements. The solid lines in figure 6.15 are calculated under the assumption of purely relaxational behaviour. It has been argued that the freezing of the ND_4 clusters gives rise to an increase in the central-peak intensity, which saturates near 80 K. The width of the quasi-elastic spectrum extrapolates smoothly to the spectral response obtained at lower frequencies. The temperature dependence of the mean relaxation rate is shown in figure 6.16. (Xhonneux *et al.* 1988). Thus the quasi-elastic line can be viewed as being caused essentially by the freezing-in of the acid protons.

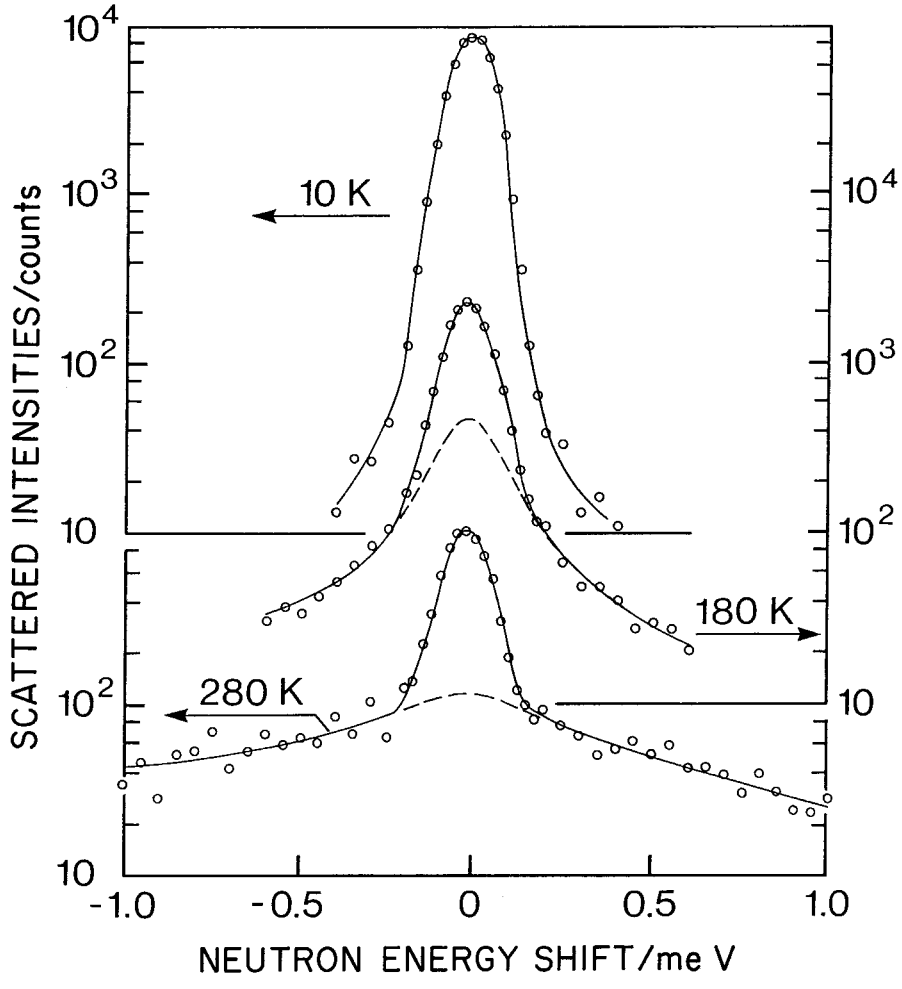

Figure 6.14. Energy scans at q_Σ as measured in D-RADP : 62 at different temperatures. The dashed lines indicate the inelastic contribution to the scattered intensities. From Xhonneux *et al.* (1988).

Short reviews of the dynamics of the IC correlations have been given by Grimm (1989) and Courtens *et al.* (1988) for the statics and dynamics. X-ray experiments have been reviewed by Terauchi (1985).

6.6. *NMR and EPR studies*

6.6.1. *Protonated compounds*

The ^{87}Rb and ^{1}H spin–lattice relaxation rate has been measured in RADP : 35 as a function of temperature (Slak *et al.* 1984). The proton T_1 is dominated by the NH_4 reorientations and exhibits a broad minimum near 175 K. From room temperature down to 125 K, the temperature dependence can be described well by a Bloembergen–Purcell–Pound (BPP) type expression and Arrhenius behaviour with an activation energy $E \approx 1600$ K and an attempt frequency $f_0 \approx 5{\cdot}6$ THz. Deviations from BPP behaviour below 120 K were related to a broad distribution of relaxation times.

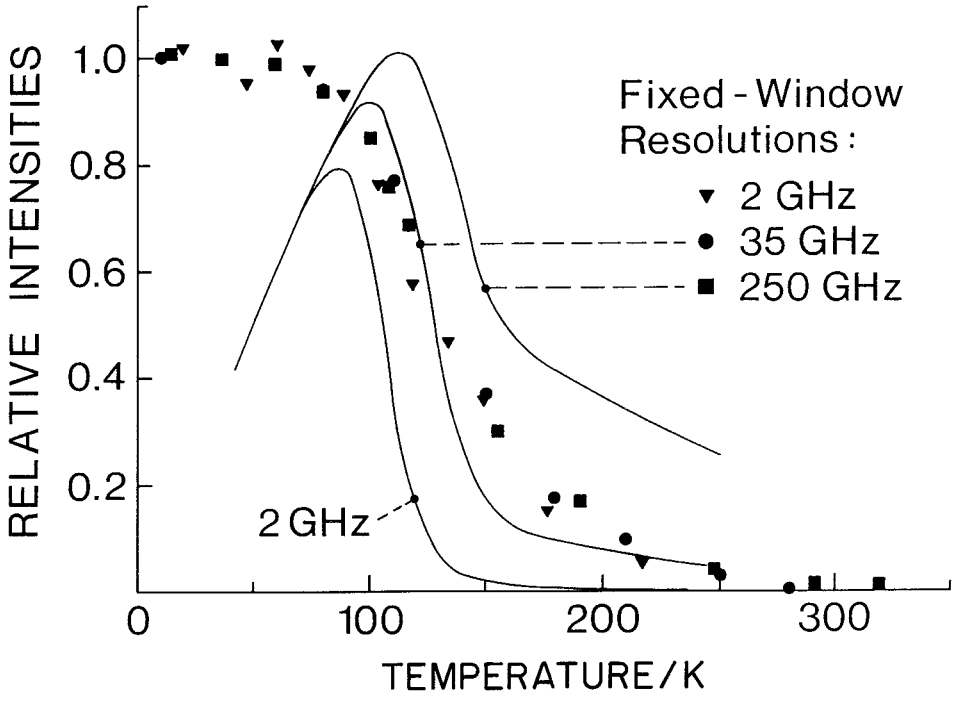

Figure 6.15. Neutron-scattering intensities in D-RADP: 62 as measured at q_Σ at zero energy transfer. The lines are calculated using a relaxational model. From Xhonneux *et al.* (1988).

From 300 to 120 K, the ^{87}Rb spin–lattice relaxation time T_1 slowly increases with decreasing T (Slak *et al.* 1984). In this regime, the relaxation processes were assigned to slow interbond jumps caused by 90° relaxations of the H_2PO_4 groups. Below 120 K, the RB T_1 decreases and passes through a minimum near 35 K. This fast relaxation was ascribed to proton intrabond jumps. The existence of a minimum demonstrated the slowing-down of the O–H···O intrabond relaxation. On the high-temperature side, the relaxation rate can be described by an Arrhenius law with $E \approx 220$ K and $f_0 \approx 130$ GHz. To explain the significant deviations from symmetric BPP behaviour, two models have been proposed: (i) an Arrhenius law with a temperature-dependent distribution of hindering barriers, and (ii) a Vogel–Fulcher law with a T-independent distribution of activation energies.

The freezing dynamics of RADP: 48 was followed in a study of the EPR spectra of Tl^{2+}, which had been substituted on the Rb sites in this mixed crystal. The anomalous broadening and the splitting of the Tl EPR lines were interpreted using a model including random bonds and random fields (Cevc *et al.* 1989).

6.6.2. *Deuterated compounds*

Deuteron and ^{87}Rb NMR data have been reported for D-RADP: 55 (Blinc *et al.* 1986). The temperature dependence of both the O–D···O deuteron and the Rb $\frac{1}{2} \rightarrow -\frac{1}{2}$ spin–lattice relaxation rates show broad and asymmetric minima near 90 K. This has to be contrasted with the findings in the pure compounds, where symmetric Bloembergen–Purcell–Pound-type minima have been observed (see Blinc *et al.* (1986), and references therein). The relaxation rates determined from these

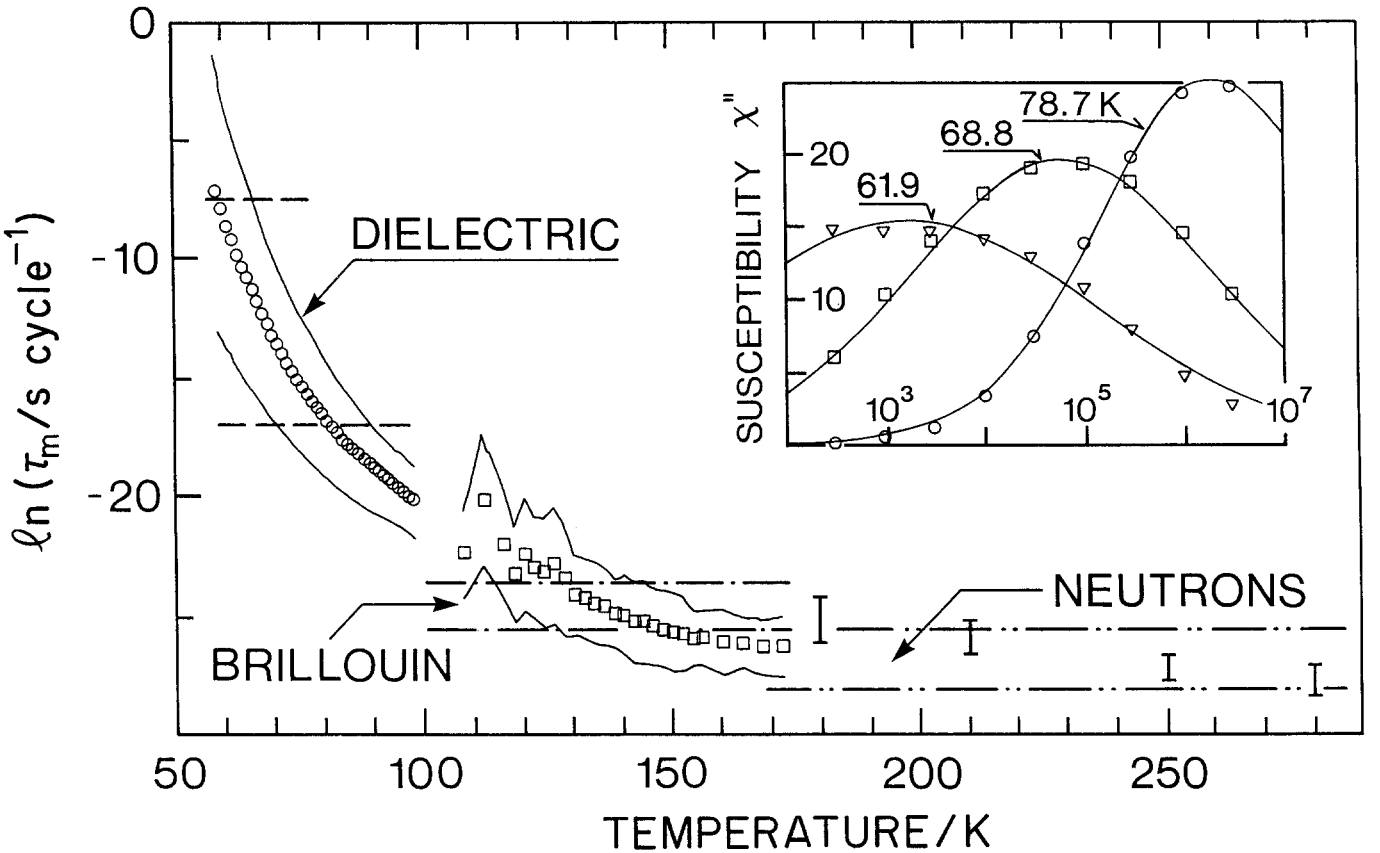

Figure 6.16. Temperature dependence of dipolar relaxation in D-RADP : 62 as measured using different experimental techniques. The inset illustrates typical data of dispersion effects in ε_2. From Xhonneux *et al.* (1988).

spectra follow an Arrhenius behaviour with an activation energy $E_b \approx 900\,K$ and an attempt frequency $v_0 \approx 10\,THz$. It was concluded that the anomalous diffusion of D_3PO_4 defects determines the O–D···O intrabond motion. The same dynamics governs the Rb relaxation.

On the other hand, in D-RADP : 55, the deuteron relaxation due to the ND_4 rotations follows a BPP-type temperature dependence with a minimum near 180 K. The Arrhenius behaviour can be parametrized using energy barriers $E_b \approx 1850\,K$. These results confirm that the ND_4 reorientations freeze-in at much higher temperatures compared with the deuterium intrabond motion.

The asymmetry of the inhomogeneously broadened ^{87}Rb lineshape has been explained in terms of a quasi-static random field component. Here the random field has to be understood in terms of the frustrated interactions that appear in the para-electric phase. The sharp increase in the second moment of the random-field distribution has been interpreted as being due to a gradual condensation of randomly polarized clusters (Blinc *et al.* 1986).

Blinc *et al.* (1989) have shown that quadrupole-perturbed nuclear magnetic resonance allows measurement of the second moment of the average distribution of local polarizations, which was thought to be directly related to the order parameter in the glass phase. Analysis of the NMR results in D-RADP : 44 suggests that the glass transition in this proton glass is a random-field smeared-out random-bond glass transition (Blinc *et al.* 1988, 1989).

6.7. *Models and model calculations*

The basic idea of a microscopic model, which was studied by Selke and Courtens (1986) using Monte Carlo techniques, is that the FE behaviour of pure RDP is suppressed by the competitive hydrogen bonding of acid protons and ammonium ions. The FE interactions are described within the framework of a pseudospin model neglecting tunnelling phenomena. All parameters are known from data on the pure crystals. The orientations of the NH_4 groups are coupled linearly with the acid protons. Using this model, the phase diagram has been calculated, including the freezing temperatures at the glass transition in accord with the experimental results. In the same spirit, an effective crystal approximation predicting the positions of the IC peaks was presented by Cowley *et al.* (1986). Their Hamiltonian, in which the ammonia position is already diagonalized out, clearly shows the presence of both random-bond and random-field terms, and elucidates their origin in terms of models used for the pure crystals.

A molecular-dynamics study of the local motion in a proton glass was performed by Parlinski and Grimm (1986, 1988). The model took into account four protons and two randomly chosen ammonium or rubidium particles per unit cell. The protons were situated in double-minimum potentials interacting with the neighbouring ions. The glassy state was characterized by a pattern of ferroelectric and antiferroelectric quasi-permanent clusters embedded in a network of disordered regions. The cluster structures of two runs, obtained as results of independent cooling processes, are shown in figure 6.17. In addition, the elementary relaxation times for glassy and crystalline systems have been calculated. At high temperatures, the dominant proton-relaxation processes are characterized by a narrow distribution peaked at short times. Below T_F, in the glass state, the spectrum evolves towards longer relaxation times, where essentially the protons of the quasi-permanent clusters give rise to slow relaxation processes. The proton dynamics is a consequence of the distribution of the proton

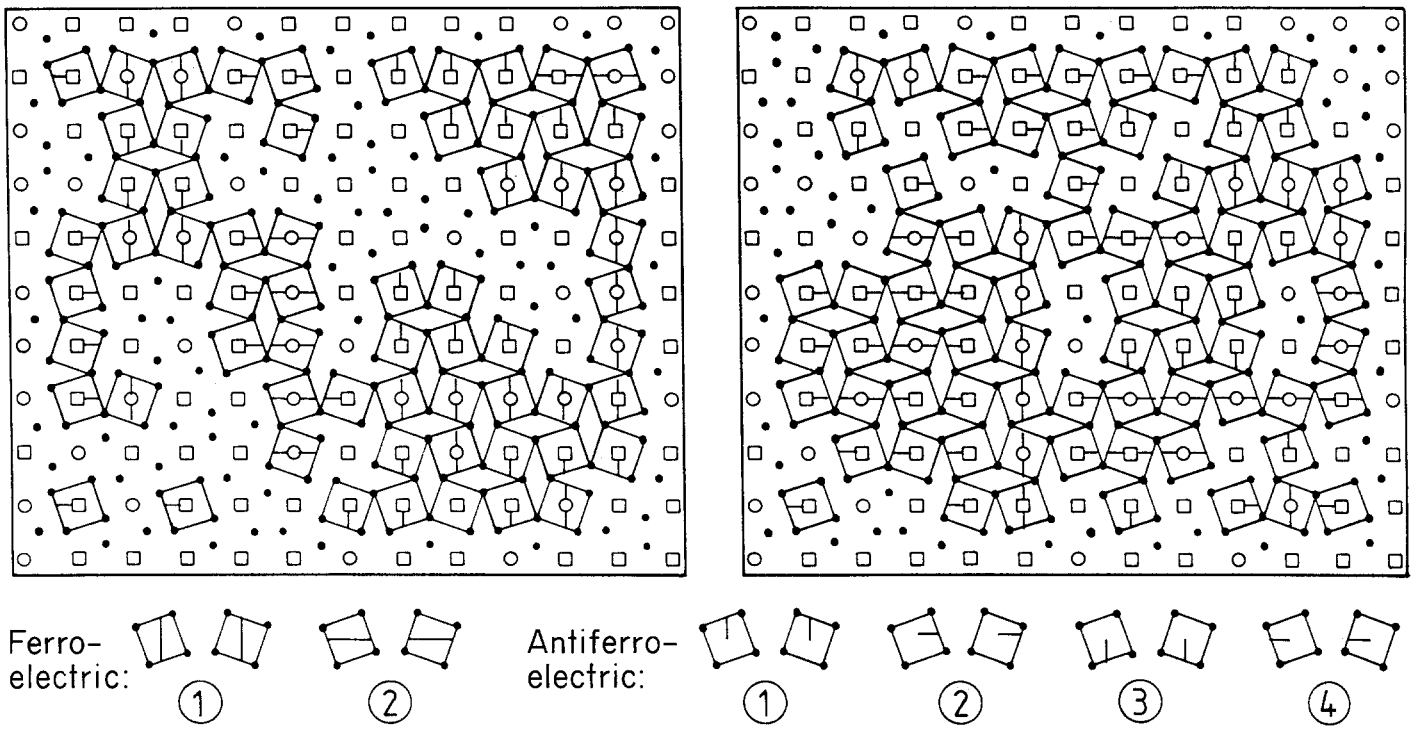

Figure 6.17. Cluster structure of two runs as obtained by molecular-dynamics simulation. The two runs simulate two independent cooling processes. The rubidium (○) and ammonium (□) ions are indicated. From Parlinski and Grimm (1988).

potential barriers, which is narrow and crystalline-like at high T and exhibits a dramatic broadening at low T.

Pseudo-spin models where the proton glasses are modelled as pseudo-Ising spins in a transverse field have been developed by Matsushita and Matsubara (1985a,b), Prelovsek and Blinc (1982), Pirc *et al.* (1985, 1987), Dobrosavljevic and Stratt (1987) and Tadic *et al.* (1989). Using these models the phase diagram and the temperature dependence of the dipolar susceptibility have been calculated. Tunnelling phenomena were included by Pirc *et al.* (1985, 1987), and it was shown that, above a threshold value of the tunnelling frequency, no ordering is possible even for $T \rightarrow 0$. The most detailed study of the influence of the tunnelling phenomena on the glass transition, including quantum fluctuations, was presented by Dobrosavljevic and Stratt (1987). The effects of random fields on the dynamics of an Ising spin system with infinite interactions was studied by Tadic *et al.* (1989). A model including random-bond and random-field effects was proposed by Blinc *et al.* (1988, 1989).

Model calculations by Schmidt *et al.* (1984, 1985) used a Slater energy ε_0 and a short-range interaction ε_a between the hydrogen bonds across the ammonium groups (ε_a is responsible for the off-centre position of the ammonium groups in the AFE state). The phase boundaries were calculated using this model, and found to be close to those experimentally observed.

The dynamic behaviour of RADP was calculated by Schmidt (1988a,b) using the concept of the creation and annihilation of intrinsic defects ($H_2PO_4 + H_2PO_4 = H_3PO_4 + HPO_4$). These defects are thermally activated and perform hindered diffusion in a random potential.

6.8. *Summary*

RADP is an interesting mixed system with glassy behaviour where tunnelling phenomena and quantum fluctuations can play an important role, at least in the protonated case. The freezing process in the glassy regime is characterized by two characteristic temperatures.

(i) $T_M = 100\,K$ is characterized by

- (*a*) the onset of diffuse scattered intensities, which reveal short-range polar order: the local order is incommensurate on the rubidium-rich side of the phase diagram and throughout the glass concentration range; it is antiferroelectric near the antiferroelectric phase boundary;
- (*b*) deviations in the static dielectric constant from Curie–Weiss behaviour;
- (*c*) deviations of the T dependence of the lattice constants from normal anharmonic behaviour;
- (*d*) the onset of birefringence effects;
- (*e*) the appearance of well defined NH_4 librational modes.

(ii) The dipolar relaxation dynamics as observed at lower temperatures point towards a 'static' glass transition temperature $T_{VF} = 10\,K$ (Vogel–Fulcher temperature).

In the deuterated compounds, both characteristic temperatures appear to be shifted to higher temperatures, the latter more than the former. This immediately reveals the importance of the acid protons (deuterons) in low-temperature relaxation.

The appearance of two characteristic freezing processes is similar to the observations in canonical glasses, in which primary relaxation is followed by secondary

processes. The primary (structural) relaxation in RADP is the appearance of a network of locally frozen NH_4 at T_M. This local order gives a distribution of double-minimum potentials, which is responsible for the broad distribution of relaxation times in the proton dynamics at much lower T. The broad distribution of hindering barriers could also be responsible for the anomalous low-temperature thermodynamic and dielectric properties observed in RADP.

In canonical glasses, the primary relaxation deviates from Arrhenius behaviour, and is broad and asymmetric when plotted against the logarithm of frequency. Secondary relaxation is Arrhenius-like, broad and symmetric. To our knowledge, RADP is the first example of a glass in which secondary relaxation shows significant deviations from pure thermally activated behaviour. This can presumably be related to the strong ferroelectric-like interactions that remain active between the sites that are not frozen in the primary process.

7. *Ortho–para*-hydrogen mixtures

7.1. *Introduction*

Solid *ortho–para*-hydrogen mixtures were the first systems in which an orientational glass state was identified for higher concentrations of the aspherical species (Sullivan *et al.* 1978). A general review of solid H_2 was given by Silvera (1980), in which references on the properties of H_2 that are not directly connected with the glass-like state can be found. A detailed review of the orientational-glass state was given by Harris and Meyer (1985).

From the requirement that the molecular wavefunction of the H_2 molecule be antisymmetric with respect to permutation of the protons, even values of the angular-momentum quantum number J are connected with the nuclear spin $I = 0$ of the molecule (p-H_2) and odd values of J with $I = 1$ (o-H_2). The concentration x of the *ortho–para* mixture will specify the fraction of *ortho* molecules. Because of the low moment of inertia, the J-states are well separated in energy. At the low temperatures where H_2 is solid, only the $J = 0$ ground state and the $J = 1$ first excited state at 171 K need be considered. The $J = 0$ *para* molecules have a spherical s-type wavefuntion. The p-type wavefunction of the $J = 1$ *ortho* molecules carries a quadrupole moment. The probability distribution for the orientation of the *ortho* molecule is represented by an ellipsoid of rotation. In solid H_2, the quantum-mechanical free-rotor states of the molecule are almost unaffected by interactions with neighbours. J is a good quantum number. The solid can be understood as a crystalline array of freely rotating molecules.

The leading anisotropic interaction between pairs of molecules is the electric quadrupole–quadrupole interaction, which is active between the $J = 1$ (*ortho*) molecules only. The interaction is of relatively short range. In theoretical treatments, frequently only the interaction between first neighbours is considered. The *ortho*-to-*para* conversion is a forbidden nuclear-spin transition; in the solid, slow conversion is induced by intermolecular magnetic interactions. The conversion rate decreases with x. A sample with $x = 0{\cdot}50$ changes to $x = 0{\cdot}49$ in about 1 h. The conversion favours the separation of a solid solution into *ortho*-rich and *para*-rich regions. This effect is counterbalanced by quantum diffusion. Thus the occupation of the lattice sites by *ortho* and *para* molecules should be regarded as a dynamic equilibrium. Long-time experiments have to face this problem. During the time window characteristic of NMR studies, the substitutional configuration can be considered as

quenched. The release of heat accompanying the small but nevertheless finite conversion can introduce thermal gradients in the sample and constitutes a major experimental problem, particularly in thermal measurements. On the other hand, the finite conversion rate makes studies with a continuous change of x possible when a given sample is investigated over a longer period.

The main experimental tool for the study of *ortho–para* mixtures is NMR. Here the NMR signal stems exclusively from the *ortho* molecules. Most results have been obtained on polycrystalline samples. Single crystals form relatively easily, but of course the growth and verification of the orientation have to be made *in situ*, for example by studying the anisotropy of the NMR signal.

The NMR results obtained for H_2 by different research groups are generally speaking consistent, but, since the analysis is model-dependent and the models have been improved over the years, there are slight differences in interpretation.

7.2. *Experimental results*

Pure o-H_2 ($x = 1$) and mixtures with higher x, $x > 0{\cdot}53$, show two crystalline phases. The high-T phase is hexagonal close-packed (h.c.p.). The symmetry and thermal properties of this structure require the *ortho* molecules to be orientationally disordered. The low-T phase is cubic, with a face-centred centre-of-mass lattice (f.c.c.), as shown by X-ray diffraction. Infrared, Raman and neutron-diffraction measurements revealed that the four molecules of the f.c.c. unit cell point into the four $\langle 111 \rangle$ body diagonals (Pa3 structure), forming four sublattices, in each of which the orientations are all parallel. Thus the cubic phase is long-range orientationally ordered. The rotational entropy of this phase is low (figure 7.1).

The hexagonal-to-cubic transition is of the martensitic type. The reconstruction of the centre-of-mass lattice can be understood as a change in the stacking sequence of the $(111)_{\text{f.c.c.}}/(001)_{\text{h.c.p.}}$ planes. The orientation of these planes is conserved. The transformation shows a complex behaviour in thermal cycling experiments, characterized by incomplete transformations and memory effects. In mixed crystals with $x < 0{\cdot}53$, the h.c.p.-to-Pa3 transition no longer occurs; these crystals conserve the h.c.p structure down to lowest temperatures. The (x, T) phase diagram is shown in figure 7.2.

In order to specify what is meant by orientational order, a pertinent order parameter has to be defined. The lowest multipole moment of the molecular orbital is the quadrupole moment, a tensor quantity. The tensor is set up with reference to the principal local axes x_i, y_i, z_i of the local electric-field gradient at the ith molecule. Thus the off-diagonal components like $\langle J_x J_y \rangle$ vanish and the two quadrupole parameters $\sigma = \langle 1 - \frac{3}{2}J_{zz} \rangle$ and $\eta = \langle J_x^2 - J_y^2 \rangle$ remain. σ measures the alignment along z_i; η is a measure of the departure from axial symmetry, and is often called the eccentricity. Working in the irreducible part of the (σ, η) plane avoids the need to consider negative values of σ. Thus σ, η and the directions define a local orientational quadrupolar order parameter. In the ordered Pa3 structure, the local axis is along $\langle 111 \rangle$, $\sigma = 1$, $\eta = 0$. In the glass state, σ, η and the local axes vary from site to site.

Information on the local quadrupolar order parameters is obtained from NMR measurements. This method makes use of the fact that the NMR lineshape is determined by the intramolecular dipole–dipole interaction between the nuclear spins. This interaction depends directly on σ and η and on the polar angles between the local axes and the magnetic field. The shape of the NMR profile, represented in particular by its second moment, is related to the distribution of the local order parameters. The

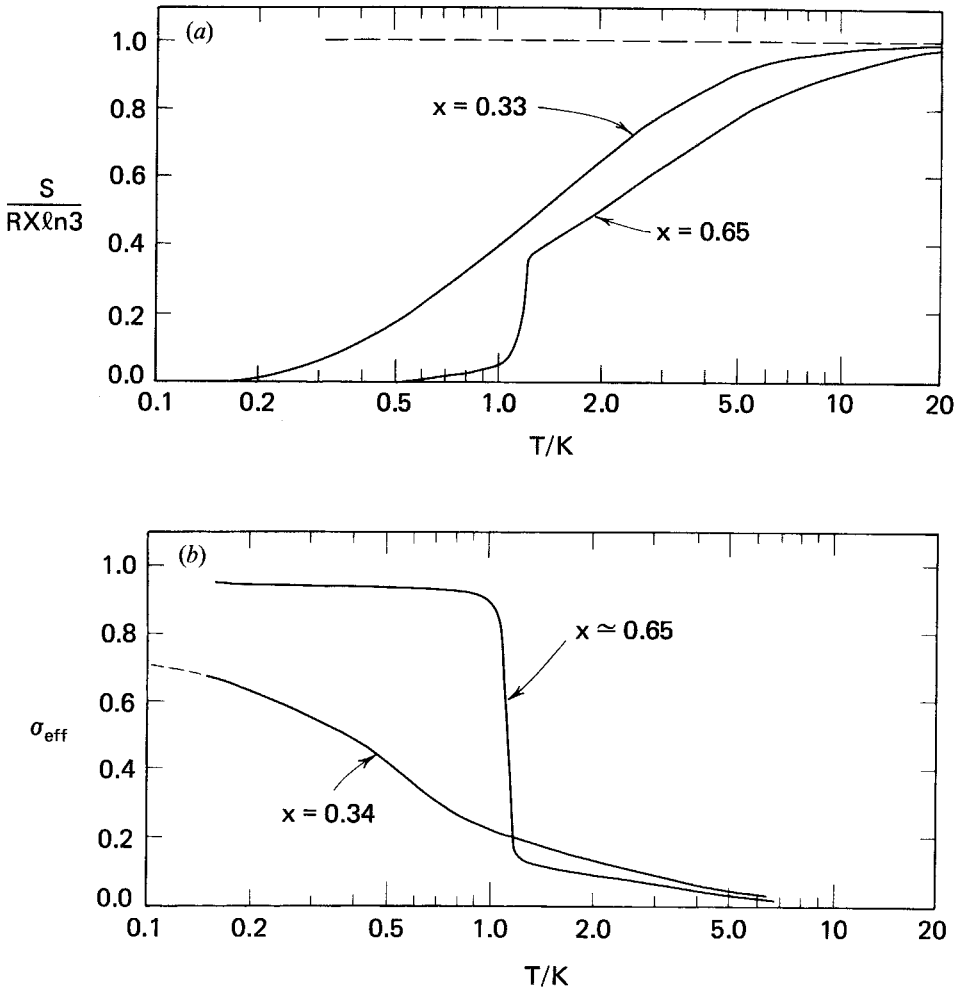

Figure 7.1. Rotational entropy (*a*) and effective local order parameter $\sigma_{\text{eff}} = \langle\sigma\rangle$ (*b*) as functions of temperature for two *ortho* concentrations x. The mixture with $x = 0{\cdot}65$ undergoes an h.c.p.-to-Pa3 phase transition at about 1 K, for $x = 0{\cdot}33$ and $0{\cdot}34$ the mixture freezes into the glass-like state. From Harris and Meyer (1985).

distribution as a function of both quadrupole parameters σ and η, that is $P(\sigma, \eta)$, was derived by Li *et al.* (1988). If one is willing to assume axial symmetry, the number of variables of this distribution may be reduced from two to one. This means taking the single quadrupole parameter as the effective order parameter $\sigma_{\text{eff}} = (\sigma^2 + \frac{3}{4}\eta^2)^{1/2}$ (Sullivan *et al.* 1978, Estève *et al.* 1982a,b, Washburn *et al.* 1982, 1983, Edwards *et al.* 1986). A δ-function-like distribution located at a finite value of σ is of course expected for the Pa3 phase of pure o-H_2 in the limit $T \to 0$, while—even within the Pa3-phase region—distributions of finite width are obtained for mixed crystals. The finite width suggests variations of the local environment from site to site and an RMS tipping angle between the local axes and the [111] directions (Harris *et al.* 1983). In the h.c.p. phase the distribution is centred at considerably smaller values of the local order parameter (figure 7.1).

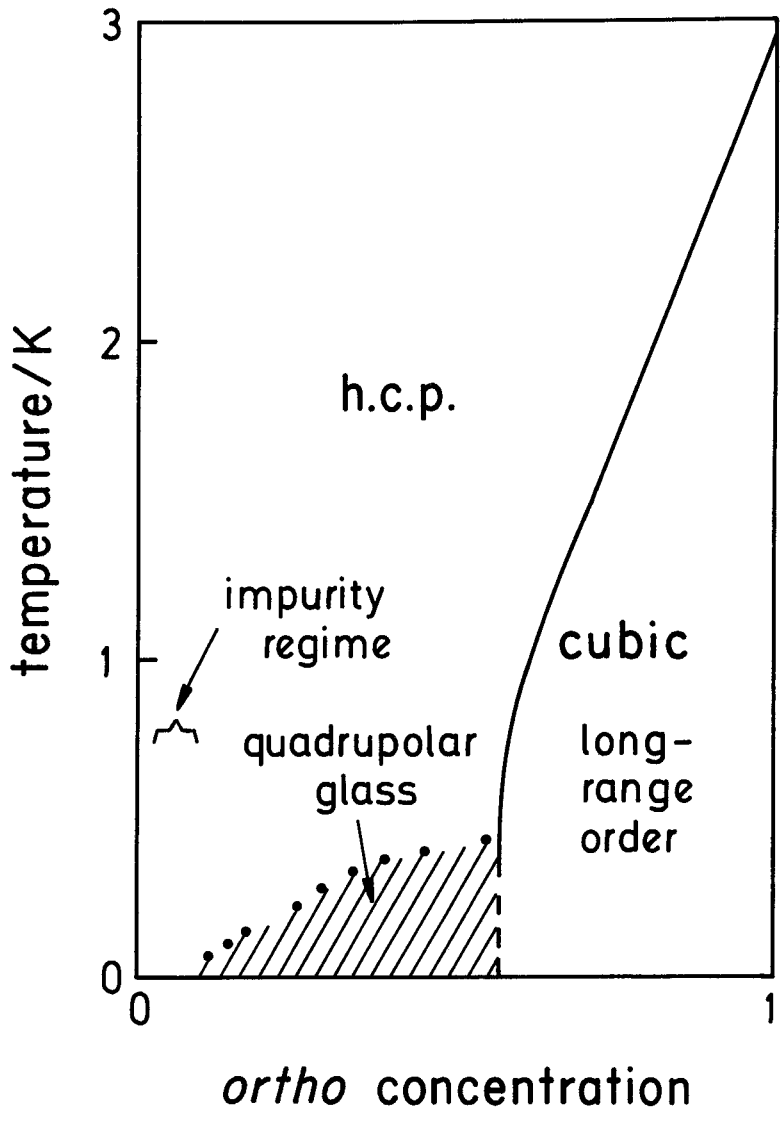

Figure 7.2. (x, T) phase diagram of o–p-H_2, adapted from Harris and Meyer (1985). The data points indicate the temperatures at which the local quadrupolar order parameter σ_{eff} has grown to 47% of the nominal value for perfect local ordering (from Li *et al.* (1988) and Meyer and Washburn (1984)). These temperatures should not be regarded as transition temperatures in the sense of phase-transition temperatures.

Evidence for orientational ordering at the hcp-to-Pa3 transition is also obtained from thermodynamic measurements and from dynamic NMR studies. The spin–lattice relaxation time T_1 increases below the h.c.p.-to-Pa3 transition temperature T_c (Ishimoto *et al.* 1976, Washburn *et al.* 1983). It is given approximately by $\exp(\Delta/k_B T)$, where Δ can be understood as the libron energy. The rotational entropy is small in the Pa3 phase, jumps to larger values at T_c and gradually approaches the value characteristic for complete orientational disorder, $k_B \ln(2J + 1)$, $J = 1$, at about 20 K (figure 7.1). Below $x = 0{\cdot}53$, the appearance of the ordered Pa3 phase is

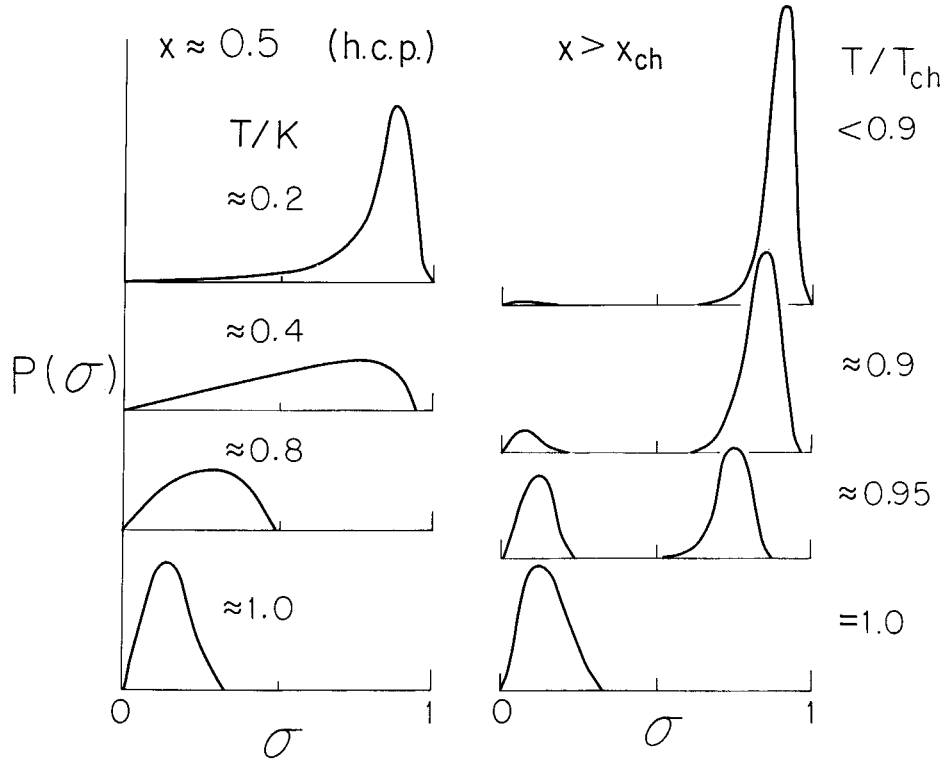

Figure 7.3. Schematic representation of the temperature evolution of the distribution $P(\sigma)$ of the local order parameter. For $x < x_{ch}$ the samples remain h.c.p. at low temperatures, whereas for higher x the h.c.p.–Pa3 phase boundary is crossed. From Harris and Meyer (1985).

suppressed. The rotational entropy decreases smoothly with decreasing T (Meyer and Washburn 1984). The orientations are said to freeze gradually into an orientational glass. When a sample with $x < 0{\cdot}53$ is cooled, the initially narrow distribution of the local order parameters broadens, and its centre $\langle\sigma\rangle$ shifts to higher values of the order parameter (Estève *et al.* 1982a,b, Washburn *et al.* 1982, Edwards *et al.* 1986). The evolution of the distribution is shown schematically in figure 7.3. Sullivan *et al.* (1978) suggested that the quadrupole parameter $\langle\sigma\rangle$ grows relatively abruptly at a characteristic temperature, giving the freezing into the orientational glass the aspect of a phase transition. This point was in contradiction with earlier NMR (Amstutz *et al.* 1969) and thermodynamic results (Hill and Ricketson 1954, Jarvis *et al.* 1969). The work of Sullivan *et al.* stimulated further investigations into the orientational-glass state of *ortho-para* mixtures. The idea of a glass phase boundary was questioned by Washburn *et al.* (1980). Analysis of the NMR line in terms of a quadrupolar distribution function has been improved over the years, and today we note an agreement between all research groups active in the field that the distribution changes smoothly with temperature, consistent with gradual freezing of the orientations. The most refined analysis has been given by Li *et al.* (1988).

For practical reasons, the T dependence of the local order parameter of figure 7.1 may be used to define a characteristic temperature T_f, for example by identifying

T_f as the temperature at which $\langle\sigma\rangle$ reaches half of its saturated $T = 0$ limit. The T_f values shown in figure 7.2 should be understood in this purely heuristic sense. (Meyer and co-workers avoid introducing T_f at all.) The use of single crystals allows the magnetic-field direction to be varied with respect to the crystal axes. Washburn *et al.* (1982) studied the anisotropy of the second moment M_2 of the NMR line. The relative anisotropy $\Delta M_2/M_2$ is essentially independent of x and T throughout the h.c.p. phase and the glass-like state. This suggests that the angular distributions of the molecular axes are quite similar in the disordered and frozen-in states. It is only the degree of alignment σ that increases with decreasing T (Washburn *et al.* 1982).

The spin–lattice relaxation time T_1 is related to the average quadrupolar fluctuation time τ_Q or more generally to the spectral density $J(\omega)$ of the quadrupolar autocorrelations. The exact shape of $J(\omega)$ is not well known except in the high-T limit. Nevertheless, there is a consensus that the quadrupolar fluctuation rate τ_Q^{-1} is roughly constant at higher temperatures and decreases strongly at lower T, as shown in figure 7.4 (Sullivan and Estève 1981, Washburn *et al.* 1983). From a practical point of view, the temperature where T_1 is a minimum (i.e. where $\omega_{\text{Larmor}}\tau_Q = 1$), can be regarded as the freezing temperature T_f; but this cannot be construed as a phase-transition temperature. T_f defined in this way decreases with x, and so does $T_1(T_f)$. Around and below T_f, T_1 is dependent on the Larmor frequency (Washburn *et al.* 1983). This behaviour is suggestive of a slowing down of the average orientational-fluctuation rate. This slowing down of the quadrupolar fluctuations is presumably the best indication of the freezing into the orientational-glass state, although it must be pointed out that neither the T evolution of the order parameter distributions nor the dynamic measurements show any discontinuity or hysteresis that would justify the assumption that any phase boundary is crossed at the freezing temperature (Washburn *et al.* 1982, Meyer and Washburn 1984).

Two unusual properties of nuclear-spin relaxation have been observed in the glass state: the spin–lattice relaxation time varies across the absorption spectrum, and the nuclear magnetization of a given isochromat decays in a non-exponential way. Together with the information on the local order-parameter distribution, the results for T_1 suggest that the spectral density $J(\omega)$ consists of a quasi-static, a fluctuating and a paralibron (or sloppy libron) part, as pointed out by Washburn *et al.* (1983). Paralibrons are local orientational excitations, which are characteristic of a state with well developed short-range order. The correlation time of the quasi-static part is longer than 10 ms.

The non-exponential decay was shown to result from the distribution of local axes and local order parameters (Sullivan *et al.* 1984, Lin *et al.* 1986). This means that, even though the quadrupolar fluctuations decay exponentially with a single relaxation time, the magnetization will show a non-exponential decay because, for a given spectral position, different combinations of axes and local order parameters contribute to the signal.

The domain of slow relations has been probed by nuclear-spin stimulated echoes (Yu *et al.* 1983, Lin and Sullivan 1988). The echoes show a logarithmic decay. This has been interpreted in terms of a hierarchical relaxation process similar to that appearing in a scaling model of short-range spin glasses: the low barriers for reorientations, as realized in small clusters, must be overcome before the higher barriers of the large clusters because the faster reorientations constrain the slower ones (Lin and Sullivan 1988). Here a cluster is a region of coherently aligned molecules. Assuming

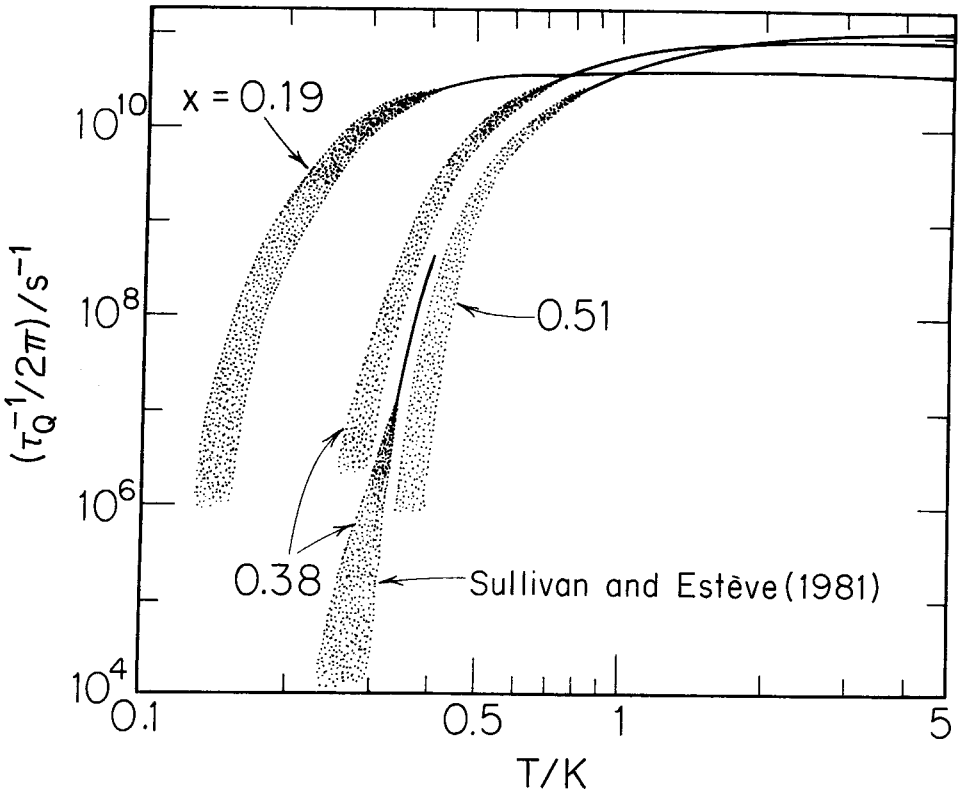

Figure 7.4. Approximate temperature dependence of the quadrupolar relaxation rate as derived from the spin–lattice relaxation time T_1 for three concentrations $x > x_{ch}$. From Harris and Meyer (1985).

a quasi-constant distribution of the energy barriers, a reasonable fit of the logarithmic decay and of the low-temperature specific heat (Haase *et al.* 1984) is obtained.

From the dynamic NMR results, the ordering of the orientations is identified as a relaxational effect. The temperature at which the freezing becomes apparent in a given experiment depends on the characteristic frequency of the method. It remains an open question as to whether there exists a finite static limit for the freezing temperature. If so, this limit must be below about 0·5 K, for $x = 0{\cdot}5$, since even at that temperature the orientational fluctuations are on a time scale shorter than 0·1 ms (Yu *et al.* 1983).

Orientational-glass formation also occurs in *ortho–para* deuterium. When comparing the results with those for H_2, the concentration x of o-p-D_2 mixtures should be read as the *para* concentration, since it is the p-D_2 molecule that is in the $J = 1$ state and thus carries the quadrupole moment. Furthermore, the temperatures should be scaled by the quadrupolar coupling constant Γ: $\Gamma(D_2) = 1{\cdot}02$ K, $\Gamma(H_2) = 0{\cdot}82$ K. Taking these points into account the NMR results for the local order parameter and the relaxation rates of the two hydrogen systems are closely related (see Calkins *et al.* (1986) and Li *et al.* (1988); earlier work on D_2 is exhaustively referenced in the former paper). Slight differences exist for $\langle\sigma\rangle$ at low temperatures, where the values for D_2 are about 10% lower than for H_2.

7.3. *Conclusions*

From a modelling point of view, o–p-H_2 mixtures are somewhat analogous to spin glasses, provided that the vector variable spin is replaced by the tensor variable quadrupole moment. The importance of frustration in combination with substitutional *ortho–para* disorder has been emphasized (Sullivan 1983). Two isolated *ortho* molecules communicating via the electric quadrupole–quadrupole interaction minimize the potential energy in a T configuration. However, it is impossible to arrange all molecules mutually perpendicular in a periodic array. The Pa3 structure is already a compromise: in it, the binding energy per pair of neighbouring molecules is only half of the binding energy of an isolated pair. It is this topological incompatibility of the centre-of-mass array and the orientational configuration that causes frustration. In the Pa3 structure, the relative orientation of neighbours is identical, and hence the bond energy is constant throughout the crystal. In the hypothetical orientational ground state on a h.c.p. lattice, the situation is more complex. There are neighbours with nearly parallel orientations and others with nearly perpendicular orientations. The bond energy is distributed inhomogeneously over the h.c.p. crystal and is smaller on average than in the Pa3 structure (James 1968). Here the dilution of the *ortho* system by *para* species will lead to significant readjustments of the orientations of the *ortho* molecules in the vicinity of the spherical *para* molecule. It has been argued that in a randomly diluted lattice with the frustration introduced by the anisotropic nature of the electric quadrupole–quadrupole interaction, the lowest-energy configurations are not unique (Sullivan 1983). As in spin glasses, the free energy mapped on configuration space shows many minima separated by barriers of varying height. The system can be caught in one of these minima without having the chance of exploring the full configuration space, a situation that is called non-ergodic. In the experiment, the non-ergodicity should lead to history effects and cooling-rate dependences. Indications of such effects have been reported in T_1 measurements (Sullivan *et al.* 1982), but have not been confirmed either in H_2 (Washburn *et al.* 1983) or in D_2 (Calkins *et al.* 1986).

The symmetries of the *ortho–para* system have been analysed theoretically by Harris and Meyer (1985). Using the replica trick, the Hamiltonian of the electric quadrupole–quadrupole interaction is translated into an effective Hamiltonian. Besides terms that couple pairs and quadruples of quadrupole operators, the effective Hamiltonian has two special field terms that result from the addition properties of the tensor operators. The first one contains an electric-field gradient, which can be regarded as the field conjugate to the order parameter of a phase with long-range quadrupolar order, analogous to the appropriate Fourier component of the magnetic field for long-range magnetic ordering. The first term is finite for any $x < 1$ in the h.c.p. lattice. The second term contains a variance of distributions of electric-field gradients, and is thus conjugate to the order parameter of the quadrupolar glass state. It is non-zero in the h.c.p. and f.c.c. lattices. Thus random dilution gives rise to 'random fields' that are conjugate to the glass order parameter. Hence the *ortho–para* mixtures are understood as orientational glasses in an 'ordering' field, and one expects the glass order to evolve smoothly without showing anomalies reminescent of a classical phase transition. It should be noted that analogous random fields due to dilution do not occur in spin glasses. Furthermore, the 'random fields' of the present problem are a consequence of the intermolecular interactions and are thus of a different origin from the random fields cited for the mixed cyanides, although both types of random fields have the same effect. The considerations described here can be

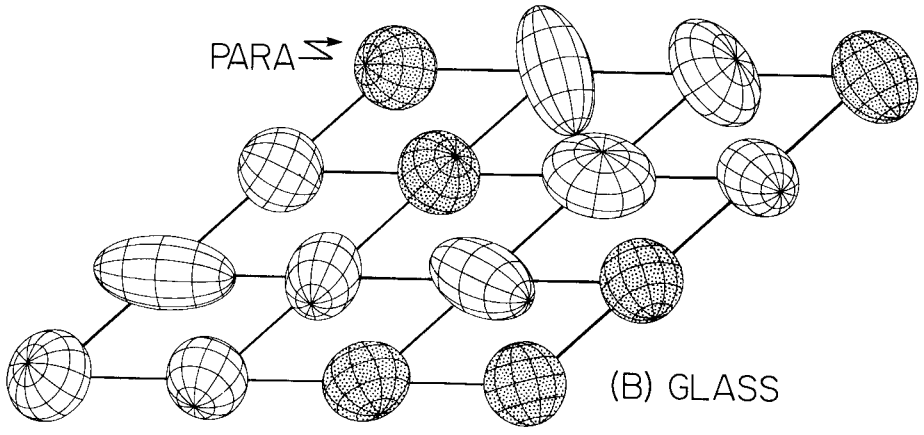

Figure 7.5. Schematic picture of the orientations in the quadrupolar glass. This picture should be regarded as a snapshot on the time scale of an NMR experiment. There are still slow orientational fluctuations and over long observation time even the substitutional configuration will change because of *ortho–para* conversion and quantum diffusion. From Sullivan (1983).

condensed in the statement that the glass order parameter of o–p-H_2 does not display broken symmetry.

Monte Carlo simulations (Devoret and Estève 1983, Klenin 1983) confirm the rather gradual freezing of the orientational modes. The calculations show that the size of the clusters with frozen orientations increases and the reorientation rate of these aggregates decreases monotonically with decreasing temperature, and thus confirm the cooperative nature of the freezing process. A schematic picture of the quadrupolar-glass state is shown in figure 7.5.

The *ortho–para* mixtures can be regarded as a model system. The fundamental interactions between the molecules are well known and are of a simple electrostatic nature. The number of ingredients necessary to produce a glass-like state is minimal —namely just one chemical species. The hydrogen allow study of the specific effects of quantum zero-point motion on the orientational ordering. Such effects have been demonstrated in the NMR spectrum on a coupled pair of *ortho* molecules (Schweizer *et al.* 1979). In the mixtures, these effects become increasingly more important as x is decreased (Meyer and Washburn 1984).

NMR is an ideal probe for the study of the hydrogen systems. On the other hand, the interpretation of the NMR results is to a certain extent model-dependent and gives information on local properties only. There are, however, relatively few complementary measurements; in particular, there is no information on the bulk quadrupolar response function, which would play a role analogous to the magnetic susceptibility in spin glasses.

8. Argon–nitrogen mixed crystals

8.1. *Introduction*

$Ar_{1-x}(N_2)_x$ mixed crystals can be regarded as the classical analogue of the quantum system *ortho–para* hydrogen. The N_2 molecule plays the role of the o- and Ar that of the p-H_2 molecule. The electron configuration of the N_2 molecule has the

shape of an ellipsoid of rotation with a ratio of long to short axis of 1·28. The N_2 molecules interact through an effective quadrupole–quadrupole interaction that incorporates both, the direct quadrupole–quadrupole and the anisotropic component of the van der Waals interaction with the neighbours.

The properties of solid N_2 that are relevant for the understanding of $Ar_{1-x}(N_2)_x$ mixed crystals are described in the following. We refer the reader to Scott's (1976) review on solid N_2.

Like solid o-H_2, pure N_2 shows two crystalline modifications, the hexagonal close-packed (h.c.p.) phase at high and the cubic Pa3 phase at low temperatures. The phase transition occurs at 35 K. The high-temperature phase is orientationally disordered. The molecules precess around the hexagonal axis. The mean aperture angle of the precession cone is close to the magic angle of 54°, indicating that the time-averaged quadrupole moment of the molecule practically vanishes. Accordingly, the c/a value of the h.c.p. lattice is very close to the ideal value for close packing of spheres. The Pa3 structure is characterized by orientational long-range order in a four-sublattice arrangement. In each of the sublattices, the molecules are all parallel, along one of the four [111] directions. The h.c.p.-to-Pa3 transition is first-order, involves a reconstruction of the centre-of-mass lattice, and shows the characteristics of a martensitic information.

8.2. *Experimental results*

Solid $Ar_{1-x}(N_2)_x$ is obtained by cooling liquid mixtures below the solidification temperature. Since the liquid–solid coexistence region is unusually narrow for N_2-rich mixtures, it is unlikely that noticeable concentration gradients are introduced by this preparation method. The preparation of large single crystals using the Bridgeman technique was reported by Press *et al.* (1982). All other studies have been carried out on polycrystalline samples.

The (x, T) phase diagram of $Ar_{1-x}(N_2)_x$ mixed crystals has been determined by X-ray diffraction (Barrett and Meyer 1965). N_2 and Ar are completely miscible. Since there are no indications of chemical ordering, it is assumed that the h.c.p. sites are randomly occupied by N_2 and Ar. When the N_2 concentration x is reduced, the h.c.p.-to-Pa3 transition temperature decreases and the martensitic hysteresis widens. For example, for $x = 0{\cdot}82$, the last traces of the h.c.p. phase disappear at 11 K, whereas, on heating, the cubic diffraction peaks can be traced up to 38 K (Klee *et al.* 1988); see figure 8.1.

Below the threshold concentration $x_c = 0{\cdot}8$, the phase transition is suppressed and the average h.c.p. lattice is stable down to the lowest temperatures. Hence the dynamical orientational disorder of the high-temperature regime should eventually freeze into a static pattern of randomly oriented N_2 molecules. Such a state is called an orientational glass. It can be conveniently studied in the concentration range $0{\cdot}5 < x < 0{\cdot}8$. For $x < 0{\cdot}5$, Barrett and Meyer (1965) reported an f.c.c. low-temperature state. The h.c.p.-to-f.c.c. transition, however, is very sluggish—for $0{\cdot}2 < x < 0{\cdot}5$, the low-temperature f.c.c. phase could be obtained only after cold working. (Nevertheless, it would be interesting to study a series of Ar-rich mixed crystals starting from dilute N_2 impurities in an Ar f.c.c. matrix and systematically increasing the N_2 concentration. Eventually an f.c.c.-based collective orientational glass should form, which might be regarded as a short-range variety of the Pa3 phase.)

The first evidence for an h.c.p.-based orientational-glass state came from an NMR study of a sample with $x = 0{\cdot}675$, containing the ^{15}N isotope with nuclear spin $\frac{1}{2}$

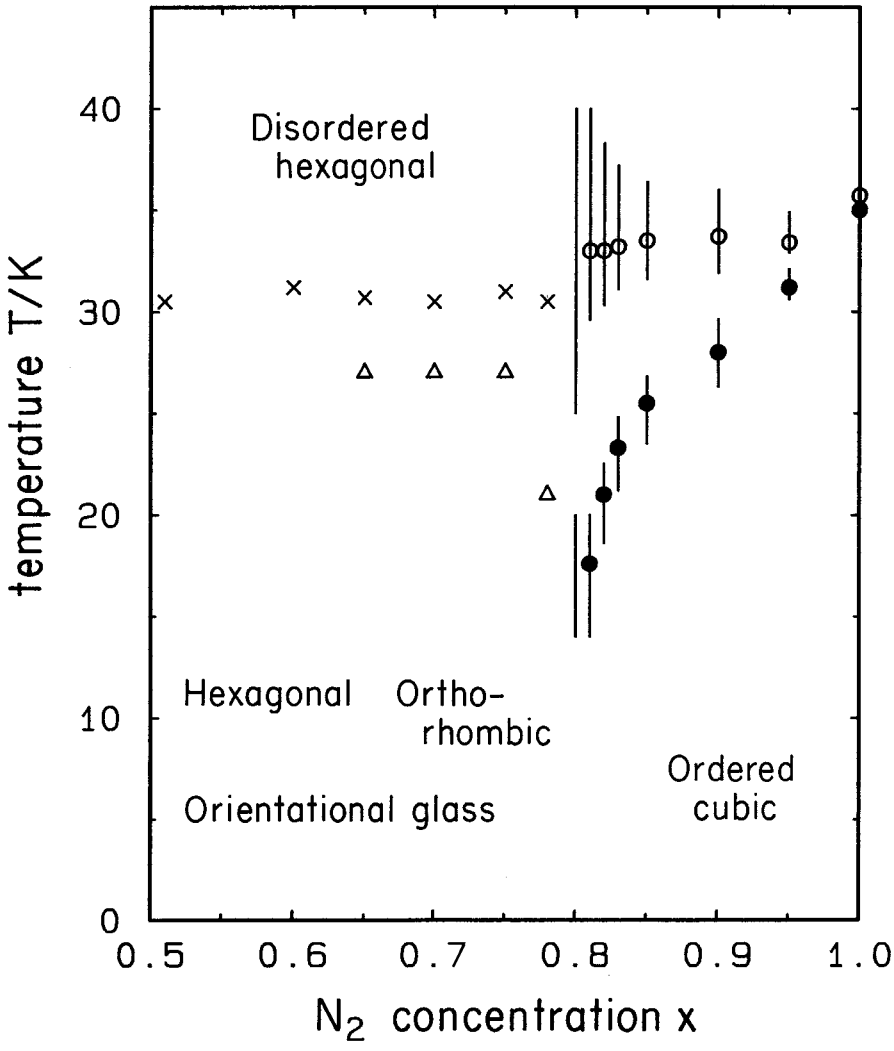

Figure 8.1. (x, T) phase diagram of $Ar_{1-x}(N_2)_x$, with $0{\cdot}5 < x < 1$: (×), temperatures at which the width of the X-ray powder lines increase most strongly on cooling (see figure 8.4); ⧫, ◇, give midpoint and width of h.c.p.-to-Pa3 transition on cooling (⧫) and on heating (◇); (△), onset of orthorhombic distortion. From Klee and Knorr (1990).

(Estève *et al.* 1982a,b). Here 75% of the molecules are *ortho* ($I = 1$). The sensitivity of the NMR transitions to the orientational state stems from the dependence of the energy levels of the intramolecular nuclear-spin Hamiltonian on the angle between the molecular axis and the magnetic field. The orientation of the molecule with respect to the field, which we define as the local quadrupolar order parameter, has axial component σ and eccentricity η. The latter is neglected in the following. The local order parameter is distributed as $P(\sigma)$, which has been deduced from the NMR lineshape (figure 8.2). The results have been further condensed into the first moment of the distribution, $\langle\sigma\rangle$ (Sullivan *et al.* 1986). (The fact that $\langle\sigma\rangle$ is non-zero results from a projection of the (σ, η) plane on positive values of σ. The average local order parameter is actually zero.)

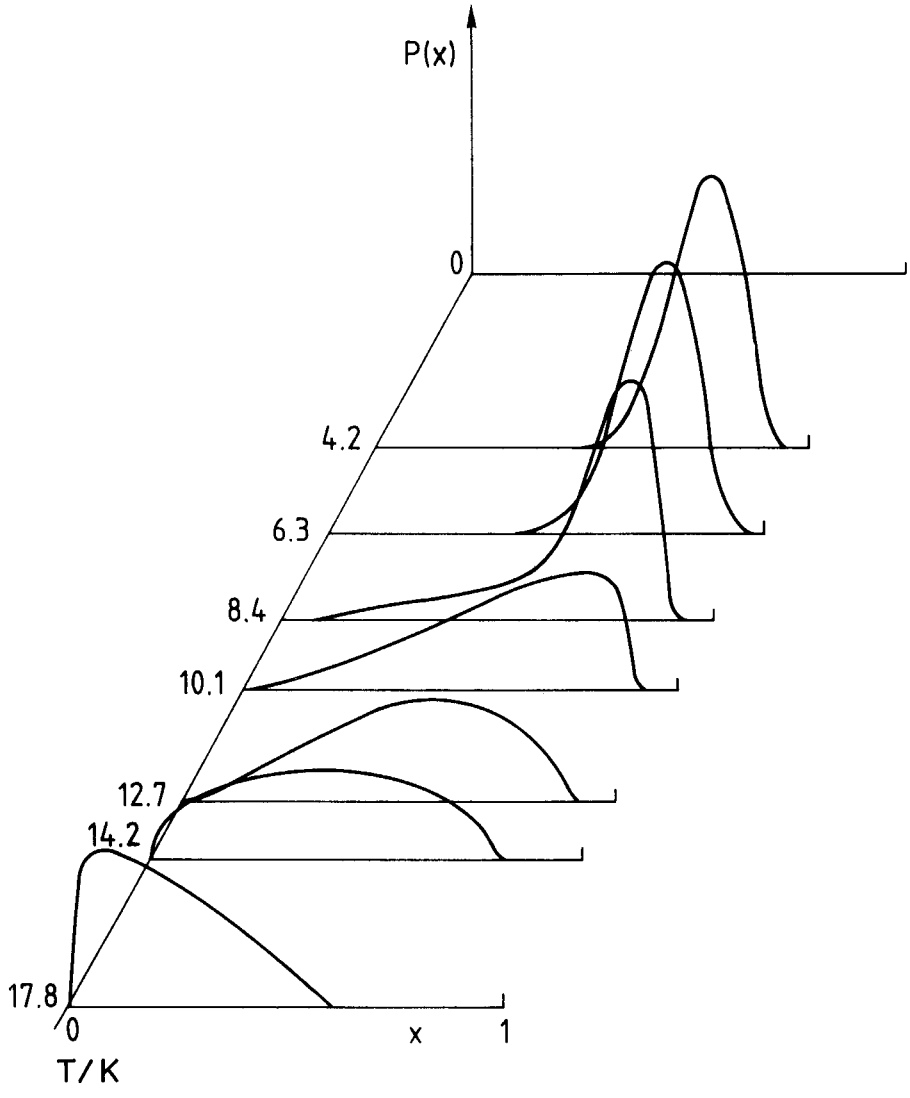

Figure 8.2. Temperature evolution of the quadrupolarization distribution function $P(\sigma)$ of $Ar_{0.33}(N_2)_{0.67}$ as deduced from the NMR lineshape. From Estève *et al.* (1982).

The results closely resemble those on o–p-H_2. As the temperature decreases, the distribution broadens and shifts progressively to higher values of σ without any apparent discontinuity that could be associated with a phase-transition-like onset of the orientational-glass state at a characteristic temperature. Pulsed-NMR experiments showed that the orientational motion was slower than 10 mHz for $4\,K < T < 20\,K$. Comparison of this result with Monte Carlo studies (Mandell 1974, Klenin and Pate 1981) led to the conclusion that the onset of local quadrupolar order is associated with collective rotations of at least 100 molecules (Estève *et al.* 1982a,b). This conclusion assumes scaling between cluster size and relaxation time.

Heat-capacity measurements support the idea of a gradual freezing of the orientational degrees of freedom (Ward *et al.* 1983). There is no anomalous contribution to

the specific heat or long-term thermal relaxation that could be connected with a phase-transition-like effect.

The neutron-scattering law $S(Q, \omega)$ was analysed as a function of energy ω at some discrete values of the momentum transfer Q for $x = 0{\cdot}72$ by Press *et al.* (1982), who argued that $S(Q, \omega)$ is mainly due to rotational rather than translational degrees of freedom. The spectrum consists of an elastic Gaussian and an additional quasielastic component, which has an approximately Lorentzian shape with width parameter Γ (see figure 8.3). When the sample is cooled down from the dynamically disordered regime, the elastic component increases by a factor of about 3 whereas the ratio of the elastic to the quasi-elastic component increases by a factor of 12. Above T_f, the Lorentzian component is interpreted as being due to rotational diffusion. The width Γ of the Lorentzian gives the rotational diffusion rate directly. Extending this concept to temperatures below T_f, one would expect Γ to decrease with decreasing temperature. Experiment shows, however, that Γ is roughly temperature-independent, showing only a shallow minimum around 20 K. Hence an alternative interpretation of the scattered intensity has to be found at low temperatures. Press *et al.* (1982) suggested that the orientations of the molecules freeze in with random directions. This static disorder gives rise to enhanced diffuse elastic scattering. The quasi-electric scattering at low temperatures is interpreted as being due to excitations of librational type. The librational energies are distributed because of variations of the local environment.

The diffuse intensity of the neutron-diffraction experiment shows broad maxima in reciprocal space. The most pronounced maximum is centred at $Q = (\frac{7}{4}, \frac{7}{4}, \frac{1}{3})$, which means that there are correlations that favour an ordering in an enlarged unit cell with appropriate dimensions $4a$, $4a$ and $3c$. The width of these broad maxima corresponds to a coherence length along c of roughly six intermolecular distances. This suggests the interesting possibility that the glass-like state can be understood in terms of short-range order in a complex superstructure, perhaps with a modulated pattern of orientations and/or displacements of the molecular centres from the h.c.p. positions.

X-ray powder diffraction on $Ar_{1-x}(N_2)_x$ with $0{\cdot}5 < x < 0{\cdot}8$ shows that the width of the h.c.p. powder lines increases with decreasing temperature (Klee *et al.* 1988, Klee and Knorr 1990); see figure 8.4. The temperature of steepest ascent of the width *versus* temperature curve may be used to locate a characteristic temperature T_f in a purely heuristic manner. X-rays are more sensitive to the translational positions, especially of the Ar atoms, than to the N_2 orientations. Thus it is evident from the broadening of the diffraction lines that the formation of the orientational glass affects the centre-of-mass lattice. Klee *et al.* (1988) suggested that the line broadening represents distributions of strains, very much as in cold-worked metals, which develop when the orientations of the N_2 molecules freeze in and then act as sources of quadrupolar strain fields. The results show that in $Ar_{1-x}(N_2)_x$ the coupling of orientations and translational degrees of freedom cannot be ignored. Another interesting detail is observed for $0{\cdot}7 < x < 0{\cdot}8$: here some powder lines not only broaden but also split at lower temperatures. Thus the lattice distortions not only have a random but also a homogeneous component. On the basis of these findings, Klee *et al.* (1988) suggested that N_2-rich $Ar_{1-x}(N_2)_x$ mixtures have a third crystallographic phase, 'δ', in addition to the h.c.p. and Pa3 phases. Above $x = 0{\cdot}8$, the δ phase is concealed by the Pa3 phase. When the h.c.p.-to-Pa3 transformation is suppressed by chemical substitution, a short-range variety of the δ phase is detected at low temperatures. The structure of the δ phase results from a homogeneous (ferroelastic) shear deformation of the h.c.p.

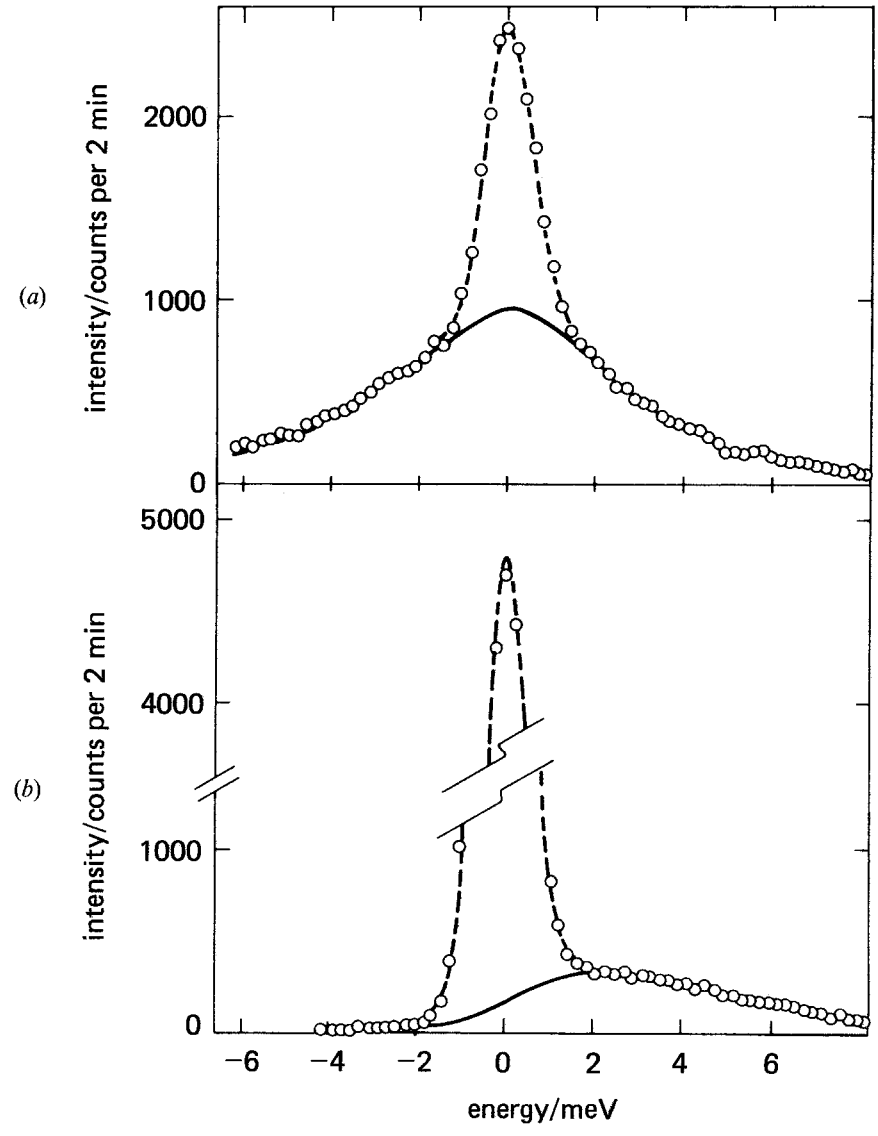

Figure 8.3. Inelastic neutron-scattering profiles of $Ar_{0\cdot28}(N_2)_{0\cdot72}$: (*a*) $T = 46\,K$; (*b*) $4\cdot5\,K$; $Q = 3\cdot5\,Å^{-1}$. The dashed line gives the Gaussian and the solid line the Lorentzian component. From Press *et al.* (1982).

lattice and a spontaneous quadrupolar polarization lying in the basal plane. Perhaps there are also internal displacements that are compatible with the modulation of the diffuse scattering discussed above.

The low-temperature heat capacity of the glassy regime shows a term linear with T and an enhanced T^3 term (Ward *et al.* 1983, Nicholls *et al.* 1987) (figure 8.5), as observed in amorphous solids and known under the keyword 'two-level systems'. For mixed cyanides (see section 5), Sethna and co-workers argued that the low-temperature anomalies arise from inversion flips of the CN ions by tunnelling. The same reorientation process, but thermally excited, was thought to be responsible for

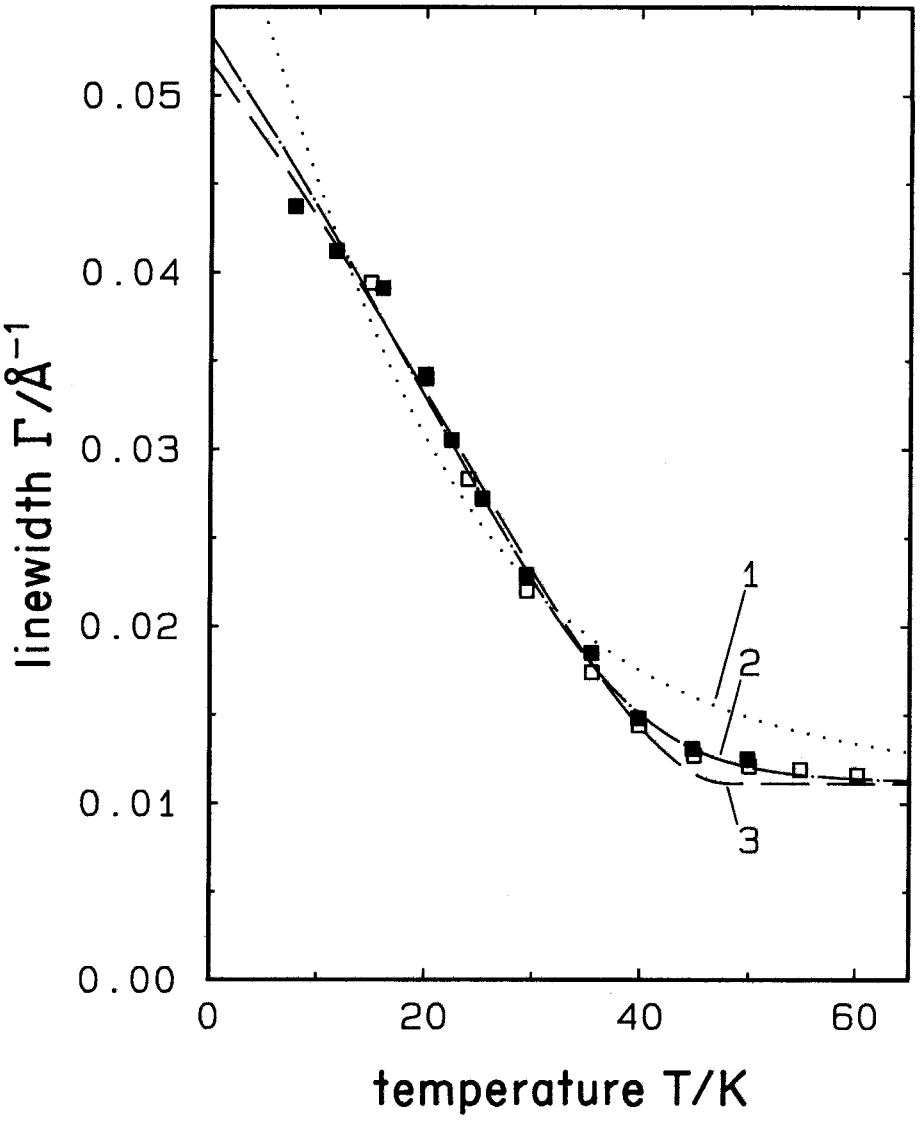

Figure 8.4. Apparent width of the (110) powder line of $Ar_{0.4}(N_2)_{0.6}$. Klee and Knorr (1990) argue that the freezing of the orientations is accompanied by the formation of random lattice strains, which in turn lead to broadening of the diffraction lines. The lines are best fits to a random-bond–random-field Ising model: 1, pure random field; 3, pure random bond; 2, random bonds and random fields. From Klee and Knorr (1990).

secondary relaxations well below the freezing of the quadrupolar modes. The connection between secondary relaxation and two-level systems is, according to these authors, prototypic for glasses in general. In cyanides, the inversion flips can easily be seen in dielectric measurements. In $Ar_{1-x}(N_2)_x$, secondary relaxations have not so far been detected. Thus it seems that the idea of Sethna and co-workers does not apply to $Ar_{1-x}(N_2)_x$ and that instead the low-temperature anomalies involve the same type of modes that contribute to the primary freezing process.

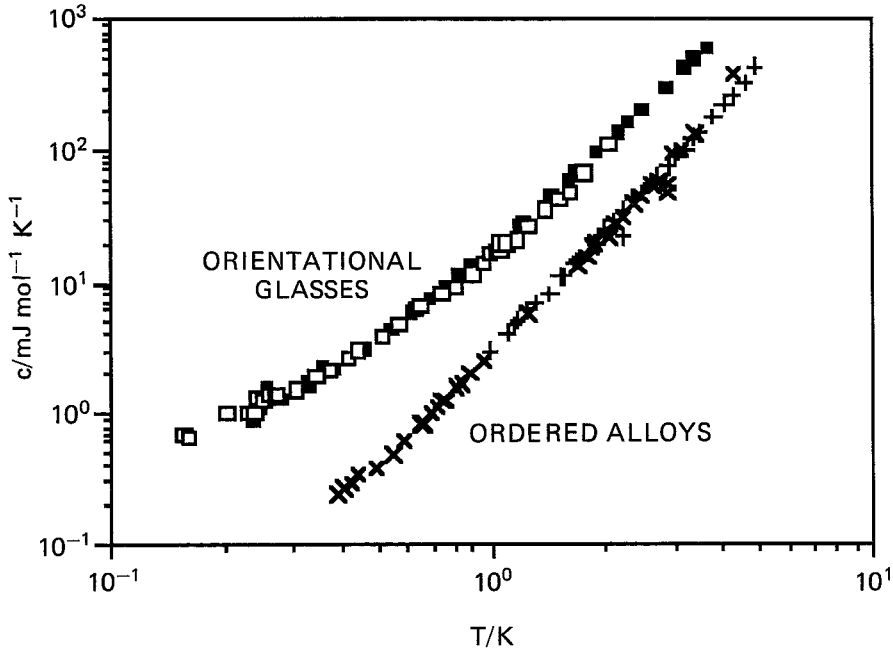

Figure 8.5. The T dependence of the heat capacity of ternary solid solutions $Ar_{1-x-y}(N_2)_x(CO)_y$. The percentages of the constituents, in the sequence $x/1-x-y/y$, are as follows: (+), 100/0/0; (x), 80/0/20; (■), 60/40/0; and (□), 40/40/20. The heat capacities of samples forming the orientational glass show strong deviations from Debye behaviour (TLS effects), regardless of whether the aspherical species is N_2 or CO. From Nicholls *et al.* (1987).

This point has been further clarified by measurements on ternary mixtures of $Ar_{1-x-y}(N_2)_x(CO)_y$, where N_2 was partially replaced by CO (Nicholls *et al.* 1987). The CO molecule has practically the same shape as the N_2 molecule, its quadrupole moment is about 1·7 times as large as that of N_2, and it carries a small electric dipole moment. (Binary mixtures $Ar_{1-y}(CO)_y$ are not stable, but $Ar_{1-x-y}(N_2)_x(CO)_y$ are.) Dielectric measurements (Liu and Conradi 1984) on the ternary mixtures show dielectric loss peaks (figure 8.6) at temperatures well below the primary freezing process. The temperature width of the loss peaks is comparable to those observed in the mixed cyanides, indicating an extraordinarily broad distribution of energy barriers, the average barrier being 180 K compared with values like 600 K for cyanides. The strength of the low-T anomalies of the ternary mixtures is practically unchanged with respect to the binary mixtures (Nicholls *et al.* 1987). It can be concluded that the head–tail asymmetry of CO, which is responsible for secondary, dipolar, relaxations, is not the main cause of the low-T anomalies. Thus it seems that the appealing idea that secondary relaxation and low-T effects are related has to be abandoned as a general rule. Of course, one could still argue, somewhat artificially, that as-yet unidentified secondary relaxations do exist in $Ar_{1-x}(N_2)_x$, although in that case these modes have to be different from inversion flips.

^{13}C NMR of the ternary mixtures $Ar_{1-x-y}(N_2)_x(CO)_y$ was studied by Walton *et al.* (1988); see figure 8.7. This method probes the local environment through the anisotropy of the chemical shift. At low temperatures, the NMR line has a characteristic

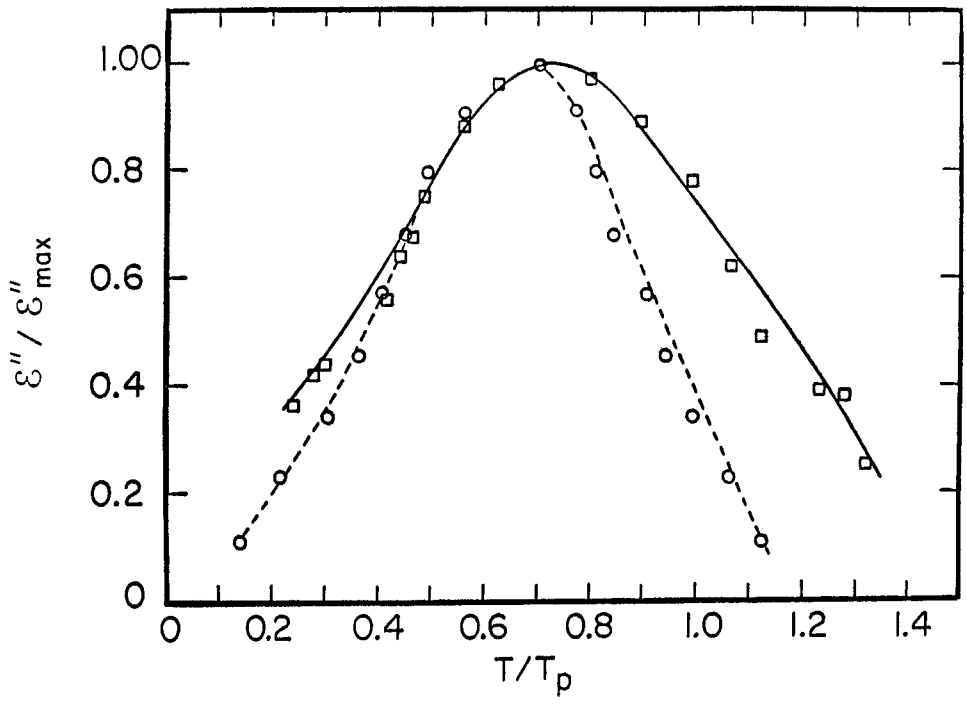

Figure 8.6. Scaled T dependence of the normalized dielectric loss of $(N_2)_{0.4}Ar_{0.4}(CO)_{0.2}$ (□) and $(KBr)_{0.5}(KCN)_{0.5}$ (○). T_p is the temperature of the maximum dielectric loss. Nicholls *et al.* (1987) suggested that the large width of the loss peak stems from a broad distribution of energy barriers for head–tail reorientations of the CO and CN molecules respectively, and emphasized the strong similarity of the two orientational glasses. From Nicholls *et al.* (1987).

profile that indicates that the molecules have static and random orientations. The line profile narrows on heating. Walton *et al.* (1988) proposed two models for the interpretation of this narrowing. The first refers to preferred orientations. It starts out from the idea of rapid reorientations of the molecule, which can be condensed into a local static orientation distribution function. The distribution is nearly spherical at high temperatures and becomes increasingly aspherical at lower temperatures. The second is a kinetic model that assumes a broad homogeneous distribution of correlation times, with each molecule sharing the entire distribution. Both models are compatible with experiment. The temperature dependence of the linewidth is shown in figure 8.7.

The spin–lattice relaxation time T_1 in $Ar_{1-x-y}(N_2)_x(CO)_y$ shows a broad minimum near 15 K, as found by Walton *et al.* (1988). Referring to the dielectric results, they suggested that 180° flips of the CO molecules are responsible for the minimum of T_1. The NMR profile signalling the quadrupolar freezing narrows at considerably higher temperatures. Thus the dipolar degrees of orientational freedom freeze at lower temperatures than the quadrupolar ones. Analogous behaviour had been observed in mixed cyanides. Walton *et al.* (1988) emphasized the similarity of the NMR results for $Ar_{1-x-y}(N_2)_x(CO)_y$ and mixed cyanides by demonstrating that it is possible to match the temperature dependences of the widths of the NMR profiles of the two systems

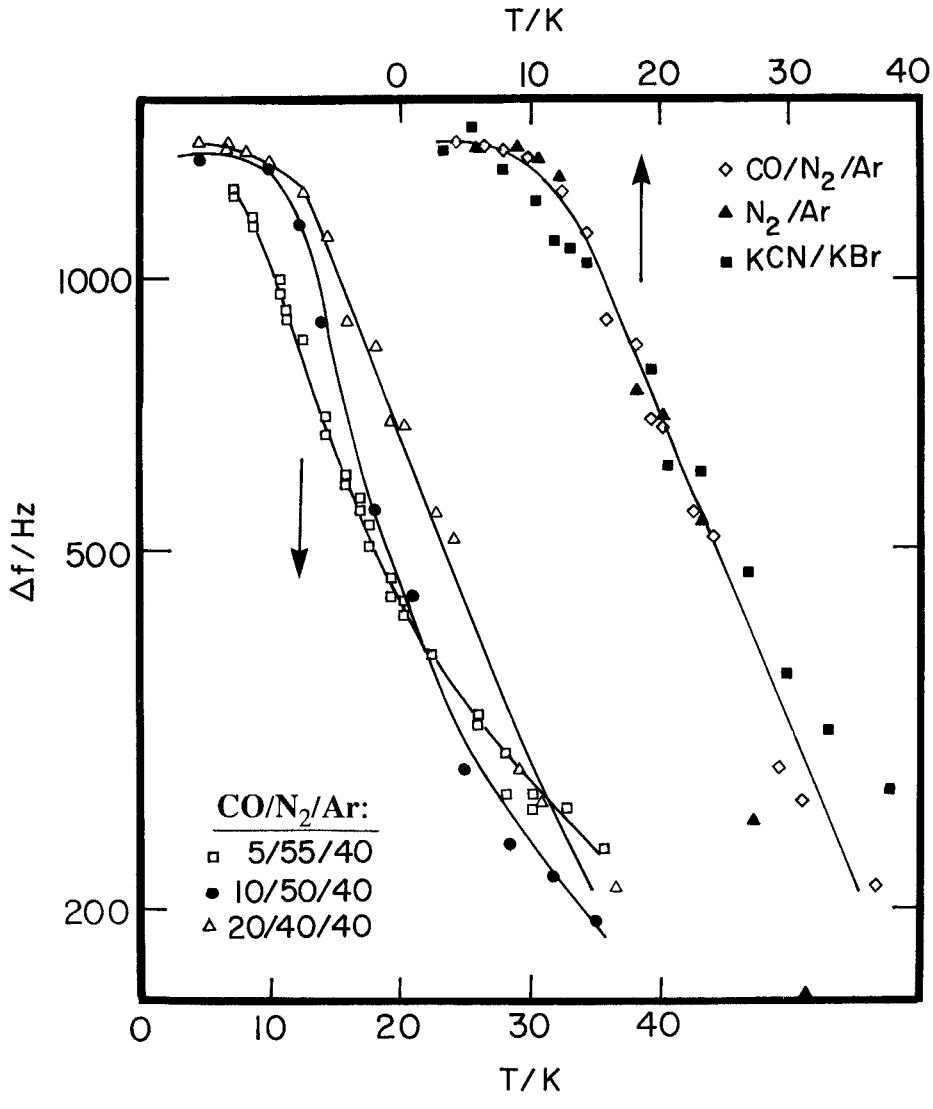

Figure 8.7. T dependence of the NMR linewidth of several $Ar_{1-x-y}(N_2)_x(CO)_y$ solid solutions. The width is regarded as a local order parameter of the orientational glass. Corresponding data on $(KBr)_{0.5}(KCN)_{0.5}$ can be scaled to coincide. From Walton *et al.* (1988).

after proper scaling of the temperature axis. On the basis of this, they claimed a certain universality of the orientational glass formation.

Raman measurements on $Ar_{1-x}(N_2)_x$ were carried out by D. Polani and R. Feile (1989 unpublished results, Mainz), in both the low-frequency regime and the range of the N–N stretching band. The measurements have not yet been analysed completely. Data on the dynamically disordered phase show a sharp stretching line sitting on a Lorentzian-shaped socket, which presumably arises from orientational modes. Below x_c, these two components merge when the temperature decreases. The temperature evolution of the profile is strongly reminescent of the inelastic neutron-scattering

results. It may be argued that the Lorentzian at high T is due to orientational diffusion, whereas at low T it represents a broad distribution of librational-type modes in a perturbed local environment. In the Pa3 phase for $x > x_c$, discrete excitations have been observed. Their width increases with increasing Ar content—again owing to perturbations of the local environment in the mixed crystals. Here, however, the perturbations are significantly smaller than in the orientational glass.

The Raman spectrum of pure N_2 has recently been reinvestigated by Pangilinan *et al.* (1989). On heating the sample in the Pa3 phase, they observed a strong increase in the intensity of the stretching band, which occurs about 10 K below the Pa3-to-h.c.p. transition. They have proposed a 'plastic' state in the intermediate temperature range (i.e. a phase with dynamical orientational disorder on an f.c.c. centre-of-mass lattice). This offers the possibility of observing an f.c.c. orientational glass for $x_c < x < 1$ (i.e. an orientational glass with a centre-of-mass lattice identical with that of mixed cyanides). On the other hand, the X-ray diffraction pattern of pure N_2 shows that those lines of the Pa3 structure that are directly related to the four-sublattice orientational arrangement persist up to the Pa3-to-h.c.p. transition. The X-ray results for the mixed crystals $Ar_{1-x}(Na_2)_x$ show different behaviour (Klee and Knorr 1990). The Pa3 specific Bragg reflections appear at the h.c.p.-to-cubic transition; on heating, the reverse cubic-to-h.c.p. transition occurs at considerably higher temperatures (figure 8.1). The Pa3-specific reflections already have disappeared below the reverse transition temperature, suggesting an f.c.c. orientationally disordered state at intermediate temperatures, in agreement with what Pangilinan *et al.* (1989) have suggested —although for pure N_2. The temperature range where the orientational order is lost coincides with the temperatures at which heat-capacity measurements show anomalies. Thus the heat-cpacity experiment seems to probe the orientational order–disorder transition and not the changes in the centre-of-mass lattice.

8.3. *Conclusion*

Several quantities have been related to the freezing into the orientational-glass state: the width of the ^{15}N and ^{13}C NMR signals, the width of the diffraction lines, and the changes in the neutron and Raman spectra. All of these quantities change rather gradually with temperature on passing from the dynamically disordered high-T state into the orientational glass. Clearly, there are no discontinuities or hysteresis effects that could be regarded as an indication that a phase boundary existed between the dynamically disordered phase and the orientational glass.

Klee and Knorr (1990) have recently compared the temperature dependence of the width of the Bragg lines with theoretical predictions of the 'glass order parameter' $q(T)$ of a random-bond–random-field Ising system (figure 8.4). They conclude that, although random fields are not negligible, they are less important than the random interactions. Within the framework of this model, a true glass-transition temperature can be defined in the spin-glass sense.

Meyer and Harris (1985) analysed a system of quadrupole moments diluted on the sites of a h.c.p. lattice and interacting via electrostatic quadrupole–quadrupole interactions. Using the replica trick, they found that the decomposition of the Hamiltonian includes a random-field and a homogeneous-field term. Concentrating on the random-field term, they argued that a phase-transition-like onset of the quadrupolar-glass state cannot be expected in such a situation. This prediction is in good agreement with the gradual change of all experimental quantities that have been

related to the freezing process of $Ar_{1-x}(N_2)_x$. The slight orthorhombic splitting observed in the X-ray diffraction experiment indicates that a spontaneous quadrupole moment develops in the basal plane of the h.c.p. lattice. It is appealing to identify this moment with the homogeneous-field term of Meyer and Harris (1985). Thus it appears that their analysis is a good starting point for understanding the glass state of $Ar_{1-x}(N_2)_x$.

Compared with *o–p*-H_2, the NMR experiments on $Ar_{1-x}(N_2)_x$ have not yet reached the same high degree of sophistication. On the other hand, study of the $Ar_{1-x}(N_2)_x$ mixtures has benefitted from the fact that the low-temperature thermal properties are not obscured by the *ortho–para* conversion and that powerful methods like neutron scattering, Raman and X-ray-diffraction experiments can be carried out at easily accessible temperatures. The fact that N_2 is a classical rotator is of great advantage for Monte Carlo (Devoret and Estève 1983) molecular-dynamics simulations (Klee *et al.* 1988).

In $Ar_{1-x}(N_2)_x$, the coupling of the orientations with the deformations of the centre-of-mass lattice is stronger than in the H_2 system, but weaker than in cyanides. Hence $Ar_{1-x}(N_2)_x$ is less ideal in terms of the generalized spin-glass concept, but closer, so to say, to the real glasses. Both $Ar_{1-x}(N_2)_x$ and the H_2 mixtures have the shortcoming that the quadrupolar response function, which would play a role analogous to the magnetic susceptibility of spin glasses, has not been investigated —although in principle it should be accessible, for example, through studies of the Kerr effect.

9. Other systems

9.1. *Solid solutions of methane and krypton*

At 90·7 K, methane condenses into an orientationally disordered f.c.c. lattice, the so-called free-rotor phase (phase I). At 20·4 K, it transforms into phase II, with a structure containing eight sublattices. On six of these, the octupoles of the CH_4 molecules are orientationally ordered, while the molecules on the two remaining sublattices are dynamically disordered and behave like slightly hindered rotators. On these two sites, the octupole–octupole interactions cancel each other completely. Fully deuterated methane transforms from phase I into phase II at 26·5 K. CD_4 exhibits a low-temperature phase (phase III), which in CH_4 can only be stabilized at pressures greater than 450 bar. The structure of phase III is still unknown. For a review see Press (1981).

Since the early heat-capacity investigation by Eucken and Veith (1936, 1937), it has been known that the specific-heat anomalies in CH_4 at the transition from phase I to phase II vanish if a sufficient amount of Kr is added to CH_4. Subsequently, the phase diagram of $Kr_{1-x}(CH_4)_x$ has been established by heat-capacity (K. J. Lushington 1986, unpublished results), NMR (Calvani *et al.* 1981, 1983, De Luca and Moraviglia 1983, Calvani and Glättli 1984, 1985) and dielectric techniques (Böhmer and Loidl 1990b). A schematic (x, T) phase diagram for $Kr_{1-x}(CH_4)_x$ is shown in figure 9.1. The solid line indicates the phase boundary between the phases I and II, and the dashed line the transition from the free-rotor phase into the glassy low-temperature state. This line indicates the freezing-in of the octupole moments in random orientations.

Calvani and Glättli (1984, 1985) measured the NMR susceptibility in solid solutions of $Kr_{1-x}(CH_4)_x$ for CH_4 concentrations $0{\cdot}6 < x < 0{\cdot}85$. The experimental results revealed that the average energy splitting of the two lowest rotational states

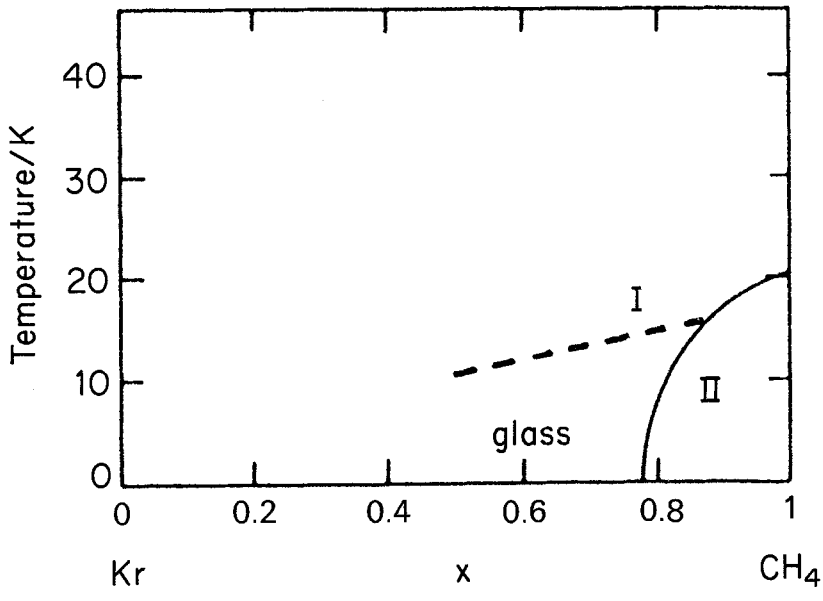

Figure 9.1. Schematic (x, T) phase diagram of solid solutions $Kr_{1-x}(CH_4)_x$. The approximate phase boundary between phase I (dynamic orientational disorder) and phase II (partial orientational order) is shown as a solid line. The glass state indicates a low-temperature state with frozen-in orientational disorder.

$\Delta = 5{\cdot}8$ K, intermediate between those found for pure CH_4 in phase II ($\Delta = 1{\cdot}9$ K) and for the free-rotor phase ($\Delta = 12{\cdot}7$ K). The temperature dependence of the spin–lattice relaxation time T_1 has been studied for various concentrations. At low temperatures and high methane concentrations, the linewidth scales as $x^{1/2}$, as predicted for a random defect dilution. A sharp increase at $x = 0{\cdot}8$ was interpeted as being due to a transition into an orientational-glass state.

The most detailed investigations of the octupolar-glass state in $Kr_{1-x}(CH_4)_x$ have been performed by Grondey *et al.* (1986, 1987). The rotational spectra in $Kr_{1-x}(CH_4)_x$ were studied for concentrations $x < 0{\cdot}65$ by means of inelastic incoherent neutron-scattering techniques. At low T and low krypton concentrations, well defined tunnelling transitions were observed in phase II (figure 9.2 (*a*)). In addition, almost-free-rotator lines were detected at somewhat higher energies (approximately 1 meV). With increasing Kr concentration, the tunnelling and rotational excitations displayed asymmetric broadening. For $0{\cdot}8 < x < 1$, distinguishable tunnelling and nearly-free-rotator scattering distributions were observable. The spectra indicated that, even for defect concentrations of 20% Kr, the structure of phase II with partial orientational order is the stable low-temperature state and that the lineshapes of the rotational excitations are modified by the disturbance of the local crystal field. Surprisingly, the spectra in the glass state were characterized by a well defined single excitation at 0·77 meV, which is intermediate between the limits of rotational tunnelling and almost-free rotation (figure 9.2 (*b*)). In the high-temperature limit, the spectra at all Kr concentrations (phase I) could be described by an almost-quasi-elastic lineshape (figure 9.2 (*c*)), and revealed dynamic disorder of the molecular orientations. These quasi-elastic scattered intensities can be described in terms of rotational diffusion.

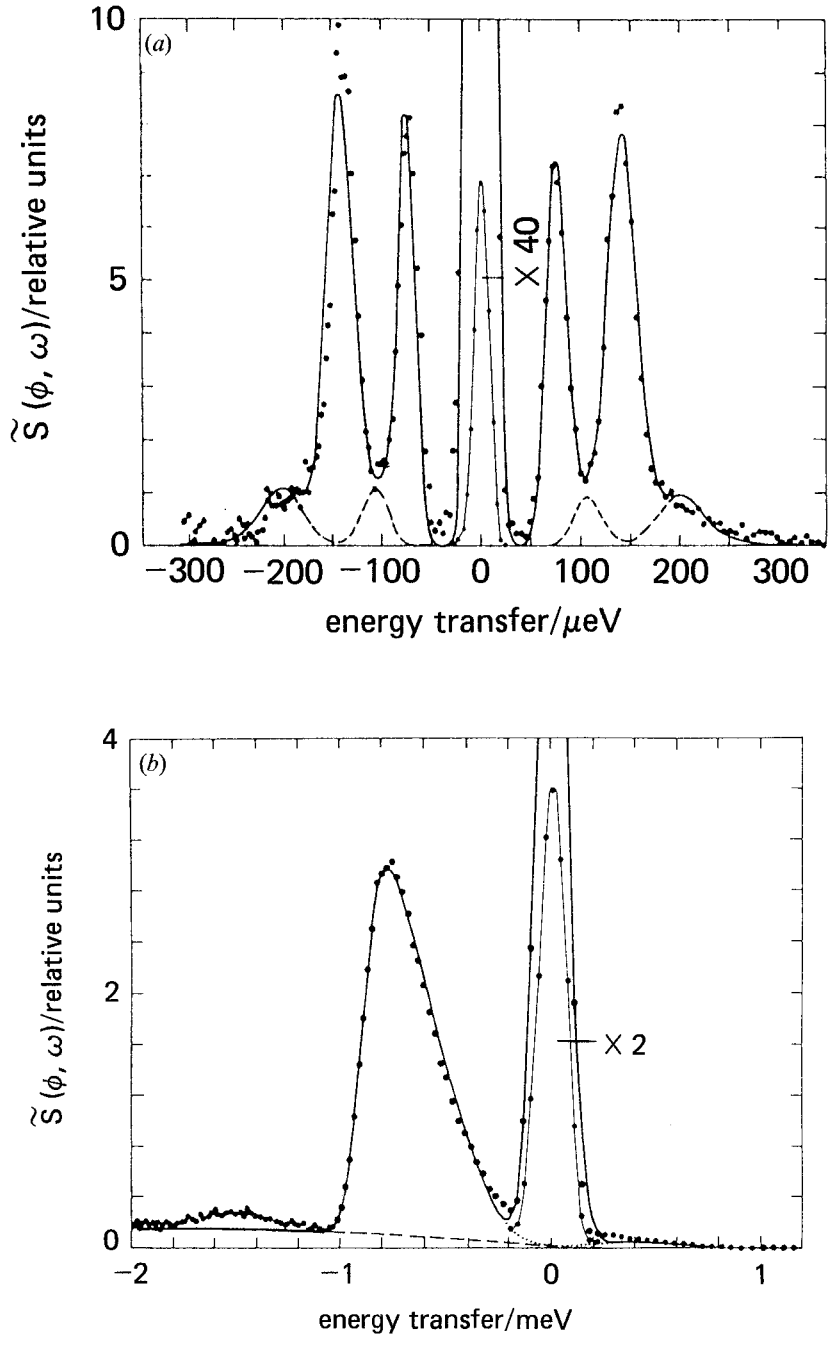

Figure 9.2. Spectra for $Kr_{1-x}(CH_4)_x$ mixtures in the different phases I, II and in the glassy low-temperature state: (*a*) tunnelling excitations for $x = 0{\cdot}976$ in phase II at $T = 4{\cdot}9$ K; (*b*) rotational excitation for $x = 0{\cdot}73$ in the glassy low-temperature state at $T = 1{\cdot}6$ K; (*c*) quasi-elastic scattered intensities due to rotational diffusion of the methane molecules in phase I for $x = 0{\cdot}73$ and $T = 29{\cdot}0$ K. (*a*) and (*b*) from Grondey *et al.* (1984) and (*c*) from Grondey *et al.* (1985).

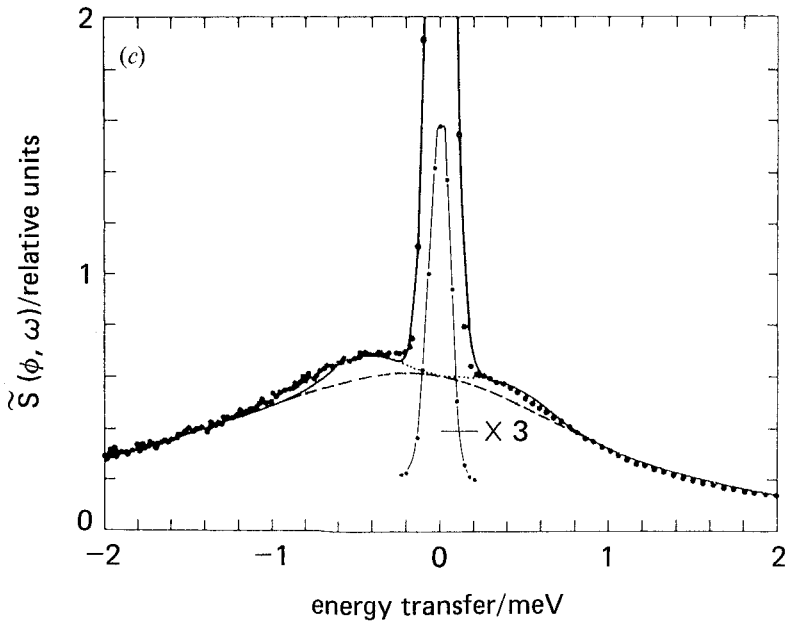

Figure 9.2. Continued.

In summary, the experimental results published so far reveal that for methane concentrations $x < 0{\cdot}8$, $Kr_{1-x}(CH_4)_x$ mixed crystals are characterized by frozen-in orientational disorder. Site disorder and anisotropic interactions seem to play an important role in establishing the low-temperature glass state. However, at present, it is still unclear the extent to which the freezing is interaction-dominated or a purely kinetic single-particle effect driven by the local lattice anisotropies.

9.2. *Potassium ammonium iodide mixed crystals*

As a function of temperature and pressure, the ammonium halides undergo a number of structural phase transitions (Parsonage and Stavely 1978). In the high-temperature α and β phases, the ammonium ions are dynamically disordered. The γ and δ modifications reveal orientational order. At room temperature and ambient pressure, NH_4I exhibits the α modification, which is a NaCl-type structure in which the NH_4 ions undergo rapid reorientation. At 256 K, it transforms into a CsCl structure. Here the NH_4 ions are located in the centres of primitive cubic iodide sublattices, with the N–H bonds directed towards the neighbouring I ions, while the ammonium tetrahedra can reorient between two energetically equivalent orientations. Finally, below 232 K, octupolar order is established in a slightly distorted CsCl structure of tetragonal symmetry. KI and NH_4I are fully miscible (Havighurst *et al.* 1925), and heat-capacity measurements by Stephenson *et al.* (1952) revealed that (i) NH_4I can easily be supercooled and (ii) a sufficient amount of potassium iodide in ammonium iodide stabilizes the α phase of the NH_4 ions down to the lowest temperatures.

It has been shown (Fehst *et al.* 1990) that the NH_4 ion in the rock-salt modification of NH_4I and $(KI)_{1-x}(NH_4I)_x$ exhibits a permanent dipole moment of 1·4 D, which is possibly due to an off-centre position of the NH_4 ion. The mismatch of the ammonium

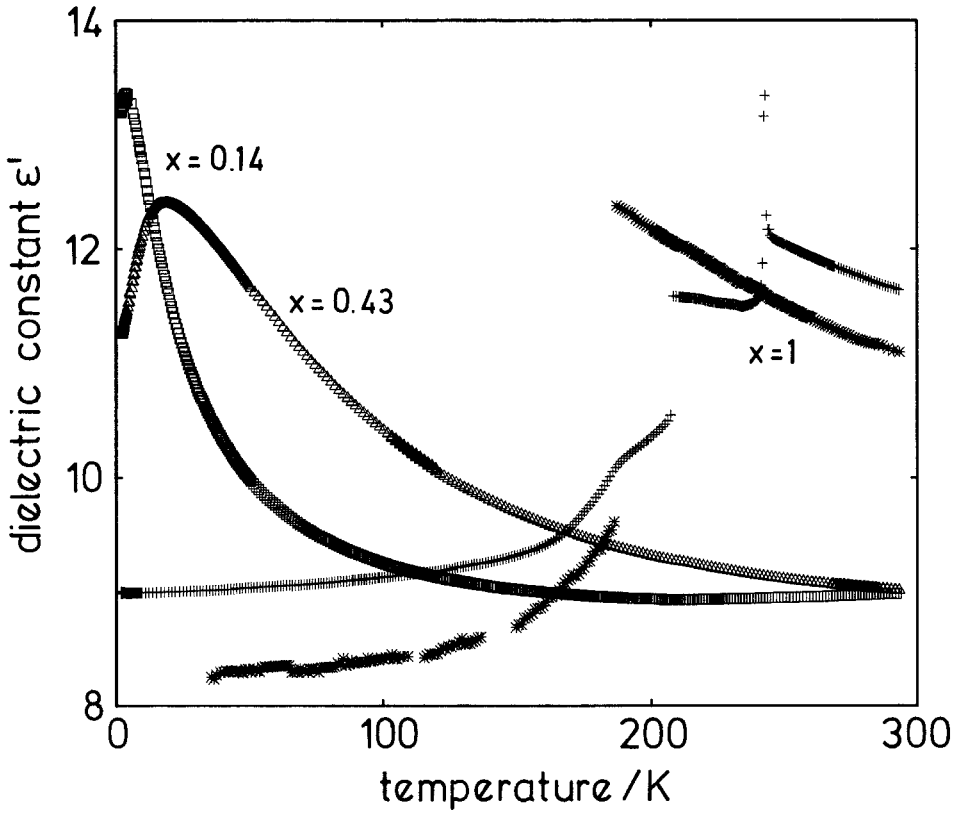

Figure 9.3. Temperature dependence of the dielectric constant ε_1 in $(KI)_{1-x}(NH_4I)_x$ for ammonium concentrations $x = 0{\cdot}14$, $0{\cdot}43$ and 1 measured at 100 kHz (the dielectric constant is also shown for a supercooled sample of pure ammonium iodide; here the probing frequency was 331 MHz). From Fehst *et al.* (1990).

ion in the octahedral environment results from the impossibility of directing all N–H bonds towards the neighbouring iodine ions. In solid solutions of NH_4I and KI, where the rock-salt structure is stabilized down to the lowest temperatures, the dipoles undergo a cooperative freezing process devoid of long-range order. Figure 9.3 (Fehst *et al.* 1990) shows the dielectric constant $\varepsilon_1(T)$ *versus* temperature in $(KI)_{1-x}(NH_4I)_x$ for ammonium concentrations $x = 0{\cdot}14$, $0{\cdot}43$ and 1. For pure ammonium iodide, the dielectric constant reveals two anomalies, which indicate the transitions from the high-temperature rock-salt structure into an intermediate CsCl and a low-temperature tetragonal structure. Apparently, for $x = 0{\cdot}43$ and $0{\cdot}14$, the NaCl structure is stable down to the lowest temperatures. A freezing process accompanied by appreciable loss sets in at low T. The temperature dependence of the dielectric loss is shown in figure 9.4 (Fehst *et al.* 1990), where $\varepsilon_2(T)$ is plotted for concentrations $x = 0{\cdot}14$ and $0{\cdot}43$ for different measuring frequencies. The upper inset in the figure shows the frequency dependence of the dielectric loss at different temperatures. The dipolar-loss spectra reveal an extremely broad distribution of relaxation times, which is a characteristic feature of transition into an orientational-glass state. The lower inset depicts the temperature dependence of the loss-peak maxima in an Arrhenius plot. Significant deviations from Arrhenius behaviour appear at low temperatures;

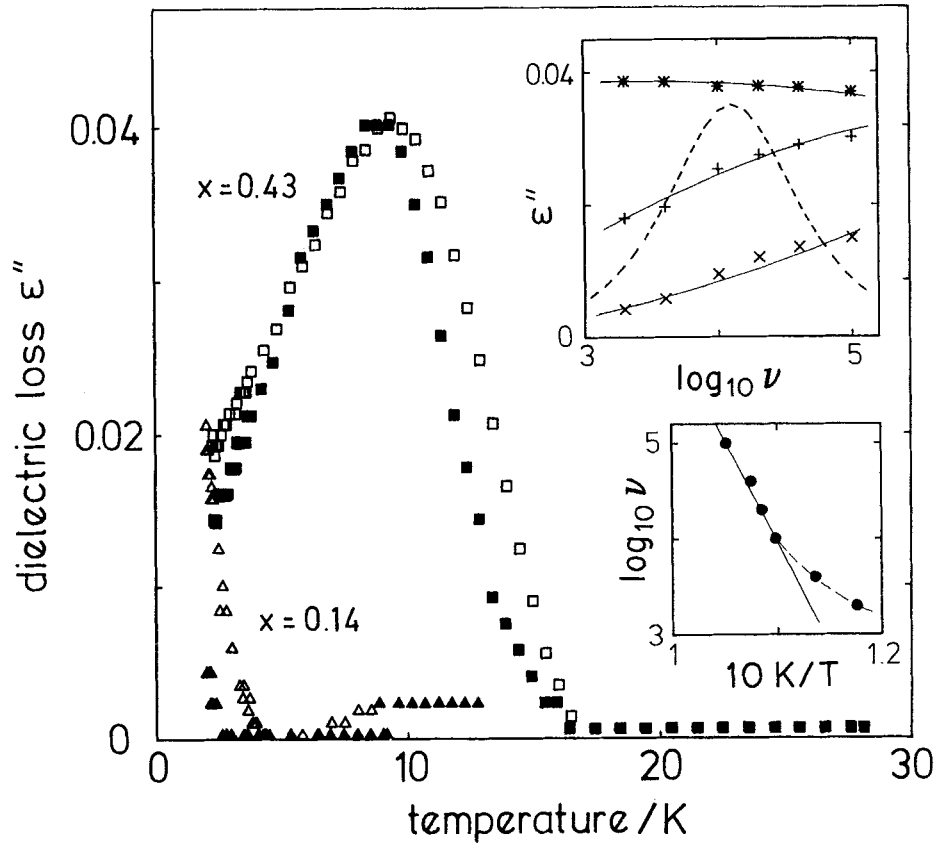

Figure 9.4. Temperature dependence of the dielectric loss ε_2 in solid solutions of $(KI)_{1-x}(NH_4I)_x$ with concentrations $x = 0{\cdot}14$ and $0{\cdot}43$, measured at different measuring frequencies: 100 kHz (filled symbols) and 4 kHz (open symbols). The upper inset shows the frequency dependence of the dielectric loss for $x = 0{\cdot}43$ as observed for various temperatures: *, 8·4 K, +, 11·9 K, ×, 14·0 K. Here the solid lines are a guide to the eye only. The dashed line indicates a monodispersive Debye relaxation. The lower inset shows the temperature dependence of the dielectric-loss maxima for $x = 0{\cdot}43$ plotted in an Arrhenius diagram. The deviations at low measuring frequencies have been interpreted as being due to additional excitations (tunnelling transitions) that become active at low T. From Fehst *et al.* (1990).

they have been interpreted as being due to a cross-over from thermally activated behaviour to tunnelling phenomena (Fehst *et al.* 1990). The conclusion that solid solutions of ammonium iodide and potassium iodide possess frustrated ground states has also been drawn from the results of inelastic incoherent neutron-scattering experiments by Bostoen *et al.* (1989, 1990).

In summary, solid solutions of NH_4I and KI comprise an interesting new class of orientational glasses. The possibly pure dipolar character, devoid of quadrupolar interference, and the transition from thermally activated to tunnelling behaviour seem a worthwhile object for further and more detailed studies.

9.3. *Mixed betaine compounds*

The structural and dielectric properties of a number of addition compounds of α-amino acids with inorganic components have been investigated in detail (Albers

1988). The best-known representative of this group is triglycine sulphate, a ferroelectric material used as infrared detector. Most of these adducts undergo a paraelectric-to-ferroelectric phase transition; for example, the betaine adducts of phosphorous and arsenic acids, betaine phosphite (BPI) and betaine arsenate (BA) exhibit ferroelectric phase transitions at 216 and 119 K respectively. In these materials, the PO_3 or AsO_4 tetrahedra are linked by quasi-one-dimensional chains of hydrogen bonds.

That betaine phosphate (BP) and deuterated betaine arsenate (D-BA) undergo antiferroelectric transitions at 119 and 86 K respectively has been found only recently (Albers 1988). In these addition compounds, the hydrogen-bonded chains are coupled antiferroelectrically. It has been argued that solid solutions of ferroelectric and antiferroelectric systems could possess frustrated ground states, similar to the case of the proton glass RADP. The first experimental evidence for a glassy low-temperature state was reported by Maeda (1989) in mixed crystals of ferroelectric BA and antiferroelectric BP. Santos *et al.* (1990) have speculated about the occurrence of a freezing transition devoid of long-range order in mixtures of antiferroelectric betaine phosphate (BP) and ferroelectric betaine phosphite (BPI). At intermediate concentrations, the dielectric constant reveals broad cusps in the real part, accompanied by appreciable loss (Santos *et al.* 1990). The first experiments on protonated and deuterated samples of betaine arsenate were reported by Rother *et al.* (1985).

In summary, mixtures of ferroelectric and antiferroelectric betaine compounds might be an interesting new family of proton glasses. It seems interesting to study the disorder in the hydrogen bonds in the linear chains as well as the disorder introduced between the chains. However, considerable further experimental work will be necessary to clarify the statics and dynamics of the low-temperature states in these mixed crystals.

9.4. *Strontium calcium titanate*

The addition of Ca to $SrTiO_3$, to give $Sr_{1-x}Ca_xTiO_3$, induces a polar phase, as was shown by Bednorz and Müller (1984) on the basis of the dielectric constant at fixed frequency. From the shape of $\varepsilon_1(T)$, these authors derived the presence of randomness in this system. This suggestion was taken up by Kleeman and Schremmer (1989), who reported a nearly monodispersive relaxation mode at about 100 kHz, with a weak low-frequency tail that is maximal at the transition. Slow relaxation of strain in pure $SrTiO_3$ was also reported by Höchli and Torre (1983) from ultrasound measurements. It is likely that randomness plays a role in these systems, but further experimental evidence is required for an assessment of its role.

9.5. *Potassium chromate (VI)*

Dielectric data taken near the order–disorder (α–β) transition at 940 K in K_2CrO_4 led Russel and Merlin (1986) to postulate a dipolar-glass phase intermediate between the two phases. Subsequently, a dispute about the validity of the data and its interpretation arose (Dissado and Haidar 1987, Merlin 1988a,b). The limited amount of data available in the literature does not allow us to settle this matter and to arrive at a definite conclusion.

9.6. *Barium lanthanum fluoride*

The low-temperature heat capacity, thermal conductivity and internal friction has been studied in solid solutions $Ba_{1-x}La_xF_{2+x}$ for concentrations $0 < x < 0{\cdot}46$ by

Cahill and Pohl (1989). With increasing x, the low-temperature behaviour gradually changes from that of a pure crystal to that characteristic of an amorphous solid. BaF_2 crystallizes in the cubic CaF_2 structure. The elementary defect is a substitutional La^{3+} at the Ba^{2+} site accompanied by a F^- ion at a neighbouring interstitial site. This elementary defect carries an electric dipole and an electric quadrupole moment.

9.7. $Ca(ND_3)_x$

Frozen-in orientational and positional disorder of the ND_3 molecules has been detected by neutron diffraction in $Ca(ND_3)_x$ with $x \approx 6$. The frustrated ground state was explained taking two different sites of the ND_3 into account (Press *et al.* 1989).

10. Survey of experimental features of orientational glasses

The orientational-glass state is observed when the elementary dipole, quadrupole or higher-order multipole moments of mixed crystals freeze in, leading to an arrangement devoid of long-range orientational order. The orientational-glass state evolves out of a high-symmetry crystalline phase where the orientations are dynamically disordered. It is formed for a certain range of chemical composition only; for other compositions, low-T phases with long-range orientational order are observed. The possible (x, T) phase diagrams are shown schematically in figures 1.1 and 1.2.

The multipole moments can be assigned to the orientations of molecular entities, such as N_2 in $Ar_{1-x}(N_2)_x$ or the displacements of specific atoms, such as the off-centre displacement of Li in $KTaO_3$:Li. It should be noted that the local moment will polarize its environment; the bare moments should be distinguished from dressed moments. Often the experimental data are not complete enough to make this distinction.

A relevant susceptibility is selected in such a way that it plays a role analogous to the magnetic susceptibility in spin glasses. This susceptibility is the bulk ($q = 0$) dielectric susceptibility in dipolar glasses and the bulk quadrupolar susceptibility in quadrupolar glasses. The quadrupolar susceptibility has not been measured directly, but at least in mixed cyanides the elastic shear constant is a linear measure of the quadrupolar susceptibility. In RADP the relevant susceptibility is a finite-q structural correlation function; it is accessible through the intensity of the side peaks of the diffraction experiment.

The relevant static susceptibility shows a Curie–Weiss T dependence $\chi \sim (T - \Theta)^{-1}$ at higher T and becomes constant below a characteristic temperature $T_f(\omega \to 0)$, which is finite and larger than Θ. This Parisi-type behaviour is known from spin glasses. $T_f(\omega \to 0)$ is regarded as a true glass-transition temperature. Of course, nobody has ever measured a strictly static susceptibility, but for $KTaO_3$:Li and $KTaO_3$:Na extrapolation to $\omega = 0$ demonstrates a Parisi-type T dependence. For mixed cyanides, there is some indication of such behaviour.

In the measurement of the T dependence of the relevant susceptibility at finite measuring frequencies, relaxations are observed, which show up as cusp-like anomalies of the real part and maxima of the imaginary part at the freezing temperature $T_f(\omega)$. These relaxations signal the slowing down of the relevant degrees of freedom. In analogy with real glasses, they are called primary or α relaxations. The primary relaxation rates show broad and asymmetric distributions. The width of the distribution is five or more decades in frequency, and thus exceeds by orders of magnitude the width of a monodispersive Debye process. The shape of the distribution is well parametrized in terms of the KWW expression. The T dependence of the average

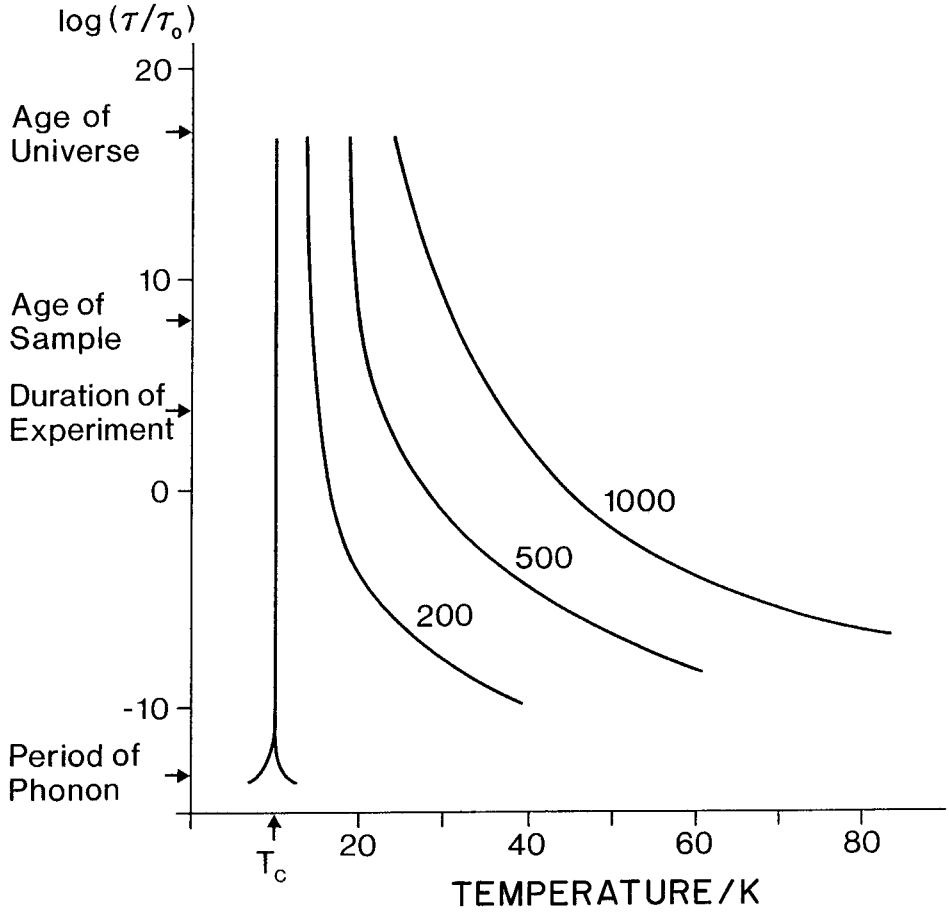

Figure 10.1. Logarithmic time scale of observation at the glass transition and at a structural transition. While the curves for $\tau(T)$ are based on extrapolation (Courtens 1986, Höchli 1982) they provide evidence for the onset of effective irreversibility far above the temperature at which τ diverges.

relaxation rate shows deviations from an Arrhenius law and is better described by the Vogel–Fulcher law. The energy barrier E_b of the Vogel–Fulcher law is of the order of 1000 K or more, it is considerably larger than what is found in the dilute limit. Thus it should not be understood in a single-particle picture—the high values rather signal that collective processes are important.

The ratio D of the mean energy barrier E_b to the Vogel–Fulcher temperature T_{VF}, $D = E_b/T_{VF}$, is greater than 20. Thus orientational glasses are strong glasses in the sense of the distinction between 'strong' and 'fragile' that is made for real glasses.

In passing, we wish to illustrate that the experimentalist's time windows cannot be blamed for the failure to access the Vogel–Fulcher temperature T_{VF}: figure 10.1 shows the relaxation rate and thus the access time to a dynamic phenomenon near T_{VF}. For a reasonably strong glass with $D = 10$, at $T = 1{\cdot}4T_{VF}$, the access time exceeds the age of the Universe. At $T < 1{\cdot}4T_{VF}$, such a glass is irreversible. Compared with a glass, a structural phase may be accessed within 10^{-10} T_c on both sides of T_c (barring

other obstacles). The large irreversible range of T is the reason why the very existence of a phase transition is often discussed in glasses.

We also mention in passing that the spin–lattice relaxation time T_1 of the NMR experiment gives valuable information on the relaxations involved in the freezing process. It must be realized, however, that here local relaxations are probed, which are not necessarily identical with the relaxations probed in measurements of the relevant susceptibility. A structural model is necessary to translate one type of process into the other. In $KTaO_3$: Li, for example, Li NMR is sensitive to the dynamics of an individual Li atom, whereas the dielectric susceptibility probes the dynamics of the elementary dipole moments. Clearly, the elementary dipole moments are ultimately caused by the off-centre Li position, but the absolute value of these moments is mainly due to displacements and polarization of the neighbouring atoms.

Often, a second relaxation regime exists at temperatures well below T_f. Again in analogy with real glasses, the relaxations are called secondary or β. The β relaxations can show up in the relevant susceptibility, as in mixed cyanides, or in non-relevant response functions, as in RADP. The distribution of the β-relaxation rates is broad, typically ten decades in frequency, but symmetric (i.e. Cole–Cole-like). The T dependence of the mean relaxation rate follows an Arrhenius law, although significant Vogel–Fulcher-like deviations have been observed for RADP.

As far as the distribution and T dependence of primary and secondary relaxation rates are concerned, we note a close analogy with real glasses.

Attempts have been made to classify the response functions investigated in orientational glasses in terms of symmetries. The first approach assumes that the classification in terms of Fourier components and irreducible representations valid for the high-T phase of the concentrated reference compound (e.g. f.c.c.-KCN for mixed cyanides) can be transferred to the orientational-glass state. This route is followed when translating experimental results on the transverse sound velocity in the orientational-glass state of mixed cyanides into the T_{2g} elastic constant c_{44}. The lifting of the cubic selection rules in Brillouin scattering is one example that this assumption is not strictly correct. The other approach refers to the symmetry of an individual defect in an environment that has the point symmetry of the host lattice. This view leads, for example, in mixed cyanides to considering the secondary relaxations in terms of 180° inversion flips of individual CN^- ions, and it might be wondered why such a motion should be visible in the elastic constant. Thus both approaches are full of pitfalls. After all, it is a basic feature of the orientational-glass state that it occurs in mixed crystals with concentrations of the active species that exceed the dilute limit. Thus neither the symmetries of the dilute limit nor those of the virtual crystal can be strictly valid. On the other hand, one is reluctant to abandon the symmetry relations of the dilute or concentrated limits completely, since they are helpful at least near the end points of the phase diagrams (figures 1.1 and 1.2).

The response and stimulus connected by the relevant susceptibility will be called polarization and field. Zero-field-cooled orientational glasses show an average spontaneous polarization that is vanishingly small. Thus the spontaneous electric polarizations of KCl:OH and $KTaO_3$: Li are less than 0·01 times the remanent polarization obtained by cooling the sample in a field. In mixed cyanides, where—as for the other quadrupolar glasses—field-cooling experiments have not yet been performed, an estimate of the quadrupolar polarization can be obtained from a comparison of the broadening of the Bragg lines in the orientational-glass state and the splitting of these lines upon the phase transitions of the pure cyanides. For the latter

compounds, the spontaneous shear of the cell angles is of the order of 10°, while the r.m.s. shear of the orientational-glass state is of order 0·1°. Thus the polarization of orientational glasses behaves in a way analogous to that in spin glasses.

In dipolar glasses, the nonlinear part of the relevant susceptibility increases strongly on approaching T_f from above. It is likely that the same effect also occurs in quadrupolar glasses.

There are no anomalies in the heat capacity at the freezing temperature. The same observation has been made in spin glasses, whereas real glasses do show a maximum or a step. The example of spin glasses shows that the absence of a heat-capacity anomaly does not automatically exclude the existence of a true glass transition at $T_f(\omega \to 0)$.

Orientational glasses show the low-temperature anomalies commonly known as two-level-system (TLS) effects. In this respect, they are analogous to real glasses. Attempts to assign specific degrees of freedom to TLS, such as 180° tunnelling of CN, are appealing but lack experimental verification.

The length over which the dipole or quadrupole moments are coherently frozen-in is definitely longer than the average distance between two neighbouring moments, and definitely shorter than the typical size of conventional domains. In principle, this length can be derived from the diffuse diffracted intensity. A value of 20 Å has been derived from the satellite peaks in RADP. In most orientational glasses, the local ordering is of the ferrotype; it is difficult to separate the weak correlation-induced diffuse intensity from the Bragg lines and thermal diffuse scattering. Nevertheless, it is presumably safe to think of ordered regions of a few hundred Ångström units in these cases. Values around 100 Å have been suggested for $KTaO_3$: Li from second-harmonic generation in optical-scattering experiments.

Several experimental quantities have been taken as the 'glass order parameter' $q(T)$. These experimental quantities have the property in common that they measure in one way or the other the variance of a distribution of polarizations. Examples are the second moment of NMR profiles, and the width of broadened Bragg lines and the intensity of the elastic component of the diffuse intensity in inelastic neutron scattering. In a more indirect way, $q(T)$ has occasionally been derived from the T dependence of the relevant susceptibility below T_f. Clearly, none of these attempts are very satisfactory, since they all depend on specific models and on the time and length windows of the methods applied. Thus the interpretation of the Bragg width in terms of a distribution of cell parameters assumes that the sample consists of individual regions of unspecified size, every one having a well defined set of cell parameters, which contribute to the diffracted intensity independently. Related problems occur in the interpretation of NMR results when, for example, the assumption of preferred orientations is made. In fact, some of the glass order parameters cited may not be related to the relevant response at all. Generally speaking, the glass order parameters derived in those ways increase monotonically with decreasing temperature. An operational T_f is usually defined as the temperature where $q(T)$ increases strongly. It should be noted that this T_f often does not coincide with the T_f derived from the relevant susceptibility. On the basis of such results, some authors have strongly objected to the existence of a true glass transition, whereas others have referred to a glass transition in the presence of random fields. That is, they have fitted $q(T)$ to the predictions of random-bond/random-field models and obtained the true glass-transition temperature from the random-bond component only. Although these attempts are to a large extent speculative, they are helpful for the understanding and comparison of

orientational glasses. We remind the reader that, even for conventional phase transitions, it is difficult to derive the parameter of long-range order from measurements of non-relevant quantities. Well known examples are the discrepancy between the long-range and short-range order parameters in the chemical ordering of β-brass or Cu_3Au and the problem of deriving an antiferromagnetic order parameter from measurements of bulk magnetic susceptibility.

As discussed here, orientational glasses are in many respects analogous to spin glasses. The main difference, as we see it, is the strong coupling of the orientational degrees of freedom to the displacements of the lattice. In spin glasses, the spin–lattice coupling can safely be ignored. In orientational glasses, the reorientation of a dipole or quadrupole moment involves changes of atomic coordinates, which automatically lead to displacements of the neighbouring atoms. These effects are weakest in *ortho–para* hydrogen and strongest in mixed cyanides. Because of this coupling, orientational glasses exhibit properties analogous to those of real glasses. On the other hand, the formation of the orientational-glass state does not involve conventional diffusion, since the chemical disorder is quenched. Thus, in contrast with real glasses, diffusion does not contribute to the relaxation processes.

The fundamental question has been posed as to whether the orientational-glass state has lost the translational symmetry of a crystalline lattice. Two pieces of experimental evidence on mixed cyanides suggest that this may be so: the elastic shear constant softens almost completely, and the Bragg spikes are replaced by weaker cusp-like singularities. It has been argued that the orientational-glass state of mixed cyanides forms out of a quasi-liquid state. As far as the crystalline point symmetry is concerned, this state is certainly not isotropic, but it is also not strictly cubic, as shown by the violation of the selection rules in Brillouin experiments.

11. Predictions from theoretical models

11.1. *Introduction*

Most theories of dilute glasses are based on interactions between moments p_i and p_j occupying random sites of a regular lattice. In spin glasses, the moments arise from constituents carrying a magnetic moment, and the other lattice sites are spinless metal ions. The interaction between the magnetic moments depends on distance r according to $\cos(k_F r)/r^3$; it can thus have either sign. Geometrical considerations involving the Fermi wavenumber k_F and even distance are sacrificed, and the interaction J_{ij} is written instead in terms of a distribution $g(J_{ij})$ with zero average $\bar{J}$ and non-zero variance $\mathrm{Var}(J)$. The solution of the Hamiltonian

$$\mathscr{H} = \sum_{i \neq j} p_j p_j J_{ij}$$

with the above-mentioned conditions has taken a decade of intensive theoretical research and is a fascinating subject in itself. It is based in part on analytical work and in part on large-scale computations. We refer the interested reader to the detailed review by Binder and Young (1986).

Much of the work on glass formation has been influenced by insight gained from the study of structural phase transitions. These two phenomena have much in common: on lowering the temperature, the time average of the moments p_i assumes a non-zero value below a particular temperature T_c. The behaviour of $p_i(T)$ and variables associated with p_i can be expressed as a function of $T - T_c$ for structural transitions (see section 11.2) and for dilute glasses.

Most previous theoretical work was devised for spin systems. Fortunately, straightforward considerations allow these findings to be translated for application to orientational systems. This will be done in section 11.3, and will enable us to present predictions for orientational glasses (section 11.4) derived mainly from random interactions; in some cases, random fields give rise to similar effects (section 11.5). The summary of the state of the art clearly emphasizes the role of random interaction (section 11.6).

11.2. *Structural transitions*

The theory of structural phase transitions is based on a Hamiltonian

$$\mathscr{H} = \sum_{i>j} J_{ij} p_i p_j + E \sum_j p_j + \text{anisotropy terms.} \tag{11.1}$$

The interaction term depends only on $r_i - r_j$ and has translational symmetry. The order parameter couples to a homogeneous field E. The predictions for the order parameter P, the static susceptibility χ_s, the correlation length ξ and the time decay $P(t)$ of the order parameter are

$$P \sim \begin{cases} (T_c - T)^{\beta} & \text{for} \quad T < T_c, \\ 0 & \text{for} \quad T > T_c \end{cases} \tag{11.2a}$$

$$\chi_s = \frac{\partial P}{\partial E} \sim |T - T_c|^{-\gamma}, \tag{11.2b}$$

$$\xi \sim \left\{ \begin{cases} \infty & \text{for} \quad T < T_c, \\ (T - T_c)^{-\nu} & \text{for} \quad T > T_c, \end{cases} \right\} \tag{11.2c}$$

and $\xi \sim |T - T_c|^{-\nu}$ also for $T < T_c$ for Ising-like models,

$$P(t) = P(0)\,e^{-\alpha t}, \quad T > T_c, \tag{11.2d}$$

where, close to T_c, $\alpha \sim (T - T_c)^z$, z being a dynamic exponent (Kadanoff *et al.* 1967, Hohenberg and Halperin 1977). Here T_c denotes a 'critical' temperature associated with divergences of χ_s and ξ. The transition temperature T_c and the proportionality constants depend on the strength of the interaction, while the parameters β, γ and ν, called critical indices, depend on the dimensionality of the solid and of the order parameter only. This 'universality' is a consequence of the uniformity of interaction, $J_{ij} = J(r_i - r_j)$, which is also assumed to be short-range here, independent of the significance of p. When moments occupy random sites, their interaction no longer has translational symmetry. In this situation, the interaction is described in terms of probabilistic distributions $g(J)$. In the following, we relate selected findings for $g(J)$ in spin glasses to the analogous findings in orientational glasses.

11.3. *Random interactions*

Brout (1965) was perhaps the first to recognize that the freezing process of particles in orientational glasses with random interactions results in glass formation, and to point out fundamental similarities between KCl:OH and Cu:Mn. We consider the analogy between dipolar interaction and spin–spin interaction in metals. The interaction between dipoles p_i and p_j separated by r is given by

$$J_{12} = \{p_1 p_2\} r^{-3} - 3\{p_1 r\}\{p_2 r\} r^{-5}. \tag{11.3}$$

The braces $\{\ \}$ denote the pseudo-scalar product, which has a negative sign for angles between the vectors larger than $\frac{1}{2}\pi$. To estimate the average and the variance of J_{12},

we express it as

$$J_{12} = p_1 p_2 r^{-3}[1 - 3\cos(r, x)].$$

For an isotropic distribution of dipoles, the average is

$$\bar{J} = \int J(r, \phi)\, \mathrm{d}\phi\, \mathrm{d}r^2 = 0$$

because of the $\mathrm{d}\phi$ term. The variance is

$$\mathrm{Var}(J) = \sqrt{\tfrac{8}{5}} p_1 p_2 r^{-3}.$$

Similar findings hold for a discrete random distribution of dipoles on a lattice:

$$\mathrm{Var}(J) = 2^{1/2} p_1 p_2 r^{-3}$$

for nearest-neighbour cubic sites. If the polar direction is allowed to be $\pm x$ and $\mathbf{r}/r$ is arbitrary then it is equally probable that $J > 0$ (ferroelectric ordering or parallel alignment) as that $J < 0$ (antiparallel alignment). For analogous findings regarding quadrupolar interaction, see Hammes *et al.* (1989). The situation is similar to that in spin glasses: the interaction

$$J_{12} = \cos(k_F r)/r^3,$$

where k_F is the Fermi wavenumber, has zero average and non-zero variance. Toulouse (1977) recognized that competing random interactions of spins on a closed loop may lead to degeneracy. The closed loop, called a plaquette (figure 11.1 (*a*)) shows that spin no. 4 should be up in the field of spin no. 1, and down in the field of spin no. 3. Such a situation, which was judged 'frustrating' for spin no. 4 (Toulouse 1977), does not occur for dipoles and quadrupoles on identical plaquettes (figure 11.1 (*c*) and (*e*)), but does on triangular plaquettes (figures 11.1 (*b*), (*d*) and (*f*)). The form of the plaquettes is of course immaterial for random sites, since many triangles and plaquettes exist in a crystal. Random multipolar interaction and random interaction in spin glasses share one important aspect, namely frustration, which is defined by a probabilistic distribution of interactions with zero average and non-zero variance. Cancellation of the average interaction arises owing to integration along the distance in spin glasses and to integration along the radial coordinates in orientational glasses. It is by virtue of this analogy that we can profit from the theory of spin glasses. Edwards and Anderson (1975) proposed a Hamiltonian of the form

$$\mathscr{H} = \sum_{i \neq j} J_{ij} S_i S_j + H \sum_i S_i, \tag{11.4}$$

where $S_i = \pm 1$ are defects with positions i and j, and J_{ij} are interactions between these defects, which are postulated to be given a probabilistic Gaussian distribution with average $\bar{J}$, often set equal to zero, and a non-zero variance. H is an external field. This model is based on coupling to nearest neighbours. An analogous model was formulated by Sherrington and Kirkpatrick (SK) (1975) for infinite-range interaction. Mean-field theory should apply to such a system. Accordingly, the use of the SK model was preferred in analytical work, in particular the solutions of the SK Hamiltonian obtained by Parisi and by Sompolinski (see Parisi (1979), Sompolinski (1981) and further works by the authors referenced in Binder and Young (1986)), which, according to Binder and Young (1986), are probably equivalent and treat static and dynamic aspects respectively. The (short-range) Edwards–Anderson (EA) model (1975) primarily laid the ground for numerical Monte Carlo (MC) computations. The consequence of this model in terms of the orientational quantities P for S and E for H are presented in the next section.

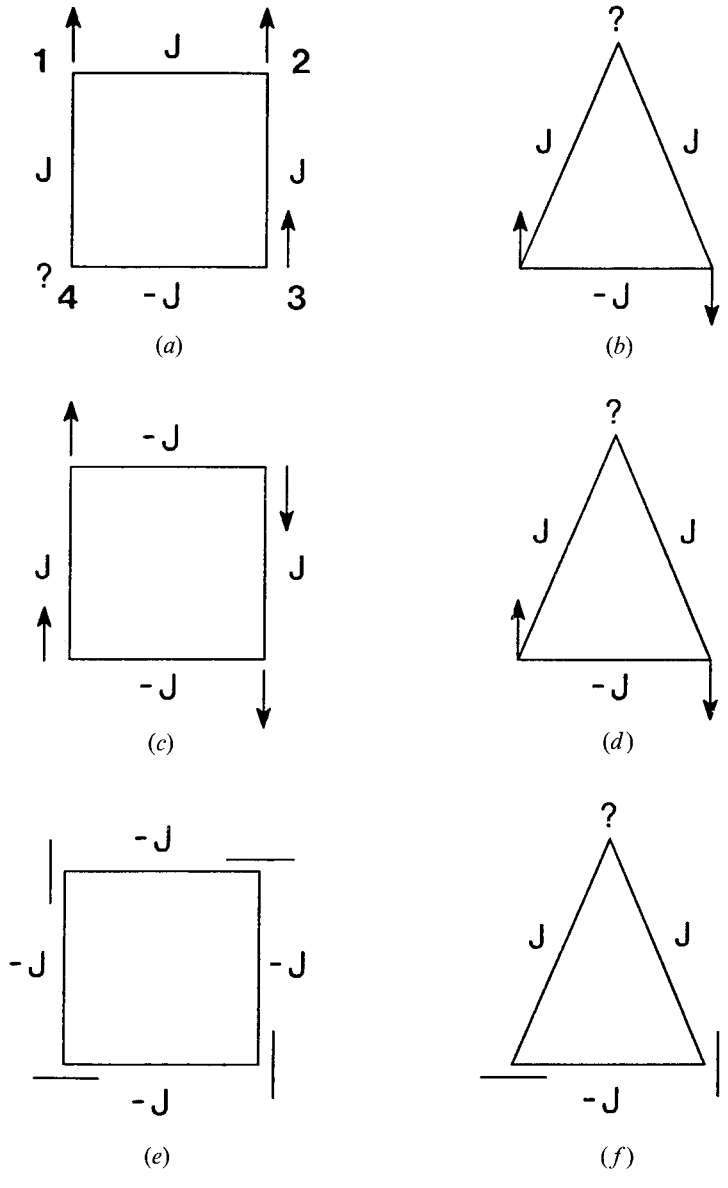

Figure 11.1. Frustration in spin and orientational glasses: In the first plaquette with spins numbered from 1 to 4, spin no. 4 'does not know how to align'. Similar situations are found for spins, dipoles and quadrupoles in triangular plaquettes.

11.4. *Results derived from spin-glass theories*

Of particular importance to the description of a glass transition is the local order parameter q_i as defined by Edwards and Anderson (1975). It corresponds to the squared-time average of the local polarization, and is non-zero below T_f. It is not directly accessible by experimental determination, since it requires observation over an infinitely long period of time, but its susceptibility χ is accessible, at least for $T > T_f$, as are the decay functions $q(t)$. The definitions of these quantities and

appropriate references are given in table 11.1. Their behaviour has been given in terms of general models involving random interaction. These interactions include nearest-neighbour Ising spin (Edwards and Anderson 1975), infinite-range Ising spin (Sherrington and Kirkpatrick 1975), nearest-neighbour quadrupole interaction (Hammes *et al.* 1989) and the random-interaction Potts model (Carmesin and Binder 1988). The findings are summarized in table 11.2. Most of the predictions were taken from Binder and Young (1986); for results prior to 1986, we simply quote this paper. The predictions appear in the order given for the experimental investigation (section 2). Of particular interest are observed phenomena whose behaviour in glasses differs markedly from that in structural phases. A list of these is given in table 11.3. We note in particular that the linear susceptibility below T_c and the correlation length above T_c both diverge on approaching the critical temperature T_c of a structural phase transition and that they are nearly constant at the freezing temperature T_f of a glass transition. On the other hand, the renormalized spin-glass susceptibility χ_{SG}/χ^4 diverges at T_f, whereas the corresponding quantity χ_{FE}/χ^4 in a ferroelectric is constant around T_c. Different behaviour is also observed for the low-temperature heat capacity and for the dependence of T_c and T_f on fields. Some of these findings are also illustrated in figure 11.2. It should be noted that diverging spin-glass correlation lengths are discussed in the theoretical literature, but these quantities do not show up in scattering experiments as the usual correlation length.

On the basis of these clear-cut theoretical predictions, the distinction between a glassy state and an ordered structure should be straightforward. Yet many disputes have arisen on this very issue. What are the origins of this uncertainty?

From a theoretical point of view, the predictions are based on only one kind of interaction, that with zero average and non-zero variance, and on the absence of random fields. Introduction of non-zero-average interactions tends to enhance order, while random fields may destroy order. The influence of these features on observable quantities is studied in much less detail, and is often restricted to a particular compound (see section 11.4). Of equal importance are the difficulties in interpreting experimental results. First of all, samples are imperfect, they contain moments that may or may not interact randomly, and, depending on dilution, they may be subject to random fields arising from unintentionally diluted impurities and other defects. Furthermore, there are experimental difficulties. In particular, it is impossible to measure a static property like χ_s. If dispersion is present then $\chi(\omega)$ (given at the lowest accessible frequency, ω_0) may be a poor approximation for χ_s. Only if the dispersion curve $\chi(\omega)$ is measured in a range sufficient to determine the decay function can χ_s be obtained by means of extrapolation. Similarly, a lack of divergence of χ_s above T_c and of ξ_{FE} is not in itself sufficient grounds for the classification of a material as a glass, since these observables always remain finite in practice. Even in a perfect ferroelectric, below the Curie point, domains form that have their origin in surface-energy contributions and a finite-size effect. Any classification along the lines of orientational glass *versus* ferroelectric or ferroelastic is arbitrary to some degree. In our review of orientational glasses, we have included the following solids: those whose susceptibility behaves similarly to Parisi's prediction in the experimentally accessible range, those whose decay function is distinctly non-exponential, those whose correlation length stays well below that of the classical ferroelectric $BaTiO_3$, and those whose diffraction pattern shows signs of disorder.

We shall now illustrate how dramatic the role of imperfections can be. Let us introduce into a ferroelectric three dipolar impurities on sites forming a regular

Table 11.1. Definition of observables.

Name of observable				
By theoreticians	By experimentalists	Symbol	Definition	Reference
Linear susceptibility	Dielectric constant	χ, ε_α	$\varepsilon_\alpha = 1 + \varepsilon_0^{-1}\partial P_\alpha/\partial E_\alpha$	Lines and Glass (1977)
	Elastic compliance	χ, $s_{\alpha\beta}$	$s_{\alpha\beta} = \partial S_\alpha/\partial T_\alpha$	Mason (1950)
Spin-glass susceptibility	Nonlinear susceptibility	χ_{SG}, χ_{NL}	$\chi_{NL} = (\chi_{SG} - \frac{2}{3})(k_B T)^{-3}$	Binder and Young (1986), p. 865
Autocorrelation function	Decay function	$q(T)$	$q(t) = \lim_{t\to\infty} [\langle S_i(0)S_j(t)\rangle_t]_{av}$	
Edwards–Anderson order parameter		$q(l)$, q_{EA}	$q_{EA} = \lim_{N,t\to\infty} q(t)$	
Correlation length				
Ferromagnetic	Polar cluster size	ξ_d (d for dipole)		Carmesin and Binder (1988)
Quadrupolar	(Structural) domain size	ξ_d		
Correlation function		$g(R)$	$g(R) = e^{-R/\xi}$	Hammes *et al.* (1989)

Notation: $\varepsilon_0 = 8{\cdot}85\,\mathrm{pF\,m^{-1}}$; P_α, E_α, $S_{\alpha,\beta}$ and $T_{\alpha,\beta}$ are polarization, electric field, strain and stress respectively; subscripts α and β are vector and tensor component indices; S_i is the spin at site i; R is distance.

Table 11.2. List of theoretical predictions.

Observable	Prediction	Reference[a]
χ	$\begin{cases}(T - T_c)^{-1} & \text{for } T > T_f \\ \text{Constant} & \text{for } T < T_f\end{cases}$	P
T_f, T_c	$T_f = \mathrm{Var}(J)/k_B f_M, f_{SK} = 1, f_{Potts} = 0{\cdot}4, f_{EA} \sim 0$	BY (p. 876), CB
$T_f(0) - T_f(E)$	$(\frac{3}{4})^{1/3}\,\mathrm{Var}(J)/[p_0 E\,\mathrm{Var}(J)]^{2/3}$	BY (p. 871)
χ_{SG}	$(T - T_f)^{-\gamma}$	BY (p. 871)
$q(t)$	$\exp[-(\alpha t)^{\beta}]$, $\delta^{-2} t^{-3/2} \exp(-\delta^2 t)$, $\delta = (T - T_f)/T_f$	BY (pp. 880, 882)
	$t^{-\beta}$, $\beta(T, E)$ given	CB, O, B, SZ
$q(l)$	$1 - 3[T/\mathrm{Var}(J)]^3$	BY (p. 875)
ξ_α	Continuous at T_f	CB
ξ_d	$(T - T_f)^{-\delta}$	CB
C	Continuous at T_f, $\sim T^\alpha$ for $T \ll T_f$	BY (p. 909)

[a] BY, Binder and Young (1986), with page number; B, Bray (1989); CB, Carmesin and Binder (1988); EA, Edwards and Anderson (1985); O, Ogielski (1985, 1987); SK, Sherrington and Kirkpatrick (1975); SZ, Sompolinski and Zippelius (1981, 1982); P, Parisi (1979).

Table 11.3. Theoretical predictions that are different in glass and ordered-phase transitions.

Glass	Ordered phase
χ constant below T_f	$\chi \sim (T_c - T)^{-1}$ below T_c
χ_{SG}/χ^2 diverges at T_f	χ_{SG}/χ^4 constant
$q(t)$ non-exponential	$q(t) \sim e^{-\alpha t}$, $\alpha \sim \lvert T - T_c \rvert$
$\chi^*(\omega)$ non-Debye	$\chi^* = \chi_{(0)}/(1 - i\omega\alpha^{-1})$, Debye
$T_f(0) - T_f(E) \sim E^{2/3}$	$T_f(E) > T_f(0)$
ξ_d zero or weakly T-dependent	$\chi_d \sim (T - T_c)^{-\delta}$
$C \sim T^\alpha$, $\alpha \sim 1$, $T \ll T_f$	$C \sim T^3$, $T \ll T_f$

triangle. Near T_c, regardless of the size σ of the triangle and barring inversion symmetry of the sites, the ferroelectric correlation induces an effective interaction between the dipolar impurities. This triangular plaquette has two degenerate ground states unrelated by symmetry (see figure 11.1), and thus possesses the basic requirement for frustration. For large triangles, frustration will set in when $\xi_{FE} > \sigma$, i.e. very close to T_c, so the effect might go unnoticed. Small triangles, i.e. large impurity concentrations, may lead to glassy behaviour in systems that otherwise undergo structural phase transitions.

11.5. *Modelling glass properties by random fields*

Random fields can be produced by static defects, that is defects that either have no orientational degree of freedom or those whose orientation is frozen during a given experimental time. Random fields cannot induce a transition by themselves, but can modify the properties of an ordered phase that is induced by other independent, non-frustrated interactions. In particular, they may break the order locally and form domains of a supposedly homogeneous order-parameter distribution. At low concentration, they merely stabilize the domain structure observed naturally in ferroelectrics and ferroelastics, sometimes called the *domain state*. At higher concentrations,

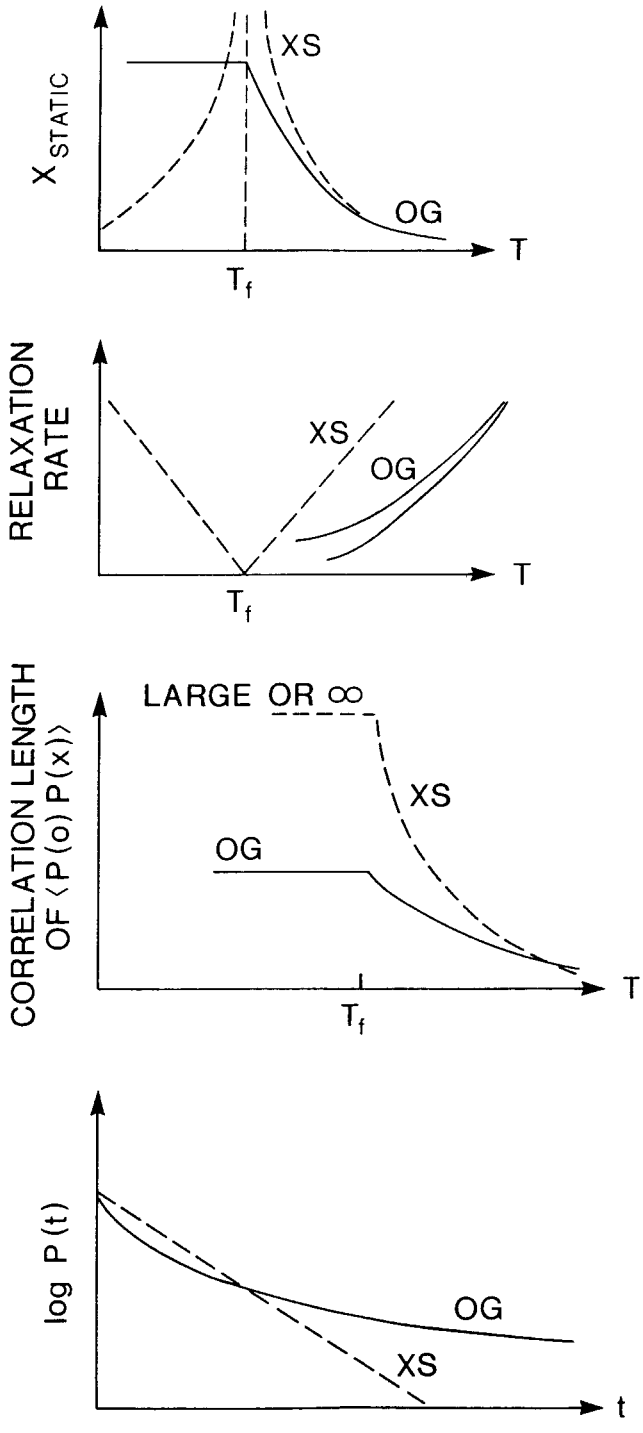

Figure 11.2. Theoretical predictions for the behaviour of the essential features in orientational glass (OG) and near structural phase transitions (XS).

they give rise to phenomena similar to those found in true glasses. We are aware of one particular instance where explicit predictions have been made on the basis of a general random-field model. The prediction concerns the decay function which, according to Fisher and Huse (1986), is given by $q(t) \sim \exp(-a \ln t)$. This decay is somewhat slower than arithmetical. It is, however, difficult to distinguish between some of the decay scenarios in random-bond glasses (Palmer *et al.* 1984). According to Binder and Young (1986), the consequences of random-field models are in need of clarification. We feel that random fields should be introduced when there is physical evidence of, or at least a plausible argument for, their presence. We offer two examples: KCN : Na, where Na has no moment, and $KTa_{1-x}Nb_xO_3$: Li, where, at least at some temperatures, Li is frozen whereas Nb and Ta are mobile. This brings us back to the physical origin of orientational interactions and its relation to sample properties.

The major shortcoming of general theories of glasses is the parametrization in terms of first and second moments, neither of which is related to its microscopic origin. Michel (1986) has attempted to account for the properties of the orientational glass KBr : CN on a microscopic basis. He expressed the forces exerted by halogens in terms of random static fields that break the quadrupolar order of CN observed in the high-concentration limit. His results were in line with those of Harris *et al.* (1976), but much more detailed. By parametrizing the field and the coupling of CN to the lattice, he was able to account for much of the experimental data on KBr : CN. In particular, he reproduced the phase diagram and the temperature-dependent elastic response nearly quantitatively. On applying the Debye transformation, he also accounted for elastic dispersion. Michel's model thus provides the most detailed and correct description of an orientational glass. Nevertheless, this model does not answer the question as to whether random interactions of quadrupolar nature between CN molecules describe the situation equally well, for example, in cases of particular systems or concentrations. If so, the assumption that alkali ions provide *static* fields would become unnecessary.

11.6. *Conclusion*

It is gratifying that general theories correctly describe essential experimental findings and that these features are different from those found at structural phase transitions. These features include the Parisi susceptibility (a Curie–Weiss-type rise of $\chi(T)$ up to a plateau below T_f), the spontaneous variance of the polarization below T_f, an essential divergence of the nonlinear susceptibility, the non-critical ferroelectric and ferroelastic correlations and non-critical arithmetical or similar decay functions of the polarization. It is less gratifying that very few reliable statements exist on the microscopic origin of the sources and the actual form of the interaction. This situation appears to be opposite to that in spin glasses, and is caused by the interaction of moments with the lattice. This interaction is important in orientational glasses, but may be neglected in spin glasses.

12. Orientational glass viewed as a structural instability. Outlook and conclusions

The determination of a wealth of experimental results (section 10) and the development of theoretical models (section 11) have taught us that a few simple concepts are at the basis of orientational-glass formation. These concepts include

Table 12.1. Classification of structural instabilities in terms of coupling parameters. The coupling between moments on random lattice is denoted by J, with cumulants $\bar{J}$ and $\mathrm{Var}(J)$; that between moments and the lattice by is denoted by K.

	$\bar{J}$ small $\mathrm{Var}(J)$ small	$\bar{J}$ large $\mathrm{Var}(J)$ small	J small $\mathrm{Var}(J)$ large	Interaction large, J undefined
K small	Supermagnet	Ferromagnet	Spin glass	Canonical glass
K medium	Super-para-electric Super-para-elastic	Ferroelectric Ferroelastic	Orientational glass	
K larger than J, $\mathrm{Var}(J)$	Glassy crystal	Glassy crystal	Glassy crystal	

moments occupying regular random lattice sites of a mixed single crystal; they imply interaction between these moments J, with a random character $\mathrm{Var}(J)$ and, possibly, an ordering component $\bar{J}$. Finally, these moments are coupled to the lattice by a coupling parameter formally denoted by K.

Pairwise interaction between particles increases their correlation and slows down their motion when T is lowered. Below a certain value of T_f, the original structure becomes unstable and a new state or configuration, sometimes called a phase, is formed. The actual form of the new state depends on the coupling parameters.

Non-interacting moments ($\bar{J} = \mathrm{Var}(J) = 0$) cannot form a glass, and are thus of interest only as a limiting case: with increasing coupling to the lattice, the moments change their magnitude and locally distort the lattice. In some cases, the lattice becomes disordered enough to take on a glassy aspect. The name 'glassy crystal' has been given to this phenomenon. We indicate this nomenclature in the first column of table 12.1. If moments are non-interacting on regular sites of the lattice then the ordering part of the interaction $\bar{J} \neq 0$, and an ordered structure may form. If K is small, as it is for some *magnetic* moments, their order does not affect the lattice, as in ferromagnets. For large K, the lattice as a whole distorts as in ferroelectrics and ferroelastics (see table 12.1, column 2). If the sites occupied by the moments are ideally random then the interaction between moments may be described by a $\mathrm{Var}(J)$ term. The presence of a small ordering term, however, does not alter the conclusions drawn. With increasing K, we encounter first the spin glass, then the orientational glass ('strong' for smaller K and 'weak' for larger K), and then for dominating K, we find the glassy crystal (table 12.1, column 3). Finally, when interactions are too large to allow a distinction between K and J, the approximation of pairwise interaction breaks down. No microscopic model exists for the canonical glass (table 12.1, column 4).

The orientational glass is thus situated between the spin glass and the glassy crystal, and can be approached from either side by reduction or enhancement of the parameter $\mathrm{Var}(J)/K$. The orientational glass is also situated between the ferroelectric and the canonical glass; it can be obtained by increasing $\mathrm{Var}(J)/\bar{J}$. To go from the orientational glass to the canonical glass, we imagine that every lattice site carries a moment and that the moment cannot arrange itself in an ordered structure owing to the way in which the sample was prepared. In this manner, $\mathrm{Var}(J)$ is further enhanced conceptionally, but the analogy breaks down at this point, since pairwise interaction is insufficient to describe a canonical glass.

We begin by considering the affinity of the orientational glass with its vertical neighbours in table 12.1 in more detail. The spin glass has a configuration with a multitude of nearly degenerate energy levels. Relaxation implies cascades through

these levels and is unending: the ground state cannot be reached. How does moment–lattice coupling influence relaxation? First, it introduces a local anisotropy to the moment. This sets a time scale τ_0 of hopping between equivalent local minima. When K increases, the density of energy levels is reduced more and more, and Arrhenius behaviour is resumed for $K > \mathrm{Var}(J)$. In the intermediate range, where K is comparable to $\mathrm{Var}(J)$, the Vogel–Fulcher law $\ln(\tau/\tau_0) = E_b/k_B(T - T_{VF})$ describes the experimental findings. The parameter $D = E_b/k_B T_{VF}$ assumes the role of the anisotropy parameter K. $D = 0$ indicates temperature-independent single-moment jumps in time τ_0 as assumed for spin glasses, where, for example, τ_0 denotes the time unit of one Monte Carlo step. $D = \infty$ indicates limiting Arrhenius behaviour as in the glassy crystal. Secondly, impurity–lattice coupling leads to distortion of the lattice. Such distortion is most pronounced at the temperature of glass formation and helps identify the nature of the low-temperature state from an experimental point of view.

Within the limit of low impurity–lattice coupling, orientational glasses are thus like spin glasses, and spin-glass theory can be successfully applied to such systems. Judging from the deviation from Arrhenius behaviour, the closest spin-glass analogues are probably $KTaO_3$:Na, $KTaO_3$:Li and KCl:OH. On doping with CN quadrupoles or heavy doping with Li, the lattices are much more distorted by the impurity. Spin-glass theory is less applicable to these cases; in particular, the Parisi susceptibility is not observed in such systems. Instead, relaxation splits into two branches with different characteristics.

The neighbours of orientational glasses on a horizontal line in table 12.1 are ordered instabilities and canonical glasses. We shall review their affinities with orientational glasses in turn. Much of the early research on spin and orientational glasses was inspired by critical phenomena at phase transitions leading to an ordering of the orientational (and magnetic) degrees of freedom. Near an ordering transition at T_c, $\chi_s \sim (T - T_c)^{\gamma}$, $\tau \sim (T - T_c)^{-\delta}$ and $\xi \sim (T - T_c)^{-\nu}$ all diverge with exponents related to scaling laws and depending on topological rather than physical features. In orientational glasses, these responses are less critical: χ_s diverges only hypothetically at $T < T_f$; τ and ξ are distributed such that their average diverges weakly at $T_{VF} \ll T_f$. It appears that the nonlinear susceptibility is the only macroscopic quantity of an orientational glass that diverges at T_f.

The distinction between critical and non-critical responses is not always straightforward. Even in the most perfect ferroelectric, the Curie–Weiss branches $\varepsilon \sim |T - T_c|^{-\gamma}$ are 'rounded' on both sides of T_c. Numerous sources report observations of rounding or smeared-out responses, and talk in terms of clusters, diffuse transitions and dirty ferroelectrics. Such observations merit completion by a search for dynamic, that is frequency-dependent, responses. They might allow a distinction between two possible microscopic origins of 'rounding'. The first implies static random fields that lead to a breakdown of long-range order in otherwise ferroelectric material, called a domain state. The second is dipolar-glass formation.

Starting from ordered systems, attempts have been made to treat mixed systems with what is called the virtual-crystal approximation. Except in the limit of large dilution, this approximation is unsuccessful, and has been superseded by random-field glass theory.

In canonical glasses, the relaxation rate is determined from the temperature-dependent viscosity. It is concluded that

$$\bar{\tau} \sim \exp[-E_b/k_B(T - T_0)],$$

which scales with configurational entropy S_c such that

$$\begin{aligned}\tau &= \tau_0 \exp(CT/S_c) \\ &= \tau_0 \exp[E_b/k_B(T - T_f)].\end{aligned}$$

The jump in the heat capacity and the cusp in the viscosity occur at the same temperature. The parameter $D = E_b/k_B T_f$ is a measure of the degeneracy of the energy landscape. Large D means that few levels are available; small D means large degeneracy. The D values of orientational glasses are in the range $10 < D < 20$, which is in the middle of the range of D values found for canonical glasses. The splitting of the relaxation distribution into an α and a β branch is apparently one of the more puzzling features in canonical glasses. Its analogy in orientational glasses and the possibility of associating π and $\frac{1}{2}\pi$ jumps with the α and β processes respectively should help to solve the puzzle. The same is true for the low-temperature anomalies in canonical glasses, which are related to wide distributions of two-level systems of unknown origin. In orientational glasses, such two-level systems are clearly associated with the tunnelling of the moment in the local potential provided by the surrounding lattice. Orientational glasses with strong lattice distortion and other near-canonical-glass behaviour are KBr : CN, KBr : Na and RADP.

We have profited from the impact that research on both phase transitions and spin glasses has had on orientational-glass research: the attempt to reconcile the apparent phase transition with the sluggish response in the metastable region has led to considerable insights. In particular, we have learned to live with these metastable states and to refrain from wasting too much thought on the inaccessible time range from 10^5 to 10^{17} s. This is true of analytical theorists who discard the slow part of the fluctuations from considerations leading to susceptibility. It is obviously true of specialists in Monte Carlo simulation, who have to end computations at a finite time, and for experimentalists facing the same limits. In addition, these workers have learned that extrapolation of the observed phenomena to infinite time leads to unphysical parameters. Restriction to the metastable state thus makes sense and is rewarded by the discovery of salient features, which have potential for application and which we will now summarize.

Metastable states are formed of coherent regions of dipolar or quadrupolar orientation with correlation lengths ranging in the tens to hundreds of Ångström units. They have strongly temperature- and field-dependent relaxation rates, and might thus be considered as units for storing and retrieving information. Such units have been simulated on a computer, which has led to the proposal of a novel fault-tolerant information-retrieval method (Kinzel 1987). What looks like a game in computer glass might be implemented in an orientational glass, provided that access to individual cells can be controlled. Local electric fields penetrating a solid are more likely to be generated than their magnetic counterparts.

Research on orientational glasses is likely to have an impact on the next complex structure: the canonical glass. In particular, we believe that connections between spin-glass theories and mode-coupling theories will be made and that important parameters such as T_g and the density of states may be predicted on a microscopic basis.

Acknowledgments

It is our great pleasure to acknowledge stimulating discussions with K. Binder, J. Joffrin, M. Maglione, K. H. Michel, R. O. Pohl and A. Rigamonti. Thanks are also

due to E. Courtens, H. Meyer, A. B. Harris and S. Washburn for their critical reading of the manuscript.

References

ABRAGAM, A., and BLEANEY, B., 1970, *Electron Paramagnetic Resonance of Transition Metal Ions* (Oxford: Clarendon).

ALBEN, A., WEAIRE, D., SMITH, J. E., and BRODSKY, M. H., 1975, *Phys. Rev.* B, **11,** 2271.

ALBERS, J., 1988, *Ferroelectrics*, **78,** 3.

ALBERS, J., ELSCHNER, S., KLÖPPERPIEPER A., and PETERSSON, J., 1984, *Ferroelectrics*, **55,** 101.

ALDERMAN, D. W., and COTTS, R. M., 1970, *Phys. Rev.* B, **1,** 2870.

AMIN, S., 1989, *Z. Phys.* B, **74,** 113.

AMIN, S., COWLEY, R. A., and COURTENS, E., 1987, *Z. Phys.* B, **67,** 229.

AMSTUTZ, L. I., MEYER, H., MYERS, S. M., and ROVER, D. C., 1969, *Phys. Rev.*, **181,** 589.

ANDERSON, P. W., HALPERIN, B. I., and VARMA, C. M., 1972, *Phil. Mag.*, **25,** 1.

ANDREWS, S. R., 1985, *J. Phys.* C, **18,** 1357.

ANSERMET, J. P., RYTZ, D., CHÂTELAIN, A., HÖCHLI, U. T., and WEIBEL, H. E., 1981, *J. Phys.* C, **14,** 4541.

ATOJI, M., 1971, *J. chem. Phys.*, **54,** 3514.

AZZINI, G. A., BANFI, G. P., GUILOTTO, E., and HÖCHLI, U. T., 1990, *Phys. Rev.* B (to be published).

BACON, G. E., 1962, *Neutron Diffraction* (Oxford: Clarendon).

BAIER, G., ENSS, C., and SCHICKFUS, M. VON, 1990, *Phys. Rev.* B (in press).

BANFI, G. P., LANZI, G., MILANI, P., and SAMOGGIA, G., 1988, *Ferroelectrics*, **80,** 245.

BANFI, G., P., GIULOTTO, E., SAMOGGIA, G., and HÖCHLI, U. T., 1989, *Europhys. Lett.*, **9,** 729.

BARRETT, C. S., and MEYER, L., 1965, *J. chem. Phys.*, **42,** 107.

BEDNORZ, J. G., and MÜLLER, K. A., 1984, *Phys. Rev. Lett.*, **52,** 2289.

BERRET, J. F., PELOUS, J., and VACHER, R., 1983, *J. Phys. Lett., Paris*, **44,** 433.

BERRET, J. F., DOUSSINEAU, P., LEVELUT, A., MEIßNER, M., and SCHÖN, W., 1985, *Phys. Rev. Lett.*, **55,** 2013.

BERRET, J. F., DOUSSINEAU, P., LEVELUT, A., and SCHÖN, W., 1988, *Z. Phys.* B, **70,** 485.

BERRET, J. F., COURTENS, E., MEISSNER, M., POHL, R. O., and WATSON, S. K., 1989a, *PHONONS 89, Proceedings of the Third International Conference on Phonon Physics and Sixth International Conference on Phonon Scattering in Condensed Matter*, Vol. 1, edited by S. Hunklinger, W. Ludwig and G. Weiss (Singapore: World Scientific), p. 597.

BERRET, J. F., FARKADI, A., BOISSIER, M., and PELOUS, J., 1989b, *Phys. Rev.* B, **39,** 13451.

BERSUKER, G. I., 1988, *Phys. Stat. Sol.*, **148,** 223.

BEYELER, H. U., 1972, *Phys. Stat. Sol.* (b), **52,** 419.

BEYELER, H. U., 1975, *Phys. Rev.* B, **11,** 3078.

BHATTACHARYA, S., NAGEL, S. R., FLEISHMAN, L., and SUSMAN, S., 1982, *Phys. Rev. Lett.*, **48,** 1267.

BIJVOET, J. M., and LELY, J. A., 1940, *Recl Trav. chim. Pays-Bas*, **59,** 908.

BINDER, K., and YOUNG, A. P., 1986, *Rev. mod. Phys.*, **58,** 801.

BIRGE, N. O., JEONG, Y. H., NAGEL, S. R., BHATTACHARYA, S., and SUSMAN, S., 1984, *Phys. Rev.* B, **30,** 2306.

BLINC, R., AILION, D. C., GÜNTHER, B., and ZUMER, S., 1986, *Phys. Rev. Lett.*, **57,** 2826.

BLINC, R., DOLINSEK, J., SCHMIDT, V. H., and AILION, D. C., 1988, *Europhys. Lett.*, **6,** 55.

BLINC, R., DOLINSEK, J., PIRC, R., TADIC, B., ZALAR, B., KIND, R., and LIECHTI, O., 1989, *Phys. Rev. Lett.*, **63,** 2248.

BOATNER, L. A., HÖCHLI, U. T., and WEIBEL, H., 1977a, *Helv. phys. Acta*, **50,** 620.

BOATNER, L. A., KAYAL, A. H., and HÖCHLI, U. T., 1977b, *Helv. phys. Acta*, **50,** 167.

BÖHMER, R., 1985, Diplomarbeit, Universität Mainz.

BÖHMER, R., and LOIDL, A., 1990a, *Phys. Rev.* B (in press).

BÖHMER, R., and LOIDL, A., 1990b, *Z. Phys.* B, **80,** 139.

BORSA, F., HÖCHLI, U. T., VAN DER KLINK, J. J., and RYTZ, D., 1980, *Phys. Rev. Lett.*, **45,** 1884.

BOSTOEN, C., and MICHEL, K. H., 1988, *Z. Phys.* B, **71,** 369.

BOSTOEN, C., and MICHEL, K. H., 1990 (to be published).

BOSTOEN, C., CODDENS, G., and WEGENER, W., 1989, *Physica* B, **156/157,** 350.

BOSTOEN, C., CODDENS, G., and WEGENER, W., 1990, *J. chem. Phys.*, **91,** 6337.
BÖTTCHER, C. J. F., and BORDEWIJK, P., 1978, *Theory of Electric Polarization*, Vol. II, second edition (Amsterdam: Elsevier).
BOUILLOT, J., SOUBEYROUX, J. L., and LÜTY, F., 1989, *Physica* B, **156/157,** 81.
BOURSON, P., GORCYCA, G., and DURAND, D., 1987, *Crystal Lattice Defects and Amorphous Materials*, **16,** 311.
BRAY, A. J., 1989, *Cooperative Dynamics in Complex Physical Systems*, Vol. 43, (Berlin: Springer-Verlag).
BROUT, R., 1965, *Phys. Rev. Lett.*, **14,** 176.
BRUCE, D. A., 1981, *J. Phys.* C, **14,** 5195.
BRÜCKNER, H. J., COURTENS, E., and UNRUH, H.-G., 1988, *Z. Phys.* B, **73,** 337.
BUFFAT, P., GANIÈRE, J. D., RAPPAZ, M., and RYTZ, D., 1986, *J. Crystal Growth*, **74,** 353.
BYER, N. E., and SACK, H. S., 1968, *Phys. Stat. Sol.*, **30,** 569.
CAHILL, D. G., and POHL, R. O., 1989, *Phys. Rev.* B, **39,** 10477.
CALKINS, M., BANKE, R., LI, X., and MEYER, H., 1986, *J. low Temp. Phys.*, **65,** 47.
CALVANI, P., and GLÄTTLI, H., 1984, *Solid St. Commun.*, **50,** 169.
CALVANI, P., and GLÄTTLI, H., 1985, *J. chem. Phys.*, **83,** 1822.
CALVANI, P., CASIERI, C., DE LUCA, F., and MARAVIGLIA, B., 1981, *Phys. Lett.* A, **86,** 490.
CALVANI, P., DE LUCA, F., and MARAVIGLIA, B., 1983, *Chem. Phys. Lett.*, **101,** 300.
CARMESIN, H. O., and BINDER, K., 1988, *J. Phys.* A, **21,** 4053.
CEVC, P., ZALAR, B., and BLINC, R., 1989, *Solid St. Commun.*, **70,** 461.
CHASE, L. L., LEE, E., PRATER, R. L., and BOATNER, L. A., 1982, *Phys. Rev.* B, **26,** 2759.
CIMINO, A., and PARRY, G. S., 1960, *Nuovo Cim.*, **19,** 971.
CIMINO, A., PARRY, G. S., and UBBELOHDE, A. R., 1959, *Proc. R. Soc. Lond.* A, **252,** 445.
CIVERA-GARCIA, E., KNORR, K., LOIDL, A., and HAUSSÜHL, S., 1987, *Phys. Rev.* B, **36,** 8517.
CORNAZ, P., HÖCHLI, U. T., and WEIBEL, H. E., 1981, *Helv. phys. Acta*, **54,** 226.
COURTENS, E., 1981, *J. Phys.* C, **14,** L37.
COURTENS, E., 1982, *J. Phys. Lett., Paris*, **43,** 199.
COURTENS, E., 1983, *Helv. phys. Acta*, **56,** 705.
COURTENS, E., 1984, *Phys. Rev. Lett.*, **52,** 69.
COURTENS, E., 1985, *Jap. J. appl. Phys.*, **24,** Suppl. 24-2, 70.
COURTENS, E., 1986, *Phys. Rev.* B, **33,** 2975.
COURTENS, E., 1987a, *Ferroelectrics*, **72,** 229.
COURTENS, E., 1987b, *Dynamics of Molecular Crystals*, edited by J. Lascombe (Amsterdam: Elsevier), p. 310.
COURTENS, E., and VACHER, R., 1987, *Phys. Rev.* B, **35,** 7271.
COURTENS, E., and VOGT, H., 1985, *J. Chim. phys.*, **82,** 317.
COURTENS, E., and VOGT, H., 1986, *Z. Phys.* B, **62,** 143.
COURTENS, E., ROSENBAUM, T. F., NAGLER, S. E., and HORN, P. M., 1984, *Phys. Rev.* B, **29,** 515.
COURTENS, E., HUARD, F., and VACHER, R., 1985, *Phys. Rev. Lett.*, **55,** 722.
COURTENS, E., VACHER, R., and DAGORN, Y., 1986, *Phys. Rev.* B, **33,** 7625.
COURTENS, E., VACHER, R., and DAGORN, Y., 1987, *Phys. Rev.* B, **36,** 318.
COURTENS, E., COWLEY, R. A., and GRIMM, H., 1988, *Ferroelectrics*, **78,** 275.
COWLEY, R. A., 1976, *Phys. Rev.* B, **13,** 4877.
COWLEY, R. A., RYAN, T., and COURTENS, E., 1985, *J. Phys.* C, **18,** 2793.
COWLEY, R. A., RYAN, T. W., and COURTENS, E., 1986, *Z. Phys.* B, **65,** 181.
DASGUPTA, C., MA, S. K., and HU, C. K., 1979, *Phys. Rev.* B, **25,** 6995.
DAVIS, T. G., 1972, *Phys. Rev.* B, **5,** 2530.
DE ALMEIDA, J. R. L., and THOULESS, D. J., 1978, *J. Phys.* A, **11,** 1983.
DE GOËR, A. M., SALCE, B., and BOATNER, L. A., 1980, *Phonon Scattering in Condensed Matter*, edited by H. J. Maris (New York: Plenum), p. 243.
DE LUCA, F., and MORAVIGLIA, B., 1983, *Chem. Phys. Lett.*, **101,** 1983.
DESCAMPS, M., and CAUCHETEUX, C., 1987, *J. Phys.* C, **20,** 5073.
DE RAEDT, B., and MICHEL, K. H., 1979, *Phys. Rev.* B, **19,** 767.
DE RAEDT, B., BINDER, K., and MICHEL, K. H., 1981, *J. chem. Phys.*, **75,** 2977.
DEVONSHIRE, A. F., 1936, *Proc. R. Soc. Lond.* A, **153,** 601.
DEVORET, M., and ESTÈVE, D., 1983, *J. Phys.* C, **16,** 1827.
DE YOREO, J. J., MEIßNER, M., POHL, R. O., ROWE, J. M., RUSH, J. J., and SUSMAN, S., 1983, *Phys. Rev. Lett.*, **51,** 1050.

De Yoreo, J. J., Pohl, R. O., and Burns, G., 1985, *Phys. Rev.* B, **32,** 5780.
De Yoreo, J. J., Knaak, W., Meißner, M., Pohl, R. O., 1986, *Phys. Rev.* B, **34,** 8828.
Dhar, D., Randeria, M., and Sethna, J. P., 1988, *Europhys. Lett.*, **5,** 485.
Diaz-Gongora, A., and Lüty, F., 1978, *Phys. Stat. Sol.* (b), **86,** 127.
Dissado, L. A., and Haidar, A., 1987, *J. Phys.* C, L929.
Dobrosavljevic, V., and Stratt, R., 1987, *Phys. Rev.* B, **36,** 8484.
Doussineau, P., Ziolkiewicz, S., and Höchli, U. T., 1989, *Europhys. Lett.*, **9,** 591.
Doverspike, M. A., Wu, M.-C., and Conradi, M. S., 1986, *Phys. Rev. Lett.*, **56,** 2284.
Dubus, M., Daudin, B., Salce, B., and Boatner, L. A., 1985, *Solid St. Commun.*, **55,** 759.
Dultz, W., 1974, *Solid St. Commun.*, **15,** 595.
Dultz, W., and Krause, H., 1978, *Phys. Rev.* B, **18,** 394.
Dultz, W., and Rehaber, E., 1983, *Phys. Rev.* B, **28,** 2114.
Dultz, W., Otto, H. H., Krause, H., and Buevoz, J. L., 1981, *Phys. Rev.* B, **24,** 1287.
Durand, D., and Lüty, F., 1977a, *Phys. Stat. Sol.* (b), **81,** 443.
Durand, D., and Lüty, F., 1977b, *Ferroelectrics*, **16,** 205.
Durand, D., Scarvada do Carmo, Anderson, A., and Lüty, F., 1980, *Phys. Rev.* B, **22,** 4005.
Edwards, S. F., and Anderson, P. W., 1975, *J. Phys.* F, **5,** 965.
Edwards, C. M., Zhou, D., and Sullivan, N. S., 1986, *Phys. Rev.* B, **34,** 6540.
Ehrhardt, K. D., Press, W., and Lefebvre, J., 1983, *J. chem. Phys.*, **78,** 1476.
Elliott, N., and Hastings, J., 1961, *Acta crystallogr.*, **14,** 1018.
Elschner, S., and Petersson, J., 1986a, *J. Phys.* C, **19,** 3373.
Elschner, S., and Petersson, J., 1986b, *Z. Naturforsch.* (a), **41,** 343.
Elschner, S., Knorr, K., and Loidl, A., 1985, *Z. Phys.* B, **61,** 209.
Elschner, S., Albers, J., Loidl, A., and Kjems, J. K., 1987, *Europhys. Lett.*, **4,** 1139.
Elschner, S., Wiotte, W., Petersson, J., and Blinc, R., 1990, Preprint.
Engstrom, H., Bates, J. B., and Boatner, L. A., 1980, *J. chem. Phys.*, **73,** 1073.
Ernst, R. M., Wu, L., Jeong, Y. H., Nagel, S. R., and Susman, S., 1988, *Phys. Rev.* B, **38,** 6246.
Estève, D., Sullivan, N. S., and Devoret, M., 1982a, *J. Phys. Lett., Paris*, **43,** 793.
Estève, D., Devoret, M., and Sullivan, N. S., 1982b, *J. Phys.* C, **15,** 5455.
Eucken, A., and Veith, H., 1936, *Z. phys. Chem.* B, **34,** 275.
Eucken, A., and Veith, H., 1937, *Z. phys. Chem.* B, **38,** 393.
Fehst, I., Böhmer, R., Ott, W., Loidl, A., Haussühl, and Bostoen, C., 1990, *Phys. Rev. Lett.*, **64,** 3139.
Feile, R., Loidl, A., and Knorr, K., 1982, *Phys. Rev.* B, **26,** 6875.
Fiory, A. T., 1971, *Phys. Rev.* B, **4,** 614.
Fischer, B., and Klein, M. W., 1976, *Phys. Rev. Lett.*, **37,** 756.
Fischer, B., and Klein, M. W., 1979, *Phys. Rev. Lett.*, **43,** 289.
Fisher, D. S., and Huse, D. A., 1986, *Phys. Rev. Lett.*, **56,** 1601.
Fisher, D. S., and Huse, D. A., 1987, *Phys. Rev.* B, **13,** 6841.
Folk, R., Iro, H., and Schwabl, F., 1976, *Z. Phys.* B, **25,** 69.
Folk, R., Iro, H., and Schwabl, F., 1979, *Phys. Rev.* B, **20,** 1229.
Fontaine, D., 1975, *C.r. hebd. Séanc. Acad. Sci. Paris*, **281,** 443.
Fossum, J. O., and Garland, C. W., 1988a, *Phys. Rev. Lett.*, **60,** 592.
Fossum, J. O., and Garland, C. W., 1988b, *J. chem. Phys.*, **89,** 7441.
Fossum, J. O., Wells, A., and Garland, C. W., 1988, *Phys. Rev.* B, **38,** 412.
Fousek, J., and Janovek, V., 1969, *J. appl. Phys.*, **40,** 135.
Fowler, P. W., and Klein, M. L., 1986, *J. chem. Phys.*, **85,** 3913.
Fröhlich, H., 1958, *Theory of Dielectrics*, second edition (Oxford: Clarendon).
Fulcher, G. S., 1925, *J. Am. Soc. Ceram.*, **8,** 339.
Fuoss, R., and Kirkwood, J. G., 1941, *J. Am. chem. Soc.*, **63,** 385.
Galam, S., 1990a, *J. appl. Phys.* **67,** 5979.
Galam, S., 1990b (to be published).
Garland, C. W., Kwiecien, J. Z., and Damien, J. C., 1982, *Phys. Rev.* B, **25,** 5818.
Garland, C. W., Fossum, J. O., and Wells, A., 1988, *Phys. Rev.* B, **38,** 5640.
Gash, P. W., 1983, *J. appl. Phys.*, **54,** 6900.
Gash, P., and Lüty, F., 1985, *J. Microscopy*, **140,** 351.
Geifman, I. N., 1981, *Soviet Phys. Solid St.*, **23,** 738.

GEIFMAN, I. N., SYTIKOV, A. A., KOLOMYTSEV, V. I., and KRULIKOVSKIL, B. K., 1981, *Soviet Phys. JETP*, **53,** 1212.
GHIVELDER, L., BASTOS, C. A. M., RIBEIRO, P. C., and VON DER WEID, J. P., 1985, *J. Phys.* C, **18,** 4037.
GLINCHUK, M. D., and SMOLYANINOV, A., 1990, *Phase Transitions* (in press).
GOPAL, E. S. R., 1966, *Specific Heats at Low Temperatures* (New York: Plenum).
GRANNAN, E. R., RANDERIA, M., and SETHNA, J. P., 1988, *Phys. Rev. Lett.*, **60,** 1402.
GRANT, M. B., and KLEIN, M. V., 1985, *Phys. Rev.* B, **32,** 1212.
GRIMM, H., 1989, *Dynamics of Disordered Materials*, edited by D. Richter, A. J. Dianoux, W. Petry and J. Texeira (Berlin: Springer-Verlag), p. 274.
GRIMM, H., and MARTINEZ, J., 1986, *Z. Phys.* B, **64,** 13.
GRIMM, H., PARLINSKI, K., SCHWEIKA, W., COURTENS, E., and AREND, H., 1986, *Phys. Rev.* B, **33,** 4969.
GRONDEY, S., PRAGER, M., PRESS, W., and HEIDEMANN, A., 1986, *J. chem. Phys.*, **85,** 2205.
GRONDEY, S., PRAGER, M., and PRESS, W., 1987, *J. chem. Phys.*, **86,** 6465.
GROSS, O. J., KANTER, I., and SOMPOLINSKI, H., 1985, *Phys. Rev. Lett.*, **55,** 304.
GRUBER, L., and KNORR, K., 1990, *Z. Phys.* B, **79,** 185.
GUINIER, A., 1956, *Théorie et technique de la radio-crystallographie*, Vol. 15 (Paris: Dunod), p. 7.
HAASE, D. G., PERELL, L. R., and SALEH, A. M., 1984, *J. low Temp. Phys.*, **55,** 283.
HALPERIN, B. I., and VARMA, C. M., 1976, *Phys. Rev.* B, **14,** 4030.
HAMMES, D., CARMESIN, H. O., and BINDER, K., 1989, *Z. Phys.* B, **76,** 115.
HANSKEPETITPIERRE, G., STERN, E. A., and YACOBY, Y., 1986, *J. Phys., Paris*, **47,** Suppl. 12, C8–675.
HARRIS, A. B., and MEYER, H., 1985, *Can. J. Phys.*, **63,** 3.
HARRIS, A. B., Lubensky, T. C., and CHEN, J. H., 1976, *Phys. Rev. Lett.*, **36,** 415.
HARRIS, A. B., WAHSBURN, S., and MEYER, H., 1983, *J. low Temp. Phys.*, **50,** 151.
HATTORI, T., ARAKI, H., NAKASHIMA, S., MITSUISHI, A., and TERAUCHI, H., 1987, *J. phys. Soc. Japan*, **56,** 781.
HATTORI, T., ARAKI, H., NAKASHIMA, S., MITSUISHI, A., and TERAUCHI, H., 1988, *J. phys. Soc. Japan*, **57,** 1127.
HAUSSÜHL, S., 1973, *Solid St. Commun.*, **13,** 147.
HAUSSÜHL, S., 1979, *Solid St. Commun.*, **32,** 181.
HAUSSÜHL, S., ECKSTEIN, J., RECKER, K., and WALLRAFEN, F., 1977, *Acta crystallogr.* A, **33,** 847.
HAVIGHURST, R., MACK, E., and BLAKE, F. C., 1925, *J. Am. chem. Soc.*, **47,** 29.
HAYASE, S., SAKASHITA, H., and TERAUCHI, H., 1985a, *Jap. J. appl. Phys.*, **24,** 985.
HAYASE, S., FUTAMURA, T., SAKASHITA, H., and TERAUCHI, H., 1985b, *J. phys. Soc. Japan*, **54,** 812.
HAYASE, S., KAMON, K., SAKASHITA, H., and TERAUCHI, H., 1986, *J. phys. Soc. Japan*, **55,** 2695.
HAYASE, T., SAKASHITA, H., and TERAUCHI, H., 1987, *Ferroelectrics*, **72,** 245.
HERZBERG, G., 1966, *Infrared and Raman Spectra of Polyatomic Molecules* (Princeton: Van Nostrand).
HESS, H. F., and DE CONDE, K., 1981, *Phys. Rev.* B, **24,** 7419.
HESSINGER, J., and KNORR, K., 1990, *Phys. Rev. Lett.*, **63,** 2749.
HILL, R. W., and RICKETSON, B. W. A., 1954, *Phil. Mag.*, **45,** 277.
HÖCHLI, U. T., 1976, *J. Phys.* C, **9,** L495.
HÖCHLI, U. T., 1981, *Ferroelectrics*, **35,** 17.
HÖCHLI, U. T., 1982, *Phys. Rev. Lett.*, **48,** 1494.
HÖCHLI, U. T., and BAERISWYL, D., 1984, *J. Phys.* C, **17,** 311.
HÖCHLI, U. T., and BOATNER, L. A., 1979, *Phys. Rev.* B, **20,** 266.
HÖCHLI, U. T., and MAGLIONE, M., 1989, *J. Phys. cond. Matter*, **1,** 2241.
HÖCHLI, U. T., and RIGAMONTI, A., 1983, *J. Phys.* C, **16,** 6321.
HÖCHLI, U. T., and TORRE, S., 1983, *Sintesi Ricerche e Lavori Riunione Annuale*, edited by F. de Pasquale, p. 1.34.
HÖCHLI, U. T., WEIBEL, H. E., and BOATNER, L. A., 1977, *Phys. Rev. Lett.*, **39,** 1158.
HÖCHLI, U. T., WEIBEL, H. E., and BOATNER, L. A., 1979, *J. Phys.* C, **12,** L563.
HÖCHLI, U. T., WEIBEL, H. E., and REHWALD, W., 1982, *J. Phys.* C, **15,** 6129.

HÖCHLI, U. T., RYTZ, D., VAN DER KLINK, J. J., and BORSA, F., 1984, *Solid St. Commun.*, **49,** 863.
HÖCHLI, U. T., KOFEL, P., and MAGLIONE, M., 1985, *Phys. Rev.* B, **32,** 4546.
HÖCHLI, U. T., GRYMASZEWSKI, E., and HUTTON, S. L., 1990, *J. Phys. cond. Matter*, **2,** 4259.
HÖCK, K. H., SCHAFER, R., and THOMAS, H., 1979, *Z. Phys.* B, **36,** 151.
HOHENBERG, P. C., and HALPERIN, B. I., 1977, *Rev. mod. Phys.*, **49,** 435.
HOLTZMARK, J., 1919, *Annln Phys., Leipzig*, **58,** 577.
HU, Z., WALTON, D., and VANDERWAL, J. J., 1988a, *Phys. Rev.* B, **38,** 10380.
HU, Z., VANDERWAL, J. J., and WALTON, D., 1988b, *Solid St. Commun.*, **66,** 99.
HU, Z., GARLAND, C. W., and WELLS, A., 1990, *Phys. Rev.* B (in press).
HUNKLINGER, S., 1977, *Advances in Solid State Physics*, Vol. 17, edited by J. Treusch (Braunschweig: Vieweg), p. 1.
HUNKLINGER, S., and SCHICKFUS, M. VON, 1981, *Topics in Current Physics*, Vol. 24 (Berlin: Springer-Verlag) p. 81.
HUSA, D., and DAUNT, J. G., 1978, *Phys. Lett.* A, **65,** 354.
HÜSER, D., WENGER, L. E., VAN DUYNEVELDT, A. J., and MYDOSH, J. A., 1983, *Phys. Rev.* B, **27,** 3100.
HÜSER, D., VAN DUYNEVELDT, A. J., NIEUWENHUYS, G. J., and MYDOSH, J. A., 1986, *J. Phys.* C, **19,** 3697.
IHM, J., 1984, *Phys. Rev.* B, **31,** 1674.
IIDA, S., and TERAUCHI, H., 1983, *J. phys. Soc. Japan*, **52,** 4044.
ISHIMOTO, H., NAGAMINE, K., KIMURA, Y., and KUMAGAI, H., 1973, *J. phys. Soc. Japan*, **35,** 300.
ISHIMOTO, H., NAGAMINE, K., KIMURA, Y., and KUMAGAI, H., 1976, *J. phys. Soc. Japan*, **40,** 312.
IVLIEV, M. P., and SAKHENKO, V. P., 1986, *Soviet Phys. Solid St.*, **28,** 356.
JAHN, H. A., and TELLER, E., 1937, *Proc. R. Soc. Lond.* A, **161,** 220.
JAMES, H. M., 1968, *Phys. Rev.*, **167,** 862.
JANSSEN, T., 1972, *Phys. kond. Materie*, **15,** 204.
JARVIS, J. F., MEYER, H., and RAMM, D., 1969, *Phys. Rev.*, **178,** 1416.
JONSCHER, A. K., 1983, *Dielectric Relaxation in Solids* (London: Chelsea Dielectric Press).
JULIAN, M., and LÜTY, F., 1977, *Ferroelectrics*, **16,** 201.
KADANOFF, L. P., GÖTZE, W., HAMBLEN, D., HECHT, R., LEWIS, E. A. S., PALCIAUSKAS, V. V., RAYL, M., and SWIFT, J., 1967, *Rev. mod. Phys.*, **39,** 395.
KAMIKATAHARA, W. A., LOONG, C. K., OSTROWSKI, G. E., and BOATNER, L. A., 1987, *Phys. Rev.* B, **35,** 223.
KÄNZIG, W., HART, H. R. JR, AND ROBERTS, S., 1964, *Phys. Rev. Lett.*, **13,** 543.
KENNEDY, N. S. J., and NEMES, R. J., 1980, *J. Phys.* C, **13,** 4841.
KINZEL, W., 1987, *Proceedings of Heidelberg Colloquium on Glassy Dynamics*, 1986, edited by J. L. van Hemmen and I. Morgenstern (*Lecture Notes in Physics*, Vol. 275) (Berlin: Springer), p. 529.
KLEE, H., and KNORR, K., 1990, *Phys. Rev.* B, **42,** 3152.
KLEE, H., CARMESIN, H. O., and KNORR, K., 1988, *Phys. Rev. Lett.*, **61,** 1855.
KLEEMANN, W., and SCHREMMER, H., 1989, *Phys. Rev.* B, **40,** 7428.
KLEEMANN, W., SCHÄFER, F. J., and RYTZ, D., 1985, *Phys. Rev. Lett.*, **54,** 2038.
KLEEMANN, W., KÜTZ, S., and RYTZ, D., 1987, *Europhys. Lett.*, **4,** 239.
KLEEMANN, W., KÜTZ, S., SCHÄFER, F. J., and RYTZ, D., 1988, *Phys. Rev.* B, **37,** 5856.
KLEIN, M. W., 1985, *Phys. Rev.* B, **31,** 1114.
KLEIN, M. W., 1989, *Phys. Rev.* B, **40,** 1918.
KLEIN, M. W., 1990 (to be published).
KLEIN, M., and BROUT, R., 1963, *Phys. Rev.*, **132,** 2412.
KLEIN, M. L., GODDARD, J. D., and BOUNDS, D. G., 1981, *J. chem. Phys.*, **75,** 3909.
KLENIN, M., 1983, *Phys. Rev.* B, **28,** 5199.
KLENIN, M. A., and PATE, S. F., 1981, *Physica* B + C, **107,** 185.
KNOP, K., and KÄNZIG, W., 1972a, *Solid St. Commun.*, **11,** 791.
KNOP, K., and KÄNZIG, W., 1972b, *Phys. kond. Materie*, **15,** 201.
KNOP, K., and KÄNZIG, W., 1974, *Helv. phys. Acta*, **46,** 889.
KNOPP, G., KNORR, K., LOIDL, A., and HAUSSÜHL, S., 1983, *Z. Phys.* B, **51,** 259.
KNORR, K., 1987, *Physica scripta* T, **19,** 531.
KNORR, K., 1990a, *Phys. Rev.* B, **41,** 3158.
KNORR, K., 1990b, *Mater. Sci. Engng* A, **127,** 265.

KNORR, K., and LOIDL, A., 1982, *Z. Phys.* B, **46,** 219.
KNORR, K., and LOIDL, A., 1985, *Phys. Rev.* B, **31,** 5387.
KNORR, K., and LOIDL, A., 1986, *Phys. Rev. Lett.*, **57,** 460.
KNORR, K., LOIDL, A., and KJEMS, J. K., 1985, *Phys. Rev. Lett.*, **55,** 2445.
KNORR, K., VOLKMANN, U. G., and LOIDL, A., 1986, *Phys. Rev. Lett.*, **57,** 2544.
KNORR, K., CIVERA-GARCIA, E., and LOIDL, A., 1987, *Phys. Rev.* B, **35,** 4998.
KOHLRAUSCH, R., 1847, *Annln Phys., Leipzig*, **12,** 393.
KOHLRAUSCH, R., 1854, *Poggendorffs Annln Phys.*, **91,** 179.
KOILLER, B., DAVIDOVICH, M. A., SCAVARDA DO CARMO, L. C., and LÜTY, F., 1984, *Phys. Rev.* B, **29,** 3586.
KONDO, Y., SCHOEMAKER, D., and LÜTY, F., 1979, *Phys. Rev.* B, **19,** 4210.
KUGEL, G., VOGT, H., KRESS, W., and RYTZ, D., 1984, *Phys. Rev.* B, **30,** 985.
KUGEL, G. E., MESLI, H., FONTANA, M. D., and RYTZ, D., 1988, *Phys. Rev.* B, **37,** 5619.
KWIECIEN, J. Z., LEUNG, R. C., and GARLAND, C. W., 1981, *Phys. Rev.* B, **23,** 4419.
Landolt–Börnstein, 1981, New Series, Group III, Vol. 16a, edited by K. H. Hellwege and A. M. Hellwege (Berlin: Springer).
LANZI, G., MILANI, P., SAMOGGIA, G., MAGLIONE, M., and HÖCHLI, U. T., 1987, *Phys. Rev.* B, **36,** 1233.
LASJAUNIAS, J. C., and LÖHNEYSEN, H. VON, 1981, *Solid St. Commun.*, **40,** 755.
LAWLESS, W. N., 1976, *Phys. Rev.* B, **14,** 134.
LAWLESS, W. N., and SCHMIDT, V. H., 1985, *Jap. J. appl. Phys.*, **24,** Suppl. 24-2, 952.
LAWLESS, W. N., RYTZ, D., and HÖCHLI, U. T., 1981, *Ferroelectrics*, **38,** 809.
LEE, E., CHASE, L. L., and BOATNER, L. A., 1985, *Phys. Rev.* B, **31,** 1438.
LEHNDORFF, M., 1986, Thesis Nr 129, Universität Konstanz, see p. 90.
LÉVY, L. P., and OGIELSKI, A. T., 1986, *Phys. Rev. Lett.*, **57,** 3288.
LEWIS, L. J., and KLEIN, M. L., 1986, *Phys. Rev. Lett.*, **57,** 2698.
LEWIS, L. J., and KLEIN, M. L., 1987a, *Phys. Rev. Lett.*, **59,** 1887.
LEWIS, L. J., and KLEIN, M. L., 1987b, *J. phys. Chem.*, **91,** 4990.
LEWIS, L. J., and KLEIN, M. L., 1989a, *Phys. Rev.* B, **40,** 7904.
LEWIS, L. J., and KLEIN, M. L., 1989b, *Phys. Rev.* B, **40,** 4877 and 7080.
LI, X., MEYER, H., and BERLINSKI, A. J., 1988, *Phys. Rev.* B, **37,** 3216.
LIDDELL, H. M., 1981, *Computer-Aided Techniques for the Design of Multilayer Filters* (Bristol: Adam Hilger).
LIN, Y., and SULLIVAN, N. S., 1988, *Phys. Rev.* B, **38,** 5158.
LIN, Y., EDWARDS, C. M., and SULLIVAN, N. S., 1986, *Phys. Lett.* A, **118,** 309.
LINES, M. E., and GLASS, A. M., 1977, *Principles and Application of Ferroelectrics, and Related Materials* (Oxford: Clarendon).
LIU, S. B., and CONRADI, M. S., 1984, *Solid St. Commun.*, **42,** 177.
LOIDL, A., 1985, *J. Chim. phys.*, **82,** 305.
LOIDL, A., 1989, *Ann. Rev. phys. Chem.*, **40,** 29.
LOIDL, A., and KNORR, K., 1986, *Ann. N.Y. Acad. Sci.*, **484,** 121.
LOIDL, A., FEILE, R., KNORR, K., RENKER, B., DAUBERT, J., DURAND, D., and SUCK, J., 1980, *Z. Phys.* B, **38,** 253.
LOIDL, A., FEILE, R., and KNORR, K., 1981, *Z. Phys.* B, **42,** 143.
LOIDL, A., FEILE, R., and KNORR, K., 1982, *Phys. Rev. Lett.*, **48,** 1263.
LOIDL, A., HAUSSÜHL, S., and KJEMS, J. K., 1983a, *Z. Phys.* B, **50,** 187.
LOIDL, A., KNORR, K., FEILE, R., and KJEMS, J. K., 1983b, *Phys. Rev. Lett.*, **51,** 1054.
LOIDL, A., FEILE, R., KNORR, and KJEMS, J. K., 1984, *Phys. Rev.* B, **29,** 6052.
LOIDL, A., SCHRÄDER, T., BÖHMER, R., KNORR, K., KJEMS, J. K., and BORN, R., 1986, *Phys. Rev.* B, **34,** 1238.
LOIDL, A., KNORR, K., ROWE, J. M., and MCINTYRE, G. F., 1988, *Phys. Rev.* B, **37,** 389.
LOIDL, A., SCHRÄDER, T., KNORR, K., BÖHMER, R., MERTZ, B., MCINTYRE, G. F., VOGT, T., MUTKA, H., MÜLLNER, M., JEX, H., and HAUSSÜHL, S., 1989, *Z. Phys.* B, **75,** 81.
LONG, D. A., 1976, *Raman Spectroscopy* (New York: McGraw-Hill).
LOPONEN, M. T., DYNES, R. C., NARAYANAMURTI, V., and GARNO, J. P., 1980, *Phys. Rev. Lett.*, **45,** 457.
LOPONEN, M. T., DYNES, R. C., NARAYANAMURTI, V., and GANRO, J. P., 1982, *Phys. Rev.* B, **25,** 1161.
LUTTINGER, J. M., and TISZA, L., 1946, *Phys. Rev.*, **70,** 954.

LÜTY, F., 1974, *Phys. Rev.* B, **10,** 3667, 3677.
LÜTY, F., 1981, *Defects in Insulating Crystals*, edited by V. M. Tuchkevich and K. K. Shvarts (Berlin: Springer), p. 69.
LÜTY, F., and ORTIZ-LOPEZ, J., 1983, *Phys. Rev. Lett.*, **50,** 1289.
LYONS, K. B., FLEURY, P. A., and RYTZ, D., 1986, *Phys. Rev. Lett.*, **57,** 2207.
LYONS, K. B., FLEURY, P. A., NEGRAN, T. J., and CARTER, H. L., 1987, *Phys. Rev.* B, **36,** 2465.
MAEDA, M., 1989, *Ferroelectrics*, **7,**
MAGLIONE, M., 1987, Ph.D. Thesis, EPF Lausanne.
MAGLIONE, M., HÖCHLI, U. T., and JOFFRIN, J., 1986, *Phys. Rev. Lett.*, **57,** 436.
MAGLIONE, M., ROD, S., and HÖCHLI, U. T., 1987, *Europhys. Lett.*, **4,** 631.
MAGLIONE, M., JOFFRIN, J., HÖCHLI, U. T., and PELOUS, J., 1988, *J. Phys., Paris*, **49,** 959.
MAGLIONE, M., HÖCHLI, U. T., JOFFRIN, J., and KNORR, K., 1989, *J. Phys. cond. Matter*, **1,** 1527.
MAHANTI, S. D., MURRAY, P., and KEMENY, G., 1985, *Phys. Rev.* B, **32,** 3263.
MANDELL, M., 1974, *J. chem. Phys.*, **60,** 4880.
MARTINEZ, J. L., AGULLO-RUEDA, F., and SCHMIDT, V. H., 1987, *Ferroelectrics*, **76,** 23.
MASON, W. P., 1950, *Piezoelectric Crystals, and Their Application to Ultrasonics* (New York: Van Nostrand).
MATHO, K., 1979, *J. low temp. Phys.*, **35,** 165.
MATSUO, T., SUGA, H., and SEKI, S., 1968, *Bull. chem. Soc. Japan*, **41,** 583.
MATSUO, T., KISHIMOTO, I., SUGA, H., and LÜTY, F., 1986, *Solid St. Commun.*, **58,** 177.
MATSUSHITA, E., and MATSUBARA, T., 1985a, *J. phys. Soc. Japan*, **54,** 1161.
MATSUSHITA, E., and MATSUBARA, T., 1985b, *J. phys. Soc. Japan*, **54,** 2032.
MATSUSHITA, E., and MATSUBARA, T., 1986, *J. phys. Soc. Japan*, **55,** 666.
MAYER, A. P., and COWLEY, R. A., 1988a, *J. Phys.* C, **21,** 4827.
MAYER, A. P., and COWLEY, R. A., 1989b, *J. Phys* C, **21,** 4835.
MEIßNER, M., and SPITZMANN, K., 1981, *Phys. Rev. Lett.*, **46,** 265.
MEIßNER, M., KNAAK, W., SETHNA, J. P., CHOW, K. S., and DE YOREO, J. J., 1985, *Phys. Rev.* B, **32,** 6091.
MERLIN, R., 1988a, *IEEE J. quant. Electron.*, **24,** 1791.
MERLIN, R., 1988b, *J. Phys.* C, **21,** 6219.
MERTZ, B., and LOIDL, A., 1985, *J. Phys.* C, **18,** 2843.
MERTZ, B., and LOIDL, A., 1987, *Europhys. Lett.*, **4,** 583.
MERTZ, B., BÖHMER, R., EISELE, B., and LOIDL, A., 1990a, *Z. Phys.* B, **79,** 431.
MERTZ, B., BÖHMER, R., LOIDL, A., BERRET, J. F., MEIßNER, M., and KNAACK, W., 1990b, *Phonons 89*, edited by S. Hunklinger and W. Ludwig (Singapore: World Scientific), p. 585.
MERTZ, B., BERRET, J. F., BÖHMER, R., LOILD, A., MEIßNER, M., and KNAAK, W., 1990c, *Phys. Rev.* B (in the press).
MESSER, C. E., and ZIEGLER, W. T., 1941, *J. Am. chem. Soc.*, **63,** 2610, 2703.
MEYER, H., and WASHBURN, S., 1984, *J. low temp. Phys.*, **57,** 31.
MICHEL, K. H., 1986, *Phys. Rev. Lett.*, **57,** 2188.
MICHEL, K. H., 1987a, *Phys. Rev.* B, **35,** 1405.
MICHEL, K. H., 1987b, *Phys. Rev.* B, **35,** 1414.
MICHEL, K. H., 1987c, *Z. Phys.* B, **68,** 259.
MICHEL, K. H., and NAUDTS, J., 1977a, *Phys. Rev. Lett.*, **39,** 212.
MICHEL, K. H., and NAUDTS, J., 1977b, *J. chem. Phys.*, **67,** 547.
MICHEL, K. H., and NAUDTS, J., 1978, *J. chem. Phys.*, **68,** 216.
MICHEL, K. H., and ROWE, J. M., 1980, *Phys. Rev.* B, **22,** 1417.
MICHEL, K. H., and THEUNS, T., 1989, *Phys. Rev.* B, **40,** 5761.
MIGONI, R. L., BILZ, H., and BÄUERLE, D., 1976, *Phys. Rev. Lett.*, **37,** 1155.
MIURA, Y., TAKASHIGE, M., TERAUCHI, H., TAKANO, Y., ISHIMOTO, H., and OGAWA, S., 1985, *Jap. J. appl. Phys.*, **24,** Suppl. 24-2, 950.
MIURA, Y., TAKASHIGE, M., TERAUCHI, H., SUGIYAMA, S., and MAYIMA, T., 1987, *Jap. J. appl. Phys.*, **26,** Suppl. 26-3, 795.
MORIYA, K., MATSUO, T., SUGA, H., and LÜTY, F., 1984, *Proceedings of the International Conference on Defects in Insulating Crystals*, p. 329.
MORIYA, K., MATSUO, T., SUGA, H., and TERAUCHI, H., 1985, *Jap. J. appl. Phys.*, **24,** Suppl. 24-2, 955.

MOY, D., POTTER, R. C., and ANDERSON, A. C., 1983, *J. low Temp. Phys.*, **52,** 115.
MOY, D., DOBBS, J. N., and ANDERSON, A. C., 1984, *Phys. Rev.* B, **29,** 2160.
MYDOSH, J. A., and NIEUWENHUYS, J. G., 1980, *Ferromagnetic Materials*, edited by E. P. Wohlfarth (New York: North-Holland), p. 71.
NARAYANAMURTI, V., and POHL, R. O., 1970, *Rev. mod. Phys.*, **42,** 201.
NICHOLLS, C. I., YADON, L. N., HAASE, D. G., and CONRADI, M. S., 1987, *Phys. Rev. Lett.*, **59,** 1317.
NICKLOW, R. M., CRUMMETT, W. P., MOSTOLLER, M., and WOOD, R. F., 1980, *Phys. Rev.* B, **22,** 3039.
NISHIHATA, Y., SAKASHITA, H., and TERAUCHI, H., 1985, *Jap. J. appl. Phys.*, **24,** Suppl. 24-2, 961.
NÜCKER, N., KNORR, K., and JEX, H., 1978, *J. Phys.* C, **11,** 1.
OGIELSKI, A. T., 1985, *Phys. Rev.* B, **32,** 3784.
OGIELSKI, A. T., 1987, *Proceedings of Heidelberg Colloquium on Glassy Dynamics, 1986*, edited by J. L. van Hemmen and I. Morgenstern (*Lecture Notes in Physics*, Vol. 275) (Berlin: Springer), p. 190.
OMARY, R., PRÉJEAN, J. J., and SOULETIE, J., 1983, *J. Phys., Paris*, **44,** 1069.
ONO, Y., HIKITA, T., and IKEDA, T., 1988, *Ferroelectrics*, **79,** 327.
ORTIZ-LOPEZ, J., 1983, Thesis, University of Utah.
ORTIZ-LOPEZ, J., and LÜTY, F., 1988, *Phys. Rev.* B, **37,** 5452, 5461.
PALMER, R. G., STEIN, D. L., ABRAHAMS, E., and ANDERSON, P. W., 1984, *Phys. Rev. Lett.*, **53,** 958.
PANGILINAN, G., GUELACHVILI, G., SOORYAKUMAR, R., NARAHARI RAO, K., and TIPPING, R. H., 1989, *Phys. Rev.* B, **39,** 2522.
PAPPA, C., HAMMAN, J., and JACOBINI, C., 1985, *J. Phys., Paris*, **46,** 637.
PARISI, G., 1979, *Phys. Rev. Lett.*, **43,** 1754.
PARLINSKI, K., and GRIMM, H., 1986, *Phys. Rev.* B, **33,** 4864.
PARLINSKI, K., and GRIMM, H., 1988, *Phys. Rev.* B, **37,** 1925.
PARRY, G. S., 1962, *Acta crystallogr.*, **15,** 596, 601.
PARSONAGE, N. G., and STAVELY, L. A. K., 1987, *Disorder in Crystals* (Oxford: Clarendon), p. 311.
PECHENYI, A. P., ANTIMIROVA, T. V., GLINCHUCK, M. D., and VUGMEISTER, B. E., 1988, *Soviet Phys. Solid St.*, **30,** 1890.
PERESSINI, P. P., HARRISON, J. P., and POHL, R. O., 1969, *Phys. Rev.*, **180,** 926.
PHILLIPS, W. A., 1972, *J. low Temp. Phys.*, **7,** 351.
PIRC, R., and VILFAN, I., 1981, *Solid St. Commun.*, **39,** 181.
PIRC, R., TADIC, B., and BLINC, R., 1985, *Z. Phys.* B, **61,** 69.
PIRC, R., TADIC, B., and BLINC, R., 1987, *Phys. Rev.* B, **36,** 8607.
POTTER, R. C., and ANDERSON, A. C., 1981, *Phys. Rev.* B, **24,** 677, 4826.
PRATER, R. L., CHASE, L. L., and BOATNER, L. A., 1981a, *Solid St. Commun.*, **40,** 697.
PRATER, R. L., CHASE, L. L., and BOATNER, L. A., 1981b, *Phys. Rev.* B, **23,** 221.
PRATER, R. L., CHASE, L. L., and BOATNER, L. A., 1981c, *Phys. Rev.* B, **23,** 5904.
PRELOVSEK, P., and BLINC, R., 1982, *J. Phys.* C, **15,** L985.
PRESS, W., 1981, *Single Particle Rotations in Molecular Crystals* (Berlin: Springer).
PRESS, W., JANIK, B., and GRIMM, H., 1982, *Z. Phys.* B, **49,** 9.
PRESS, W., DAMAY, P., LECLERCQ, F., and CHIEUX, P., 1989, *J. chem. Phys.*, **91,** 1167.
PRICE, D. L., ROWE, J. M., RUSH, J. J., PRINCE, E., HINKS, D. G. and SUSMAN, S., 1972, *J. chem. Phys.*, **56,** 3697.
RANDERIA, M., 1987, Thesis, Cornell University.
RANDERIA, M., and SETHNA, J. P., 1988, *Phys. Rev.* B, **38,** 12607.
RANDERIA, M., and SETHNA, J. P., and PALMER, R. G., 1985, *Phys. Rev. Lett.*, **54,** 1321.
REHWALD, W., and ROSINELLI, M., 1977, *Phys. Stat. sol.* (a), **42,** 699.
RIGAMONTI, A., 1984, *Adv. Phys.*, **33,** 115.
RIGAMONTI, A., and TORRE, S., 1985, *Solid St. Commun.*, **56,** 619.
RIGAMONTI, A., and TORRE, S., 1986, *Phys. Rev.* B, **33,** 2024.
ROD, S., BORSA, F., and VAN DER KLINK, J. J., 1988, *Phys. Rev.* B, **38,** 2267.
ROTHER, H. J., ALBERS, J., KLÖPPERPIEPER, A., and MÜSER, H. E., 1985, *Jap. J. appl. Phys.*, **24,** Suppl. 24-2, 384.
ROWE, J. M., HINKS, D. G., PRICE, D. L., SUSMAN, S., and RUSH, J. J., 1973, *J. chem. Phys.*, **58,** 2039.

ROWE, J. M., RUSH, J. J., VEGELATOS, N., PRINCE, D. L., HINKS, D. G., and SUSMAN, S., 1975, *J. chem. Phys.*, **162,** 4551.
ROWE, J. M., RUSH, J. J., and PRINCE, E., 1977, *J. chem. Phys.*, **66,** 5147.
ROWE, J. M., RUSH, J. J., CHESSER, N. J., HINKS, D. L., and SUSMAN, S., 1978a, *J. chem. Phys.*, **68,** 4320.
ROWE, J. M., RUSH, J. J., CHESSER, N. J., MICHEL, K. H., and NAUDTS, J., 1978b, *Phys. Rev. Lett.*, **40,** 455.
ROWE, J. M., RUSH, J. J., HINKS, D. G., and SUSMAN, G., 1979, *Phys. Rev. Lett.*, **43,** 1158.
ROWE, J. M., RUSH, J. J., SHAPIRO, S. M., HINKS, D. G., and SUSMAN, S., 1980, *Phys. Rev.* B, **21,** 4863.
ROWE, J. M., RUSH, J. J., and SUSMAN, S., 1983, *Phys. Rev.* B, **28,** 3506.
ROWE, J. M., RUSH, J. J., and LÜTY, F., 1984, *Phys. Rev.* B, **29,** 2168.
ROWE, J. M., BOUILLOT, J., RUSH, J. J., and LÜTY, F., 1986, *Physica* B, **136,** 498.
RUPPRECHT, G., and WINTER, W. H., 1966, *Phys. Rev.*, **155,** 1019.
RUSSELL, S. D., and MERLIN, R., 1986, *Phys. Rev.* B, **33,** 1871.
RYTZ, D., 1983, Dissertation No. 475, EPF Lausanne.
RYTZ, D., and SCHEEL, H. J., 1982, *J. Crystal Growth*, **59,** 468.
RYTZ, D., HÖCHLI, U. T., and BILZ, H., 1980, *Phys. Rev.* B, **22,** 359.
RYTZ, D., CHÂTELAIN, A., and HÖCHLI, U. T., 1983, *Phys. Rev.* B, **27,** 6830.
SACK, H. S., and MORIARTY, M. C., 1965, *Solid St. Commun.*, **3,** 93.
SAHU, D., and MAHANTI, S. D., 1982a, *Phys. Rev. Lett.*, **48,** 936.
SAHU, D., and MAHANTI, S. D., 1982b, *Phys. Rev.* B, **26,** 2981.
SAINT-PAUL, M., and GILCHRIST, J. LE G., 1986, *J. Phys.* C, **19,** 2091.
SAINT-PAUL, M., NAVA, R., and JOFFRIN, J., 1984, *Phonon Scattering in Condensed Matter*, edited by W. Eisenmenger (Berlin: Springer-Verlag), p. 252.
SALCE, B., DE GOËR, A. M., and BOATNER, L. A., 1981, *J. Phys., Paris*, Suppl. 12, C6–424.
SAMARA, G. A., 1984, *Phys. Rev. Lett.*, **53,** 298.
SAMARA, G. A., 1985, *Jap. J. appl. Phys.*, **24,** Suppl. 24-2, 80.
SAMARA, G. A., 1988, *Physica* B, **150,** 179.
SAMARA, G. A., and SCHMIDT, V. H., 1986, *Phys. Rev.* B, **34,** 2035.
SAMARA, G. A., and TERAUCHI, H., 1987, *Phys. Rev. Lett.*, **59,** 347.
SANTOS, M. L., AZEVEDO, J. C., ALMEIDA, A., CHEVES, M. R., PIRES, A. R., MÜSER, H. E., and KLÖPPERPIEPER, A., 1990, *Ferroelectrics*, **108,** 363.
SATIJA, S. K., and WANG, C. H., 1978, *Solid St. Commun.*, **28,** 617.
SCHICKFUS, M. VON, 1982, *Coherence, and Energy Transfer in Glasses*, edited by P. A. Fleury and B. Golding, *NATO Conference Series VI, Materials Science*, Vol. 9, p. 69.
SCHMIDT, V. H., 1987, *Ferroelectrics*, **72,** 157.
SCHMIDT, V. H., 1988a, *J. molec. Struct.*, **177,** 257.
SCHMIDT, V. H., 1988b, *Ferroelectrics*, **78,** 207.
SCHMIDT, V. H., WAPLAK, S., HUTTON, S., and SCHNAKENBERG, P., 1984, *Phys. Rev.* B, **30,** 2795.
SCHMIDT, V. H., WANG, J. T., and SCHNAKENBERG, P., 1985, *Jap. J. appl. Phys.*, **24,** Suppl. 24-2, 944.
SCHRÄDER, T., LOIDL, A., KNORR, K., and KJEMS, J. K., 1985, *Phonon Physics*, edited by J. Kollar, N. Kroo, N. Menyhard and T. Siklos (Singapore: World Scientific), p. 111.
SCHRÄDER, T., LOIDL, A., and VOGT, T., 1989a, *Phys. Rev.* B, **39,** 6186.
SCHRÄDER, T., LOIDL, A., VOGT, T., and FRANK, V., 1989b, *Physica* B, **156/157,** 195.
SCHRÄDER, T., MÜLLER, M., and LOIDL, A., 1989c, *Dynamics of Disordered Materials*, edited by D. Richter, A. J. Dianoux, W. Petry and J. Texeira (Berlin: Springer), p. 256.
SCHRÄDER, T., LOIDL, A., and VOGT, T., 1990a, *Ferroelectrics*, **106,** 181.
SCHRÄDER, T., LOIDL, A., and VOGT, T., 1990b, *Z. Phys.* B, **79,** 423.
SCHRÄDER, T., LOIDL, A., and VOGT, T., 1990c, *Phonons 89*, edited by S. Hunklinger, W. Ludwig and G. Weiss (Singapore: World Scientific), p. 594.
SCHREMMER, H., KLEEMANN, W., and RYTZ, D., 1989, *Phys. Rev. Lett.*, **62,** 1896.
SCHWEIZER, R., WASHBURN, S., and MEYER, H., 1979, *J. low Temp. Phys.*, **37,** 309.
SCOTT, T. A., 1976, *Phys. Rep.*, **27,** 89.
SEKIMOTO, K., YOSHIMITSU, K., and MATSUBARA, T., 1982, *Solid St. Commun.*, **44,** 979.
SELKE, W., and COURTENS, E., 1986, *Ferroelectrics Lett.*, **5,** 173.
SETHNA, J. P., 1986a, *Phys. Today*, **39,** 20.
SETHNA, J. P., 1986b, *Ann. N.Y. Acad. Sci.*, **484,** 130.

SETHNA, J. P., and CHOW, K. S., 1985, *Phase Transitions*, **5,** 317.
SETHNA, J. P., NAGEL, S. R., and RAMAKRISHNAN, T. V., 1984, *Phys. Rev. Lett.*, **53,** 2489.
SEWARD, W. D., and NARAYANAMURTY, V., 1966, *Phys. Rev.*, **148,** 463.
SEWARD, W. D., REDDY, V., and SHANER, J. W., 1972, *Solid St. Commun.*, **11,** 1569.
SHERRINGTON, D., and KIRKPATRICK, S., 1975, *Phys. Rev. Lett.*, **35,** 1972.
SHIMADA, T. MATSUO, T., SUGA, H., and LÜTY, F., 1986, *J. chem. Phys.*, **85,** 3530.
SILVERA, I. S., 1980, *Rev. mod. Phys.*, **52,** 393.
SLAK, J., KIND, R., BLINC, R., COURTENS, E., and ZUMER, S., 1984, *Phys. Rev.* B, **30,** 85.
SLATER, J. C., 1941, *J. chem. Phys.*, **9,** 16.
SLATER, J. C., 1950, *Phys. Rev.*, **78,** 748.
SMOLENSKY, G. A., NADOLINSKAYA, E. G., YUSHIN, N. K., and SHILNIKOV, A. V., 1986, *Ferroelectrics*, **69**, 275.
SOMMER, D., KLEEMANN, W., LEHNDORFF, M., and DRANSFELD, K., 1989, *Solid St. Commun.*, **72,** 731.
SOMPOLINSKI, H., 1981, *Phys. Rev. Lett.*, **47,** 935.
SOMPOLINSKI, H., and ZIPPELIUS, A., 1981, *Phys. Rev. Lett.*, **47,** 359.
SOMPOLINSKI, H., and ZIPPELIUS, A., 1982, *Phys. Rev.* B, **25,** 6860.
SOULETIE, J., and TOURNIER, R., 1969, *J. low temp. Phys.*, **1,** 95.
STACCHIOTTI, M. G., and MIGONI, R. L., 1990, *J. Phys. cond. Matter*, **2,** 4341.
STANKOWSKI, J., TRYBULA, Z., and SCHMIDT, V. H., 1988, *Ferroelectrics*, **79,** 351.
STEPHEN, M., and CWILICH, G., 1987, *Phys. Rev. Lett.*, **59,** 285.
STEPHENSON, C. C., LANDERS, L. A., and COLE, A. G., 1952, *J. chem. Phys.*, **20,** 1044.
STRUKOV, B. A., SORKIN, E. L., Yuskin, N. K., and TARASKIN, S. A., 1986, *Soviet Phys. Solid St.*, **28,** 1785.
SUGA, H., 1986, *Ann. N. Y. Acad. Sci.*, **484,** 248.
SUGA, H., and SEKI, S., 1974, *J. non-crystalline Solids*, **16,** 171.
SUGA, H., MATSUO, T., and SEKI, S., 1965, *Bull. chem. Soc. Japan*, **38,** 1115.
SUGA, H., MATSUO, T., and SEKI, S., 1968, *Bull. chem. Soc. Japan*, **41,** 583.
SUGISAKI, M., MATSUO, T., SUGA, H., and SEKI, S., 1968, *Bull. chem. Soc. Japan*, **41,** 1747.
SULLIVAN, N. S., 1983, *AIP Conf. Proc.*, **103,** 121.
SULLIVAN, N. S., and ESTÈVE, D., 1981, *Physica* B, **107,** 189.
SULLIVAN, N. S., DEVORET, M., COWAN, B. P., and URBINA, C., 1978, *Phys. Rev.* B, **17,** 5016.
SULLIVAN, N. S., DEVORET, M., and VAISSIERE, J. M., 1979, *J. Phys. Lett., Paris*, **40,** 559.
SULLIVAN, N. S., ESTÈVE, D., and DEVORET, M., 1982, *J. Phys.* C, **15,** 4895.
SULLIVAN, N. S., DEVORET, M., and ESTÈVE, D., 1984, *Phys. Rev.*, **B,** 4935.
SULLIVAN, N. S., EDWARDS, C. M., and BROOKMAN, J. R., 1986, *Molec. Crystals liq. Crystals*, **139,** 365.
TADIC, B., PIRC, R., and BLINC, R., 1989, *Z. Phys.* B, **75,** 249.
TAKASHIGE, M., TERAUCHI, H., MIURA, Y., HOSHINO, S., and NAKAMURA, T., 1985a, *Jap. J. appl. Phys.*, **24,** Suppl. 24-2, 947.
TAKASHIGE, M., TERAUCHI, H., MIURA, Y., and HOSHINO, S., 1985b, *J. Phys. Soc. Japan*, **54,** 3250.
TAMURA, S., and WOLF, S. P., 1987, *Phys. Rev.* B, **36,** 3491.
TERAUCHI, H., 1985a, *Ferroelectrics*, **64,** 87.
TERAUCHI, H., 1985b, *Jap. J. appl. Phys.*, **24,** Suppl. 24-2, 75.
TERAUCHI, H., 1986, *Phase Transitions*, **7,** 315.
TERAUCHI, H., FUTAMURA, T., NISHIHATA, Y., and NIDA, S., 1984, *J. phys. Soc. Japan*, **53,** 483.
THOLENCE, J. L., and TOURNIER, R., 1970, *Phys. Rev. Lett.*, **25,** 867.
TORRE, S., and RIGAMONTI, A., 1987, *Phys. Rev.* B, **36,** 8274.
TOULOUSE, G., 1977, *Commun. Phys.*, **2,** 115.
TOULOUSE, G., 1980, *J. Phys. Lett., Paris*, **41,** L447.
TRUELL, R., ELBAUM, C., and CHICK, B. B., 1969, *Ultrasonic Methods in Solid State Physics* (New York: Academic).
TRYBULA, Z. Z., STANKOWSKI, J., SZCZEPANSKA, L., BLINC, R., WEISS, AL, and DALAL, N. S., 1988, *Physica* B, **153,** 143.
UWE, H., LYONS, K. B., and FLEURY, P. A., 1986, *Phys. Rev.* B, **33,** 6436.
VAN DER KLINK, J. J., and BORSA, F., 1984, *Phys. Rev.* B, **30,** 52.
VAN DER KLINK, J. J., and RYTZ, D., 1982, *J. Crystal Growth*, **56,** 673.
VAN DER KLINK, J. J., and RYTZ, D., 1983, *Phys. Rev.* B, **27,** 4471.

VAN DER KLINK, J. J., RYTZ, D., BORSA, F., and HÖCHLI, U. T., 1983, *Phys. Rev.* B, **27,** 89.
VAN DER KLINK, J. J., ROD, S., and CHÂTELAIN, A., 1986, *Phys. Rev.* B, **33,** 2084.
VANDERWAL, J. J., HU, Z., and WALTON, D., 1986, *Phys. Rev.* B, **33,** 5782.
VERWEEL, H. J., and BIJVOET, J. M., 1983, *Z. Kristallogr.*, **100,** 201.
VIKHNIN, V. S., and BORKOVSKAYA, Y. B., 1978, *Soviet Phys. Solid St.*, **20,** 2082.
VIKHNIN, V. S., and ORLOV, O. L., 1983, *Soviet Phys. Solid St.*, **25,** 22.
VIKHNIN, V. S., NADOLINSKAYA, E. G., SHILNIKOV, A. V., and YUSHIN, N. K., 1988, *Soviet Phys. Solid St.*, **30,** 349.
VOGEL, H., 1921, *Z. Phys.*, **22,** 645.
VOGT, H., 1974, *J. appl. Phys.*, **5,** 85.
VOIGT, P., BETZLER, K., SCHMIDT, N., and KAPPHAN, S., 1990, *Ferroelectrics* **106,** 149.
VOLKMANN, U. G., BÖHMER, R., LOIDL, A., KNORR, K., HÖCHLI, U. T., and HAUSSÜHL, S., 1986, *Phys. Rev. Lett.*, **56,** 1716.
VUGMEISTER, B. E., 1985, *Soviet Phys. Solid St.*, **27,** 716.
VUGMEISTER, B. E., and ANTIMIROVA, T. V., 1990, *Phys. Stat. Sol.* (in the press).
VUGMEISTER, B. E., and GLINCHUK, M. D., 1979, *Soviet Phys. Solid St.*, **21,** 735.
VUGMEISTER, B. E., and GLINCHUK, M. D., 1980, *Soviet Phys. JETP*, **52,** 482.
VUGMEISTER, B. E., and GLINCHUK, M. D., 1985, *Soviet Phys. Usp.*, **28,** 606.
VUGMEISTER, B. E., and STEPHANOVICH, V. A., 1987, *Solid St. Commun.*, **63,** 323.
VUGMEISTER, B. E., and STEPHANOVICH, V. A., 1988, *Solid St. Commun.*, **66,** 673.
VUGMEISTER B. E., LAGUTA, V. V., BYKOV, P. I., KONDAKOVA, I. V., and SYRNIKOV, P. P., 1989, *Soviet Phys. Solid St.*, **31,** 205.
WAGNER, K. W., 1913, *Annln Phys., Leipzig*, **40,** 817.
WALTON, P., 1990 (to be published).
WALTON, D., MOOK, H. A., and NICKLOW, R. M., 1974, *Phys. Rev. Lett.*, **33,** 412.
WALTON, J. H., WU, M.-C., and CONRADI, M. S., 1988, *Can. J. Chem.*, **66,** 680.
WANG, C. H., and SATIJA, S. K., 1977, *J. chem. Phys.*, **67,** 851.
WANG, J. C., 1980, *Phys. Rev.* B, **22,** 2725.
WARD, L. G., SALEH, A. M., and HAASE, D. G., 1983, *Phys. Rev.* B, **27,** 1832.
WASHBURN, S., SCHWEIZER, R., and MEYER, H., 1980, *Solid St. Commun.*, **35,** 623.
WASHBURN, S., CALKINS, M., MEYER, H., and HARRIS, A. B., 1982, *J. low Temp. Phys.*, **49,** 101.
WASHBURN, S., CALKINS, M., MEYER, H., and HARRIS, A. B., 1983, *J. low Temp. Phys.*, **53,** 585.
WASHBURN, S., CALKINS, M., MEYER, H., and HARRIS, A. B., 1984, *J. low Temp. Phys.*, **57,** 31.
WECHSLER, M. S., LIEBERMAN, D. S., and READ, T. A., 1953, *Trans. Am. Inst. Mining metall. Engrs*, **197,** 1503.
WENGENMAYR, R., 1988, Diplomarbeit, TH Darmstadt.
WILLIAMS, G., and WATTS, D. C., 1970, *Trans. Faraday Soc.*, **66,** 80.
WINDHEIM, R., 1976, *Solid St. Commun.*, **18,** 1183.
WIOTTE, W., ELSCHNER, S., and ALBERS, J., 1986, *Proceedings of the 23rd Congress Ampère on Magnetic Resonance*, edited by M. Maraviglia, F. de Luca and R. Campanello, p. 142.
WOCHNER, P., 1988, Ph.D. Thesis, Ludwig-Maximilians-Universität, München.
WOCHNER, P., BURKEL, E., PEISL, J., ZEYEN, C. M. E., and PETRY, W., 1989, *Dynamics of Disordered Metals*, edited by D. Richter, A. J. Dianoux, W. Petry and J. Texeira (Berlin: Springer), p. 280.
WU, L., ERNST, R. M., JEONG, Y. H., NAGEL, S. R., SUSMAN, S., 1988, *Phys. Rev.* B, **37,** 10444.
XHONNEUX, P., COURTENS, E., and GRIMM, H., 1988, *Phys. Rev.* B, **38,** 9331.
YACOBY, Y., 1978, *Z. Phys.* B, **31,** 275.
YACOBY, Y., and JUST, S., 1974, *Solid St. Commun.*, **15,** 715.
YACOBY, Y., and LINZ, A., 1973, *Phys. Rev.* B, **9,** 2723.
YACOBY, Y., AGRANAT, and A., and OHANA, I., 1983, *Solid St. Commun.*, **45,** 757.
YAMAMOTO, S., and SHINNAKA, Y., 1981, *J. phys. Soc. Japan*, **50,** 1417.
YU, I., WASHBURN, S., CALKINS, M., and MEYER, H., 1983, *J. low Temp. Phys.*, **51,** 401.
ZELLER, R. C., and POHL, R. O., 1971, *Phys. Rev.* B, **4,** 2029.
ZIEMATH, E. C., and AEGERTER, M. A., 1986, *Solid St. Commun.*, **58,** 519.
ZIMMERMANN, J., and WEBER, G., 1981, *Phys. Rev. Lett.*, **46,** 661.